Characterization and impact of cellular senescence during mammary gland involution

Elsa Charifou

▶ **To cite this version:**

HAL Id: tel-04219252

https://theses.hal.science/tel-04219252

Submitted on 27 Sep 2023

Sorbonne Université

École Doctorale Complexité du Vivant (ED515)

Équipe Plasticité cellulaire dans les pathologies liées à l'âge
Développement et Biologie des Cellules Souches
Institut Pasteur

Characterization and impact of cellular senescence during mammary gland involution

Thèse de doctorat en Biologie

Présentée par **Elsa CHARIFOU**

Soutenue publiquement le 26 Septembre 2022

Devant le jury composé de:

Chahrazade EL AMRI – Présidente du jury

Serge ADNOT – Rapporteur

Felicity DAVIS – Rapportrice

Dmitry BULAVIN – Examinateur

Bethan LLOYD-LEWIS – Examinatrice

Louis GERVAIS – Membre invité

Han LI – Directrice de thèse

If your dreams do not scare you, they are not big enough.

Mike Horn, world explorer

Acknowledgments

I would like to thank all the members of my Ph.D. jury. First, **Dr. Felicity Davis** and **Dr. Serge Adnot** for putting their expertise in the mammary gland and senescence fields to review my work. Thanks also to **Dr. Bethan Lloyd-Lewis**, **Dr. Charhazade El Amri**, **Dr. Dmitry Bulavin,** and **Dr. Louis Gervais** for accepting to participate in my Ph.D. defense. It would be an honor to discuss my work with you all.

Thanks to my thesis director, **Dr. Han Li**, for the opportunity to do a Ph.D. in your lab. After four challenging years, I feel proud of the work we achieved together. Thanks for giving me the opportunity to participate in ENBDC and ISCA meetings and for your trust in presenting my data at the retreat and for the Dev'Club. Overall, your advice improved my capacity to present my work.

À mon équipe de folie:

Aurélie, ma dealeuse d'œufs, mon grain de café, mon petit Kévin, mon éleveuse de chèvres, ma Céline Dion, mon arnaqueuse de tredlnik, ma reine des crop. C'est simple, sans toi je n'aurais jamais écrit ces lignes… Merci de m'avoir retourné le cerveau pour faire une thèse, je ne regrette finalement pas (enfin je crois) ! Merci de m'avoir prise sous ton aile pour me transmettre ton savoir et ton amour des glandes mammaires. Merci d'avoir porté et partagé ce projet avec moi. Et merci d'avoir été là tous les jours pour que j'y arrive. Dans les moments compliqués, avec notre confessionnal en pièce de culture. Mais surtout dans les moments de joie. Et mon Dieu (Arrête de jurer !), ils ont été nombreux !! **Lamia**, merci d'avoir été une étudiante aussi appliquée et impliquée. Ton aide dans les marquages, les scans, et les quantifications a été précieuse. Merci aussi pour ton attitude vaillante qui m'a motivée quand j'en avais le plus besoin. Merci aussi d'avoir montré ton côté vulnérable et de m'avoir fait confiance. Et enfin, merci pour tous les fous rires qu'on a pu avoir à la cantine… ou à Prague ! **Laurianne**, à l'héritière de mon bureau et de mes pipettes. Je garde en tête nos moments d'extase au microscope devant les adipocytes différenciés en forme de fleur, ou les sublimes organoides au confocal… qui étaient quand même bien difficiles à trouver parfois ! Merci de m'avoir suivie dans tous mes vices culinaires pour combler mes pulsions rédactionnelles. On se paiera uber eats premium quand tu rédigeras ta thèse ;) **Cheng**, thanks for being the mom of the lab and for comforting me anytime I needed. Thanks for teaching me all the techniques of mice injections and optimizing the program for automatic quantification! **Jérémy**, à mon petit poulain, aussi connu comme l'homme au bonnet, aka le roi

To my international IP girls squad, thank you for all the moments we shared together. **Miriam** my German top model, thanks for always coming to my office. I will remember our Coldplay concert as a highlight of the last four years! **Ralitza**, my best Bulgarian girl, thanks for your kindness and your adventurous mindset. And **Tanya**, my Canadian friend from a previous life. Thanks for simply being you. You made me feel so comfortable in such a short amount of time. Thanks for our self-defense class/food trip nights/bubble teas, it helped me to survive this crazy writing time.

Thanks to **Jakub** and **Zuzana** first for the collaboration we established on organoids. It was a really motivating period of my Ph.D. Thank you also for inviting me to your wedding in Czech Republic. I felt privileged to witness so much love.

A mes amis qui m'ont toujours soutenue :
Merci à **Yassin** pour toutes nos aventures à travers le monde. Merci de m'avoir toujours poussée à aller plus loin. Merci aussi pour ta positivité légendaire qui m'a toujours permise de dédramatiser. Tu as été un soutien précieux pendant toutes ces années. Merci à mes meilleurs amis **Mick Mick**, **Mélo, Léa** et **Marina** pour vos encouragements constants, nos soirées jeux de société, nos dimanche matins piscine… tous ces moments qui m'ont rappelé qu'il n'y avait pas que la thèse qui comptait ! Merci à ma team Vis Ma Vie De Chercheur **Helena**, **Antoine**, **Ségolène**, **Flaminia**, **Virginia**, **Yoann**, **Léonor**, et **Natalia**. J'ai vécu certains des moments les plus magiques de ma thèse à vos côtés, à encadrer de nombreux lycéens et à (peut-être ?) créer des vocations.

Et enfin, merci à ma famille sans qui je n'en serai pas arrivée jusque-là :
A ma **Maman**, merci pour ton accueil. Tu as tout fait pour me rendre la vie plus facile et que je puisse me concentrer sur la rédaction de ma thèse. Tu es depuis toujours ma plus grande fan, merci pour ton soutien inconditionnel. Et enfin à mon **Papa**, moi qui pensais que la thèse serait l'épreuve la plus dure que j'aurais à traverser… J'espère que de là-haut, tu es fier de ce que j'ai pu accomplir.

Parce que ce travail n'aurait jamais pu avoir lieu sans toutes les personnes bienveillantes qui m'ont aidée, encouragée, soutenue, et fait rire, pendant ces quatre années. Je pourrais écrire à nouveau 200 pages pour vous exprimer ma gratitude. Un grand merci à tous.

Abstract

Résumé

La sénescence est une réponse à un stress biologique, caractérisée par un arrêt stable du cycle cellulaire. Néanmoins, les cellules restent métabolliquement actives et acquièrent un phenotype sécrétoire associé à la sénescence, avec la production d'un sécrétome complexe composé de cytokines, chémiokines, facteurs de croissance et modulateurs du remodelage de la matrice extracellulaire. La sénescence est associée à de nombreux processus pathologiques, comme la tumorigénèse et le vieillessement. Cependant, où, quand et comment la sénescence contribue aux processus physiologiques reste méconnu. Pour répondre à cette question, nous avons tiré profit de la glande mammaire (GM), un organe avec une plasticité remarquable pendant le développement post-natal. L'involution de la GM est l'un des évenements majeurs de mort cellulaire et de remodelage tissulaire chez les mammifères, lorsque les cellules épithéliales produisant le lait sont éliminées et que la GM retourne à son état pré-grossesse, attendant la prochaine gestation. Au cours de ma thèse, nous avons montré que la sénescence était induite transitoirement pendant la phase irréversible de l'involution. De plus, le programme de sénescence apparaissait spécifiquement dans les cellules luminales productrices de lait et corrélait à l'expression de l'inhibiteur du cycle cellulaire p16. En parallèle, nous avons établi un nouveau modèle d'organoides pour mimer la gestation, la lactation et l'involution de la GM. Dans ce modèle *ex-vivo*, nous avons aussi relever la présence de cellules sénescentes strictement lors du processus d'involution. Pour évaluer l'impact biologique de la sénescence *in vivo*, nous avons utilisé une méthode de scellement des mamelons pour découpler les phases réversible et irréversible de l'involution. Nous avons dévoilé une association étroite entre le sevrage des hormones lactogéniques qui a lieu lors de la seconde phase d'involution, et l'induction du programme de sénescence. Pour mieux définir les rôles physiologiques de la sénescence pendant l'involution, nous avons traités des souris avec de l'ABT-263, un composé sénolytique induisant l'apoptose des cellules sénescentes. Nous avons observé une altération du remodelage tissulaire suite à l'élimination des cellules sénescentes, avec des alvéoles résiduelles plus larges et un remplissage adipocytaire retardé. De plus, dans des organoides provenant de souris transgéniques p16-3MR, nous avons éliminé les cellules sénescentes avec succès grâce à l'administration de ganciclovir, ce qui a retardé le processus d'involution. Dans leur ensemble, les modèles *in vivo* et *ex-vivo* suggèrent un rôle important de la sénescence pour moduler la phase de remodelage tissulaire dans l'involution de la GM. Enfin, le processus d'involution est intiment lié avec le cancer du sein post-partum, un cancer diagnostiqué dans les 10 ans suivant une grossesse et associé à un mauvais pronostic. Explorer comment la sénescence impacte le microenvironnement lors de l'involution pourrait ainsi fournir de nouvelles connaissances pour mieux comprendre le cancer du sein post-partum.

Abstract

Cellular senescence is a biological stress response characterized by a stable cell cycle arrest. Nonetheless, cells remain metabolically active and acquire a senescence-associated secretory phenotype (SASP), a complex secretome composed of cytokines, chemokines, growth factors, and extracellular matrix remodeling modulators. Senescence is associated with various pathological processes, such as tumorigenesis and aging. However, it is unknown when, where and how senescence contributes to physiological processes. To answer this question, we took advantage of the mammary gland (MG), an organ with remarkable plasticity throughout postnatal development. The MG involution is one of the major mammalian cell death and tissue remodeling events, when milk-producing epithelial cells are removed, and the MG returns to its pre-gestation state, resting for further pregnancy. During my Ph.D., we showed that senescence was transiently induced during the irreversible phase of involution. The senescent program occurred specifically in the alveolar milk-producing luminal cells and correlated with the expression of the cell cycle inhibitor p16. In parallel, we established a novel organoid system to mimic MG gestation, lactation, and involution. In this *ex-vivo* model, we also highlighted the presence of senescent cells strictly during the involution-like process. To assess the biological impact of senescence *in vivo,* we used a teat sealing method to uncouple the reversible and irreversible phases of involution. We unveiled a close association between the withdrawal of lactogenic hormones occurring in the second phase of involution and the induction of the senescence program. To further define the physiological roles of senescence during involution, we treated mice with ABT-263, a senolytic compound inducing apoptosis of senescent cells. Interestingly, we observed an impaired tissue remodeling upon senescence elimination, with larger remaining alveolar structures and delayed adipocyte refilling. Moreover, in organoids from transgenic p16-3MR mice, we successfully removed senescent cells with ganciclovir and delayed the involution-like process. Taken together, both *in vivo* and *ex-vivo* models suggest an essential role of senescence in modulating the tissue remodeling phase of MG involution. Importantly, the involution process is intimately associated with postpartum breast cancer (PPBC), a cancer diagnosed within 10 years following delivery with a poor prognosis. Investigating how senescence impacts the microenvironment during the involution process might provide major insights to understand PPBC.

Introduction

I.   __Cellular senescence__

A.   General introduction of senescence

Senescence is a term deriving from the latin root "senex", which can be translated by the adjective "old". Cellular senescence has been historically described by Hayflick and Moorhead in the early 60s as the failure of non-transformed cells to divide indefinitely (Hayflick and Moorhead 1961). They showed that human fetal lung fibroblasts could proliferate *in vitro* up to a defined number of divisions, termed the "Hayflick's limit". Independently of the origin of the human tissues, cells stopped replicating after 50±10 mitosis. This pioneering work refuted Carrel's long-standing dogma of cell immortality, based on chicken embryonic heart cells, which were supposedly grown *in vitro* for more than 34 years (Carrel 1912). After identifying technical issues in Carrel's methodology and reproducing Hayflick's observations worldwide for six decades, it is now widely accepted that cells have a limited replicative lifespan, after which they enter a state of cellular senescence.

Following this groundbreaking discovery and 60 years of broad research in this field, cellular senescence is now commonly defined as a permanent proliferative arrest due to the increased expression of cyclin-dependent kinase inhibitors (e.g., p16^{INK4A}; p21^{CIP1}). A plethora of biological stresses can induce the irreversible cell cycle arrest (e.g., telomere exhaustion, DNA damage, oncogene activation, oxidative stress...). Depending on the cell type of origin or on the senescence-inducing signal, senescent cells do not exhibit a unique common biological barcode but a wide range of non-exclusive biomarkers (e.g., senescence-associated beta-galactosidase (SAβGal) histological staining, overexpression of cell cycle inhibitors, lack of proliferation hallmarks, enlarged morphology, or chromatin rearrangements). Although senescent cells are non-proliferative, they are resistant to apoptosis and remain metabolically active, acquiring secretive phenotypes called Senescence-Associated Secretory Phenotypes (SASPs). SASPs are heterogeneous and are composed of a variety of

key cell players (e.g., inflammatory cytokines, chemokines; matrix remodeling factors, growth modulators...) ([Campisi and d'Adda di Fagagna 2007](#)).

The heterogeneity of senescent features is reflected in diverse *in vivo* roles of senescence. The senescence program has been conserved through evolution as an intrinsic defense mechanism to prevent the proliferation of damaged cells. Therefore, senescence is a potent tumor suppression mechanism, avoiding uncontrolled replication of preneoplastic cells. The counterpart of this senescence-induced growth arrest is the exhaustion of stem and progenitor proliferative cells, contributing to aging ([Rodier and Campisi 2011](#)).

Senescence also has a major extrinsic role in tissues. Through the secretion of SASPs, senescent cells interact with neighboring cells and modify the tissue microenvironment. Transient induction of senescence has been recently shown to be beneficial in different contexts (e.g., wound healing, cellular plasticity upon tissue damage, or embryonic development). Whereas the inability to eliminate senescent cells leading to their accumulation is associated with well-exemplified detrimental effects (e.g., cancer cell proliferation, age-related diseases, chronic inflammation, or fibrosis) ([Munoz-Espin and Serrano 2014](#)).

Focus has been mainly placed on the deleterious dark side of senescence, leading to the flourishing of senotherapies ([Childs et al. 2017](#)). These newly developed therapeutic strategies aim to eliminate senescent cells or to modulate SASP functions, to extend healthy lifespan and improve age-related diseases. However, senescence contribution and regulation in *in vivo* physiological processes still remains elusive. Better understanding the spatio-temporal regulation of physiological *in vivo* senescence is therefore essential to comprehend its pathological outcomes and its clinical relevance.

## B.	Main inducers of cellular senescence

Entrance into the senescence cell state can be triggered by a wide range of intrinsic and extrinsic signals, such as telomere dysfunction, persistent DNA damage, oncogenic activation, oxidative stress, or cytotoxic drugs. The developed senescence phenotype depends on the type of trigger signals, leading to the production of stimuli-specific SASP. Therefore, the senescence program can be categorized according to inducer stimuli, most of them being deeply characterized *in vitro* (Collado and Serrano 2006).
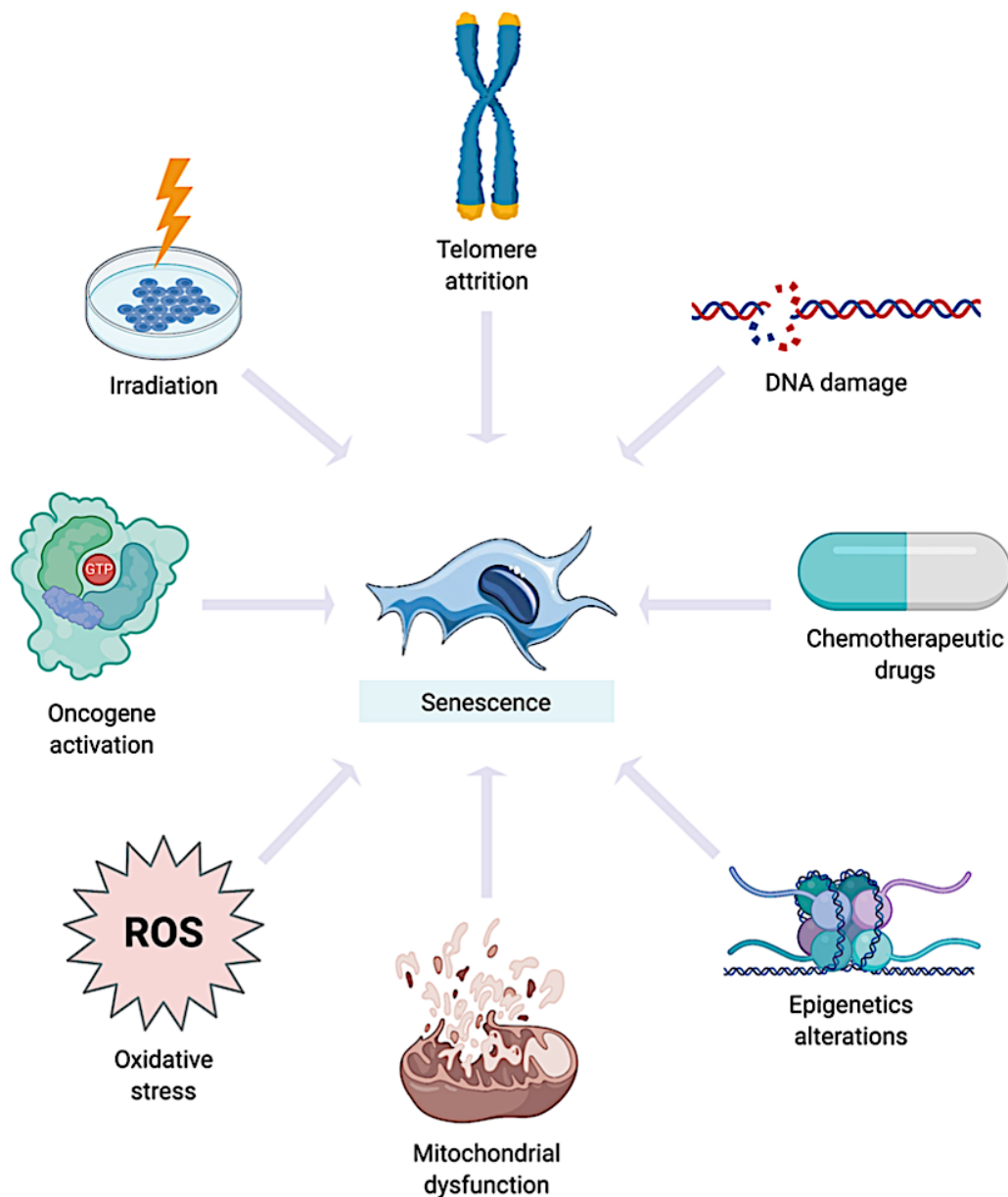
Figure 1. Inducers of cellular senescence. The senescence program can be triggered by various stresses such as telomere erosion, persistent DNA damages, or oncogene activation. The cells interpret these signals as sub-lethal stresses and respond by entering an irreversible cell cycle arrest. Senescence can therefore be classified regarding its inducing stressor in replicative senescence, DNA damage-induced senescence, or oncogene-induced senescence. Adapted from (Ngoi et al. 2021).

1.   *Replicative senescence*

Replicative senescence is the first type of senescence historically identified by Hayflick and is triggered by telomere attrition. Telomeres are repetitive sequences capping the end of linear chromosomes and function as a molecular clock, keeping track of the number of cell divisions. These sequences of 10-15kb are replicated by the telomerase, an enzyme competent only in embryonic stem cells but inactive in somatic stem cells. During each somatic cell division, normal DNA polymerases fail to replicate DNA ends, and as telomerases are inactive, each chromosome loses 50-200bp per S phase. Telomeres are shortened until reaching a critical size, which triggers the DNA damage response (DDR) machinery, and permanent cell cycle arrest (Allsopp et al. 1992).

2.   *DNA damage-induced senescence*

Various stressors such as metabolites, chemical reagents, or physical agents also induce DNA damage and trigger DDR (Jackson and Bartek 2009). When DDR attempts to repair DNA fail, and damages remain unresolved, cells can either enter apoptosis or senescence. Events leading towards one or the other outcome are still not well defined, but it has been proposed that severe short-term DNA damages activate apoptosis, whereas mild DNA damages tend to promote senescence (Petrova et al. 2016).

Reactive oxygen species (ROS) accumulations are perceived as an oxidative stress and can lead to mutations in nuclear and mitochondrial DNA (Busuttil et al. 2003). For example, an increase of ROS due to UVB exposure has been shown to induce senescence in keratinocytes (Lewis et al. 2008). Chemotherapies using ionizing irradiation or chemotherapeutic agents such as doxorubicin are also proposed to induce senescence through the formation of double-strand breaks (Suzuki and Boothman 2008; Roberson et al. 2005).

3. *Oncogene-induced senescence*

Oncogene-induced senescence (OIS) is a cell cycle arrest triggered by abnormal oncogene overexpression. OIS was described for the first time in response to Ras overexpression in human and mouse fibroblasts (Serrano et al. 1997). Upon oncogene activation, cells enter into a burst of proliferation, perceived as a replicative stress signal triggering premature senescence. Nowadays, OIS induction is reported after the deregulation of one of more than 50 genes classified as oncogenes. Therefore, OIS is a robust tumor suppression mechanism (Gorgoulis and Halazonetis 2010).

C. Biomarkers of senescent cells

Senescent cells are highly heterogeneous, especially *in vivo*, due to the variety of inducing signals and the cell type. Moreover, senescent cells exhibit a heterogeneous transcriptional profile if they respond directly to the cellular stress (primary senescence) or if they respond to a paracrine signal from a cell already senescent (secondary senescence) (Kirschner et al. 2020) *(see "Autocrine/Paracrine reinforcement of senescence" for further details)*. Finally, most of the described characteristics to define a senescent cell have been identified *in vitro,* and some, but not all, are valuable indicators of *in vivo*

senescence. Therefore, it remains challenging to characterize senescence by a unique signature, and a set of combined features is required to define a senescent cell in a tissue ([Di Micco et al. 2021](#)).
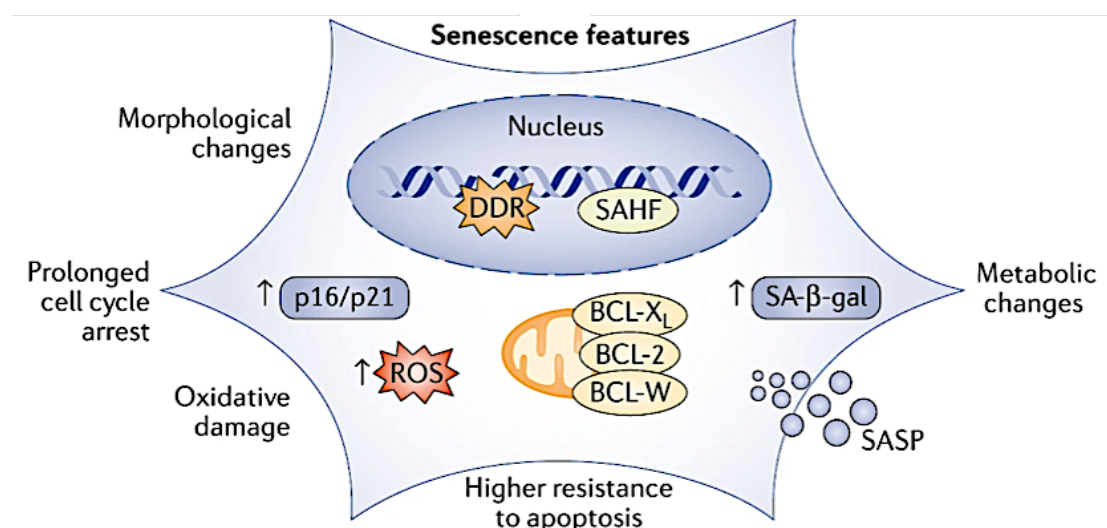
Figure 2. Markers of senescent cells. There is no unique but a combination of biomarkers used to identify senescent cells, most of them characterized *in vitro*. Senescent cells are in an irreversible cell cycle arrest and overexpress cell cycle inhibitors such as p16 and p21. They remain metabolically active and acquire a secretory phenotype (SASP), composed of various cytokines, chemokines, growth factors, and extracellular matrix remodelers. Due to their extended lysosomal content, senescent cells have increased β-galactosidase activity and are positive for SAβGal staining. They are resistant to apoptosis with an up-regulation of Bcl2 family proteins. Morphologically, senescent cells have an enlarged phenotype, and remodeling of the heterochromatin leads to the appearance of senescence-associated heterochromatin foci (SAHF). From ([Di Micco et al. 2021](#)).

1. *Cell cycle arrest*

One prominent feature of senescent cells is their stable cell cycle arrest. Therefore, senescent cells lack proliferative markers, typically incorporation of 5-bromodeoxyuridine (BrdU) *in vitro* or Ki-67 immunostaining *in vivo*.

However, stable cell cycle arrest is not exclusive to senescent cells, as quiescent and differentiated post-mitotic cells are also not replicating. Unlike senescent cells, quiescent cells are in a temporary arrest, called the G0 phase, with low metabolism and can re-enter into the G1 phase upon adequate mitogen stimuli (Pardee 1989). Regarding post-mitotic cells, precursors differentiate into specialized cells upon a defined developmental program distinct from stress response inducing senescence. Thus, effectors mobilized for this permanent cell cycle arrest are different between terminally differentiated cells (p18^{INK4c}, p27^{KIP1}) and senescent cells (p16^{INK4a}, p21^{CIP1}, ARF, p53, and RB) (He and Sharpless 2017).

Quiescence
Cell cycle: Reversible arrest
Macromolecular damage: No
Signaling: p27^{KIP1} - dependent
Secretion: No

Differentiation
Cell cycle: Generally irreversible arrest
Macromolecular damage: No
Signaling: Various (e.g. Hedgehog, Wingless, Notch, RB, p16^{INK4A})
Secretion: Yes/No

Senescence
Cell cycle: Generally irreversible arrest
Macromolecular damage: Yes
Signaling: p21$^{WAF1/Cip1}$/p16^{INK4A} up-regulation
Secretion: Yes

Figure 3. Differences in cell cycle arrest in quiescent, differentiated, and senescent cells. Quiescence, differentiation, and senescence are three cellular states with a withdrawal from the cell cycle, but they can be separated based on the reversibility of the cell cycle arrest, the presence of macromolecular damages, the activated signaling pathways, and the production of a secretome. Arrows figure the interconnection between the states; once senescent, cells cannot reverse their cell fate. From (Gorgoulis et al. 2019).

2. *Expression of cyclin-dependent kinase (CDK) inhibitors*
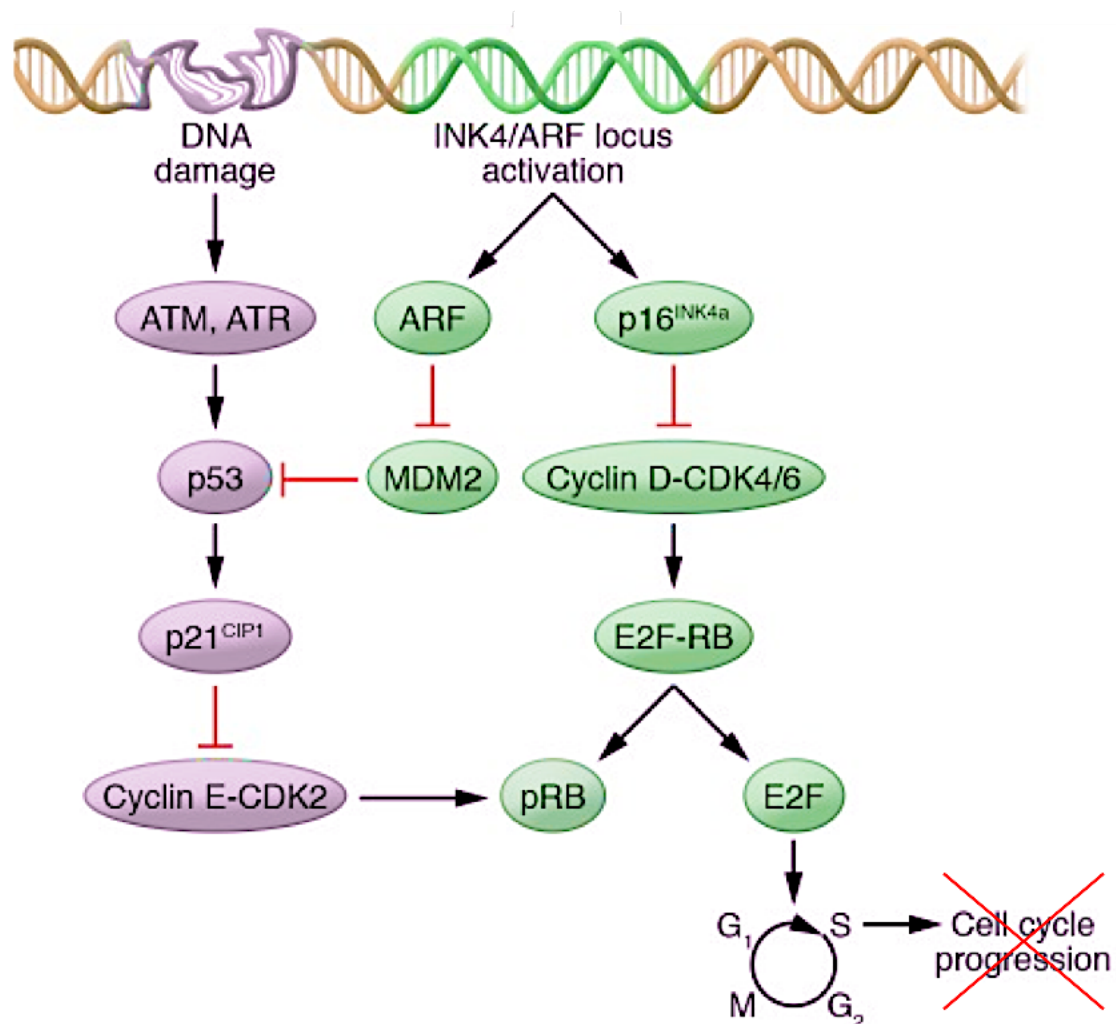
Figure 4. Molecular pathways activated in senescent cells. Senescent-associated cell cycle exit is regulated by two main pathways, p16[INK4A]- or p21[CIP1]-dependent. Both p16[INK4] and p21[CIP1] are cyclin-dependent kinase inhibitors,

respectively targeting Cyclin D-CDK4/6 and Cyclin E-CDK2, kinases responsible for phosphorylating RB to release the transcription factor E2F. Upon p16^{INK4A}- or p21^{CIP1} activation, RB remains non-phosphorylated and sequestrates E2F, preventing the transcription of genes involved in the cell cycle progression. Adapted from ([Herranz and Gil 2018]).

a)   *p16^{INK4A}-Rb pathway*

p16^{INK4A}, or p16, is a cyclin-dependent kinase inhibitor involved in the interruption of the cell cycle and commonly overexpressed in senescent cells. p16 is produced by the INK4A/ARF locus, which comprises *CDKN2A* encoding for p16 and ARF (p19^{ARF} in mice, p14^{ARF} in humans) and *CDKN2B* encoding for p15. CDKN2A locus is epigenetically repressed in normal proliferative cells ([Gil and Peters 2006]). Thus, Cyclin D-CDK4/6 can phosphorylate Rb, dissociating from a complex with the transcription factor E2F. Free E2F enters the nucleus and transactivates genes involved in the progression of the cell cycle. Upon senescence induction, epigenetic de-repression of *CDKN2A* locus, higher promoter accessibility, and increased protein stability are combined strategies to express p16 ([Hernandez-Segura, Nehme, and Demaria 2018]). p16 binds to CDK4/6, preventing its kinase activity. Rb is maintained in a hypo-phosphorylated state and sequestrates E2F, preventing transcription of proliferative genes and leading to G1 cell cycle arrest ([Serrano 1997]). Therefore, p16 expression is a robust and powerful biomarker of *in vivo* senescence ([Krishnamurthy et al. 2004]).

b)   *p53/p21^{CIP1} pathway*

p21^{CIP1}, or p21, is also a critical cyclin-dependent kinase inhibitor transcriptionally induced by p53 activity. p21 inhibits the kinase activity of Cyclin E-CDK2, leading to hypo-phosphorylation of Rb, sequestration of E2F, and inhibition of cell cycle progression ([Deng et al. 1995]).

3. *Morphological changes*

a) *Nucleus*

Lamin B1 is a protein present on the nucleoplasmic side of the inner nuclear membrane, necessary for nuclear 3D structure and chromatin organization (Gerace, Blum, and Blobel 1978). In many types of senescence, Lamin B1 is down-regulated, destabilizing the nuclear integrity (Freund et al. 2012). This decline induces large-scale chromatin rearrangements, as lamina-associated domains spatially cluster within the nucleus and lose their condensation state. Senescence-associated heterochromatin foci (SAHFs) enriched in repressive heterochromatin marks are proposed to be a compensatory mechanism to maintain heterochromatin status in senescent cells (Chandra and Kirschner 2016). SAHFs heterochromatinization specifically represses cell cycle genes normally activated transcriptionally by E2F (Narita et al. 2003) *(see "Expression of cyclin-dependent kinase inhibitors" for further details)*. Loss of Lamin B1 and appearance of SAHFs are found in different types of senescence but are not universal markers.

b) *Cytoplasm*

In vitro, senescent cells as fibroblasts present an enlarged size, with a flattened morphology, mainly due to cytoskeleton rearrangements (Wang and Gundersen 1984). However, *in vivo* senescent cells preserve their 3D structure, presumably due to constraints applied by the tissue architecture (Herranz and Gil 2018).

4. *Senescence-associated β-galactosidase (SAβGal)*

Senescent cells exhibit an expansion of lysosomes in number and size. This extended lysosomal content is correlated with overexpression and higher activity of a lysosomal enzyme named β-galactosidase (Kurz et al. 2000). This enzyme is not required for a functional senescence program, as patients deficient

for the *β*-galactosidase encoding gene *GLB1* do not show any impairment in establishing or maintaining a senescent phenotype ([Lee et al. 2006](#)). However, *β*-galactosidase activity is a predominant marker of senescence. This enzyme is active at acidic pH 4.0 in lysosomes of normal cells under physiological conditions. In senescent cells, reflecting the expanded lysosomal compartment, this enzyme is active under sub-optimal pH 6.0. This pH-linked property is widely used in the classical cytochemical assay termed "SA*β*Gal staining", in which the chromogenic substrate X-Gal (5-Bromo-4-chloro-3-indolyl β-D-galactopyranoside) is cleaved by SA-*β*-galactosidase, forming a blue-dyed precipitate observed in bright-field ([Dimri et al. 1995](#)). A newly developed fluorogenic compound, $C_{12}FDG$ (5-Dodecanoylaminofluorescein Di-β-D-galactopyranoside) ([Cahu and Sola 2013](#)), can replace X-Gal substrate for fluorescent analyses as fluorescence-activated cell sorting (FACS).

SA*β*Gal staining is a powerful labeling of expanded lysosomal content, which is a characteristic non-exclusive to senescent cells. Indeed, other cell types with autophagy properties as macrophages can be positive for SA-*β*Gal staining ([Bursuker, Rhodes, and Goldman 1982](#)), rising the need to combine this widely used assay with additional senescent markers.

5.   ***Resistance to apoptosis***

Apoptosis is an extreme stress-response inducing a tightly controlled cell death, destroying cellular components and leading to clearance by engulfing cells ([Kerr, Wyllie, and Currie 1972](#)). Apoptosis and senescence are described as alternative cell fates for damaged cells beyond repair. Decision to undergo one or the other program is not fully understood yet, especially as the same stressors can trigger both pathways. However, once engaged in senescence, cells lock this decision by mechanisms to resist the alternative fate.

Compared with normal proliferating cells, senescent cells are more resistant to various pro-apoptotic stimuli *in vitro*, such as UV damage, withdrawal of serum

in culture, oxidative stress, or addition of cytotoxic compounds ([Soto-Gamez, Quax, and Demaria 2019](#)).

More specifically, senescent cells are proposed to become resistant to apoptosis by either up-regulating transcription or increasing transcripts stability of BCL-2 anti-apoptotic genes ([Ryu, Oh, and Park 2007](#)) ([Yosef et al. 2016](#)). Senescent cells can also epigenetically repress the pro-apoptotic gene *Bax* ([Sanders et al. 2013](#)).

Therefore, resistance to apoptosis is an interesting property of certain senescent cells. Furthermore, chemical compounds specifically targeting the apoptosis resistance/increased survival pathways is a newly developed strategy to specifically eliminate senescent cells ([van Deursen 2019](#)) *(see "Senolytics" for further details)*.

6. *Acquisition of Senescent Associated Secretory Phenotype (SASP)*

Senescent cells do not proliferate but remain metabolically active and secrete a set of molecules termed senescent-associated secretory phenotype (SASP). The composition of this secretome is cell type-, stress-, and time-dependent and is a highly heterogeneous combination of cytokines, growth factors, and extracellular matrix proteases ([Coppe et al. 2010](#)). Moreover, SASP functions depend on the nature of the secreted factors and the responsiveness of the microenvironment (see *"SASP"* for further details on SASP composition and functions). Consequently, the utility of SASP as a biomarker to identify senescent cells *in vivo* is limited ([Herranz and Gil 2018](#)).

1.   Heterogeneity of SASP composition

Senescent cells can influence their microenvironment through the secretion of a combination of molecules termed Senescence Associated Secretory Phenotype (SASP). Large-scale transcriptomic studies have been performed to attempt to define a widely common core of SASP. But SASP is dynamically regulated and is highly heterogeneous depending on the tissue of origin and the senescence-inducing-stress (Hernandez-Segura et al. 2017). Despite its heterogeneity, SASP is commonly composed of various soluble factors such as interleukins (e.g., IL-1α, IL-6), chemokines (e.g., IL-8, CXCL2), growth factors (e.g., bFGF, VEGFA), extracellular matrix proteases (e.g., MMP-3, MMP-14), insoluble extracellular matrix components (e.g., fibronectin), and exosomes containing various cytosolic components (e.g., bioactive lipids, ROS, miRNA) (Basisty et al. 2020).

2.   Mechanistic regulation of SASP

SASP expression is massively regulated at different scales by controlling transcription, mRNA stability, translation, and secretion levels. SASP initiation is not fully understood yet, but diverse signaling pathways can trigger SASP regulation, such as DNA damage response (DDR), p38/MAPK, cGAS/STING, and mTOR (Kumari and Jat 2021). Most converge on activating two major SASP drivers, NF-κB and C/EBPβ. NF-κB and C/EBPβ are potent transcription factors with synergistic inflammatory effects. They accumulate on the chromatin of senescent cells, upregulating the transcription of numerous SASP as IL-1α, IL-6, and IL-8 (Chien et al. 2011; Kuilman et al. 2008).

3.   *Autocrine/paracrine reinforcement of senescence*

SASP functions are pleiotropic and depend not only on SASP composition but also on the response of surrounding cells exposed to this senescence-messaging secretome.

SASPs factors, such as IL-1α, Il-6, and IL-8, are proposed to reinforce senescence growth arrest in an autocrine manner. *Via* a positive feedback loop, they enhance NF-κB and C/EBPβ activity, amplifying SASP signaling (Orjalo et al. 2009).

SASP secreted from senescent cells also propagates the senescence growth arrest to surrounding proliferative cells, a phenomenon termed paracrine senescence or secondary senescence. Both *in vitro* treatment of non-senescent cells with conditioned medium from senescent cells and *in vivo* injections of senescent cells in recipient mice induce a complete senescence response of neighboring cells. As revealed by unbiased quantitative transcriptomic analysis, paracrine senescence is mediated mainly by various members of the TGF-β family, VEGF, and chemokines (Acosta et al. 2013). Mediation of senescence to neighboring cells can also be done *via* Notch signaling in a juxtacrine manner (Kirschner et al. 2020). Interestingly, as primary and secondary senescent cells can activate different senescent pathways, they might have a distinct gene expression profile, adding complexity to the heterogeneity of the senescent phenotype (Kirschner et al. 2020).
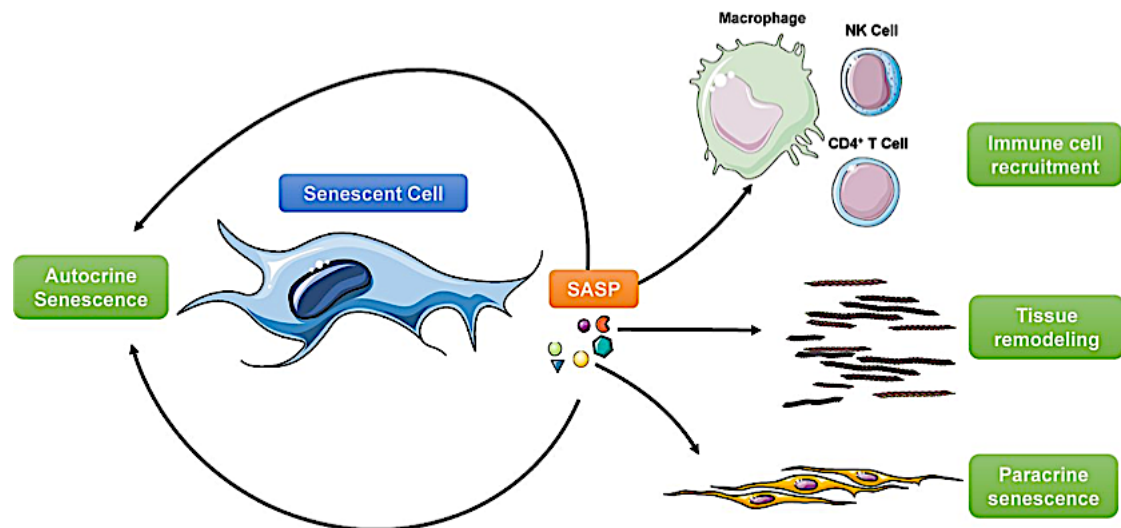
Figure 5. Multiple functions of senescence-associated secretory phenotype (SASP). The secretome of a senescent cell can be composed of various molecules such as cytokines, chemokines, growth factors, or tissue remodeling modulators. This SASP can act in an autocrine manner, reinforcing the senescent phenotype and the production of SASP via a positive feedback loop. It can also spread the senescent phenotype to neighboring cells in a paracrine manner. Moreover, *via* the secretion of cytokines, senescent cells can chemoattract immune cells to help with tissue clearance. Senescent cells also promote tissue remodeling through the secretion of metalloproteinases degrading the extracellular matrix or through the release of growth factors stimulating angiogenesis and alleviating fibrosis. From (McHugh and Gil 2018).

4. *Interaction with the immune system*

One of the major roles of the immune system is to remove dying cells to preserve the integrity of the body. Communication between senescent cells and immune cells is very complex and poorly defined but proposed to occur via SASP production. Indeed, many SASPs are revealed to be pro-inflammatory as IL-6, IL-8, monocyte chemoattractant proteins (MCPs), macrophage inflammatory proteins (MIPs), or TGFβ. Through their SASP, it is proposed that senescent cells could promote inflammation, chemoattract immune cells, and favor immune cell migration by remodeling the extracellular matrix. Then, activated immune cells would help for the specific removal of senescent cells while leaving surrounding healthy cells intact (Prata et al. 2018).

Among immune cells, senescent cells might preferentially interact *via* the SASP with neutrophils, macrophages, natural killer (NK) cells, and T lymphocytes to help for their clearance (Xue et al. 2007).

a)   *Neutrophils*

Via the sensing of chemoattractant IL-8, neutrophils are generally the first actors to be recruited on the inflammation site. They perform a cytotoxic process known as NETosis, with the formation of extracellular traps by releasing of chromosomal DNA into the extracellular environment. Neutrophils might contribute to senescence surveillance as neutrophil depletion using antibodies impairs senescence clearance from liver (Kang et al. 2011).

b)   *Macrophages*

Multiple studies showed a strong correlation between macrophages, professional phagocytic actors, and senescence clearance. For example, *in vitro*, macrophages migrate in response to senescent conditioned medium from human fat progenitor cells (Xu et al. 2015). *In vivo*, macrophages are proposed to participate in the clearance of senescent cells during salamander limb regeneration, as depletion of macrophages induces accumulation of senescent cells (Yun, Davaapil, and Brockes 2015). How macrophages trigger senescent cells is not fully elucidated, but proposed mechanisms involve the secretion of cytotoxic factors (M1 subtype) and phagocytosis (M2 subtype).

c)   *NK cells*

NK cells might also be involved in senescence clearance*. In vitro*, senescence was induced in lung fibroblasts IMR90 cells, and both senescent and proliferating cells were incubated with NK cells. Interactions in the co-culture system were followed using time-lapse imaging and showed a preferential killing of senescent cells mediated by NK cells (Krizhanovsky et al. 2008). Moreover, impairing NK

functions correlates with levels of senescent cells. Indeed, in a model of liver fibrosis, treatment with NK neutralizing antibodies revealed an impaired clearance of senescent hepatic stellate cells, whereas stimulation of NK cell activity correlated with a decreased number of senescent cells (Krizhanovsky et al. 2008).

d)   *T lymphocytes*

Correlative studies suggest that T lymphocytes might also participate in senescence surveillance as well as macrophages and NK cells. IL-6, one of the major SASP components, is a cytokine known to activate two populations of lymphocytes, CD8+ cytotoxic T lymphocytes (T-CD8+) and T-CD4+ helper cells (T-CD4+) (Bettelli et al. 2006). T-CD8+ express the receptor NKG2D, a receptor expressed in NK cells and stimulated for their cytotoxicity against senescent cells *in vitro* (Hu et al. 2016; Sagiv et al. 2016). T-CD4+ helpers might also be involved in senescence surveillance. Indeed, patients with HIV infection, which depletes the pool of T-CD4+ helper, present an accumulation of senescent cells induced by cirrhosis (Kang et al. 2011).

To summarize, it is proposed that senescent cells could interact *via* their SASP with many key immune system players for their clearance. Therefore, impairment of immune surveillance could be a central mechanism leading to the accumulation of senescent cells.

E.   *In vivo* roles of senescence

Senescence is a complex mechanism influencing a plethora of *in vivo* processes. Depending on cell types, secreted factors, and spatio-temporal dynamic, senescent cells exhibit beneficial or detrimental effects that are detailed thereafter.
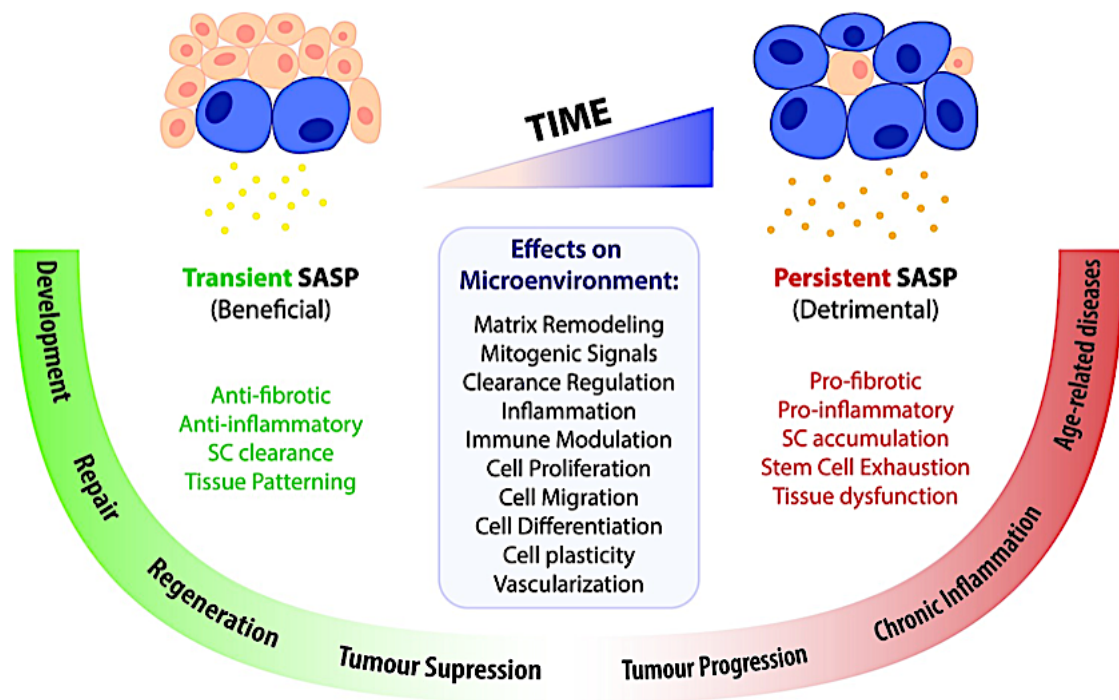
Figure 6. Pleiotropic roles of senescence. Senescent secretome can influence the microenvironment through different aspects, such as cell proliferation and differentiation, matrix remodeling, or immune reaction. Therefore, senescence is involved in many processes and plays beneficial roles as in embryogenesis, tissue repair upon injury, and tumor suppression. However, senescence is also associated with detrimental processes, promoting tumor progression, chronic inflammation, and age-related diseases. This balance between beneficial and detrimental effects might be time-dependent, as transient SASP is proposed to be salutary, whereas persistent SASP creates a deleterious microenvironment. From (Paramos-de-Carvalho, Jacinto, and Saude 2021).

1. *Senescence and cancer*

Senescence has dichotomous roles in cancer. In essence, senescence is a potent tumor mechanism. Indeed, senescent cells are irreversibly cell cycle arrested and are not responding to mitotic signals, which are intrinsic obstacles to oncogenesis. Cells mutated for p53 or p16 proteins fail to senesce, and corresponding p53 or p16 knockout mice show a premature tumor development

due to unrestrained proliferative capacity (Ghebranious and Donehower 1998). Moreover, when exposed to oncogene overexpression, cells preferentially enter into oncogene-induced senescence (OIS) state, which restricts their tumor-forming capacity (O'Brien, Stenman, and Sager 1986).

Anti-tumor effect of senescence is mainly attributed to the intrinsic cell cycle arrest, but senescent cells are also anti-tumorigenic via their secretome. Many SASPs factors induce senescence in a paracrine manner *(see "Autocrine/paracrine reinforcement of senescence" for further details)* and therefore could prevent excessive proliferation of surrounding precancerous cells during early tumorigenesis (Perez-Mancera, Young, and Narita 2014). Moreover, through their SASPs, senescent cells might recruit and stimulate the immune system *(see "Interaction with the immune system" for further details),* and this immune surveillance contributes to tumor clearance (Swann and Smyth 2007). In p53 deficient hepatocellular carcinomas, reactivation of p53 was sufficient to induce senescence, production of inflammatory cytokines, and activation of an immune response against cancerous cells, reducing tumor size (Xue et al. 2007).

However, senescent cells can also display potent antagonistic pro-tumorigenic effects in a SASP-dependent manner. First of all, senescent cells can specifically stimulate the proliferation of premalignant and malignant cells, which are more sensitive to SASP, notably composed of growth factors. *Via* their SASPs, senescent cells promoted the growth of S1 human mammary epithelial cells co-cultured in transwells without affecting normal epithelial cells. Co-injection of epithelial cells with senescent cells also favored tumorigenesis in recipient mice (Krtolica et al. 2001). Secondly, senescent cells can promote angiogenesis and tumor vascularization, notably *via* secretion of pro-angiogenic factors such as VEGF, increasing the size and number of blood vessels (Coppe et al. 2006). Thirdly, senescent cells secrete a variety of proteases as MMP-2 and MMP3, degrading the extracellular matrix and disrupting tissue structures. This permissive microenvironment supports cancer cell dissemination *in vivo*.

Moreover, senescent fibroblasts can promote epithelial-mesenchymal transition (EMT), thus enhancing cell migration and invasion (Coppe et al. 2008).

Therefore, senescence can inhibit or enhance tumor progression. It has been proposed that this balance between anti- and pro-tumorigenic effects depends on the heterogeneous SASP composition and the time senescent cells have to modulate their microenvironment. Transient presence of senescent cells might be beneficial to limit tumor development, whereas persistence of senescent cells might favor tumorigenesis *(See "Acute versus chronic senescence" for further details)* (Yang et al. 2021).
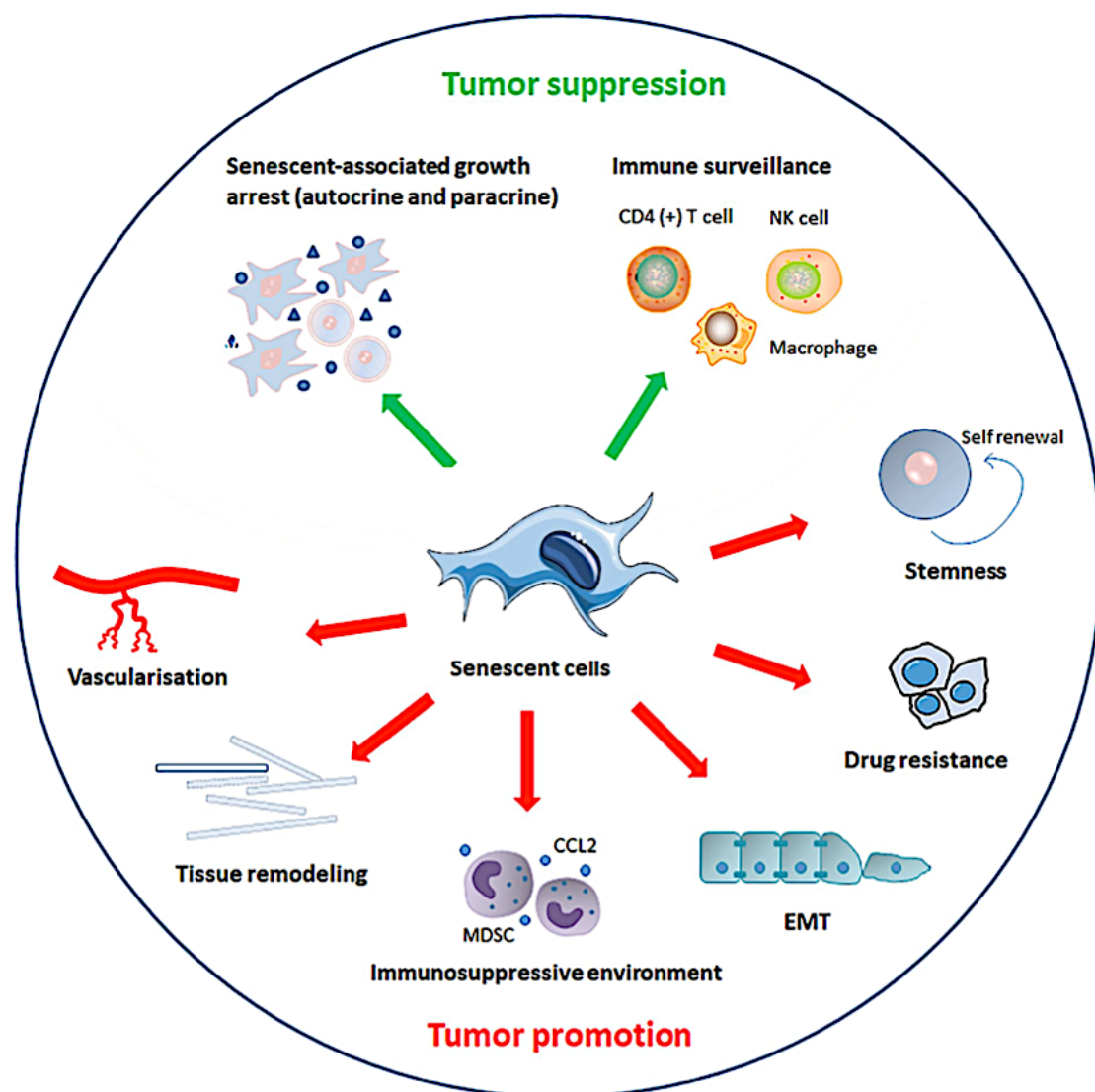
Figure 7. The paradoxical roles of senescence in cancer development. Senescence is a major tumor suppression mechanism, as the main characteristic of senescence is the irreversibility of the cell cycle arrest, limiting the proliferation of pre-cancerous cells. Moreover, through SASP, senescent cells stimulate immune surveillance, promoting the elimination of tumor cells. However, senescence can also promote tumorigenesis in different ways. SASP can help with the maintenance of stem cell features and increases cellular plasticity. The growth of cancerous cells is also supported *via* angiogenesis and the recruitment of immature immunosuppressive cells, impairing immune surveillance. SASP also favors the dispersion of tumor cells by promoting the epithelial-to-mesenchymal transition (EMT) and tissue remodeling of the microenvironment. Finally, senescence can confer drug resistance, as chemotherapies classically target hyperproliferative cells. Senescent cancerous cells can stay dormant, prone to events to escape senescence, such as mutation of cell cycle inhibitors, inducing tumor relapse. From (Yang et al. 2021).

2. *Senescence and aging / age-related pathologies*

It has been postulated for decades that senescence is linked to aging and age-related pathologies. Senescent cells accumulate in aged mice and in various tissues such as the lung, liver, or gut (Wang et al. 2009). In primates, senescent cells even represent up to 15% of total cells in old animals (Herbig et al. 2006). Removing senescent cells *in vivo* throughout life in the INK-ATTAC model extended the median lifespan of naturally aged mice and demonstrated the causative link between senescence and aging (Baker et al. 2016) *(see "Strategies to target senescent cells" for further details on INK-ATTAC mouse model).*

The presence of senescent cells also correlates with the development of numerous age-related pathologies such as Alzheimer's disease or chronic obstructive pulmonary disease (COPD) (Bhat et al. 2012; Adnot et al. 2015). Moreover, senescence abolition using INK-ATTAC also alleviated age-associated disorders in multiple organs such as skeletal muscle or adipose tissue, extending healthspan (Baker et al. 2011).

Age-associated impaired tissue regenerative capacity is possibly due to stem cell exhaustion. Indeed, to avoid pre-neoplastic transformation, stem cells are prone

to senescence induction, limiting their self-renewal capacity (Oh, Lee, and Wagers 2014). In aged muscle, satellite muscle stem cells switch from their quiescence status to a senescent phenotype, impairing regenerative muscle functions. The microenvironment also regulates cell stemness, and aging of the niche also leads to an impairment of their stem cell functions (Fujita and Tsumaki 2013). Overall, stem cell aging is partially accountable for loss of tissue regeneration (Sousa-Victor et al. 2014).

Accumulation of senescent cells has been mainly described as detrimental in cancer and age-related pathologies. However, artificial induction of senescence might also have beneficial effects on chronic diseases. Nutlin-3a is an inhibitor of murine double minute 2 (MDM2), preventing the interaction between MDM2 and p53 and related p53 degradation. Interestingly, administration of Nutlin-3a induced p21-p53 senescent associated cell cycle arrest in pulmonary artery smooth muscle cells (PA-SMCs). This senescent inducer treatment showed therapeutic effects as it partially reverted pulmonary hypertension (Mouraret et al. 2013).

3.   *Senescence and tissue repair*

Emerging evidence suggests that senescence has beneficial roles in tissue repair. Senescent cells can curb fibrosis, notably through over-secretion of enzymes responsible for extracellular matrix degradation and stimulation of immune surveillance. Indeed, upon liver damage, induced senescent hepatic stellate cells create a fibrotic scar, whose elimination by the immune system, in turn limits liver fibrosis. In mice deficient for p16 and p53, hepatic stellate cells bypass senescence and proliferate abnormally, leading to exacerbated liver fibrosis (Krizhanovsky et al. 2008). During wound closure, skin senescent fibroblasts also secrete proteins from the extracellular matrix as CCN1, which induces anti-fibrotic gene expression. CCN1 deficient mice present excessive fibrosis, a phenotype restored with topical application of purified CCN1 protein (Jun and Lau 2010).

A transgenic mouse model allowing targeted elimination of p16⁺ cells has been used to confirm the beneficial role of senescence in wound healing, as removal of senescent cells delayed the proper kinetic of wound closure. Secretion of SASP component PDGF-AA during early wound healing has been proposed to drive differentiation of myofibroblasts, thus optimizing wound closure. Topical application of recombinant PDGF-AA on the skin of these transgenic mice, treated to eliminate senescent cells, was sufficient to restore a correct wound closure (Demaria et al. 2014).

Tissue repair has also been studied in salamanders, an organism with a remarkable capacity for regenerating complex structures such as sections of its nervous system, portions of its heart, and the totality of its limbs and tail (Joven, Elewa, and Simon 2019). Upon limb ablation, senescence is rapidly triggered at the blastema, where progenitors are generated and proliferate. Senescent cells disappear in the fully regrown limb, emphasizing the potential beneficial role of senescence in tissue regeneration (Yun, Davaapil, and Brockes 2015).

4.   *Senescence and embryogenesis*

Senescence has been mainly studied as a response to a stress signal. Surprisingly, a growing number of studies fuel the hypothesis that senescence might have a role in programmed development. Indeed, senescent cells were spotted in embryos from a wide variety of species, including human, mouse, chicken, or zebrafish (Munoz-Espin et al. 2013; Storer et al. 2013; Villiard et al. 2017). Interestingly, developmental senescence seemed to be induced preferentially in transient tissues such as the mesonephros and structures intensively remodeled as the apical ectodermal ridge (AER), region of limb outgrowth, and patterning. In mice and humans, embryonic senescent cells were positive for p21 but independent of other common markers such as p16, ARF, or DNA damage. In mice embryos genetically ablated for p21, mesonephros regression was delayed but finally caught up by a compensatory apoptosis program, resulting in no significant developmental defects at birth (Munoz-Espin et al. 2013; Storer et al. 2013). Interestingly, senescence appears tightly regulated in time and space

during embryonic development, as well-defined senescent patterns were identical in each studied embryo. Therefore, these studies suggested for the first time that senescence was not only a stochastic response to cellular damage but might play a beneficial role in programmed physiological events. Especially, the senescence program might contribute to the removal of transient structures and to the precise tissue remodeling associated with embryonic development (Rhinn, Ritschka, and Keyes 2019). Senescent cells have also been detected in the placenta, an organ of fetal origin, allowing exchanges between the mother and the fetus. Senescence is proposed to be a stress-response to the cell fusion at the origin of the formation of the syncytiotrophoblast, where it prevents cell proliferation (Chuprin et al. 2013).

Interestingly, programmed physiological senescence has been mainly documented in embryonic tissues but remains poorly defined in adult homeostasis. Recently, it has been shown that senescent cells appear in the human uterus. To favor embryo implantation, endometrial stromal cells specialize in secretory decidual cells, which promote the formation of the placenta. From the mid to the late luteal phase of the menstrual cycle, differentiation in the decidual lineage was associated with a cell cycle arrest, and some decidual cells exhibited a senescent phenotype, with SAβgal and p16$^+$ cells noticed in the uterus. It is proposed that SASP secreted by decidual senescent cells created a pro-inflammatory microenvironment promoting tissue remodeling, which makes the uterus prone to embryo implantation (Brighton et al. 2017). This process might be evolutionary conserved, as senescent cells have also been detected in the murine uterus (Egashira et al. 2017).

5. *Acute versus chronic senescence*

In conclusion, senescence is dichotomic and triggers beneficial or detrimental effects depending on the context. Currently, the proposed paradigm defines acute senescence as beneficial. Proliferation arrest and transient SASP exposure limit cancer development, favor immune surveillance, and promote

embryogenesis and tissue repair. However, upon chronic damage or impairment of senescence clearance, senescent cells accumulate and become deleterious to the tissue. Persistent SASP production induces persistent inflammation, fibrosis and promotes cancer progression (Munoz-Espin and Serrano 2014).
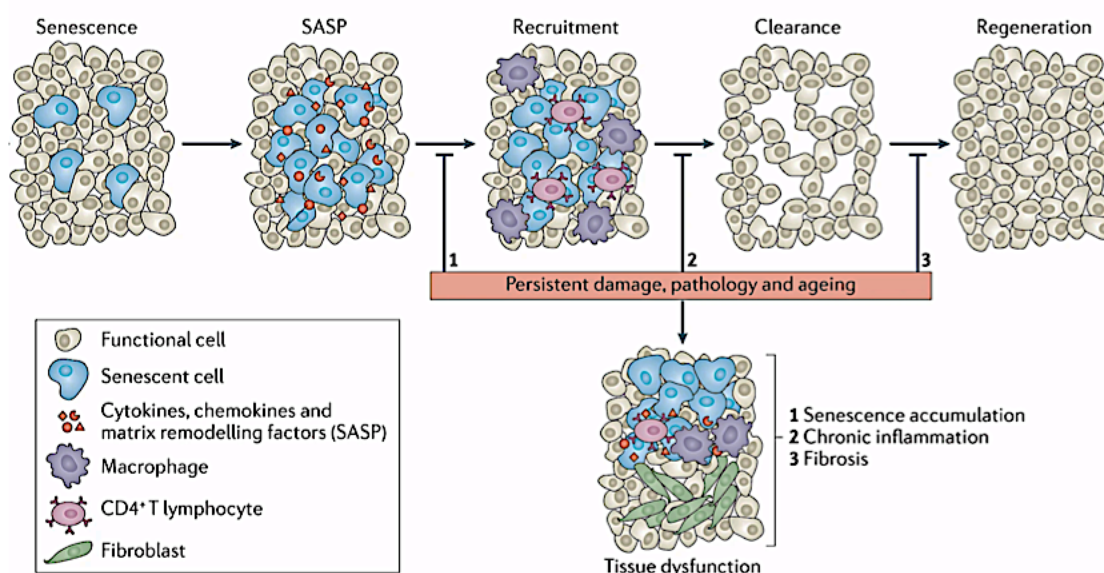
Figure 8. Consensual dichotomic model of senescence. When senescent cells appear in a tissue, they secrete a SASP, stimulating the immune surveillance and the remodeling of the microenvironment. Senescent cells are then cleared from the tissue and this transient presence of senescent cells is beneficial as it promotes tissue regeneration. However, upon persistent damage, disease or ageing, senescent cells accumulate in the tissue, leading to the permanent alteration of the microenvironment with chronic inflammation and fibrosis. Adapted from (Munoz-Espin and Serrano 2014).

F.   Strategies for senescent cells identification or elimination

1. *Genetically modified mouse models*

As previously discussed, a common marker solely expressed in all senescent cell types has not been discovered yet. However, as many senescent cells express the cell cyclin-dependent kinase inhibitor p16, we propose to review the genetic

approaches to visualize or eliminate senescent cells based on p16 increased expression.

a)   *INK4A/ARF knockout*

INK4A/ARF locus is a genomic sequence containing the gene Cdkn2a, encoding for two overlapping cyclin-dependent inhibitors, p16 and p19/Arf. Both proteins originate from two different transcripts, sharing common exons 2 and 3 but with an alternative reading frame in the first exon. Therefore, p16 and p19/Arf proteins do not share a sequences homology and have distinct effects. INK4A/ARF knockout (KO) mice were generated by homologous recombination of exons 2 and 3, depleting both p16 and p19 ([Stone et al. 1995](#)). Homozygous INK4A/ARF^{-/-} mice are viable and fertile, possibly due to early compensatory mechanisms with other cell cycle inhibitors. However, they are prone to premature tumor induction, as 69% of INK4A/ARF^{-/-} mice develop tumor at the average age of 29 weeks, whereas none of the littermates INK4A/ARF^{+/+} or INK4A/ARF^{+/-} display any health impairment. Thus, this mouse model demonstrated the hypothesis that INK4A/ARF is a primordial tumor suppressor locus ([Serrano et al. 1996](#)).
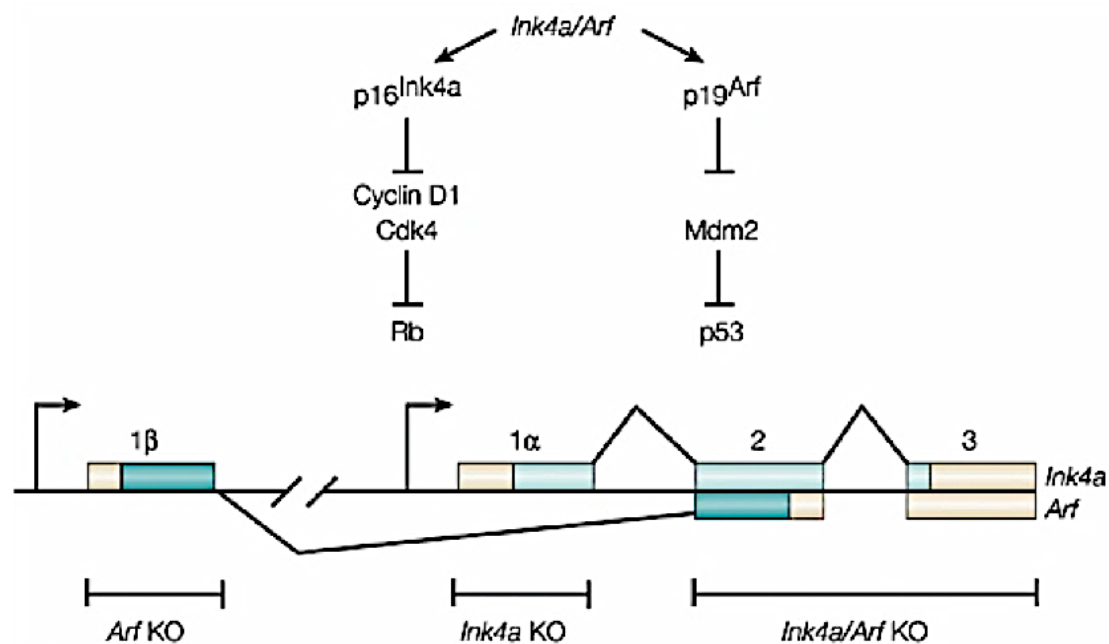
Figure 9. Knockout of the CDKN2A locus. CDKN2A locus is encoding for two proteins, p16^{Ink4a} and p19Arf, sharing the DNA sequence of exons 2 and 3 but with an alternative reading frame due to two different first exons. INK4A/ARF knockout mice are depleted for exons 2 and 3. Adapted from (Sherr 2001).

b)   *INK-ATTAC*

INK-apoptosis through targeted activation of caspase (ATTAC) is a transgenic mouse model inducing specific cell death of p16 positive cells. The ATTAC transgene allows the expression of an intracellular membrane-bound myristoylated FK506-binding-protein-caspase 8 (FKBP-Casp8). Upon administration of a synthetic drug, AP20187, FKBP-Casp8 forms an active dimer inducing apoptosis. The ATTAC transgene was firstly described in FAT-ATTAC mouse model, in which expression was regulated under a *Fabp4* promoter, therefore promoting apoptosis specifically in adipocytes (Pajvani et al. 2005). In INK-ATTAC mice, a fragment of 2,6 kb of *p16^{INK4A}* promoter replaces *Fabp4*, leading to apoptosis and clearance of p16 positive cells under AP20187 treatment. Using this INK-ATTAC model, it was shown for the first time that removing p16$^+$ senescent cells delays and attenuates age-related disorders, especially in adipose tissue and skeletal muscle (Baker et al. 2011). However, some senescent cells from various tissues such as liver or colon, are not

efficiently triggered by the INK-ATTAC system ([Baker et al. 2016](#)). This tissue-selective elimination of senescent cells remains unclear but has raised concerns about the truncated p16 promoter sequence that might not fully resemble endogenous p16 expression.
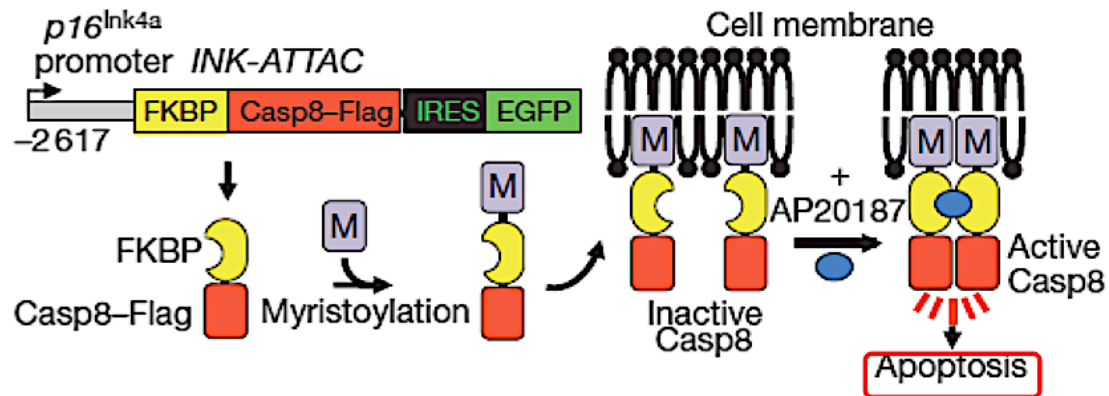
Figure 10. Transgenic INK-ATTAC. INK-ATTAC transgenic mouse model has a FKBP-Casp8 cassette under p16 regulation, allowing the production of an inactivated Casp8. Upon administration of AP20187, Casp8 forms an active dimer and induces apoptosis of p16-expressing cells. From ([Baker et al. 2011](#)).

c)   *p16-3MR*

p16-trimodality reporter (3MR) is a transgenic mouse model taking advantage of the artificial protein LUC/mRFP/HSV-TK containing fused functional domains of Renilla luciferase (LUC), monomeric red fluorescent protein (mRFP), and truncated herpes simplex virus 1 thymidine kinase (HSV-TK) ([Ray et al. 2004](#)). In p16-3MR, 3MR fused protein was inserted in a bacterial artificial chromosome (BAC) containing 50kb of *p16^{INK4}* locus, with inactivated adjacent *p16^{INK4}* and *p19^{ARF}* genes, ensuring that the full promoter of p16 drove expression of 3MR fusion. p16-3MR mice were described as an effective model to detect p16^{+} senescent cells by luciferase luminescence; to sort them using mRFP fluorescent signaling; and to kill them using the synthetic drug ganciclovir (GCV). GCV has a low affinity for endogenous cellular TK but is metabolized specifically by HSV-

TK. HSV-TK converts the drug into a toxic DNA chain terminator, which fragments mitochondrial DNA. This cell death signal triggers apoptosis in p16^{+} senescent cells. *In vivo* elimination of p16^{+} senescent cells in p16-3MR mice demonstrated for the first time a beneficial role of SASP in wound healing (Demaria et al. 2014). However, the 3MR cassette was not highly expressed *in vivo* due to low level of p16 mRNA expression. By correlation, this model failed to efficiently track all p16^{+} cells due to a low p16-driven level of mRFP fluorescence (Grosse et al. 2020).
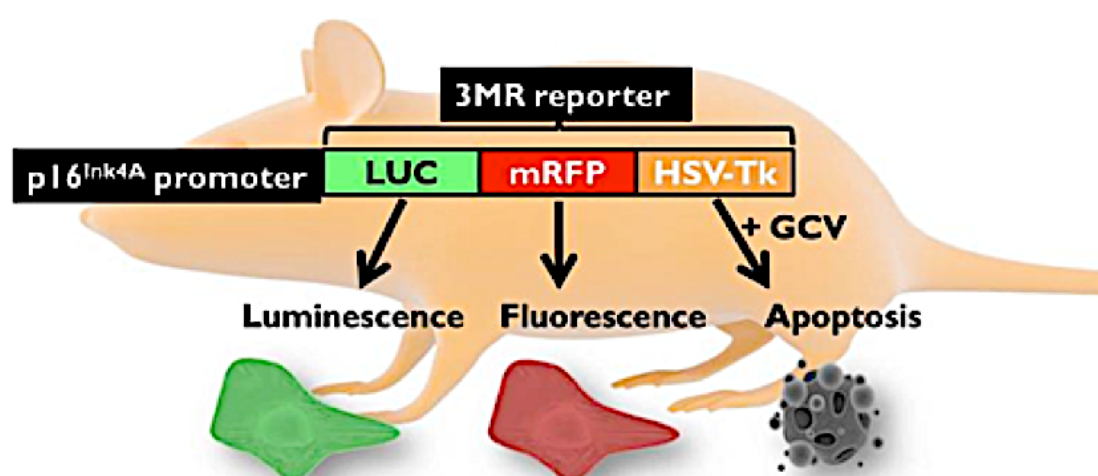
Figure 11. Transgenic p16-3MR construct. The p16-3MR transgenic mouse model has a 3MR reporter cassette, allowing the identification of p16 expressing cells via luciferase and mRFP synthesis. Moreover, p16^{+} cells produce a HSV-TK, metabolizing the ganciclovir compound and inducing apoptosis upon ganciclovir treatment. From http://demarialab.com/research.html

d)   *INKBRITE*

To tackle the low abundance of mRFP reporter in p16-3MR, which correlates with the low level of p16 mRNA transcript, a high sensitive tracking mouse model was generated. INK4A H2B-GFP Reporter-In-Tandem (INKBRITE) mouse model is a transgenic line with three tandems of H2B-GFP inserted in frame with p16 under the endogenous regulation of p16 promoter. This construct allows the

expression of numerous stable GFP proteins incorporated *via* H2B into nucleosomes of p16+ cells. This strategy increases the fluorescent signal emitted by p16^{+} cells, facilitating their detection *in vivo* (BioRXiv reference https://doi.org/10.1101/2020.06.10.142893).

INKBRITE
INK4A H2B-GFP Reporter-In-Tandem

Cdkn2a locus

Figure 12. Transgenic INKBRITE construct. INKBRITE transgenic mouse model has a supersensitive cassette inserted under the endogenous regulation of p16. This construct allows the identification of p16+ cells with GFP fluorescence. From (BioRXiv reference https://doi.org/10.1101/2020.06.10.142893).

e)   *p16-Cre/R26-mTmG and p16-Cre/DTA*

In parallel, two complementary mouse models were developed to trace and ablate p16+ cells efficiently. Three elements, a constitutive CRE recombinase, a thymidine kinase, and a fluorescent dtTomato reporter, were fused at the end of the third exon of p16. This knock-in p16-Cre mouse line was then crossed with two different reporter mouse models, p16-Cre/R26-mTmG, to trace p16^{+} cells and p16-Cre/DTA to eliminate constitutively p16^{+} cells without the use of an exogenic compound. These models were used to define a population of senescent vascular endothelial cells in liver sinusoids of aged animals. Depleting this p16[+] population disrupted the blood-liver barrier, leading to health deterioration (Grosse et al. 2020).

2. ***Senolytics***

Senolytics are chemicals able to target and kill senescent cells. As senescent cells are resistant to apoptosis, the primary hypothesis-driven strategy to kill senescent cells is to find compounds that could break down pro-survival barriers ([Kirkland and Tchkonia 2020](#)).

a) *Dasatinib and Quercetin*

Dasatinib and quercetin were the first senolytics identified to induce senescent cell death ([Zhu et al. 2015](#)). Dasatinib is an approved anti-cancer tyrosine kinase inhibitor targeting Src kinase ([Araujo and Logothetis 2010](#)). Quercetin is a natural flavonoid, which can impair glycolysis and inhibit anti-apoptotic Bcl-2 and Bcl-XL proteins ([Wu et al. 2019](#); [Primikyri et al. 2014](#)). Dasatinib and quercetin have senolytic activities against senescent human primary adipocyte progenitors and senescent human umbilical vein endothelial primary cells respectively. But the combination of dasatinib + quercetin (D+Q) synergizes their senolytic effects and *in vivo* administration of the combination D+Q extends healthspan and lifespan of treated mice ([Xu et al. 2018](#)). Co-administration of D+Q has been used in clinical trials to improve the health conditions of patients with idiopathic pulmonary fibrosis and diabetic kidney disease ([Hickson et al. 2019](#)). However, the mechanisms of action of combined drugs remain unclear. Moreover, their senolytic activity remains restrained to specific cell types. As the senescent phenotype is heterogeneous, there is a need to identify senolytics with broad-spectrum activity to target larger populations of senescent cells.

b) *ABT-263*

In this optic, a wide *in vitro* screen of compounds was performed to find new senolytics. Senescence was triggered in WI-38 fibroblasts by an extensive range of inducers such as irradiation, replicative stress, or oncogene overexpression. The survival of these senescent fibroblasts was then compared to the survival of non-senescent human WI-38 fibroblasts upon treatment with different chemicals. This study identified ABT-263, a compound also known as Navitoclax,

as a potent senolytic ([Chang et al. 2016](#)).

ABT-263 is an orally bioavailable inhibitor of anti-apoptotic proteins Bcl-2, Bcl-XL, and Bcl-W, which are upregulated in various senescent cell types. Bcl-2 family proteins sequestrate pro-apoptotic molecules and prevent senescent cell death. ABT-263 is a Bcl-2 homology domain 3 (BH3) mimetic, which binds to BCL-2 anti-apoptotic proteins. These interactions prevent the sequestration of pro-apoptotic proteins as BIM, which freed acts to induce apoptosis ([Tse et al. 2008](#)).

ABT-263 drug has a very powerful *in vitro* senolytic activity species- cell type- and senescence-inducing stress signal-independent. It exhibits cytotoxicity against senescent mouse embryonic fibroblasts, senescent human fibroblasts, and senescent human renal epithelial cells ([Chang et al. 2016](#)). ABT-263 has also been used *in vivo* to target senescent hematopoietic stem cells (HSCs) induced by ionizing irradiation, allowing the expansion of normal HSCs and the rejuvenation of the hematopoietic system ([Chang et al. 2016](#)). Despite its potent senolytic activity, ABT-263 induces long-term severe side effects such as thrombocytopenia ([Kaefer et al. 2014](#)). Indeed, platelets overexpress Bcl-XL for their survival, making them an off-target for ABT-263 cytotoxicity.
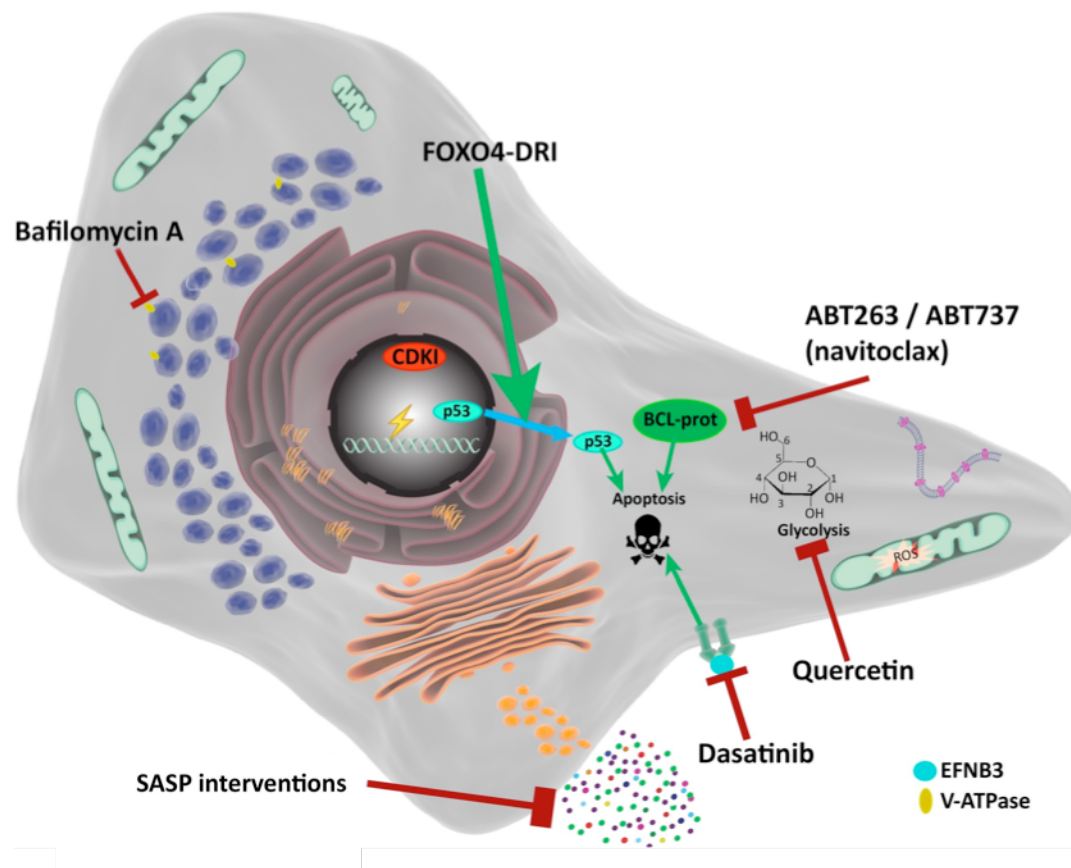
Figure 13. Senolytic approaches to remove senescent cells. Numerous compounds have been developed to target senescent cells. ABT-263/Navitoclax targets BCL2 family proteins to alleviate apoptosis resistance. Dasatinib induces apoptosis via the pro-apoptotic EFN3 pathway. Quercetin inhibits glycolysis, usually upregulated in senescent cells for SASP production. FOXO4-DRI promotes the nuclear exclusion of p53. Bafilomycin inhibits the V-ATPase, responsible for lysosomal acidification. In addition to these senolytic approaches inducing senescent cell death, new compounds known as senomorphics aim to impair SASP, to alter senescent functions without killing the cells. Adapted from (Hernandez-Segura, Nehme, and Demaria 2018).

c)   *New approaches to target senescent cells*

Nowadays, new strategies are developed to specifically deliver drugs only to senescent cells and minimize the possible off-targets of senolytics. Nanoparticles have been designed to target senescent cells specifically, by covering them with galacto-oligosaccharides. Galactose-encapsulated nanoparticles are preferentially digested into lysosomes of senescent cells overexpressing the lysosomal enzyme β-galactosidase. Nanoparticles remain intact in normal cells

and do not release their cargo, preserving non-senescent cells from cytotoxicity ([Munoz-Espin et al. 2018](#)). This promising strategy has been applied recently to ABT-263. Galacto-conjugation of prodrug Navitoclax activated by β-galactosidase activity reduces *in vivo* senescent lung cancer cells. Senolytic activity of ABT-263 is preserved while reducing platelet-induced apoptosis and thrombocytopenia in murine lung cancer model ([Gonzalez-Gualda et al. 2020](#)).

Cell surface biomarkers can also be targeted to eliminate senescent cells specifically. A new extracellular epitope, B2M, has been recently identified in some senescent cells, allowing their isolation by FACS ([Althubiti et al. 2014](#)). Commercially available antibodies recognizing B2M epitope are internalized after binding at the surface of senescent cells. This allows the design of senolytic drugs coupled to antibodies anti-B2M through a cleavable enzymatic linker, digested into lysosomes once internalized, releasing active senolytics specifically into B2M-expressing senescent cells ([Poblocka et al. 2021](#)). Chimeric antigen receptor T (CAR-T) cells are T cells genetically designed to express an artificial T cell receptor. This chimeric receptor recognizes a chosen epitope of interest and activates the cytotoxic function of the T cell ([Kuwana et al. 1987](#)). After identifying a new cell surface protein upregulated in some senescent cells, the urokinase-type plasminogen activator receptor (uPAR), CAR-T cells were designed to specifically target uPAR-expressing senescent cells. These CAR-T cells were efficient *in vitro* and *in vivo* in eliminating senescent cells and extending the lifespan of mice with lung adenocarcinoma ([Amor et al. 2020](#)). These two approaches are promising to target senescent cells specifically and reduce toxicity toward non-senescent cells. However, both strategies are based on cell surface markers, which are not commonly expressed by all senescent cell types, reducing the range of targeted senescent cells.

Undoubtedly, the field of senolytics is expanding fast, and new strategies will continue to emerge, increasing the promising possibility of targeting all types of senescent cells without off-targets.

II.   **<u>Mammary Gland</u>**

A.   <u>General introduction</u>

The mammary gland (MG), from the Latin root *mamma* or "breast", is a highly specialized exocrine gland whose main function has been selected through evolution to produce milk to feed the offspring (Oftedal 2002). Moreover, various molecules are conveyed through milk secretion, which contributes to the newborn's immune protection by transmitting antibodies against infection and colonization of the gut microbiota (Camacho-Morales et al. 2021). Finally, breastfeeding promotes mother-infant bonding in numerous species (Nagasawa et al. 2012). The presence of MG is one of the main characteristics defining the taxon of mammals, with a slight heterogeneity of MG structure amongst mammalian species. Indeed, ruminants exhibit an udder, a single massive MG with multiple teats, whereas primates and rodents have breasts, where each MG ends with its own nipple. Moreover, breasts usually operate by pair, but number of MGs depends on the anatomy of the animal and the mean litter size of the specie. In humans, only one pectoral pair of glands is developed, while mice have five pairs symmetrically localized all along the ventral area, from the neck to the perianal zone. As discussed later, a few other discrepancies between humans and mice are noticed, especially in the stromal composition of the mammary tissue and some slightly different developmental behaviors (McNally and Stein 2017).
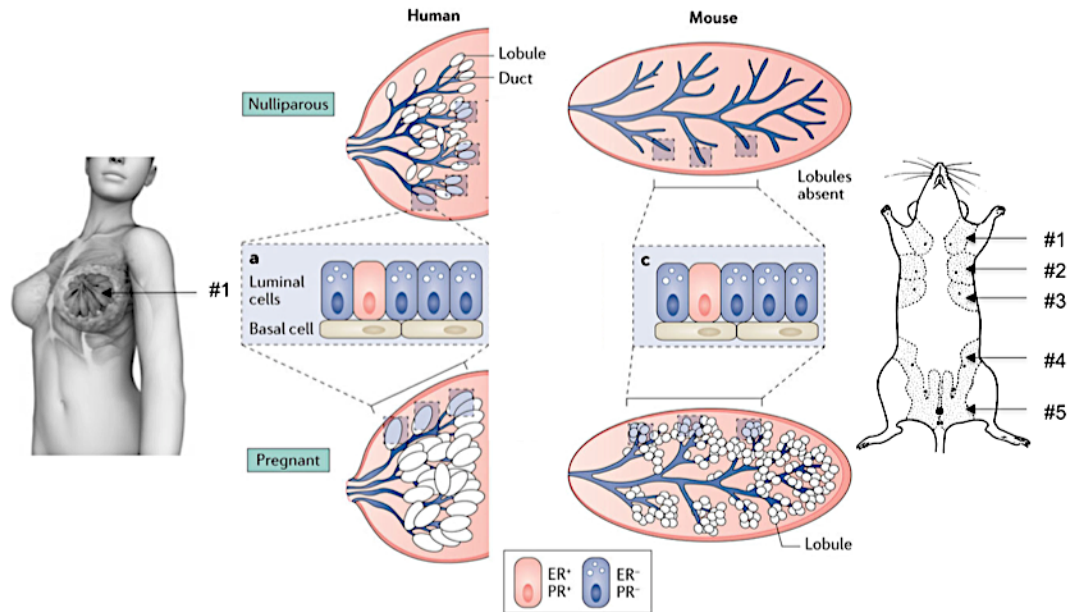
Figure 14. Mammary gland (MG) morphology in humans and mice. Women have only one pair of MGs, commonly termed breast, whereas mice possess five pairs of MGs distributed all along the ventral face. At the nulliparous stage, lobules are thinly developed in humans (left) while they are absent in mice (right). At the pregnant stage, MG architectures from both species are similarly developed, with ducts and functional milk alveoli. Adapted from (Carroll et al. 2017).

However, these anatomical differences between humans and mice are negligible compared to their developmental similarities. MGs are composed of an intricate network of epithelial ducts enclosed into a vascularized mammary fat pad composed of various stromal cells such as adipocytes, fibroblasts, and immune cells. To reach this adult mammary morphology, MGs are highly dynamic and respond to hormonal changes. Rudimentary epithelial development occurs in both sexes during embryogenesis, but only females undergo a complete post-natal mammary morphogenesis. During puberty, under the action of hormones, the primary epithelial duct expands into the fat pad to form a typical branched-tree network of epithelial ducts. MGs are maintained in this resting stage, only responding to the estrus cycle by a slight phase of expansion/regression until pregnancy-associated massive hormonal changes. During pregnancy and lactation, MGs go through intense proliferation and differentiation of milk-

producing alveolar structures, blooming from the end of epithelial ducts, to ensure adequate nourishment of the progeny. Upon weaning, MGs undergo a process of involution, where milk-producing cells are eliminated, and MGs are remodeled to a pre-gestation state, ready for a subsequent pregnancy (Richert et al. 2000).

MG is a potent model for developmental studies as most of its morphogenesis occurs post-natally. Moreover, MG is the organ of origin of breast cancer, the most prevalent cancer, with more than 2.3 million women diagnosed and 685.000 deaths worldwide in 2020 alone (Source: World Health Organization, July 2022). Understanding the physiological development of MG is a major health concern in unraveling underlying mechanisms leading to tumorigenesis.

B.   Cellular organization of mammary tissue

Mammary tissue comprises many cell types contributing to its development and structure. Epithelial cells are surrounded by a stroma rich in fibroblasts and immune cells, all enclosed in a vascularized and innerved fat pad. However, the main focus has been done on the epithelial compartment, primarily because it undergoes massive alterations during morphogenesis and is critical for the mammary function of milk production (Inman et al. 2015).
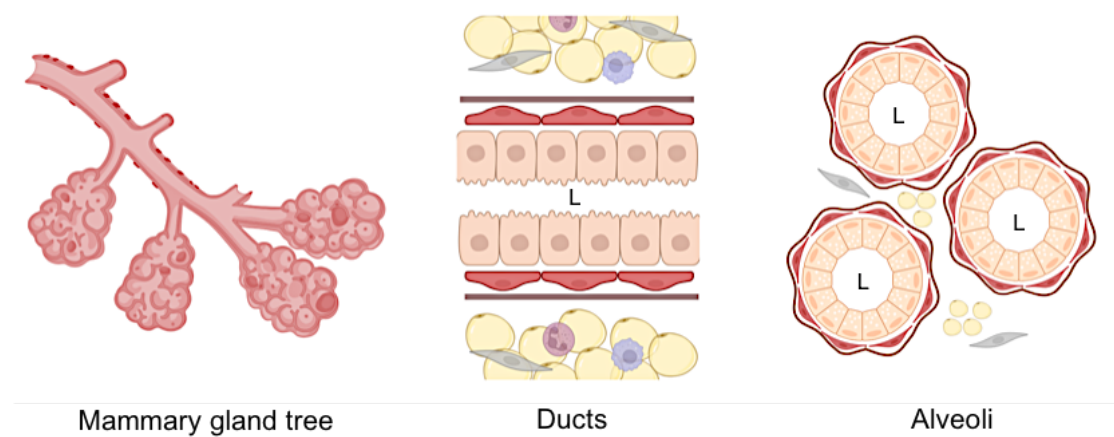
Figure 15. MG architecture and cell composition in ducts and alveoli. In the virgin state, MGs are composed of resting ducts, whereas during pregnancy and lactation, MGs are composed of a network of ducts ending with milk-producing alveoli. In the ducts, luminal cells (light pink) face the lumen and are covered by a continuous layer of myoepithelial cells (dark pink). This epithelium is enclosed by a basement membrane (brown), which separates the surrounding vascularized stromal compartment composed of adipocytes (yellow), fibroblasts (grey), and immune cells (purple). In alveoli, luminal cells fully differentiate into secretory cells, and myoepithelial cells adopt a star-like shape to help alveolar contraction. The stromal compartment adapts its size to the alveolar growth by de-differentiation of adipocytes. Designed with Biorender.

1. *Epithelium*

The mammary epithelium consists of two functionally different entities, alveoli, and ducts. Mammary alveoli are the secretory lobules producing milk during lactogenesis, whereas lactiferous ducts connect the secretory units to the nipple to transport milk (Visvader and Stingl 2014). Both structures are composed of two different cell types, luminal and basal cells, surrounded by a basement membrane. In ducts, the epithelium is stratified, with cuboidal luminal cells forming an inner lumen and a layer of spindle-shaped myoepithelial cells on top. In alveoli, the epithelium is pseudostratified, with each star-shaped contractile basal cell in contact with multiple milk-producing luminal cells underneath.

Basal and luminal cells have distinct functions and specific markers for their identification. Thanks to the specific cytoskeletal structural components expressed either by basal or luminal cells, the two populations can be detected *in vivo* by immunostaining. Anti-K5, anti-K14, or anti-SMA antibodies allow the identification of basal cells, and anti-K8 or anti-K18 antibodies specifically mark luminal cells (Mikaelian et al. 2006). Moreover, flow cytometry can separate isolated basal and luminal cells from each other and from the stromal compartment. Indeed, CD24 and α6 stainings segregate mammary cells into three populations: CD24$^-$, α6$^-$ non-epithelial cells; CD24^{low}, α6^{high} basal cells; and CD24^{high}, α6^{low} luminal cells (Sleeman et al. 2006; Asselin-Labat et al. 2006).

a)   Basal cells

Basal cells inherit their name due to their position in contact with the basement membrane. They exhibit an epithelial phenotype with expressions of intermediate filaments, more specifically cytokeratin 5 (K5) and cytokeratin 14 (K14) (Deugnier et al. 2002). They also exhibit a muscle-like phenotype *via* smooth muscle actin (SMA) expression, giving them contractility properties (Deugnier et al. 1995).

The primary function of alveolar basal cells is to contract to help milk expulsion. Myoepithelial cells respond to pituitary oxytocin, released into the systemic circulation after suckling stimulation (Gimpl and Fahrenholz 2001). Contractions of basal cells act on the release of lipids droplets from luminal cells and on the propulsion of milk out of the lumen of alveoli and all along ducts, helping maintain a continuous milk flow (Gieniec and Davis 2022). Moreover, in ducts, myoepithelial cells form a continuous layer on top of the basement membrane, separating the connective tissue from the luminal layer and mediating their interactions.

b)   _Luminal cells_

Mouse luminal cells lie on the myoepithelial layer on their basal side while their apical pole faces the mammary lumen. Luminal cells express cytokeratins K8 and K18, with a strong signal at all stages of MG development except during lactation, where the signal is weaker ([Mikaelian et al. 2006](#)).

Luminal cells can be classified by their function and position in the mammary tissue. Indeed, the main function of ductal luminal cells is to line the inner face of ducts, whereas alveolar luminal cells produce and secrete milk. ~15% of luminal cells also express hormonal estrogen (ER) and progesterone receptors (PR). ER^+, PR^+ double positive cells can be found only in ducts, whereas alveolar luminal cells are ER^-, PR^- ([Clarke et al. 1997](#)). Double immunostainings showed a co-expression of both ER and PR in 96% of cells positive for at least one receptor ([Clarke et al. 1997](#)). ER activation regulates pubertal elongation of the ductal network, whereas PR activation is required during pregnancy to form tertiary ducts ([Tanos et al. 2012](#)). Mechanistically, in their inactive form, ER and PR are bound to heat shock proteins (HSP). Upon hormonal stimulations, receptors dissociate from HSP, form homo- or hetero-dimers, and enter the nucleus, where they induce changes in the transcription levels of various genes notably involved in cell proliferation ([Brisken and O'Malley 2010](#)). ER and PR can also mediate non-genomic crosstalks with major signaling pathways such as EGFR ([Acconcia and Kumar 2006](#)). As only a tiny fraction of luminal cells is hormone-sensitive, it is proposed that activation of surrounding ER^-, PR^- cells is mediated by paracrine signals, efficiently coordinating multiple cell types ([Tanos et al. 2012](#)).

c)   _Mammary stem cells_

The mammary epithelium is a dynamic tissue, which undergoes many cycles of development and regeneration during the reproductive lifetime. The existence of mammary stem cells to explain this plasticity was proposed in the late 50s. Epithelial fragments were transplanted into a cleared fat pad and were sufficient

to regenerate a fully branched epithelium, itself capable of regeneration after a second serial transplantation (Deome et al. 1959; Daniel et al. 1968). Mammary stem cell characterization was then on standby for fifty years until the rise of flow cytometry and the identification of cell surface markers to differentiate basal and luminal lineages. Interestingly, by transplanting a single cell into the mammary fat pad, it has been shown that only single cells isolated from the basal compartment can regenerate a full bi-layered mammary epithelium, with ducts and alveolar structures (Shackleton et al. 2006; Stingl et al. 2006). However, this bi-potent capacity of mammary stem cells has been identified in transplantation assays, which do not mimic physiological development. Using genetic-lineage tracing, $K5^+$, $K14^+$ multipotent stem cells giving rise to both basal and luminal lineages were identified during embryonic development (Van Keymeulen et al. 2011). There is an active debate on the potency of mammary stem cells during post-natal development. Some bi-potent mammary stem cells in the basal compartment could give rise to both basal and luminal lineages during postnatal morphogenesis and adult homeostasis (Rios et al. 2014). Or two distinct types of unipotent stem cells, basal stem cells, and luminal stem cells, could respectively give rise to basal and luminal lineages and maintain mammary gland homeostasis (Taddei et al. 2008; Van Keymeulen et al. 2011). This discrepancy might be due to technical difficulties in individually tracing each epithelial population. Using an unbiased lineage tracing approach, limiting the number of tracked cells drastically, single cells were stochastically labeled and traced in virgin and lactating mice. Interestingly, labeled clones were lineage-restricted to basal or luminal layers during both ductal and alveolar morphogenesis, promoting the theory of unipotent stem cells to maintain MG homeostasis (Davis et al. 2016).
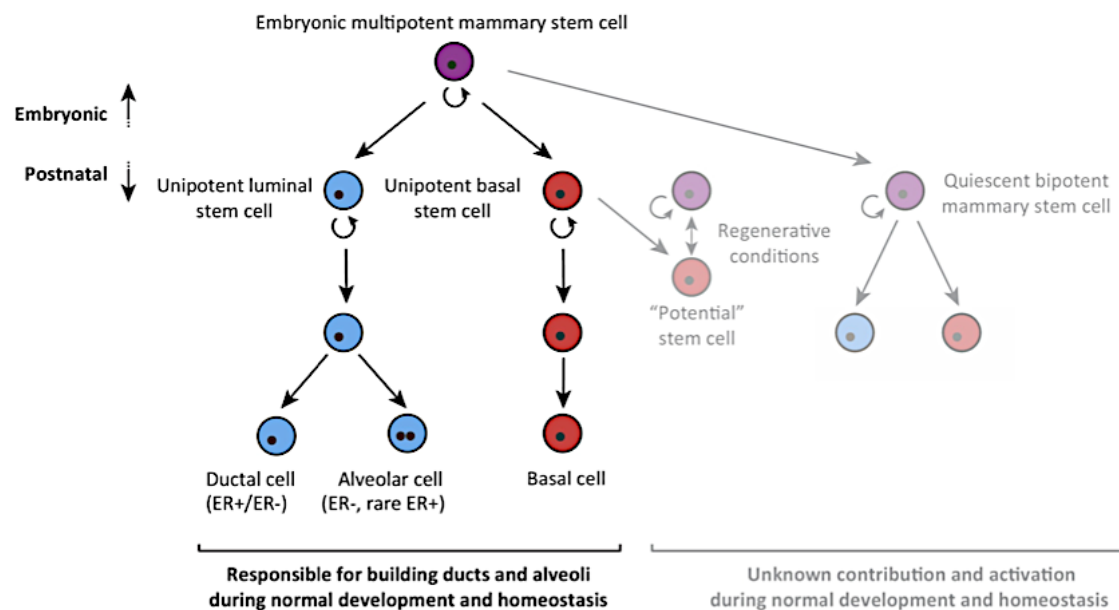
Figure 16. Model of mammary epithelial stem cell hierarchy. During embryonic development, multipotent stem cells give rise to both basal and luminal lineages. Multipotent stem cell contribution in postnatal development remains more controversial, but evidence supports the hypothesis of unipotent lineage-restricted stem cells in postnatal development and homeostasis. From (Lloyd-Lewis, Harris, et al. 2017).

2. *Stroma*

The main difference between human and murine MG resides in the stromal composition. Indeed, in mice, the fibrous tissue remains a minority, and the stromal compartment is mainly composed of fat tissue, enclosing the epithelium directly. In contrast, in humans, fibrous tissue surrounds the epithelium forming lobules, enclosed by an interstitial stroma and a fat tissue less extended (Ingthorsson et al. 2016).

a) *Adipocytes*

Virgin mouse mammary epithelium is encapsulated in a stromal fat pad mainly composed of white adipocytes. This mammary fat tissue serves as massive

energy reserve thanks to lipid storage and is highly plastic during the MG reproductive cycle (Colleluori et al. 2021). Two decades ago, it has been proposed that adipocytes could transdifferentiate into epithelial cells during pregnancy and lactation and could reversely transdifferentiate back to adipocytes during involution (Morroni et al. 2004). However, the Cre-mouse model used in this study was based on the expression of adipocyte fatty acid binding protein (AFABP, also known as aP2), which is now known to be a fat-derived circulating protein (Kralisch and Fasshauer 2013). Using a specific tracking system of mature adipocytes, it is now proposed that, during pregnancy and lactation, mature adipocytes de-differentiate into adipocyte precursors positive for platelet-derived growth factor receptor α (PDGFRα$^+$). Then, they re-differentiate into mature adipocytes upon involution (Wang et al. 2018). Adipocyte involution-associated hypertrophy is facilitated *via* lipid refilling derived from epithelial-produced milk (Zwick et al. 2018).

b)	*Fibroblasts*

Fibroblasts are essential components of the mouse mammary stroma. In MG, periductal fibroblasts are localized in the fat pad, in close proximity to the epithelial basement membrane, and create a sheath separating epithelial ducts from surrounding adipocytes. Interstitial and perivascular fibroblasts are, for their part, disseminated between adipocytes (Sumbal, Belisova, and Koledova 2021). There is no unique marker to label fibroblasts. However, there is a consensus, and fibroblasts are usually characterized as PDGFRα$^+$ or vimentin$^+$ cells, with a characteristic spindle shape and a stromal localization (Sahai et al. 2020).

Fibroblasts are key mediators of the crosstalk between stroma and epithelial cells to support MG development, from rudimentary embryonic morphogenesis to pubertal branching (Wiseman and Werb 2002). Fibroblasts are also critical during the reproductive cycle, especially during MG involution, where they secrete metalloproteinases and contribute to the deposition of a fibrotic-like

extracellular matrix (ECM). This ECM has been proposed to promote epithelial cell death and reorganization of the mammary tissue (Schedin et al. 2004; Simian et al. 2001).

c)   *Immune cells*

Macrophages and eosinophils are major immune system components recruited during pubertal morphogenesis to assist epithelial cells in the fat pad invasion (Gouon-Evans, Rothenberg, and Pollard 2000). Macrophages are also critical for the involution process, promoting epithelial cell clearance and tissue remodeling (O'Brien et al. 2012).

C.   Mammary gland morphogenesis

1.   *Pre-natal development*

Embryonic morphogenesis is succinct and is limited from E10.5 to E18.5 to the formation of epithelial buds at the position of the future nipples. At birth, each mammary fat pad only contains a rudimentary epithelial tree with ~15 ducts. (Veltmaat et al. 2003).

2.   *Puberty*

MGs remain quiescent from birth to ~4 weeks old, when puberty-associated hormonal signals orchestrate a massive expansion of the ductal network. Ductal extremities called terminal end buds (TEBs) drive MG pubertal development. They consist of two different cell types, one external layer of cap cells, precursors of myoepithelial cells, and multiple internal layers of body cells, which will give

rise to ductal luminal cells. Following ovarian secretion of estrogen and progesterone, TEBs will become hyper-proliferative regions, allowing the epithelial elongation in the mammary fat pad. Puberty is considered complete when the branched network of ducts has finished invading the whole mammary fat pad (Howlin, McBryan, and Martin 2006).

3. *Estrus cycle*

After puberty, MG is considered quiescent in adult virgin mice. However, mammary tissue is dynamic, and there is a cyclic turnover of epithelial cells in response to hormonal variations caused by the 4-day estrous cycle in rodents. Estrogen and progesterone lead to the proliferation of a subset of cells to form secondary ducts and budding alveoli, which then enter into apoptosis at the end of the estrus cycle (Fata, Chaudhary, and Khokha 2001).

4. *Reproductive cycle*

During pregnancy, MGs undergo massive changes to mature into a functional milk-producing gland for lactation. Under progesterone action, ductal basal and luminal progenitors will go through substantial proliferation to establish tertiary ductal branches and then form alveolar buds at the extremities of ducts (Hennighausen and Robinson 2005). As shown with mutant mice for progesterone and prolactin receptors, once developed, alveoli require a hormonal combination of progesterone and prolactin to mature into secretory bodies (Ormandy et al. 1997; Brisken et al. 1998). To promote epithelial development, the stromal compartment is also remodeled during pregnancy with de-differentiation and shrinkage of adipocyte lipid content, in parallel with extensive angiogenesis (Vernon and Pond 1997; Zygmunt et al. 2003). At the end of pregnancy, most of the fat pad is filled with mature lobulo-alveolar structures. After parturition, due to progesterone drop concomitant to a high level of

prolactin, lactation is initiated with the formation of the colostrum. Alveolar luminal cells are fully differentiated into their secretory phenotype, producing and ejecting milk into the lumen; and myoepithelial cells contract in response to oxytocin and calcium oscillations to synchronize and favor milk expulsion (Soloff 1982; Stevenson et al. 2020). Suckling stimulation further promotes alveolar proliferation and maturation and increases milk production gene expression (Neville, McFadden, and Forsyth 2002). Milk production requires much energy to breastfeeding mothers. Therefore, after weaning, when milk production is dispensable, MGs undergo a tightly controlled process of involution to return to a pre-pregnant resting state.
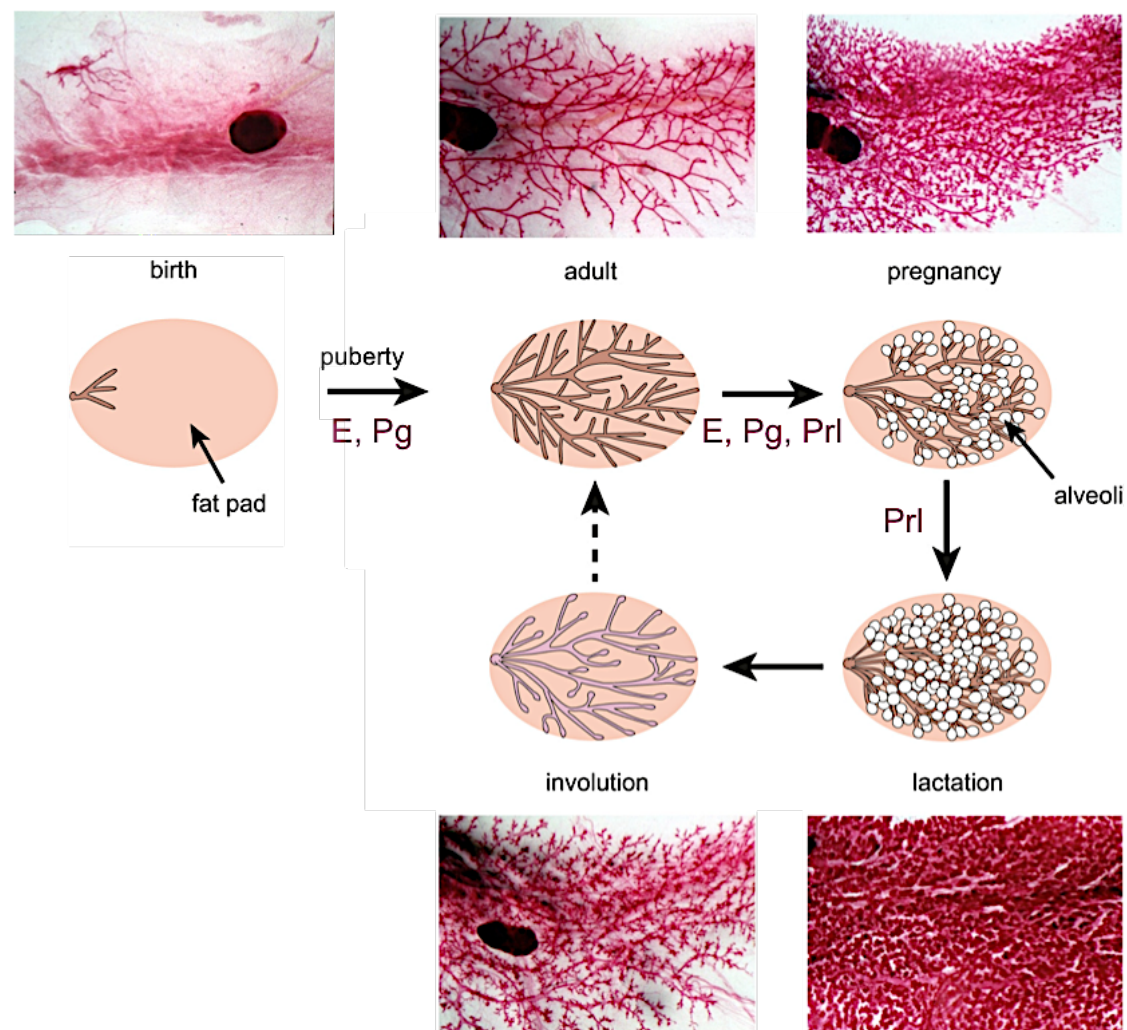
Figure 17. Murine MG developmental cycle through post-natal life. Post-natal MG development begins with a primary duct connected to the nipple. Upon puberty, the ductal network invades the mammary fat pad, and secondary ducts are developed without terminal lobules to reach a resting state in the virgin adult. During pregnancy and lactation, alveolar units are developed and fully differentiated, giving MG its milk-producing organ functionality. After weaning, a process of involution leads to the disappearance of the milk-secreting alveoli and allows MG to return to its resting pre-pregnancy stage before a further gestation. MG development is under hormonal regulation. E: estrogen; Pg: progesterone; Prl: prolactin. Adapted from (Fu et al. 2020).

D. Involution: a chaos carefully-orchestrated

1. *Overview*

The MG involution is one of the main cell death and tissue-remodeling events in the adult mammalian organism. This process occurs naturally after suckling arrest when pups diversify their food intake and do not consume milk anymore. Therefore, involution is critical for removing milk-producing epithelial cells, which are no longer needed (Watson 2006). To study mechanisms underlying the involution process, it can also be synchronized by the physical separation of the progeny from the mother at the peak of lactation at 10 days post-delivery, also termed involution day 0 (Inv0) (Lloyd-Lewis, Sargeant, et al. 2017). This strategy allows temporally defining involution, commonly divided into two distinct morphological phases (Lund et al. 1996). During the first stage of involution, there is an extensive programmed cell death, but the global architecture of the gland is not impaired. In contrast, a major tissue remodeling of mammary tissue occurs during the second phase of involution. At the end of involution, around 14 days after the initiation, MGs recover their pre-pregnant morphology and return to the quiescent state, ready for a subsequent pregnancy (Watson 2006).
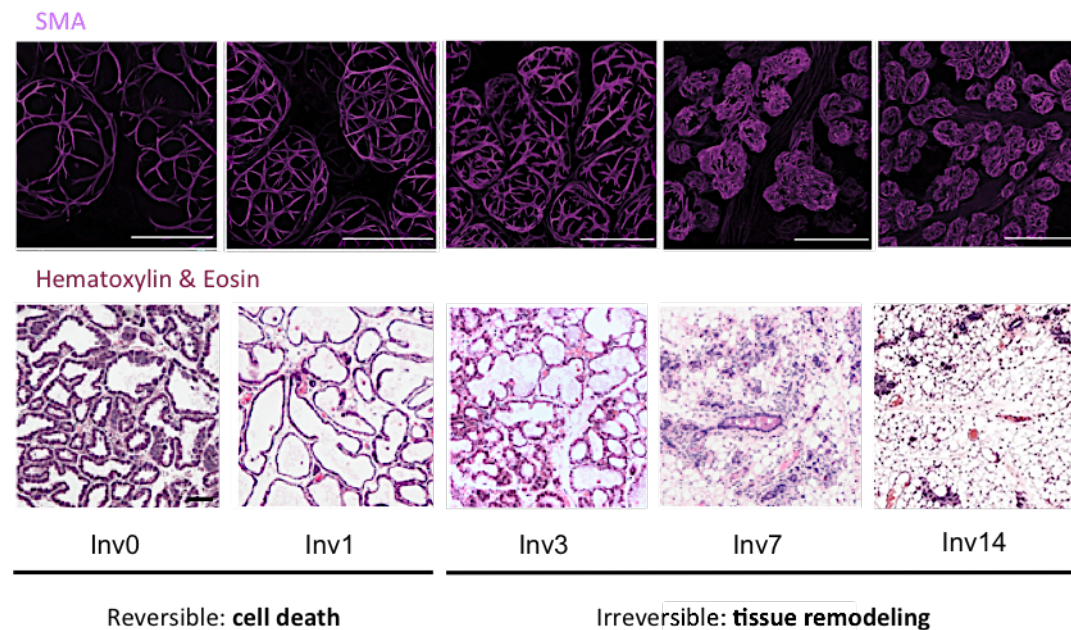
Figure 18. MG histology during the kinetic of involution. MG involution is separated into two phases based on its reversibility and the capacity to resume lactation. The first reversible phase is characterized by massive cell death, with dying cells shredded in the lumen (H&E staining at Inv1), while alveoli maintain their global architecture (SMA staining at Inv1). At Inv3, the process becomes irreversible, with shrinkage of alveoli and remodeling of the extracellular matrix (SMA and H&E stainings at Inv3). The involution process is considered completed by Inv14, with only small remaining alveoli buddings at the end of ducts. Smooth Muscle Actin (SMA) stains the myoepithelial cells. Inv0, Inv1, Inv3, Inv7, and Inv14 correspond respectively to involution day 0 (physical pups removal), or 1, 3, 7, or 14 days after the initiation of involution. Adapted from (Hitchcock et al. 2020; Sutherland et al. 2006; Kreuzaler et al. 2011).

2. *The first reversible phase of involution*

Mouse MG involution is characterized by two phases of involution based on the reversibility of the process. During the first 48h of the process, involution is reversible. Indeed, as pups are placed back with the mother and resume the suckling stimulation, involution is halted, and lactation can be re-initiated (Li et al. 1997). This reversibility has been evolutionary conserved, as it is crucial that

pups can be nursed after a long absence of the mother in search of food (Watson and Kreuzaler 2011).

This first involution phase starts as early as 12h after the last feed and is closely linked to the stagnation of milk in the alveolar structures. Sealing of mammary nipples with veterinary glue is a creative approach to study involution inducers by uncoupling the influence of the build-up of local factors versus the response to lactogenic hormones. Indeed, some MGs can be physically sealed, whereas other nipples from the same animal are left untouched. Suckling on unsealed nipples preserves lactation and maintains the production of lactogenic hormones. Interestingly, the teat sealing leads to a regular milk accumulation and does not disturb the early involution phase, emphasizing the role of milk stasis in the process (Li et al. 1997).

It has been proposed that cells perceive both chemical and mechanical signals due to milk stasis and respond by extensive cell death (Quaglino et al. 2009). Apoptosis was proposed as a major mechanism during this first cell death wave. However, apoptotic cells have a typical morphology: the chromatin is condensed, and the plasma membrane is fragmented into apoptotic bodies (Saraste and Pulkki 2000). During the first phase of involution, epithelial cells detached and discharged into the lumen do not exhibit this classical apoptosis-associated morphology but instead have a swollen shape, and their membrane is intact without blebbing. Moreover, cells are not positive for TdT-mediated dUTP nick end label (TUNEL), a classical apoptotic staining (Watson and Kreuzaler 2011). Instead of apoptosis, lysosomal membrane permeabilization (LMP) has been shown to occur in the mammary epithelium during the first phase of involution (Kreuzaler et al. 2011). Lysosomes are important acid organelles containing enzymes, which primary function is to degrade cellular macromolecules. In LMP, lysosomal proteins as cathepsins leak from lysosomes and remain active in the cytosol, where they replace caspases in their role of death executing-proteases, inducing cell death.

Mechanistically, milk stasis induces a wide range of stimuli with the build-up of local factors as an overload of intracellular Ca^{2+} and mechanical stretching of the epithelial cells (Stewart et al. 2021). In response, epithelial cells up-regulate the expression of numerous cytokines as LIF and TGFβ3, linked to the phosphorylation of the master regulator of involution, the transcription factor Stat3 (Kritikou et al. 2003; Nguyen and Pollard 2000). Activated pStat3 modifies the lysosomal content by up-regulation of lyosomal proteases cathepsins B and L and down-regulation of the endogenous cathepsins inhibitor Spi2A. While the lysosomal membrane is dismantled, by a down-regulation of LAMP, a major lysosomal membrane structural protein (Kreuzaler et al. 2011). In early involution, the leakage of lysosomal content in the cytoplasm is then responsible for the LMP cell death mediated by Stat3. Importantly, mice genetically KO for Stat3 in the mammary epithelium exhibit a dramatic delay of involution (Humphreys et al. 2002). Activation of Stat3 in its phosphorylated form is concomitant with the dephosphorylation of Stat5, which is a crucial survival factor implicated in the proliferation and differentiation of epithelial cells in the alveolar lobules, during pregnancy and lactation (Barash 2006). pStat5 dephosphorylation is required to initiate cell death, as constitutive activation of Stat5 delays MG involution in transgenic mice by the maintenance of pro-survival signals (Iavnilovitch, Groner, and Barash 2002).

During the first phase of involution, the global architecture of the gland is not impaired as there is no remodeling of the stroma concomitant with the extensive epithelial cell death. Indeed, tissue inhibitors of metalloproteinases (TIMPs) are highly expressed during the first 48h, allowing to maintain the reversibility of the involution process. More specifically, tightly controlled TIMP-3 and TIMP-1 expressions are crucial during the first involution phase. Indeed, MGs from mice KO for TIMP-3 exhibited an accelerated cell death and remodeling, whereas, surprisingly, TIMP-1 overexpression promoted a faster adipogenic re-differentiation (Fata et al. 2001; Alexander et al. 2001).

3.   The second irreversible phase of involution

The second involution phase starts 48h after the removal of the litter (Inv3) and is irreversible. Indeed, when pups are placed back with the mother and resume the suckling stimulation after 48 hours, lactation cannot be re-initiated, and involution continues until the end of the process (Li et al. 1997).

While the first phase of involution was defined by extensive cell death without changes in the MG structure, the second phase is characterized by massive tissue remodeling. Briefly, the alveolar structures are collapsed; the extracellular matrix (ECM) is profoundly restructured notably due to the high expression of metalloproteinases (MMPs) and the deposition of new ECM fibers as fibrillar collagen; immune cells are recruited to help in the clearance of the tissue; and re-differentiation of adipocytes occurs in the stroma for the refilling of the mammary fat pad. After two weeks of involution, the majority of the MG recovers its pre-gestation state and returns back to the quiescent state (Watson and Kreuzaler 2011).

Signals to switch from the first to the second phase of involution are not clearly defined. However, it has been proposed that it depends on lactogenic hormones regulated at the systemic level. Indeed, teat sealing does not affect the progression of the early phase of involution. However, maintenance of lactogenic hormones completely disturbed the entrance in the second phase of involution, with an absence of tissue remodeling persistent at Inv6 (Li et al. 1997). Moreover, implantation in the MG of pellets releasing exogenous hormones such as glucocorticoids was sufficient to impair the entrance in the second phase of involution (Feng et al. 1995).

Mechanistically, a decrease of lactogenic systemic hormones might induce the expression of metalloproteinases (MMPs), such as MMP-2 (gelatinase-A), or MMP-3 (stromelysin-1), concomitant to a decrease in expression of MMPs inhibitors TIMP-1 and TIMP-3 (Talhouk, Bissell, and Werb 1992). MMPs are broad-spectrum proteases and use their catalytic domains to cleave components

of the extracellular matrix (ECM) as collagens of the basement membrane, fibronectin, or laminin (Uria and Werb 1998).

The degradation of the ECM might be sensed as a stress signal favoring apoptotic cell death, characteristic of the beginning of the second phase of involution (Watson and Kreuzaler 2011). Indeed, mitochondria-mediated intrinsic cell death, also known as the "classical apoptosis" is induced during the early irreversible phase, marked by the presence of cleaved-caspase 3 (CC3) as well as TUNEL positive cells in alveoli walls (Marti et al. 2001). Apoptosis is regulated through the balanced expression of pro- and anti-apoptotic proteins from the Bcl2 family (Hardwick and Soane 2013). During the first phase and the early second phases of involution, when cell death is induced *via* LMP or mitochondria-mediated apoptosis, there is an overexpression of pro-apoptotic proteins Bax, Bak, and Bad; whereas anti-apoptotic proteins such as Bcl-2, Bcl-X and Bcl-W are down-regulated (Metcalfe et al. 1999). This correlates with the transgenic overexpression of Bcl-2 under WAP promoter, specific to alveolar luminal cells, which delays mammary epithelial cell death during *in vivo* involution (Jager et al. 1997). Surprisingly, the expression of anti-apoptotic proteins Bcl-2, Bcl-X, and Bcl-W increases as early as Inv3 up to Inv12 (Metcalfe et al. 1999).

Immune cells contribute significantly to the mammary involution process. In early involution, the immune response is limited to the recruitment of neutrophils *via* the expression of the neutrophil chemoattractant CXCL1 at Inv1 (Stein et al. 2004). Mast cells contribute to the second phase of involution, promoting apoptosis of alveolar cells and remodeling of the stromal compartment (Lilla et al. 2009). Notably, macrophages are the main immune cell type participating in MG involution, especially in the irreversible phase. Indeed, depletion of macrophages using the Mafia mouse model, containing a transgene-inducing cell death of CSF1R-expressing cells, dramatically delays the second phase of MG involution (O'Brien et al. 2012). Massive macrophage infiltration occurs from Inv3, possibly to promote phagocytosis of apoptotic bodies and cell debris. However, non-professional phagocytes could also fulfill this phagocytic

role. Indeed, intact epithelial cells are proposed to engulf dying epithelial cells, contributing to the fast clearance of the tissue (Monks et al. 2008). Recently, a new population of tissue-resident CD11b^{low}, CD11c^{+} macrophages has been imaged in the mammary ducts. During pregnancy, they expand to cover alveolar structures, and *via* dendrite movements, they monitor the epithelium and can react fast to cell death signaling. Therefore, ductal macrophages are well positioned to proceed to milk-producing cell phagocytosis upon early involution (Dawson et al. 2020). Then, another population of macrophages infiltrating MGs during the late phase of involution exhibits an expression of the M2 subtype, known to participate in wound healing and tissue repair, in which they promote clearance of debris but also restructuration of the ECM and angiogenesis (O'Brien et al. 2010).

Finally, the stromal compartment is extensively remodeled throughout involution, and the withdrawal of epithelium is concomitant to the replenishment of adipocytes in the mammary fat pad. During pregnancy and lactation, adipocytes dedifferentiate and delipidate to create a local source of lipids supporting milk production (Hovey and Aimo 2010). Upon involution, adipocytes fully re-differentiate and undergo hypertrophy due to the uptake of lipids released in the alveolar lumen from milk-producing dying cells. Adipocyte refilling is proposed to participate actively in the proper remodeling of the tissue, as specific depletion of MG white adipose tissue prior to involution impairs MG restructuration (Zwick et al. 2018).

To conclude, the second phase of involution displays many similarities with the tissue remodeling associated with wound-healing, such as removal of damaged epithelium; proliferation of mesenchymal cells; inflammatory response; and restructuration of the ECM with collagen deposition (Gosain and DiPietro 2004).
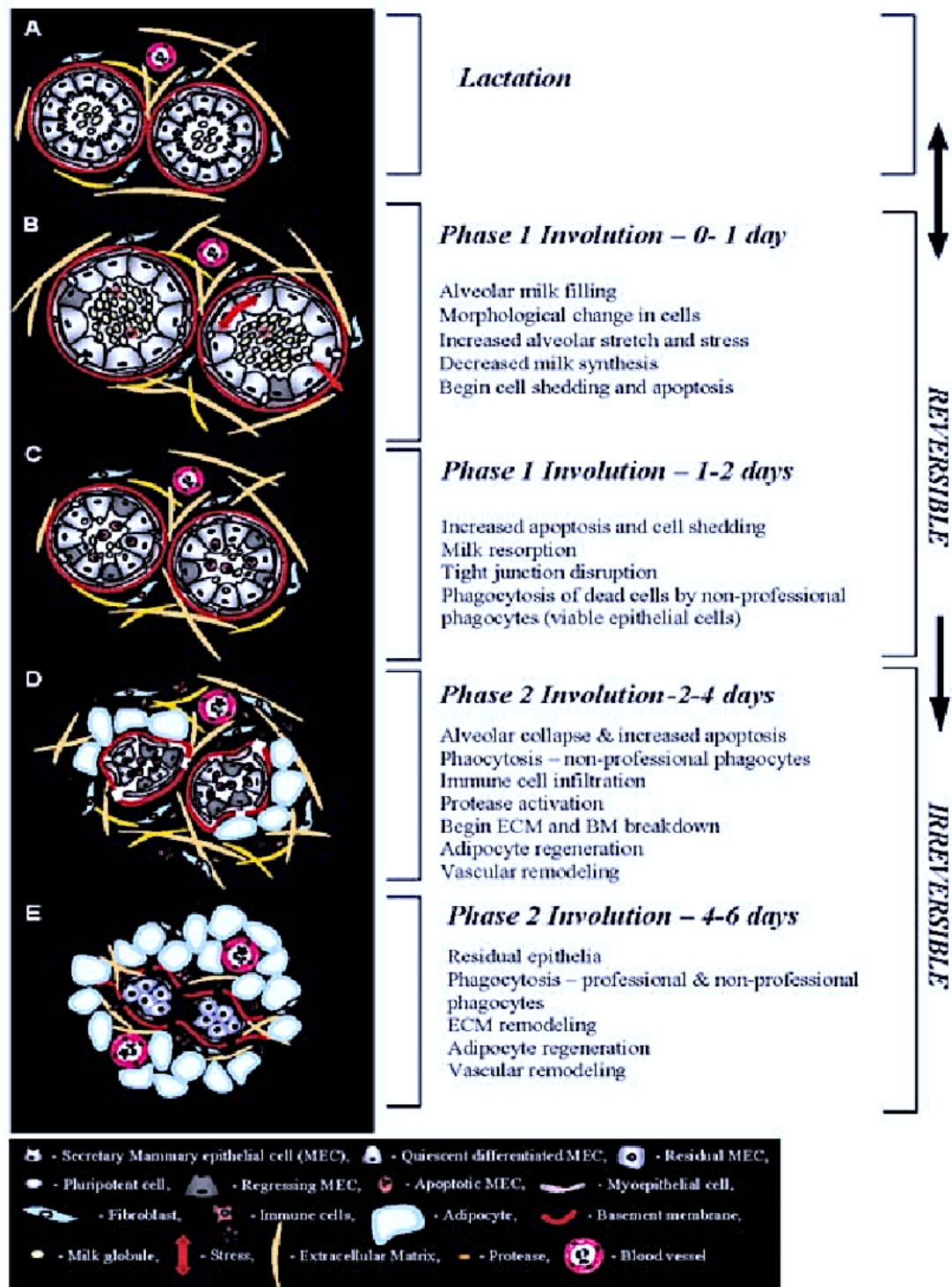
Figure 19. MG involution as a sum of dynamic intricate processes. MG involution can be precisely timed and described in details as a succession of various processes. From ebook *"Mammary Gland Involution: Events, Regulation and Influences on Breast Disease" Pai, V.P., & Horseman, N.D. (2012).*

4. *Back to the future*

MG involution is completed around two weeks after induction, with the removal of alveolar structures and the refilling of the fat pad by adipocytes. MGs remain resting until a further pregnancy. Interestingly, how epithelial stem cells are protected from pro-death signals and conserve their plasticity through multiple reproductive cycles remains unclear (Watson and Kreuzaler 2011).

Classical or "post-lactational" involution is to differentiate with lobular involution, where mammary epithelial gradually disappears with age progression. Indeed, lobular involution is characterized by reduced size and complexity of the ductal network during menopause (Radisky and Hartmann 2009). Interestingly, it is proposed that removing epithelial tissue after the end of the reproductive life span is a mechanism protective against breast cancer (Milanese et al. 2006). In contrast, post-lactational involution is associated with an increased transient risk of pregnancy-associated breast cancer (Schedin 2006).

As conclusion, post-lactational MG involution is a very complex process, extensively studied for more than two decades. However, essential questions remain open in the field. What are the precise signals associated with milk stasis initiating the first involution phase? How is the switch from the reversible to the irreversible phases of involution controlled? How are the multiple cell types involved in the tissue remodeling phase coordinated to restructure the tissue? Are there other mechanisms regulating the elaborate changes of the involuting microenvironment? Unraveling this physiological process is crucial to understanding why the post-lactational involution is associated with pro-tumorigenic development.

5.   Involution and postpartum-associated breast cancer

Epidemiologic studies suggest that pregnancy at an early age is protective against general forms of breast cancer, supposedly due to the maturation of epithelial cells during pregnancy and the reduction of the total number of menstrual cycles (Rosner, Colditz, and Willett 1994). However, there is a transiently increased risk of developing breast cancer after pregnancy, and diagnosis of breast cancer within 10 years after delivery is categorized as postpartum breast cancer (PPBC) (Albrektsen et al. 2005). PPBC is correlated with a worse prognosis, as women diagnosed with PPBC have a 40% increased risk of breast-cancer-associated death within 5 years compared to breast cancer in nulliparous women, principally due to the development of metastasis (Daling et al. 2002).

Involuting MG microenvironment has intrinsic characteristics that can promote tumorigenesis (Watson and Kreuzaler 2011). Indeed, during involution, mammary tissue is pro-inflammatory with the recruitment of immune cells, the intense remodeling of the ECM, and the impairment of the integrity of the basement membrane due to increased metalloproteinases activity. *In vitro*, ECM from involuting MGs stimulated tumor cell invasion. *In vivo*, co-injection of mammary tumor cells with involution ECM in mammary fat pad promoted invasiveness and metastasis in various organs, as well as angiogenesis (McDaniel et al. 2006).   Therefore, it has been proposed that involution creates a microenvironment permissive for tumorigenesis and metastasis, promoting PPBC (Schedin 2006).
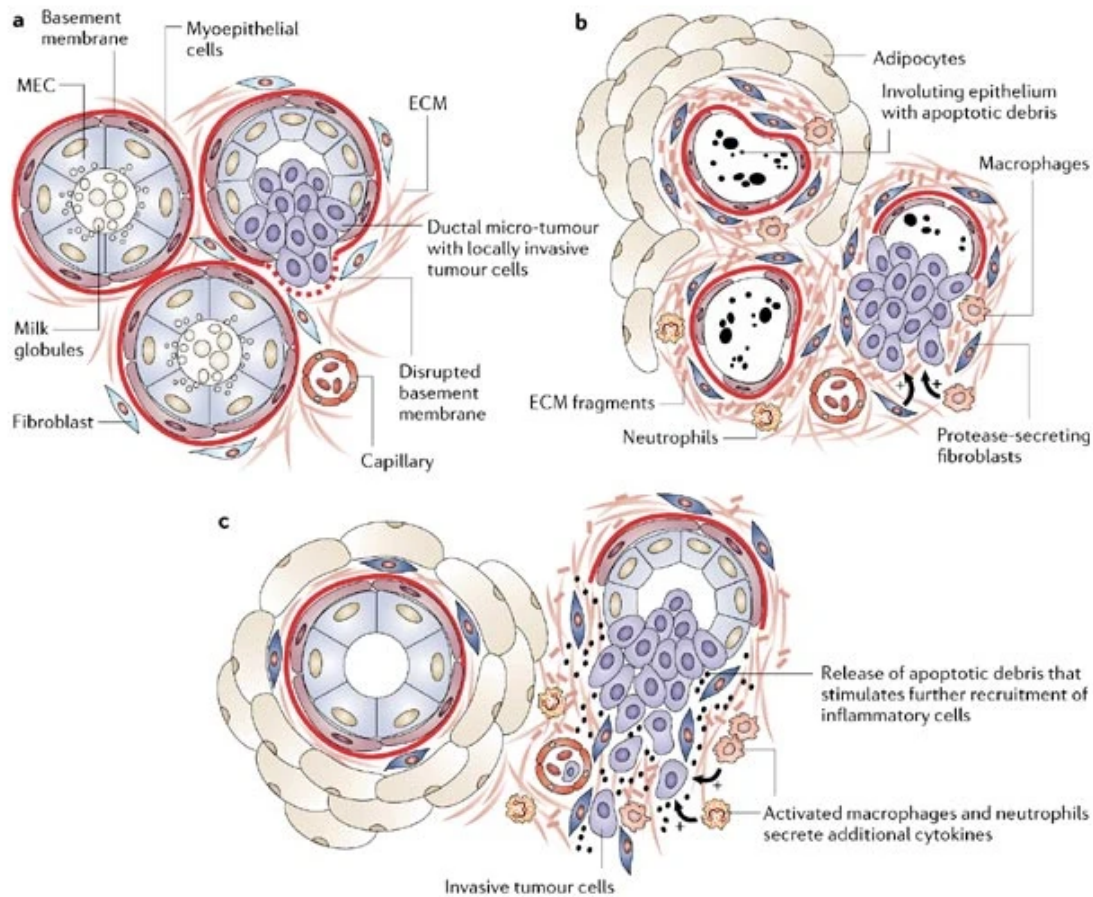
Figure 20. MG involution creates a pro-tumor microenvironment favoring the development of human postpartum breast cancer. Postpartum breast cancer is characterized by its poor prognosis, mainly due to the presence of metastasis. Pre-cancerous cells can stochastically appear in the alveolar structures of lactating MG, creating micro lesions. Upon involution, the MG microenvironment is disrupted with a major remodeling of the extracellular matrix, promoting growth, motility, and invasion of tumor cells. Moreover, immune cells recruited during involution secrete numerous cytokines and growth factors, which in turn can activate quiescent tumor cells. From (Schedin 2006).

E. *In vitro* 3D models to recapitulate MG development

MG development has been extensively studied *in vivo,* but three-dimensional (3D) culture provides many advantages regarding optical observation and live

imaging, or genetic manipulations while conserving a complex tissue architecture missing in 2D cultures (Shamir and Ewald 2014).

Spheroids are 3D cell aggregates, but they do not fully recapitulate either the complex 3D organization or the function of the mammary tissue. Organoids are 3D assays intrinsically different from spheroids, as they can form complex 3D structures with a spatial organization of multiple cell lineages, mimicking organ functions (Gilazieva et al. 2020). Various mammary organoids have been developed to mimic MG morphogenesis and understand the crosstalk between organoids derived from epithelial cells and the ECM or the fibroblasts population from the stromal compartment (Ewald et al. 2008; Simian et al. 2001; Sumbal and Koledova 2019). Some organoids were derived from single basal cells and reproduced a functional bilayer of basal and milk-producing luminal cells (Jamieson et al. 2017). However, prior to our study (see Annexes (Sumbal et al. 2020) (Charifou et al. 2021)), no organoid system resuming the three key stages of mammary gland reproductive cycle, gestation-lactation-involution, was characterized yet (Srivastava et al. 2020).
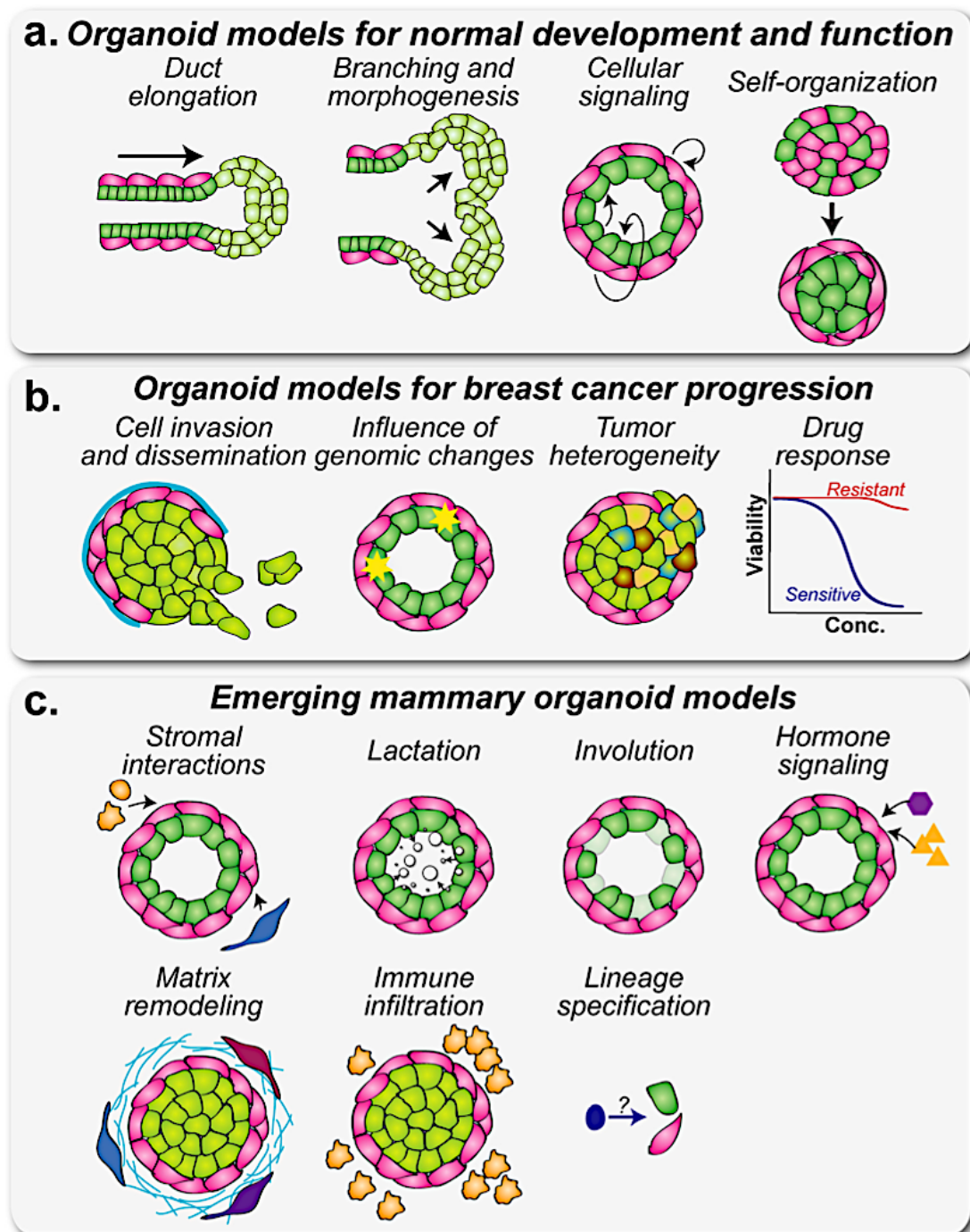
Figure 21. Mammary organoid models. Various organoid models have been developed from mammary epithelial cells to study physiological MG morphogenesis and pathological emergence of breast cancer. From (Srivastava et al. 2020).

Context of the project

Cellular senescence is a form of stress response characterized by a stable cell-cycle arrest and acquisition of a robust secretome, termed senescence-associated secretory phenotype (SASP). The permanent growth arrest is a potent cell-intrinsic tumor suppression mechanism comparable to apoptosis, whereas SASP paracrine signaling is important for optimized wound healing and tissue regeneration. Meanwhile, senescent cells accumulate during aging, contributing to aging and age-related diseases. Importantly, the elimination of senescent cells can improve a variety of aging-dependent pathologies, including cancer, and enhance tissue regeneration. Although it has become increasingly clear that senescence plays multifaceted roles during many physiological and pathological processes, its involvement in most physiological processes remains largely unknown. *Where and when does senescence occur during a lifetime? How does senescence contribute to different physiological processes?* Addressing these questions is crucial for our understanding of the pleiotropic roles of senescence and for providing necessary precision in specifically targeting the detrimental effects of senescence.

To start answering these relevant questions, we took advantage of the mammary gland (MG) system. The MG is an organ with remarkable plasticity and its development mainly occurs postnatally. Importantly, it is also the origin of breast cancer. My Ph.D. project assessed the contribution of senescence during MG development *in vivo* and *ex vivo*. Interestingly, we detected the presence of senescent cells exclusively during the MG involution. Built upon this interesting observation, my Ph.D. project characterized the involution-associated senescence program and assessed the role of senescence role in this physiological process using mouse models, senolytic treatment, bulk RNA sequencing, and a novel *ex vivo* mammary organoid system.

Results

Cellular senescence is induced during mammary gland involution associated with the onset of tissue remodeling

To assess whether senescence occurs during mammary gland (MG) postnatal development and reproductive cycle, we collected murine MGs at different developmental stages, including mature young virgin (8 weeks), pregnancy (D18.5), and lactation (L10). After 10 days of lactation (L10/Inv0), we physically removed the pups to induce synchronized involution and harvested involuting MGs (Lloyd-Lewis, Sargeant, et al. 2017). In addition, we also collected MGs from old females, both multiparous (10 months) and nulliparous (18 months) (Figure 1A). We use senescence-associated beta-galactosidase (SAβGal) staining, a widely used assay (Cahu and Sola 2013) as the primary method to detect senescent cells in the mammary gland sections. Of note, in most time points collected except involution, we failed to detect any SAβGal positive cells, including the MGs from old females (Supplementary Figure 1A).

Involution is characterized by the massive cell death of the secretory alveolar structures and tissue remodeling (Watson and Kreuzaler 2011). To determine the dynamic of SAβGal positive cells during this process, we collected involuting MGs from different time points (Figure 1A). At Inv0, fully developed alveoli were the dominant structures in the section (Figure 1B, i). At Inv1, dead cells with condensed nuclei were discharged in the lumen of alveoli while alveolar structures remained intact, indicating that the involution process was initiated (Figure. 1B, ii). At Inv3, alveolar structures started to shrink and adipocytes refilling becomes evident, indicating the onset of the tissue remodeling phase of involution (Figure 1B, iii). Interestingly, SAβGal positive cells started to appear only at Inv3. The intensity of SAβGal staining increased gradually and peaked at Inv7 (Figure 1B, iv). The presence of SAβGal positive cells was limited to the alveolar structures whereas ductal regions were negative (Figure 1B, iv). Of note, alveolar structures are eventually removed by the end of involution while ductal structures last. SAβGal staining decreased afterwards and by Inv14, we barely detected any blue cells while some of the collapsed alveolar structures remained (Figure 1B, v). The SAβGal staining suggested that there was a transient

induction of senescence during the tissue remodeling phase of mammary involution.

Transcriptomic analysis of involuting mammary gland

To confirm the SAβGal staining results, we performed bulk RNA sequencing on whole MG at different time points during involution. Principle-component analysis (PCA) revealed that samples from the same time point cluster together (Supplementary Figure 1B). To gain an unbiased global view on which biological pathways/responses occurred during involution process, we compared our datasets at different time points with hallmark gene set. Comparing Inv7 vs Inv0 or Inv3 vs Inv0, we found that similar pathways are significantly enriched or depleted, with more changes detected in Inv7 than in Inv3 (Supplementary Figure 1C).

Next, we created our customized mouse senescence gene set based on the SeneQuest (http://Senequest.net) (Gorgoulis et al. 2019). We considered a gene as associated with senescence when there were at least 5 consistent reports in one direction (upregulation or downregulation). We generated multiple gene sets separated in two categories: SENESCENCE-UP and SENESCENCE-DOWN, based on how many consistent reports where found in the Senequest.net. The higher is the reports number, the stronger is the association to senescence. Next, we performed gene set enrichment analysis (GSEA) using the customized gene sets (SENESCENCE-UP5) and our transcriptomic datasets. We found a significant enrichment of senescence upregulation in Inv3 and Inv7 comparing to Inv0 (Figure 1C). We also detailed a list of senescence-associated genes significantly upregulated at both Inv3 and Inv7 (Figure 1D). Interestingly, CDKN2a and Trp53 were also significantly upregulated in Inv7 (Supplementary Figure 1D). Taken together, the transcriptomic data analysis further confirmed the induction of senescence program in the involuting MG, specifically at Inv3 and Inv7.
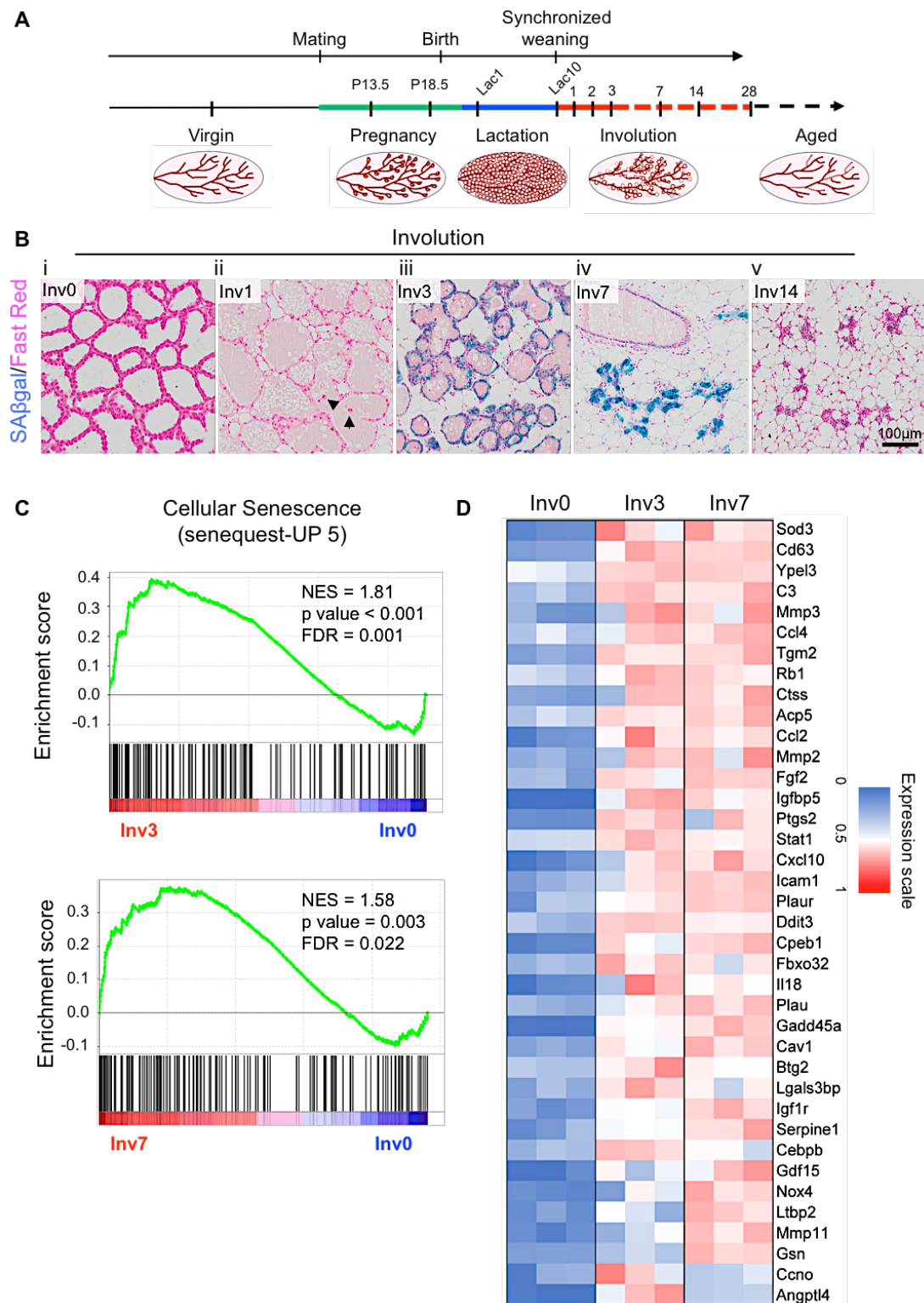
Figure 1. Transient induction of senescence during mammary gland involution.

A. Experimental design highlighting the time points of MGs collect at: mature virgin (8 weeks old) or old virgin (18 months old), pregnant (p18.5), after 10 days of lactation (L10/Inv0), or after 1, 3, 7 and 14 days of involution

(respectively Inv1, Inv2, Inv3, Inv7, and Inv14). **B.** SAβgal staining during MG involution. **C.** GSEA enrichment plots. Reference gene set: customized senescence-upregulation 5. **D.** Heat map of RNA-seq transcriptome analysis for 38 selected senescence-associated genes (customized gene set) that are significantly enriched in both Inv3 and Inv7 comparing to Inv0 (based on the GSEA analysis). Scale bar: 100μm.

Milk-producing alveolar luminal cells are the main senescent cell type during mammary gland involution

To define cell types that were becoming senescent in the mammary tissue during involution, we first performed SAβgal staining, co-stained either with Keratin 5 (Krt5), marker of basal cells (Figure 2A); or Keratin 8 (Krt8), marker of luminal cells (Figure 2B), using histological sections of MGs collected at Inv3, when the epithelial structure of the alveoli is still well preserved. We found that the majority of SAβGal+ cells were alveolar luminal cells while few Krt5+ basal cells were also positive for SAβGal staining.

To further define senescent cell types within involuting MG and gain a quantitative idea on the tissue level, we optimized a fluorescent staining of senescent cells using C_{12}FDG. Briefly, we harvested MGs from mice at Inv0 and Inv5. After cell dissociation, we incubated mammary cells with C_{12}FDG and performed a cytometry analysis to separate stromal cells (CD31$^-$, CD45$^-$, CD24$^-$, α6$^-$); basal cells (CD31$^-$, CD45$^-$, CD24^{low} and α6^{high}); and luminal cells (CD31$^-$, CD45$^-$, CD24^{high} and α6^{low}) (Supplementary Figure 2A-B). In every cell population, we then counted the number of cells positive for C_{12}FDG-GFP. Only ~6% of stromal cells were positive at Inv5 (Supplementary Figure 2C). Interestingly, in the epithelial compartment, ~15% of basal cells were C_{12}FDG-GFP+ at Inv5 compared to Inv0 (Supplementary Figure 2C). And more than ~52% of luminal cells were positive for C_{12}FDG-GFP at Inv5, suggesting that luminal cells were the main cell type to become senescent (Supplementary Figure 2C).

It is well established that alveolar luminal cells are removed via programmed cell death during involution ([Kreuzaler et al. 2011](#)), while a senescent cell does not undergo cell death. Therefore, we performed cleaved caspase 3 (CC3) and SAβGal co-staining on Inv3 to further confirm SAβGal⁺ luminal cells were distinct from dying cells. We could detect many CC3⁺ cells consistent with the literature. Interestingly, most of SAβGal⁺ cells were negative for CC3 staining (Figure 2C). Moreover, these SAβGal⁺ cells were also non-proliferating, as they were negative for proliferative maker, Ki67 (Figure 2D). Therefore, SAβGal+ cells were non-apoptotic and non-proliferating, two mutually exclusive cell states from senescence.

Mammary involution-associated senescence might be mediated by p16 *in vivo* and *ex vivo*

Senescence cell cycle arrest can be mediated by two major cyclin-dependent kinase inhibitors, either p21 or p16 ([Kumari and Jat 2021](#)). The bulk RNAseq analysis of the whole MG at different time point revealed that CDKN2a but not CDKN1a was significantly upregulated at Inv7 vs Inv0 (Supplementary Figure 1C). To confirm the bioinformatic analysis result, we took advantage of a new p16-reporter mouse model (*[https://doi.org/10.1101/2020.06.10.142893)](https://doi.org/10.1101/2020.06.10.142893)* *(BioRXiv reference)*) known as INKBRITE, with a GFP cassette under the regulation of endogenous p16 promoter, to detect p16 protein expression pattern during involution. At Inv0, the p16 expression was rather heterogenous. There were few GFP⁺ cells located in the stromal compartment, outside of the alveolar structures marked by Krt5 (Figure 2E, upper panel). Within the mammary epithelium, we found some alveolar structures without any GFP⁺ cells (Figure 2E, upper panel, asterisk), while some alveolar structures did contain GFP⁺ cells (Figure 2E, upper panel, zoom-in). Interestingly, we detected many more GFP⁺ cells at Inv3 compared to Inv0. A good proportion of the GFP⁺ cells were located within the alveolar structures facing the lumen (Figure 2E, lower panel). Therefore, p16 expression correlated with senescence induction during involution, and some alveolar luminal cells were p16⁺ at Inv3.

Previously, we established a mammary organoid model to mimick pregnancy, lactation, and involution *ex vivo* ([Sumbal et al. 2020](#)). We wondered whether senescence was also induced during involution-like process in this organoid model. Therefore, we cultured primary organoids in FGF_2 for 6 days to mimic pregnancy-associated proliferation, followed by 4 days in prolactin and hydrocortisone to induce lactation-like process. Then, we induce involution-like process by removing hormonal stimulation (basal organoid medium, BOM). We used organoids maintained in a lactation-like state (LM) for additional 8 days as control (Figure 2F, experimental scheme, upper panel). We harvested organoids on the indicated days and performed whole mount SAβGal staining. The organoids from 6 days of FGF_2, or in the lactation-like state after 4 more days in LM, were not positive for SAβgal staining (Supplementary Figure 2D). However, we noticed a significant increased intensity of SAβgal staining in organoids from D14 and D18, during involution-like process (Supplementary Figure 2E). When we examined the histological sections from whole mount organoids, we found that involuting-like (BOM) organoids were much smaller than lactating-like (LM) organoids consistent to our previous findings (Figure 2F). Moreover, there were many SAβGal+ cells in the involuting-like (BOM) organoids. This was specific to involuting organoids and not due to a long period in culture, as organoids maintained in lactation-like state were not positive for SAβgal staining (Figure 2F). Next, we extracted RNA from organoids at D10 of culture, or in involution-like (BOM D18) or maintained lactation-like (LM D18) states and performed qPCR analysis. p16 was up-regulated by 16-fold in involution-like organoids compared to D10 (Figure 2H). In contrast, p21 expression was not significantly changed between D10 and D18 BOM (Figure 2H). Taken together, we showed that organoids undergoing involution-like process contain senescent cells and this was coincident with the upregulation of p16 but not p21, consistent with our *in vivo* observations. Therefore, organoids can be used as a simplified model to study involution-associated senescence.

Next, we wondered whether involution-associated senescence was triggered by DNA damage, a common inducer of senescence. There were many γH2AX positive cells in Inv3 and most of them were alveolar luminal cells, while we did

not detect any at the Inv0 (Figure 2G), suggesting DNA damage response was induced during involution process. Interestingly, GFP+ and γH2AX+ cells were mutually exclusive (Figure 2G), which was further confirmed by SAβGal and γH2AX co-staining in WT involuting MG (Supplementary Figure 2E). Taken together, these results suggest involution-associated senescent cells did not contain a significant amount of DNA damage.
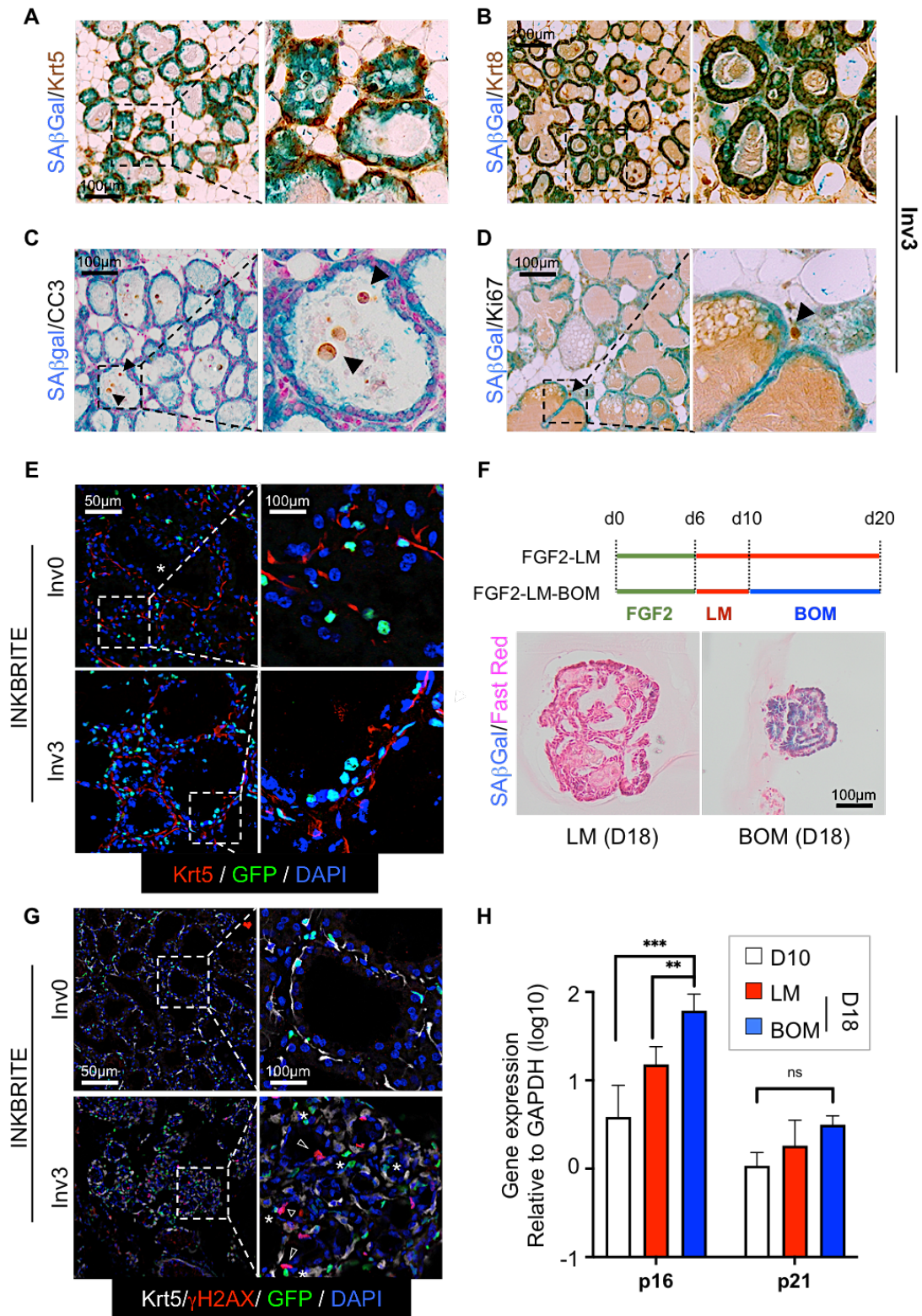
Figure 2: Alveolar luminal cells are the major senescent cell type.

A-D. Representative pictures of co-stainings SAβGal with multiple markers on WT mammary glands from Inv0 and Inv3 (N=2). **(A)** SAβGal/Krt5 (basal cells), **(B)** SAβGal/Krt8 (luminal cells), **(C)** SAβGal/cleaved caspase 3 (CC3) and **(D)**

SAβGal/Ki67. **E.** Representative pictures of co-staining of GFP with Krt5 and DAPI on INKBRITE involuting MG from Inv0 and Inv3 (N=2). **F.** Experimental design of ex vivo culture of organoids (upper panel). SAβGal staining (bottom panel) of involuting organoids from involuting (BOM, D18) and lactation control (LM, D18) (N=3). **G.** Co-staining of GFP with Krt5, γH2AX, and DAPI on INKBRITE involuting mammary glands from Inv0 and Inv3. **H.** qPCR analysis of p16 and p21 of organoids from different conditions. p-values **<0.01, ***<0.005.

Persistence of lactogenic hormones prevents the involution-associated senescence induction

We showed that senescence was specifically induced on Inv3, coinciding with the beginning of the irreversible phase of involution. Next, we wondered whether entering to the irreversible phase of involution was important for the senescence induction. We took advantage of the nipple sealing method, where some nipples are bonded with veterinary glue to mimic involution by preventing their accessibility while other nipples are still in lactation (Li et al. 1997). This approach enables the sealed MG to enter the first phase of involution caused by milk stasis. However, due to maintenance of systemic lactogenic hormones, entrance to the irreversible phase of involution is blocked and massive tissue remodeling does not occur (Li et al. 1997).

We sealed nipples from one side of lactating female and collected MGs 2 or 3 days after sealing. We compared sealed MGs to control MGs going through regular involution, at Inv2 and Inv3 (Figure 3A). First, we confirmed the correct sealing of MGs during tissue harvesting (Supplementary Figure 3A). Lactating-MGs exhibited an enlarged morphology, without milk stasis as alveoli were regularly emptied. Sealed contralateral MGs were comparable in size as lactating MGs, but milk stasis gave them a characteristic yellow color. Involuting-MGs were smaller (Supplementary Figure 3B). To further characterize MGs morphology, we stained involuting and sealed MGs with Carmine. The first phase of involution is characterized by cell death without regression of alveolar structures, and MGs kept their typical "bunch of grapes" shape as seen in Inv2

and sealed day 2 MGs (Supplementary Figure 3C). At Inv3, we noticed a regression of alveoli size, exposing ducts underneath in the involuting-MGs, while sealed-MGs maintained similar morphology (Figure 3B-left panel). Moreover, on tissue sections, we observed many dying cells shredded into the lumen of alveolar structures in both involuting-MGs and sealed-MGs at day 2, indicating that the first phase of involution was initiated (Supplementary Figure 3C-right panel, black arrow head). On day 3, involuting-MGs exhibited hallmarks of the onset of tissue remodeling events, with easily identifiable shrinking alveoli and refilling of the adipocytes, while sealed-MGs remain the same morphology as day 2 (Figure 3B, right panel). Moreover, we confirmed the correct sealing of MGs by qPCR analysis. Indeed, sealed MGs stopped their milk production, as seen by a decreased of CSN2 and WAP expressions, as involuting MGs. However, adipocyte refilling was impaired, as seen with Adipoq level at day 3, which was only upregulated in involuting MGs (Figure 3D). Taken together, these data showed that we succeeded to correctly seal MGs while maintaining lactogenic stimulation in mice. Sealing enabled MGs to start the involution process without entering the irreversible remodeling phase.

To test whether senescence program was impaired in sealed MGs, we determined the number of senescent cells using SAβgal staining. In accordance with our previous results, we showed the appearance of SAβgal positive cells at Inv3 (Figure 3B & C). Surprisingly, in sealed-MGs, we did not detect any SAβgal positive cell on day 3 (Figure 3B & C). We also collected MGs on day 5 and we could start to see a few SAβGal+ cells in the sealed-MG (Supplementary Figure 3D). Of note, we also observed a delayed adipocyte refilling in the same sections (Supplementary Figure 3D, asterisk), suggesting sealing significantly delays the tissue remodeling phase of involution on day 5. We further confirm the impairment of senescence program by qPCR analysis. Indeed, from day 2 (D2) to day 3 (D3), p16 gene was only significantly increased in the involuting MGs (Figure 3D). Taken together, we confirmed that using teat sealing to maintain lactogenic hormones was sufficient to block entrance into the irreversible phase of MG involution. More importantly, we showed that teat sealing impaired the

senescence induction. Therefore, senescence is closely associated to the irreversible remodeling phase of involution.
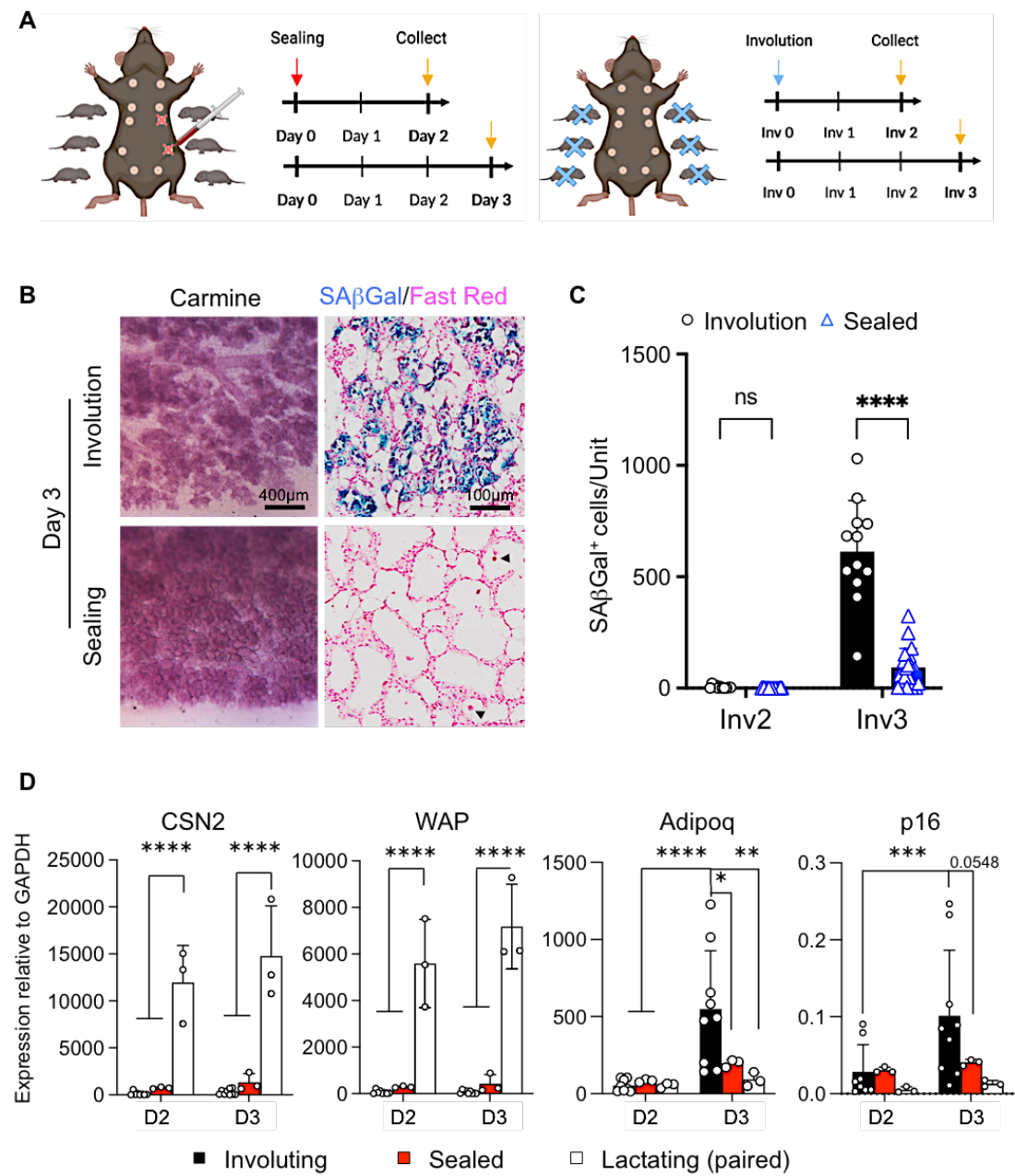
Figure 3. Persistent lactogenic hormone prevents the induction of senescence.
A. Experimental design of teat sealing of MG #3L and #4L (red), while other MGs are maintained in lactation. MGs were collected 2 or 3 days after sealing and compared with MGs from mice undergoing normal involution (blue). **B.** Left panel: Whole mount MGs after Carmine staining, magnified 5x, from involuting (top) or sealed (bottom) MGs at day 3; Right panel: SAβgal staining from involuting (top) or sealed (bottom) MGs at day 3, on cryosections, counterstained with FastRed. **C.** Automatic quantifications of SAβgal staining at day 2 (left) and day 3 (right), from involuting (blue) or sealed (red) MGs. (≥5 representative pictures/mouse; n≥3 per group). **D.** qPCR analysis of the indicated genes from MGs collected at day 2 or day 3, from involuting (blue) or sealed (red) tissues. p-values **<0.01, ***<0.005, ****<0.0001.

Removing senescent cells with senolytic ABT-263 delays mammary gland involution *in vivo*

To determine the functional link of senescence in the involution process, we specifically eliminated senescent cells using a senolytic compound, ABT-263 ([Chang et al. 2016](#)), to assess the impact of senescence on physiological involution. Mice were treated with ABT-263 by force-feeding daily, for 3 days prior to harvest at Inv3, Inv4, and Inv5 (Figure 4A). Importantly, as ABT-263 is inducing apoptosis of senescent cells, we first assessed the apoptosis level using cleaved-caspase 3 staining comparing control to ABT-263 treated samples. We showed an increase of apoptotic epithelial cells from 11% in control up to 30% in ABT-263 treated MGs at Inv5 (Figure 4B & G). As highlighted with SAβgal staining, ABT-263 treatment efficiently cleared senescent cells. Indeed, we showed that the number of SAβgal positive cells was significantly reduced at all time points in treated MGs, compared to controls (Figure 4C & 4G, Supplementary Figure 4A-C). Therefore, ABT-263 treatment could efficiently eliminate senescent cells *via* apoptosis during involution.

To further characterize the phenotype induced by ABT-263 treatment, we stained MGs with Carmine to reveal their morphology (Figure 4D, Supplementary Figure 4A & B). In control MGs, from Inv3 to Inv5, we observed the expected shrinkage of alveoli clusters, unveiling epithelial ducts, and major

adipocytes refilling of fat pad (Figure 4D, Supplementary Figure 4A & B). The ABT-263 treated MGs exhibited the same morphology as controls on Inv3 (Supplementary Figure 4A). Surprisingly, we followed the kinetic of regression of treated MGs and noticed a potential morphological defect of involution at Inv4 and Inv5, with enlarged alveoli clusters (Figure 4D, Supplementary Figure 4B).

To refine the phenotype induced by senescent cells removal, we stained MG histological sections with smooth-muscle actin (SMA), a specific marker of the mammary basal cells. This label allowed us to quantify the area of alveoli during the kinetic of involution. From Inv3 to Inv5, we showed an expected regression of alveoli size (Figure 4E, Supplementary Figure 4A & B). This shrinkage correlated with a diminution of the percentage of epithelium remaining in the tissue, from 35% of coverage per picture area at Inv3 to only 6% at Inv5 (Figure 4H). In contrast, in ABT-treated MGs, alveoli remained enlarged from Inv3 to Inv5, with more than 17% of epithelium occupying the fat pad at Inv5 (Figure 4E & H). Therefore, the kinetic of alveoli regression is slower in the ABT-263 treated MGs comparing to control.

Moreover, we characterized adipocytes refilling using adipocyte intra-membrane perilipin staining. In controls, conversely to epithelium dynamic, adipocytes were small and numerous at Inv3 and enlarged up to cover 45% of picture area by Inv5 (Figure 4F, Supplementary Figure 4A & B). In treated MGs, adipocytes number was similar to control MGs (data not shown). But the size of adipocytes and covered area were smaller on Inv5 compared to control sections (Figure 4F, Supplementary Figure 4 A & B). Therefore, the adipocytes refilling process was impaired upon ABT-263 treatment.

Taken together, our results showed that elimination of senescent cells by ABT-263 impedes the MG involution, specifically the tissue remodeling process, evidenced by slower alveoli regression and less adipocyte refilling. These results provide evidence supporting an important role of senescence induction in tissue remodeling phase of MG involution.
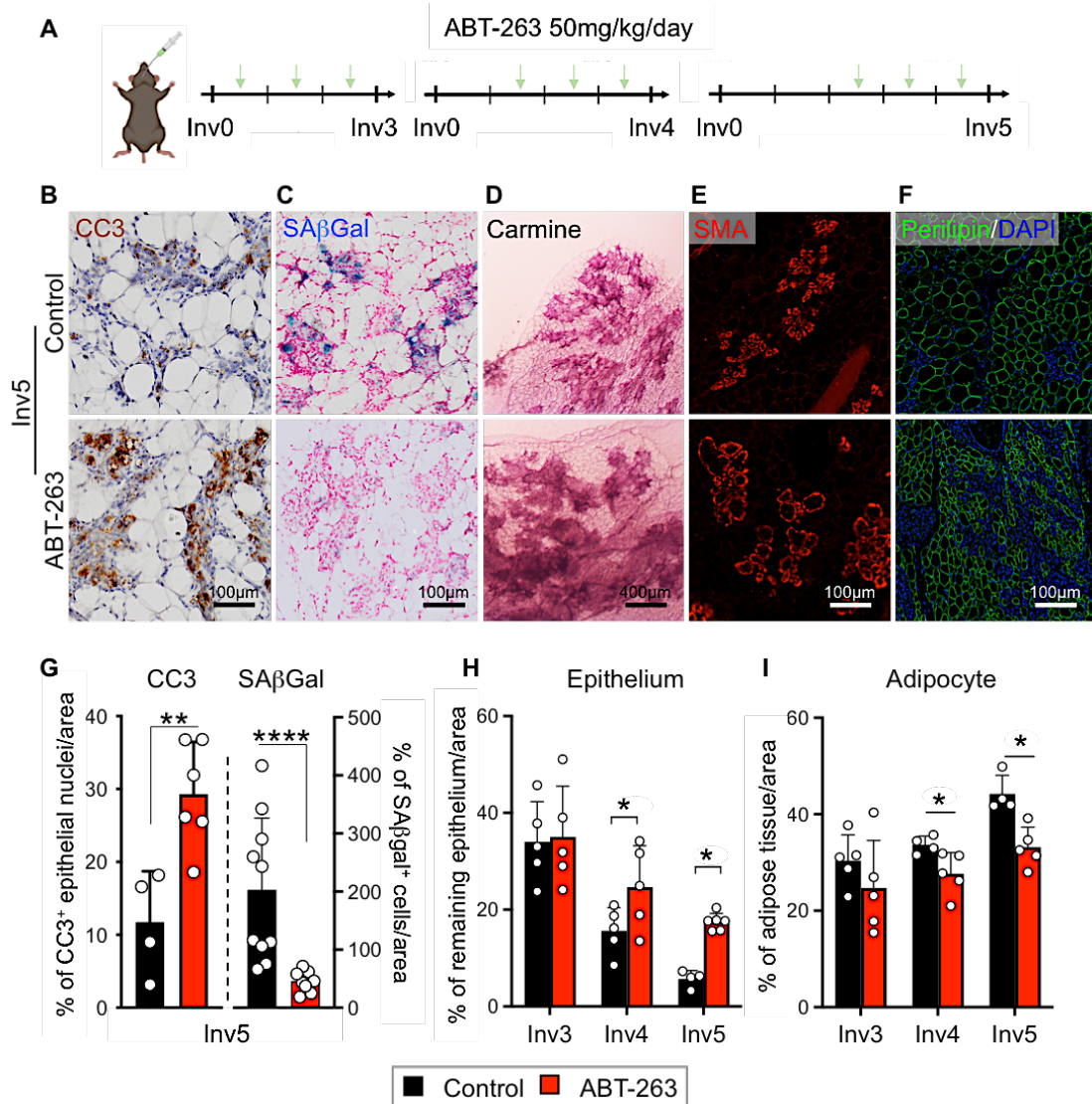
Figure 4. ABT-263 treatment specifically eliminates senescent cells and delays involution.

A. Experimental design of *in vivo* treatment with ABT-263 at 50mg.kg^{-1}.day^{-1} or vehicle only. Mice were force-feeded every day for 3 days prior to collect either at Inv3, Inv4 or Inv5. **B-F.** MG sections from control or ABT-263 treated mice at Inv5, respectively stained for (**B**) cleaved caspase 3 (CC3), (**C**) SAβGal, (**D**) Carmine, (**E**) a-SMA, and (**F**) perilipin. **G-I.** Quantification of indicated staining. (≥5 representative pictures/mouse; n≥4 per group). p-values *<0.05, **<0.01, ****<0.0001.

Removing senescent cells with ganciclovir in p16-3MR organoids delays involution-like process *ex vivo*

To consolidate the critical role of senescence and provide direct evidence of removing senescent epithelial cells on involution kinetic, we used another strategy to remove senescent cells. Since the induction of senescence correlates with p16 expression (Supplementary Figure 1C, Figure 2E & 2H), we took advantage of the p16-3MR mouse model, which induces cell death of p16 positive senescent cells upon ganciclovir treatment (Demaria et al. 2014) (Supplementary Figure. 5A). First, we showed by qPCR analysis that 3MR cassette was expressed during *in vivo* involution process, with a ~10-fold increase in Inv5 compared to Inv0 (Supplementary Figure 5B). Then, we treated mice with 50mg/kg ganciclovir (GCV) by intraperitoneal injection every day from Inv0 to Inv4 and collected glands on Inv5 (Supplementary Figure 5C). However, we did not observe a significant reduction of senescent cells, judged by the SAβGal staining, on the treated samples compared to controls (Supplementary Figure 5D). Consistently, the ratio of luminal cells remains the same in GCV treated mice at Inv5 compared to the controls (Supplementary Figure 5E). There are several potential explanations for this negative result (see Discussion).

Next, we wondered whether we could use mammary organoid, the simplified *ex vivo* system, to examine the direct consequence of removing p16$^+$ senescent epithelial cells during involution-like process. Therefore, we generated mammary organoids from p16-3MR mice and treated them with GCV *in vitro* during the involution-like process (Figure 5A). First, we confirmed by qPCR that 3MR cassette was induced by a ~15-fold from Inv0 to Inv8 (Figure 5B). Moreover, upon GCV treatment, there was a trend of decrease of the 3MR cassette expression (Figure 5B). Importantly, there was a significant reduction of endogenous p16 expression in the GCV treated organoids compared to the controls (Figure 5C). Consistently, we observed a reduction of SAβGal$^+$ cells in the GCV treated organoids (Figure 5D). Therefore, the GCV treatment could reduce the senescence induction in the involution-like organoids *ex vivo*.

Next, we evaluated the impact of removing senescent cells on the involution-like process using time-lapse imaging. At Inv0, organoids were branched forming a complex 3D structure. Consistent with our previously observation, during the involution-like process, organoids progressively lost their branched shape, recovering a circular conformation at the end of the involution process (Figure. 5D, upper panel) ([Sumbal et al. 2020](#)). However, upon GCV treatment, the morphological changes of the organoids were delayed, evidenced by persistent branching (Figure 5D-5F), suggesting a slower regression of the mammary epithelium. Taken together, we showed that removing p16[+] senescent mammary epithelial cells directly hindered the involution-like process in the *ex vivo* organoid system.
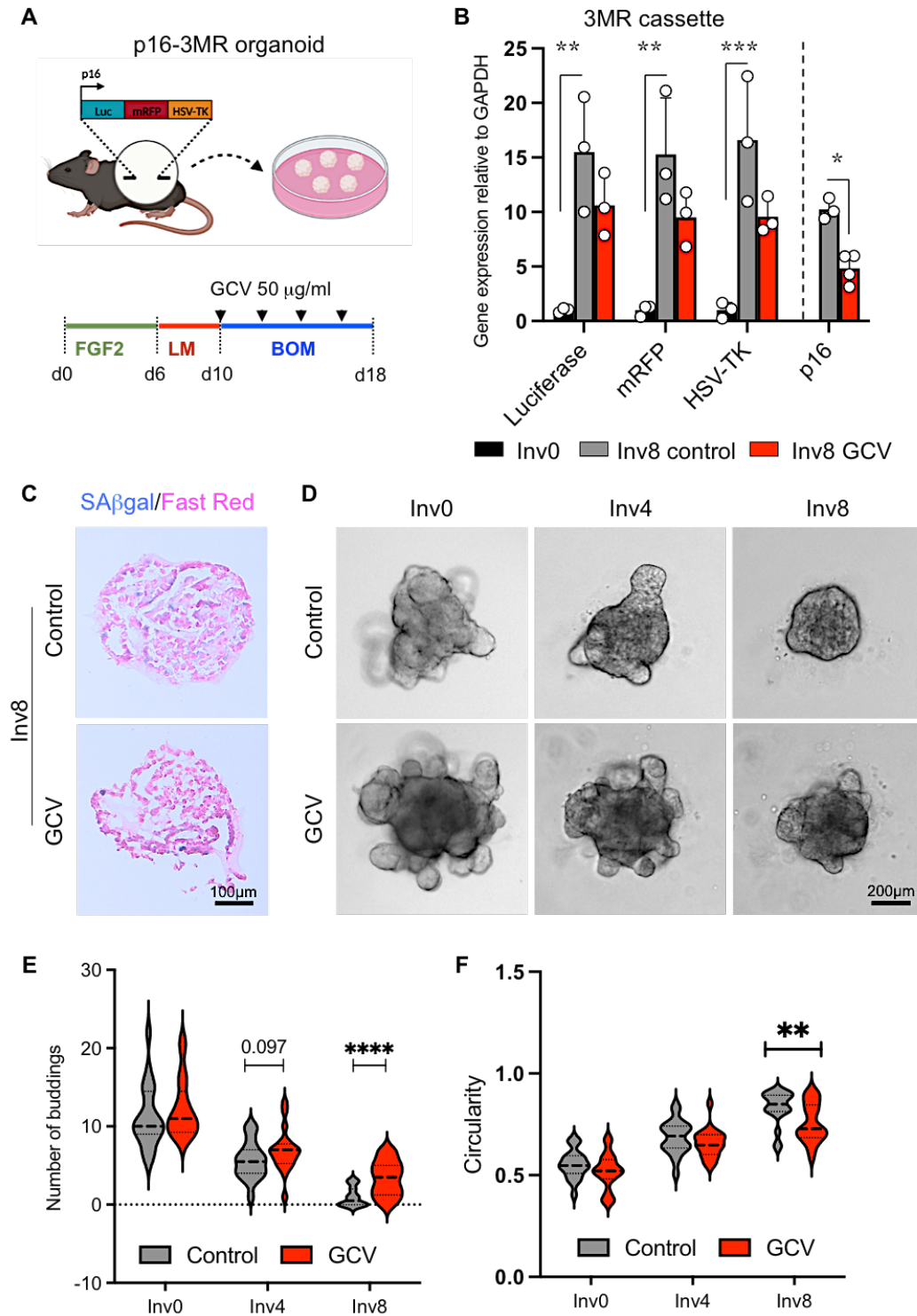
Figure 5. Removing p16+ senescent epithelial cells delays involution-like process in *ex vivo* organoid model.

A. Experimental design. Organoids from transgenic mouse model p16-3MR with integration of 3MR cassette expressing artificial Luciferase/mRFP/HSV-TK reporter, under p16 promoter regulation (upper panel). Administration of ganciclovir 50µg.ml^{-1} in BOM (GCV) or BOM only (Control), every two days

during involution-like process from Inv0 to Inv8 (lower panel). **B.** qPCR analysis of indicated genes in different conditions. **C.** SAβgal staining on cryosections of organoids at Inv8 from control (top) or GCV treated (bottom), counterstained with FastRed. **D.** Bright field images from time lapse imaging of organoids morphogenesis during involution-like process from Inv0 to Inv8, in control (top panel) or GCV treated (bottom panel). **E & F**. Morphometric analysis of (**E**) number of buddings and (**F**) organoids circularity from time lapse images; n=20 organoids/condition. p-values *<0.05, **<0.01, ***<0.005, ****<0.0001.

Overall, our study revealed that senescence is induced during MG physiological involution, coincident with the onset of tissue remodeling phase. The alveolar luminal cells are the major cell type becoming senescent, which is correlated with the upregulation of p16 expression and is independent of DNA damage. Importantly, removing senescent cells by ABT-263 treatment delays tissue remodeling process during involution. Consistently, targeting p16$^+$ senescent cells hinders the involution-like process in an *ex vivo* organoid system. Collectively, our study demonstrates, for the first time, that senescence plays a relevant role during a postnatal physiological process.

Supplementary Figures

93

A

Virgin | Pregnancy D18.5 | 10 month Multiparous | Old (nulliparous)

SAβgal/Fast Red

100μm

B

PCA2(20.20%)

- Inv0
- Inv3
- Inv7

PCA1(38.03%)

D

Inv0 | Inv3 | Inv7 | Genes

Gpnmb
Mmp12
Ifng
Cdkn2a
Ccl5
Igf1
Aldh1a3
Il7
Cxcr2
Bmp2
Bid
Trp53
Cxcl16
Ptx3
Gpr155
Ccl3
Ppp1r3c
Ccl8

Expression scale

C

HALLMARK Dataset

Inv7 vs Inv0 | Inv3 vs Inv0

INTERFERON GAMMA RESPONSE
KRAS SIGNALING UP
NOTCH SIGNALING
COAGULATION
ALLOGRAFT REJECTION
ADIPOGENESIS
EPITHELIAL MESENCHYMAL TRANSITION
UV RESPONSE DN
IL6 JAK STAT3 SIGNALING
TNFA SIGNALING VIA NFKB
WNT BETA CATENIN SIGNALING
INTERFERON ALPHA RESPONSE
APICAL JUNCTION
APICAL SURFACE
IL2 STAT5 SIGNALING
COMPLEMENT
INFLAMMATORY RESPONSE
TGF BETA SIGNALING
XENOBIOTIC METABOLISM
HEDGEHOG SIGNALING
ESTROGEN RESPONSE EARLY
HYPOXIA
MYOGENESIS
APOPTOSIS
REACTIVE OXIGEN SPECIES PATHWAY
PANCREAS BETA CELLS
GLYCOLYSIS
MYC TARGETS V2
PI3K AKT MTOR SIGNALING
HEME METABOLISM
CHOLESTEROL HOMEOSTASIS
ANDROGEN RESPONSE
MYC TARGETS V1
MTORC1 SIGNALING
PROTEIN SECRETION
UNFOLDED PROTEIN RESPONSE

NES | NES

FDR
0.05
0.04
0.03
0.02
0.01
0.00

94

Supplementary Figure 1. Transient induction of senescence during mammary gland involution.

A. SAβgal staining during MG homeostasis, pregnancy and aging. **B.** Principal Component Analysis (PCA) for involuting MGs collected at Inv0, Inv3, and Inv7. **C.** Bi-directional bar chart of hallmark gene sets, comparing Inv7 to Inv0, and Inv3 to Inv0. **D.** Heat map of RNA-seq transcriptome analysis for 18 selected senescence-associated genes (customized gene set) that are only significantly enriched in Inv7 vs. Inv0 (based on the GSEA analysis).

A — MG dissociation · Bafilomycin A1 1h · C₁₂FDG 2h · Cytometry

B

C

| Stromal cells | Basal cells | Luminal cells |

Inv0
Inv5

5.77% ±1.05 · 15.19% ±11.42 · 52.2%±8.50

C12FDG-488

D Whole mount SAβgal

D6 · D10 · D14 · D18

200μm

FGF2 · FGF2+LM · FGF2+LM+BOM · FGF2+LM+BOM

Involution-like

E SAβgal/γH₂AX

Inv3

100μm

96
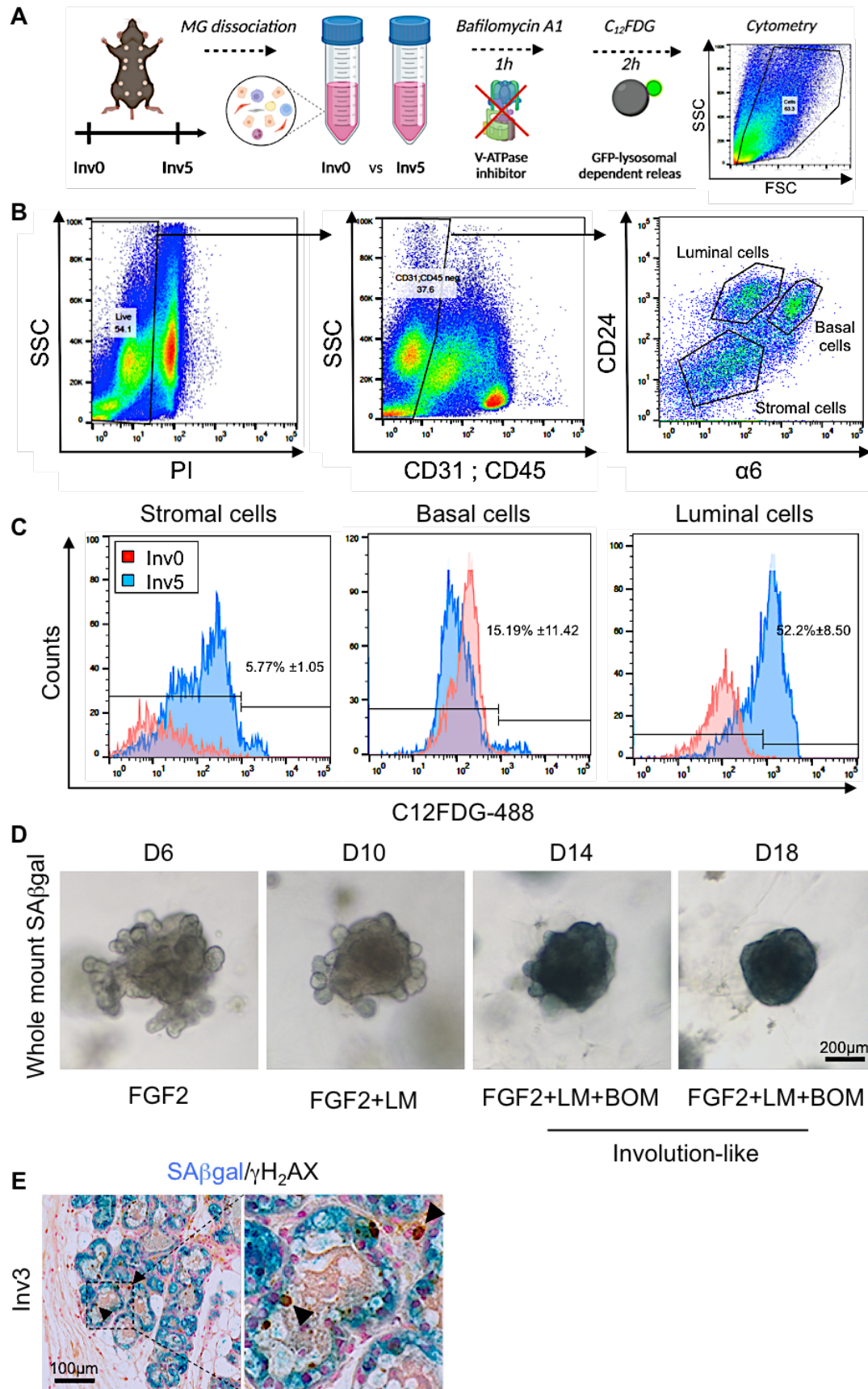
Supplementary Figure 2. Alveolar luminal cells are the major senescent cell type.

A. Experimental design of C_{12}FDG staining in dissociated involuting MGs at Inv0 and Inv5. **B.** FACS gating strategy to separate stromal, basal and luminal cells. **C.** FACS analysis of C_{12}FDG staining in stromal, basal and luminal cells, from MG of mice at Inv0 (red) or Inv5 (blue) (n=3). **D.** Whole-mount SAβGal staining of organoids at different time points indicated. **E.** Representative pictures of co-stainings SAβGal with γH2AX on WT MGs at Inv3.
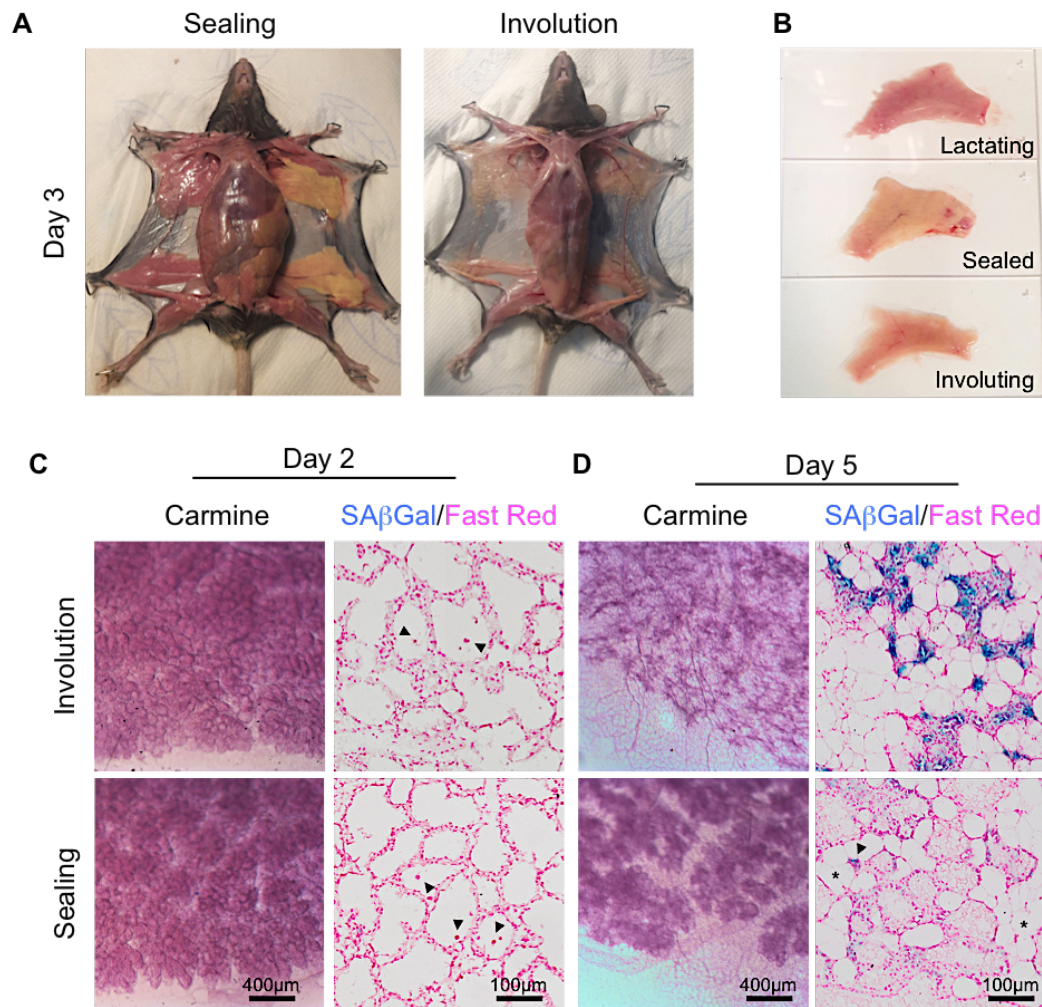
Supplementary Figure 3. Persistent lactogenic hormones prevent the induction of senescence.

A. Proper sealing controlled by typical morphology during harvesting of MGs from sealed (left) or involuting (right) mice. **B.** MGs spread out on slides after harvesting clearly exhibit milk stasis in sealed MGs. **C & D.** Left panel: Whole mount MGs after Carmine staining, magnified 5x, from involuting (top) or sealed (bottom) MGs, at day 2 (**C**) and day 5 (**D**); Right panel: SAβgal staining from involuting (top) or sealed (bottom) MGs, at day 2 (**C**) and day 5 (**D**), on cryosections, counterstained with FastRed. n≥3 per group.
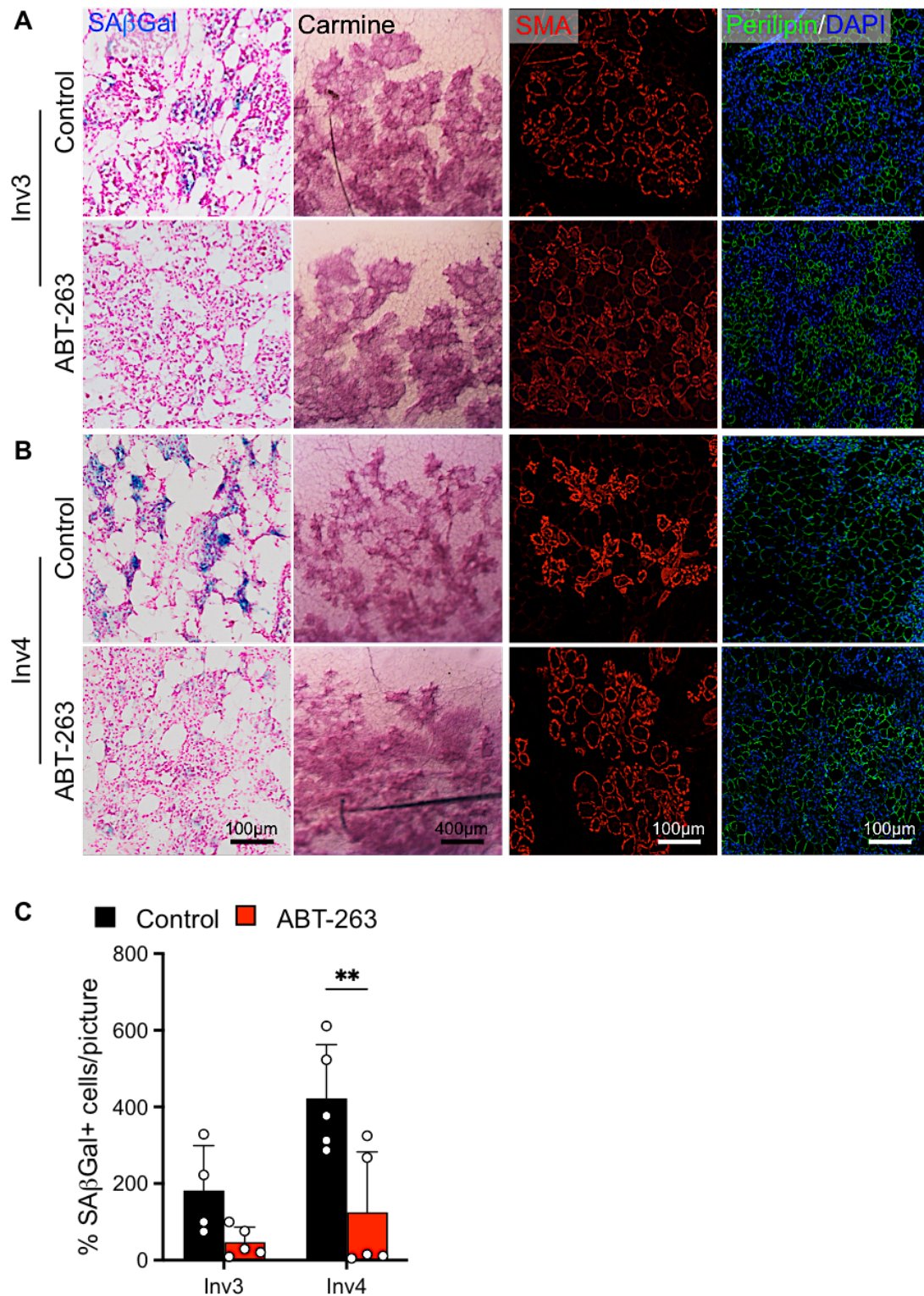
Supplementary Figure 4. ABT-263 treatment specifically eliminates senescent cells and delays MG involution.
A & B: MG sections from control or ABT-263 treated mice at Inv3 (**A**) and Inv4 (**B**), respectively stained for SAβGal, Carmine, a-SMA, and perilipin. **C.** Quantification of SAβGal staining at Inv3 and Inv4. p-values **<0.01.
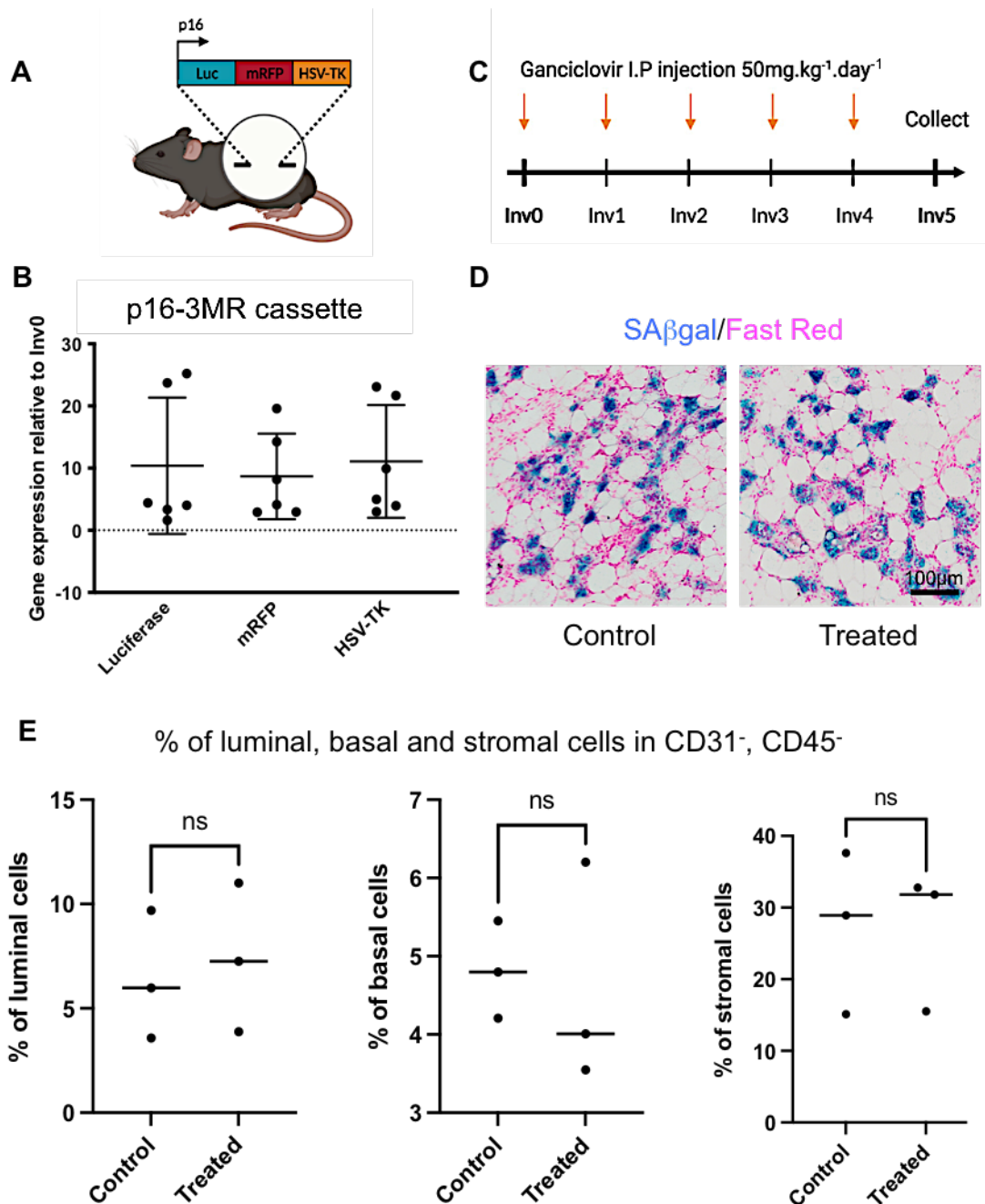
Supplementary Figure 5. Senescent cells are not efficiently removed from MG using p16-3MR mouse model.
A. Transgenic mouse model p16-3MR with integration of the 3MR reporter cassette expressing artificial Luciferase/mRFP/HSV-TK, under p16 promoter regulation. **B.** qPCR gene expression of 3MR luciferase, mRFP and HSV-TK in MG at Inv5 relative to Inv0. **C.** Design of *in vivo* administration of ganciclovir 50 mg.kg^{-1}.day^{-1} by intraperitoneal injection, every day from Inv0 to Inv4 and collect of mammary tissue at Inv5. **D.** SAβgal staining in MG from control (left) or ganciclovir treated mice (right) at Inv5, counterstained with FastRed. **E.** Quantifications of luminal, basal and stromal cells, from MG of control (left) or treated mice (right) at Inv5, counted by flow cytometry as percentage of CD31^{-}, CD45^{-} population.

Discussion

Cellular senescence is a major mechanism of cell cycle arrest associated with functional alterations, notably the acquisition of secretory-associated phenotype (SASP). Prior to our study, senescence was associated mainly with pathological processes such as aging or tumor progression, and the involvement of senescence in physiological processes remained largely unknown. Understanding when, where, and how senescence contributes to physiological processes are crucial questions to address. Indeed, senescence exhibits a plethora of roles *in vivo* that remain to be fully characterized. A better comprehension of its physiological functions might bring new insights into the pathological perspective of senescence and how to specifically target the detrimental effects associated with senescence.

MG involution is a complex process allowing the MG to return to its resting state after lactation. This process has been extensively reviewed and various mechanisms have been shown to occur in regulating MG involution, such as cell death, alveoli shrinkage, remodeling of the ECM, adipocytes refiling and immune cell clearance. With this work, we showed for the first time that senescence occurs physiologically, beyond embryonic development and tissue regeneration, during physiological MG involution. The senescence program occurs more specifically during the irreversible phase of the MG involution, to promote proper tissue remodeling.

A. Characterization of the senescence program

1. *Kinetic of MG development using SAβgal staining*

We used SAβgal staining to mark senescent cells during whole MG development. Interestingly, we showed the presence of SAβgal+ cells, appearing transiently during the irreversible phase of involution. We confirmed the senescent phenotype of these SAβgal+ cells, which were non-proliferative and non-apoptotic.

Detecting senescent cells *in vivo* remains challenging due to the lack of exclusive markers. SAβgal staining is the most widely used assay to detect senescent cells based on their extended lysosomal content. It allows the identification of the senescent cells in their native environment, which is particularly important for *in vivo* study. However, other cells with a high level of lysosomal activity, such as macrophages, can be SAβgal[+] without being senescent. Thus, we showed that only a few SAβgal cells were positive for pan-macrophage marker F4/80 (Annexes Figure 1). Therefore, SAβgal staining remains a powerful technique to detect senescent cells in the MG and has been combined with other analyses to truly identify a new senescent population during MG involution.

2. *C$_{12}$FDG optimization and identification of senescent cell types*

We optimized C12FDG staining in the mammary tissue to define precisely the senescent cell populations. As detailed in the established C$_{12}$FDG staining protocol, we used bafilomycin, an inhibitor of V-ATPase, which blocks the entrance of H^{+} into lysosomes, to decrease their acidity ([Cahu and Sola 2013](#)). Thus, we confirmed that only cells with high lysosomal content as senescent cells cleaved the C$_{12}$FDG-GFP compound, and bafilomycin incubation efficiently reduced GFP false-positive mammary cells (data not shown).

We combined C$_{12}$FDG staining with cell surface markers to identify different mammary cell populations *via* flow cytometry. As expected, in the CD31^{+}; CD45^{+} population containing endothelial and immune cells as macrophages, we detected some C$_{12}$FDG^{+}, representing ∼43% of the CD31^{+}; CD45^{+} population (Annexes Figure 1). But more importantly, in the CD31^{-}; CD45^{-} population comprising epithelial and remaining stromal cells, we detected some C$_{12}$FDG^{+} cells, especially in luminal (∼52%) and basal (∼15%) compartments. We used SAβgal staining to confirm that luminal and basal cells were also SAβgal[+] in their native environment with intact tissue architecture. Interestingly, we found a discrepancy between the number of luminal C$_{12}$FDG[+] (52%) and SAβgal[+] (91%)

cells. Indeed, $C_{12}FDG^+$ is a prominent technique to precisely define cell types in combination with cell surface markers. However, the panel of antibodies used to identify luminal cells did not distinguish between the two subpopulations of luminal cells, from ducts or from alveoli. Therefore, negative ductal luminal cells diluted the percentage of positive alveolar luminal cells. In contrast, we did not observe SAβgal$^+$ ducts in the SAβgal assay. As we manually counted the number of double-positive cells over the number of total cells in the alveolar structures, it increased the ratio of positive luminal cells. To conclude, SAβgal and $C_{12}FDG$ were outstanding techniques that, once combined, allowed us to identify senescent cells in the epithelial compartment, mostly in the alveolar luminal cell population. Interestingly, these populations are the ones mainly removed during mammary gland involution.

3. *p16 expression correlated to involution-associated senescence*

p16 and p21 are two key mediators of senescence and are often used as prominent markers to support the senescent phenotype of a cell. To assess the dynamic of senescence mediators, we performed an RNA sequencing analysis on sorted epithelial cells. We decided to analyze first the whole MG, as we planned to perform later a deep characterization of each cell population using single-cell RNA sequencing. We showed that p21 expression was increased at both RNA and protein levels at Inv1 during the first reversible phase of MG involution and did not correlate with SAβgal and $C_{12}FDG$ stainings (data not shown).

In contrast, p16 RNA expression was upregulated during the second phase of MG involution, especially at Inv7. Confirming p16 expression at the protein level was more challenging, as efficient anti-p16 antibodies were not available at the time of our study. We tried to take advantage of the p16-3MR mouse model to visualize and isolate p16$^+$ cells during involution ([Demaria et al. 2014](#)). This system contains a cassette expressing luciferase, mRFP, and HSV-TK under p16 regulation, and we showed an increased expression of the cassette at the mRNA level during MG involution. Unfortunately, the reporter cassette was not

sensitive enough to detect p16$^+$ cells, as the mRFP level remained undetectable in dissociated involuting MGs (data not shown). Indeed, induction of p16-associated mRFP during MG involution might not be as strong as in the various pathological settings in which the p16-3MR model was previously described. Therefore, we used the super sensitive reporter mouse model INKBRITE, with a GFP reporter cassette under the endogenous p16 promoter regulation, to follow p16 expression. We detected the presence of a few p16$^+$ cells in the stroma of lactating MGs. Importantly, we noticed an increase in p16 protein from Inv0 to Inv3 and Inv7, especially in luminal cells, which correlates with SAβgal and C$_{12}$FDG stainings. Therefore, we showed a strong correlation between p16 expression and the senescence program. However, it also confirmed that there is no unique marker for senescence, and multiple biomarkers should be combined to label senescent cells correctly.

4. *Deep characterization using single-cell RNA sequencing*

To deeply characterize the involution-associated senescence program, we performed a single-cell RNA seq on luminal and basal populations at different time points of involution: Inv0, Inv1, Inv3, Inv7, and Inv28. We aimed to identify inducers of senescence, define new senescent biomarkers, and detect specific SASPs upregulated in senescent cells to understand their roles in the mammary tissue. We used a MARS-seq approach, which comports more than sixty steps for sample processing. Unfortunately, we had technical issues with the quality of cDNA and their barcoding before pooling. We plan to try single-cell RNA sequencing again, this time with the 10x Genomics technique, which is much easier to use.

B. Teat sealing and senescence induction

To characterize senescence induction, we used the previously described technique of sealing ([Li et al. 1997](#)). This strategy offers the possibility to uncouple the first reversible phase of involution, triggered by milk stasis, from the second irreversible phase, induced by withdrawal of lactogenic hormones. Indeed, MGs from sealed nipples entered the first phase of involution characterized by cell death, whereas the second phase was not initiated, with the absence of tissue remodeling. We previously described the appearance of senescent cells three days after physical pups weaning. Interestingly, we did not observe senescent cells in sealed tissue on day 3, when lactogenic hormones are maintained in the system, and tissue remodeling is inhibited. Therefore, initiation of the senescence program might be closely linked to the withdrawal of lactogenic hormones and the onset of tissue remodeling. This *in vivo*-driven hypothesis is supported by the *ex vivo* organoid model developed in our laboratory ([Sumbal et al. 2020](#)) ([Charifou et al. 2021](#)). Indeed, after branching with FGF_2 and lactation using prolactin, we removed lactogenic stimulations to induce the involution of organoids. As controls, we maintained organoids in culture with prolactin stimulation. Interestingly, in organoids, milk is not expulsed from the system and accumulates with days in culture. This milk stasis and continuous lactogenic stimulation artificially mimic the sealing strategy *ex vivo*. Interestingly, in this system with the maintenance of lactogenic stimuli, we did not observe senescence induction, as in sealed MGs. Both systems support the idea that senescence induction is closely linked to the tissue remodeling phase thanks to the withdrawal of lactogenic hormones. Therefore, we aimed to find an efficient strategy to remove senescent cells during MG involution, to assess whether the senescence program was crucial for tissue remodeling.

1.   *Constitutive senescence-free mouse model Cdkn2a; Cdkn1a KO*

We illustrated that senescent cells were present during the MG involution. However, the physiological impact of senescence on MG homeostasis remains unknown. We took advantage of a genetic "senescence-free" mouse model available in our laboratory, constitutively knockout for Cdkn2a and Cdkn1a loci (abbreviated DKO thereafter), thus depleting for p16, Arf, and p21 proteins. To decipher the role of these senescence mediators in MG involution, we induced involution in the DKO mice, and we did not observe any difference in the kinetic of involution between DKO and WT (Annexes Figure 2A). We showed previously that p21 expression during involution was not associated with senescence and might be more related to apoptosis activation. We proposed that pleiotropic functions of p21, lacking in this DKO mouse model, might hide potential p16-dependent defects. Another possibility is that constitutive knock-out of these cell cycle inhibitors might be bypassed by activating redundant senescent mediators to maintain viability from early embryonic development. This hypothesis is supported by SAβgal⁺ cells still observed during the involution of MGs from DKO mice (Annexes Figure 2B). Therefore, instead of a constitutive depletion of senescence, we switched strategy by targeting the senescence program only during the MG involution process.

2.   *Senolytic treatment with ABT-263 during involution*

To further study and characterize the role of senescent cells, we established a loss-of-function system by treating mice with ABT-263 during MG involution. This senolytic is an inhibitor of anti-apoptotic Bcl-2 family proteins Bcl2, Bcl-W, and Bcl-XL and induces apoptosis of senescent cells both *in vitro* and *in vivo* (Chang et al. 2016). We showed that depleting senescent cells during the irreversible phase impaired the kinetic of involution. More specifically, tissue

remodeling was affected by the removal of senescent cells, as assessed with larger remaining alveoli and delayed adipocyte refilling. This loss-of-function approach confirmed the central role of senescence in MG tissue remodeling. However, as the mechanism of action of ABT-263 is based on inhibiting anti-apoptotic Bcl2 family proteins, ABT-263 administration might induce harmful effects by depleting other cells expressing high levels of anti-apoptotic proteins, such as platelets (Kaefer et al. 2014). Therefore, we attempted to confirm our results on the impact of senescence on tissue remodeling with a complementary strategy, using the p16-3MR mouse model.

3.   *Ganciclovir treatment in p16-3MR mice/organoids*

As we showed a strong correlation between p16 expression and involution-associated senescence, we decided to take advantage of the p16-3MR genetic mouse model available in the laboratory. Indeed, this system induces apoptosis of p16$^+$ cells upon ganciclovir administration (Demaria et al. 2014). Interestingly, as p16 was expressed during involution, we detected an associated increased expression of the 3MR cassette. However, we failed to target p16$^+$ cells efficiently with this system (Supplementary Figure 5). This can be explained by the non-optimal concentration of GCV or unsuitable ways of administration to target MG. Therefore, we would like to continue to explore the p16-3MR mouse model and find an efficient method to clear senescent cells *in vivo*. However, using the reporter INKBRITE mouse model, we showed that some non-senescent cells were also p16$^+$, especially in the stromal compartment. It raises the concern that eliminating p16+ cells in vivo might also trigger non-senescent cells and interfere in biological processes independent of senescence. To overcome this constraint, we decided to produce organoids from p16-3MR virgin mice, as organoids originate purely from the epithelial compartment, and to treat them with GCV *ex vivo* during the organoid involution. We showed a delay in the involution-like process when senescent cells were depleted from the system, with more remaining buddings. This phenotype consolidated our hypothesis that senescence was primordial for proper tissue remodeling. Moreover, whereas

previous data established a strong correlation between p16 expression and senescent epithelial cells, this system confirmed that senescence was p16-dependent *ex vivo*.

4. *Long-term effects of senescence removal*

Strikingly, when we administrated ABT-263 for a short period of only three days, we saw a delay in the kinetic of involution. We also tried to assess the impact of long-term ABT-263 treatment by drug administration from Inv3 to Inv9 and MG harvest at Inv10. The delayed phenotype observed at Inv5 was not noticeable anymore and treated MGs recovered to exhibit a completed process at the end of the involution (Annexes Figure 3). This result was not surprising, as the MG involution process is very dynamic. In many knockout mouse models, depletion of key mediators of involution delayed MG involution, but compensatory mechanisms restored a normal phenotype at the end of the process (Radisky and Hartmann 2009). We are now interested in the consequences of removing senescent cells during involution in subsequent pregnancies. Indeed, even if the morphology of the MG might not be impaired at the end of the involution process after senescent cell removal, the plasticity of the whole tissue might be reduced and impact the development of the gland in the next reproductive cycle. This hypothesis could also be assessed *in vitro* by multiple re-seeding of GCV-treated organoids to mimic subsequent pregnancy-lactation-involution cycles and evaluate the remodeling while senescent cells are removed.

5. *Senolytics versus senomorphics and senoinducers*

We targeted senescent cells using two strategies: senolytic ABT-263 and GCV administration in p16-3MR mice. However, both approaches are similar conceptually, as they induce senescent cell apoptosis. This massive cell death induction could be detrimental to the tissue. Indeed, as lots of cells are removed at once, it can be detected as critical stress and might impair tissue integrity.

Therefore, instead of using senolytics, it can be interesting to use senomorphics. These drugs target the effects of senescent cells *via* the inhibition of their SASP, without killing them and disrupting the organization of the tissue.

Another interesting approach would be to do a gain-of-function system. Senoinducers such as Palbociclib, an inhibitor of cyclin-dependent kinases CDK4 and CDK6, are compounds with the ability to induce senescence ([VanArsdale et al. 2015](#)). As senescent cell removal delayed MG involution both *in vivo* and *ex vivo*, we would like to increase the number of senescent cells and assess the kinetic of involution. From this experiment, we might observe a diversity of phenotypes. Indeed, in opposition to the senescence removal experiments, an increased number of senescent cells might accelerate the kinetic of regression, which could be measured by smaller alveoli and accelerated adipocyte refiling. However, the number of senescent cells is already high at Inv3. This level might already be optimal, and adding more senescent cells might not affect the effective progression of involution. Another interesting approach would be to induce senescent cells when they are not present yet in the tissue. We showed that senescence was closely associated with tissue remodeling during the second phase of involution. By using senoinducers during the first phase of involution, the presence of senescence might be sufficient to initiate remodeling, reinforcing the causative link between senescence and tissue remodeling.

D.   Proposed roles of senescence in MG

We demonstrated a close link between senescence and tissue remodeling during mammary gland involution. However, this tissue-remodeling phase is a sum of various intricate processes, such as removing epithelial cells concomitant with adipocyte refilling, restructuring the extracellular matrix, and recruiting immune cells for clearance of cells and debris.

By depleting senescent cells with ABT-263, we showed a delay of involution with more remaining epithelial cells, which correlated with slower adipocyte refilling. Adipocyte refilling can be either a passive phenomenon to fill emptied space in the fat pad or an active phenomenon helping alveoli shrinkage. We proposed that senescent cells might secrete SASPs promoting adipocyte refilling. To test this hypothesis, we successfully established an *in vitro* model of adipogenic differentiation using sorted mammary Pdgfr-α^+ cells, precursors of fibroblasts, and adipocytes (Annexes Figure 4). GFP$^+$ cells were isolated from a Pdgfr-α-GFP mouse model, and as previously described, we induced differentiation using an adipogenic cocktail of dexamethasone, IBMX, and insulin ([Joshi et al. 2019](#)). We would like to test the effect of conditioned medium collected from non-senescent or senescent cells to assess whether SASPs could promote adipogenic maturation and accelerate the filing of lipids.

During the tissue-remodeling phase of mammary involution, numerous compounds are secreted to degrade the extracellular matrix (ECM), such as matrix metalloproteinases (MMPs). It is also well exemplified that in the SASPs factors produced by senescent cells, many regulate the composition and the organization of the extracellular matrix ([Mavrogonatou et al. 2019](#)). Therefore, we wondered whether senescent cells are helping the remodeling of mammary tissue *via* ECM reorganization. As we detected senescent cells in the epithelial compartment, specifically during the second phase of involution, we performed RNA sequencing on epithelial cells at Inv1 and Inv7. Interestingly, we showed a significant up-regulation of tissue remodeling and matrix disassembly gene ontology biological processes (GOBPs) (Annexes Figure 5). We are now interested in finding in our RNA seq data specific candidates secreted by senescent cells, which could explain part of their impact on tissue remodeling during MG involution.

SASP factors are also usually composed of various cytokines and chemokines ([Coppe et al. 2010](#)). During the tissue-remodeling phase of involution, there is an influx of immune cells recruited to remove dead cells and debris. Therefore, we hypothesized that senescent cells present during MG involution might promote

immune cell recruitment. In MGs treated with ABT-263, we assessed the number of different types of immune cells. Interestingly, we showed a decrease in the number of total mammary macrophages, and ductal macrophages in MGs depleted for senescent cells (Annexes Figure 6). This phenomenon could be due to delayed involution, where immune cell influx might be passively lagged. However, it could also reflect the active recruitment of immune cells by senescent cells, lacking in ABT-263 treated glands. To assess this question, we would like to test whether sorted mammary senescent cells can chemoattract macrophages *in vitro.* Moreover, we could use compounds to induce senescence during the first phase of involution and evaluate if the presence of senescent cells is sufficient to recruit immune cells earlier *(See "Senolytics versus senomorphics and senoinducers" for further details).*

How mammary stem cells maintain their stemness through reproductive cycles is not fully understood. It has been shown recently that senescence, *via* ectopic expression of Rank in the luminal cells of virgin MG, promotes stemness properties of both basal and luminal populations ([Benitez et al. 2021](#)). Therefore, we could assume that physiological senescence associated with involution might protect mammary stem cells by increasing their stemness before a new development cycle. To test this hypothesis, we would like to take advantage of the mammosphere assay, an *in vitro* technique to quantify stem cells in the mammary tissue and evaluate their self-renewal capacity ([Shaw et al. 2012](#)). We propose to collect conditioned medium from sorted luminal cells at Inv0 (non-senescent) and Inv7 (senescent), culture mammospheres in both conditions, and assess any difference in the number of mammary stem cells or their stemness when cultured in senescent conditioned medium.

E.   Fate of senescent cells

At the end of the involution process, we did not detect SAβgal$^+$ cells suggesting that senescence induction was transient. It correlated with the fact that short-

term senescence is associated with beneficial processes, as in embryonic development. In contrast, the persistence of senescent cells in tissues is associated with pathological conditions. However, how senescent cells are removed from the tissues remains unclear. One assumption could be that senescent cells are removed through apoptosis. However, it is well described that senescent cells up-regulate intrinsic pathways to resist apoptosis (Childs et al. 2014). Another hypothesis is that senescent cells might be eliminated through immune cell clearance, primarily *via* macrophages. Indeed, evidence shows that immune cell-mediated response is critical in senescent cell clearance. To validate this hypothesis, we proposed to deplete macrophages and quantify the number of senescent cells not cleared from the tissue. We successfully established a model of macrophage depletion during involution using clodronate liposomes (Van Rooijen and Sanders 1994). As previously described using a transgenic MAFIA mouse model inducing macrophages apoptosis, we also showed a delay of involution upon macrophages depletion with clodronate liposomes (Annexes Figure 7). We would like to measure senescence levels in MGs depleted for macrophages. Moreover, we will take advantage of the *in vitro* system to analyze interactions between sorted senescent cells and immune cells *(See "Proposed roles of senescence in the mammary tissue" for further details)* to see if chemoattracted macrophages can engulf senescent cells.

F.   Pathological perspectives of involution-associated senescence

It is well established that pregnancy and involution transiently increase the risk of breast cancer. Postpartum breast cancer (PPBC), defined as breast cancer diagnosed within ten years of most recent childbirth, accounts for over half of all breast cancers diagnosed in women under age 40. Notably, PPBC exhibits increased rates of metastasis and poorer long-term survival compared to non-PPBC, highlighting a cancer-promotional microenvironment explicitly associated

with the postpartum period ([Schedin 2006](#)). Concomitantly, it is well described that senescent cells promote tumorigenesis in a paracrine manner *via* their SASP ([Faget, Ren, and Stewart 2019](#)). Therefore, we hypothesized that the involution-associated senescence might promote initiation, progression, and metastasis of PPBC. Indeed, in a paracrine manner, senescent cells might secrete SASPs factors during involution, contributing to the pro-inflammatory microenvironment and promoting proliferation and plasticity of pre-existing pro-tumoral cells. Interestingly, postlactational involution, in which the senescence program is crucial, is associated with an increased risk of PPBC. In contrast, lobular involution related to aging of the reproductive capacity, in which we did not detect senescent cells, correlates with a decreased risk of developing breast cancer ([Radisky and Hartmann 2009](#)).

This exciting pathological perspective of involution-associated senescence is explored in another project in our laboratory. Using a breast cancer mouse model and our *ex vivo* 3D organoid culture system, we aim to investigate how senescent cells might induce plasticity of existing pre-cancerous cells. Moreover, we established a partnership with Paris Curie Institute to obtain samples from PPBC patients, to measure the number of senescent cells in cancerous mammary tissue. Linking involution-associated senescence characterized in this Ph.D. project to PPBC might unravel new mechanisms involved in PPBC emergence and enlarge therapeutic options for women affected by PPBC.

Annexes Figures Discussion

A. SAβgal / F4/80

Inv5

B.

Histogram

56,8%   43,2%

$C_{12}FDG^-$ $C_{12}FDG^+$

$C_{12}FDG$-GFP
in CD31⁺ CD45⁺
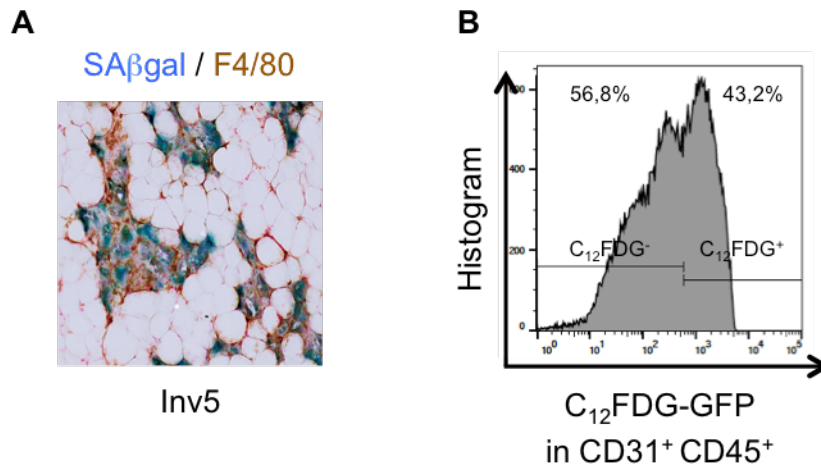
Annexes Figure 1. A. Co-staining SAβgal and F4/80 at Inv5. **B.** FACS analysis of $C_{12}FDG$ staining in CD31⁺, CD45⁺ population (immune and endothelial cells), from MG at involution day 5.

A Whole mount Carmine
Inv5 WT   Inv5 DKO

B Wholemount SAβgal
Inv5 WT   Inv5 DKO
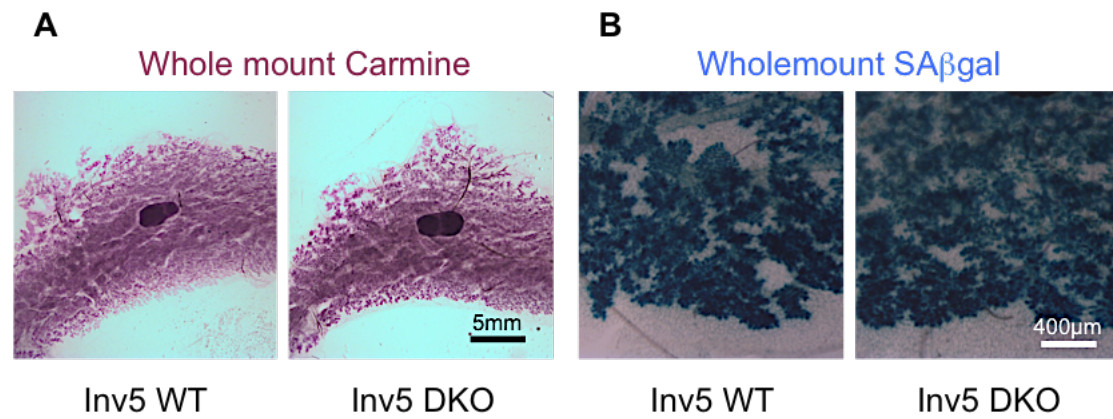
Annexes Figure 2. A. Whole mount MGs after Carmine staining from wild-type mouse (WT, left) or CDKN2A, CDKN1A double knockout (DKO, right), at involution day 5. **B.** Whole mount MGs after SAβgal staining, from wild-type mouse (left) or double knock-out (right), at involution day 5.
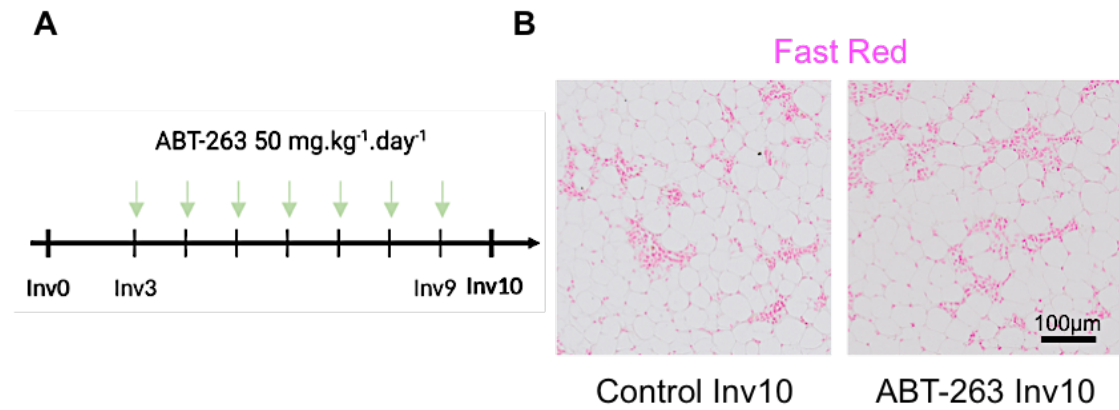
Annexes Figure 3. A. Design of *in vivo* treatment with ABT-263 at 50mg.kg^{-1}.day^{-1} or vehicle only. Mice were force-feeded every day from Inv3 to Inv9 prior to collect at Inv10. **B.** Fast Red staining from control or ABT-263 treated mice at Inv10.
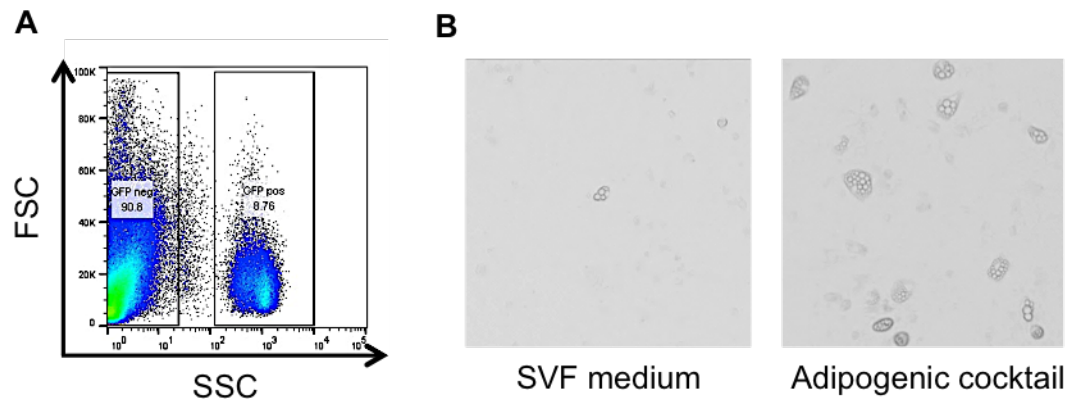
Annexes Figure 4. A. Flow cytometry panel of PDGFRα-GFP⁺ cells from dissociated virgin MGs. **B.** Pictures of adipocytes derivated from isolated PDGFRα-GFP⁺ cells, after 5 days of spontaneous differentiation (SVF medium) or after 3 days in an adipogenic cocktail of dexamethasone, IBMX and insulin, followed by 2 days of recovery in SVF medium.
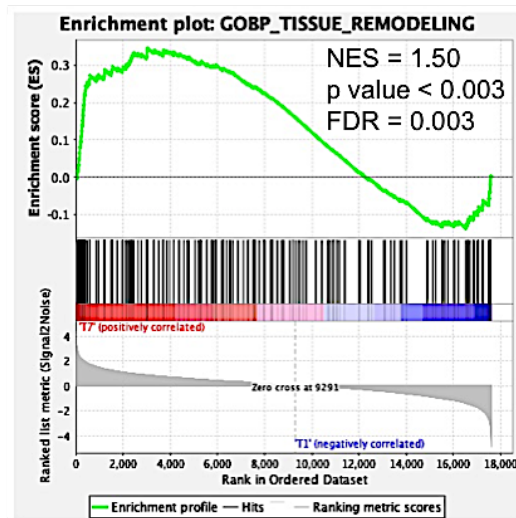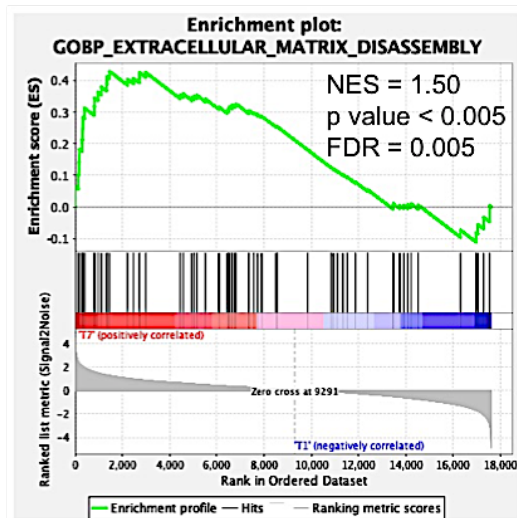
Annexes Figure 5. A-B. Enrichment plots of GOBP tissue remodeling **(A)** and GOBP extracellular matrix disassembly **(B)** in isolated epithelial cells, at Inv7 versus Inv1.
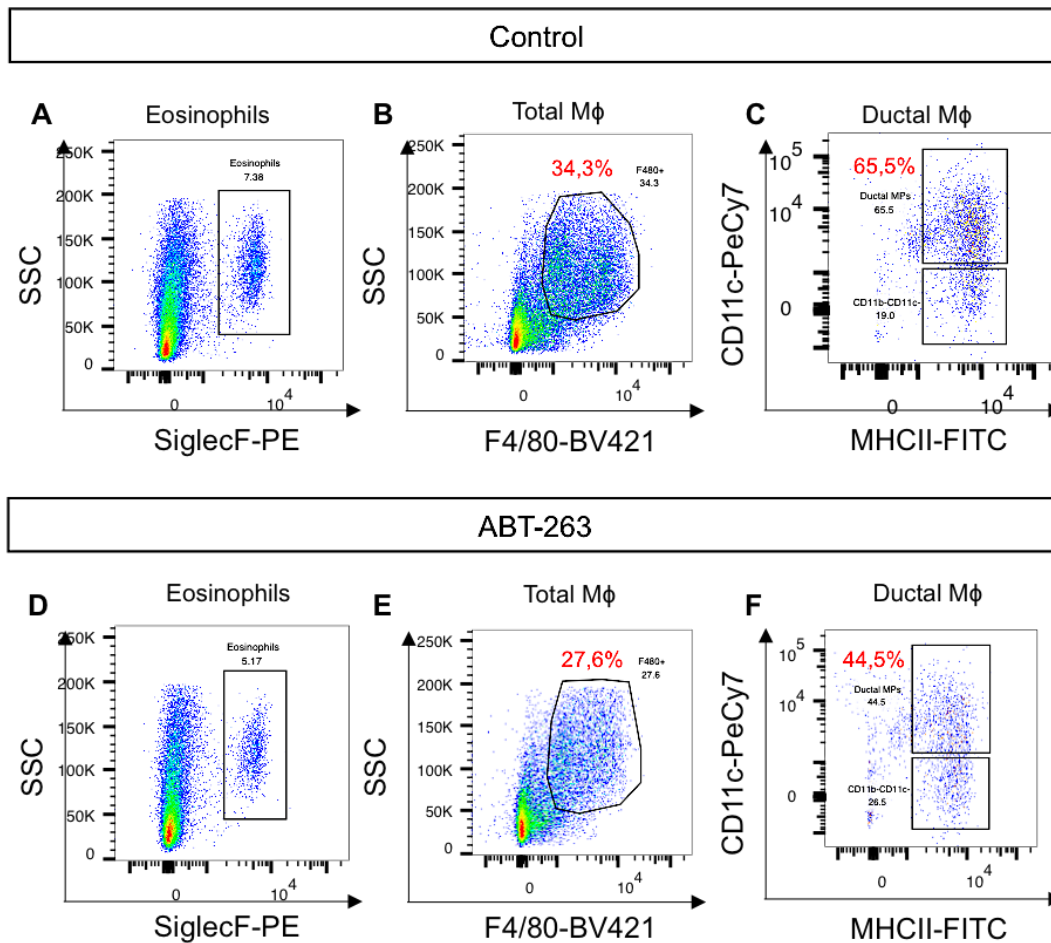
Annexes Figure 6. A-F. Flow cytometry analysis of dissociated MGs from control **(A-C)** or ABT-263 treated **(G-I)** MGs at Inv5. Cells were analyzed from the CD45^{+} population (immune cell fraction). **A.** and **D.** SSC/SiglecF from CD45^{+} population to isolate eosinophils. **B.** and **E.** SSC/F4/80 from CD45^{+} population to isolate total macrophages population. **C.** and **F.** CD11c/MHCII from CD45^{+} ; F4/80^{high} ; CD11b^{low} population to isolate ductal CD11c^{high} ; MHCII^{high} macrophages.
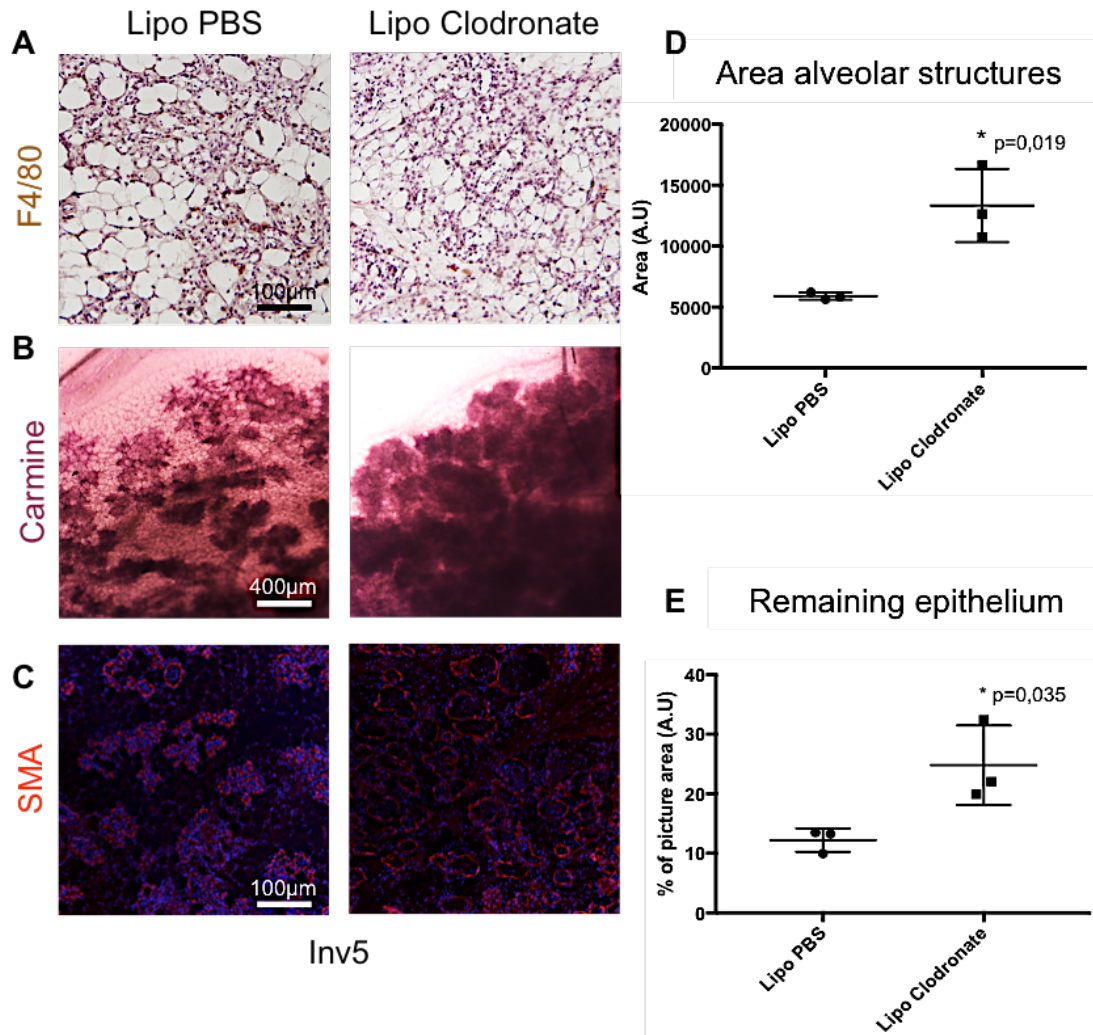
Annexes Figure 7. A. F4/80 staining in MGs from control (Lipo PBS) or from mice injected with liposomes containing clodronate (Lipo Clodronate) at Inv5. **B.** Whole mount MGs after Carmine staining, magnified 5x, from control (left) or clodronate (right) treated mice at Inv5. **C.** MG sections from control (left) or clodronate (right) treated mice at Inv5 stained for SMA. **D-E.** Quantifications of pictures stained with SMA, representing the mean area of alveolar structures **(D)** and the total coverage of epithelium per picture **(E)** (≥5 representative pictures/mouse; n=3 per group).

Material and Methods

A. Mice models

1. *Authorizations and genotypes*

Experiments involving animals were approved by French legislation in compliance with European Communities Council Directives (A 75-15-01-3) and the regulations of Institut Pasteur Animal Care Committees (CETEA). Wild-type inbred strain C57BL/6J mice were bred at the Monod Animal Facility of the Institut Pasteur. p16-3MR mouse model was obtained from J. Campisi's laboratory (Demaria et al. 2014). INKBRITE mouse model was kindly provided by Dr. Peng's laboratory. Pdgfrα^{EGFP} were obtained from The Jackson Laboratory (JAX mice number #007669).

2. *Standardization and synchronization of involution*

To study MG involution, adult virgin females were mated between 8 to 10 weeks old. To homogenize lactation stimuli, litters were evenly distributed to 6 pups per female after birth and fed by the mother for ten days. Then, pups were physically separated to allow a synchronized involution of MGs. The day of removal of the progeny was considered as the beginning of involution, also called involution day 0 or Inv0. The involution process was let to progress from Inv0, for which mice were euthanized right after offspring removal, to 1, 2, 3, 4, 5, or 7 days of involution (respectively named Inv1, Inv2, Inv3, Inv4, Inv5, Inv7) up to the end of the process 14 days after the initiation (Inv 14).

3. *Mammary glands harvesting and processing*

Mice were euthanized by cervical dislocation, and specific mammary glands were collected, respectively: MG #2L for RNA; MG #3L for wholemount SA-β-Gal staining; MG #3R for OCT cryopreservation; MG #4L for formalin fixation; MG #4R for methacarn fixation.

a) *OCT cryopreservation*

MGs were embedded in OCT to obtain cryosections. Tissues were placed in OCT cassettes right after harvesting, covered by tissue freezing medium [Leica #14020108926] and kept at -80°C until cutting. Frozen samples were cut using a cryostat and slices of 10µm were spread on SuperFrost glass slides and kept at -80°C for further stainings.

b) *Formalin fixation*

MGs were spread on glass slides and fixed overnight in a solution of formalin 10%. After 16h at room temperature, tissues were briefly washed in Phosphate-Buffered Saline (PBS) and dehydrated with ethanol (successive 45 min baths, increasing concentration of ethanol, 50%; 70%; 95% and twice 100%). Samples were then transferred in cassettes and disposed into two baths of 1h of xylenes before a mix of 50/50 xylenes/paraffin during 1h at 65°C. Then, the cassettes were placed in a first solution of 100% paraffin for 1h at 65°C, and in a second bath of pure paraffin for an overnight at the same temperature. The next day, samples were embedded in paraffin and kept at room temperature to solidify. Embedded tissues were cut using a microtome and slices of 5µm were disposed on SuperFrost glass slides for further stainings.

c) *Methacarn fixation*

MGs were spread on glass slides and fixed overnight in a solution of methacarn (60% methanol; 30% chloroform; 10% acetic acid) before being processed for Carmin coloration (see Whole mount Carmin). Tissues were then washed and dehydrated as described for formalin fixed samples and embedded in paraffin.

B.   Histological and immunohistochemical analysis

1.   *Whole mount Carmin*

Straight away after harvesting, mammary glands #4 were fixed overnight in methacarn. After 16h of incubation, MGs were washed twice in EtOH 70%, once in H_2O, and incubated overnight in Carmin Alum staining [Stem Cell Technologies #07070] at room temperature, protected from light in aluminum covers. MGs were then washed twice in EtOH 70% and processed as Formalin samples to be embedded in paraffin. During the second clearing with xylenes, pictures of whole mounts stained MGs were taken using a binocular magnifier (zoom-in x0.7 and x5) before the embedding to obtain a global histology of MGs.

2.   *Deparaffinization*

Formalin or methacarn fixed samples were embedded in paraffin and sliced at 5µm as described. Paraffin was removed prior to any staining by using successive 5 min baths of: xylenes twice, and decreasing concentration of ethanol from EtOH 100% to EtOH 50%. Finally, slides were washed in H_2O and PBS.

3.   *Hematoxylin and Eosin H&E*

After deparaffinization, sections were stained in hematoxylin for 5 to 10 min and washed with tap water for 5 min to mark nuclei in purple. Sections were then stained with eosin for 2 to 5 min and rinsed in PBS to mark cytoplasm and extracellular matrix in pink. The intensity of each staining was checked under the microscope before washing. Tissues were finally dehydrated with one 5 min bath of EtOH 95%, two 5 min baths of EtOH 100% and dried for 30 sec under a laminar flow hood before mounting with Eukit.

C. Immunohistochemistry and immunofluorescence

For immunohistochemistry, prior to the blocking step, an inhibition of endogenous peroxidase was performed using H_2O_2 1% during 10min. After secondary antibodies incubation, tissue sections were then counterstained with Hematoxylin, dehydrated and mounted with Eukitt.

For immunofluorescence, after secondary antibodies incubation, nuclei were stained during 15min with DAPI (1g/mL in H_2O) in the corresponding blocking solution, washed in PBS and mounted with Immu-Mount.

Primary antibody	Antigen retrieval	Dilution	Secondary antibody
CC3 (Asp175) (IHC) [Cell Signaling #9661T]	Acid pH=6,0	1:200	Anti-rabbit
F4/80 (IHC) [Biorad #MCA497]	No retrieval	1:100	Anti-rat
GFP (IF) [Abcam #13970]	No retrieval	1:200	Anti-chicken
Gamma H2AX (IHC) [Cell Signaling #80312S]	Acid retrieval	1:200	Anti-mouse
Gamma H2AX (IF) [Cell Signaling #80312S]	No retrieval	1:200	Anti-mouse
Ki67 (IHC) [Abcam #15580]	Acid pH=6,0	1:200	Anti-rabbit
KRT5 (IHC) [Biolegend #905501]	Acid pH=6,0	1:200	Anti-rabbit
KRT8 (IHC) [Abcam #59400]	Acid pH=6,0	1:200	Anti-rabbit
KRT5 (IF) [Biolegend #905501]	Acid pH=6,0	1:200	Anti-rabbit
KRT8 (IF) [Biolegend #904801]	Acid pH=6,0	1:100	Anti-mouse
Perilipin (IF) [Abcam #61682]	No retrieval	1:200	Anti-goat
SMA (IF) [Sigma #A5228]	No retrieval	1:200	Anti-mouse

1. *SAβGal staining on sections*

Slides of 10μm OCT cryopreserved MGs were removed from -80°C storage and dried at room temperature for 30 min. Samples were fixed in a fixation solution of PFA 2% and glutaraldehyde 0.2% in PBS at room temperature during 15 min. After three PBS washes of 5 min, MGs were incubated 6h at 30°C in a SAβGal solution containing 40mM of citrate buffer pH 6,0; 5mM of $K3Fe(CN)_6$; 5mM of $K4Fe(CN)_6$; 2mM of $MgCl_2$; 150mM of NaCl ; 0.1% of NP40 ; 0.5mg/mL of X-gal [Euromedex EU0012] and MQ water. After incubation, samples were washed in PBS, post-fixed in PFA 4% for 15 min and washed again in PBS. Tissue sections were then counterstained with Nuclear FastRed [Vector H-3403] for 2 to 5 min (checked under the microscope for a good contrast), dehydrated by one 5 min bath of EtOH 95% and two 5 min EtOH 100% baths before mounted with Eukitt [Sigma Aldrich #49629].

2. *SAβGal staining on whole mount MGs*

Straight away after harvesting, MG #3 were incubated in a fixation solution of PFA 2% and glutaraldehyde 0.2% in PBS at room temperature during 30min, on a swing. After brief washes in PBS, mammary glands were incubated overnight at 30°C in the SAβGal solution (see SAβGal staining on sections). After 16h of incubation, samples were washed in PBS, and post-fixed during 8h in 10% formalin on a swing. Then, MGs were briefly washed in PBS, dehydrated and embedded in paraffin as described for formalin fixed samples. Tissue sections were then counterstained with Nuclear FastRed [Vector H-3403] for 2 to 5 min (checked under the microscope for a good contrast), dehydrated by one 5 min bath of EtOH 95% and two 5 min EtOH 100% baths before mounted with Eukitt [Sigma Aldrich #49629].

3. *OilRedO staining*

Slides of 10μm OCT cryopreserved MGs were removed from -80°C storage and dried at room temperature for 30 min. Sections were fixed in a fixation solution

of PFA 2% and glutaraldehyde 0.2% in PBS at room temperature during 15 min. After successive 5 min washes in PBS, MQ water, and isopropanol 60%, tissue sections were stained for 15 min with a OilRedO solution [Sigma Aldrich #O1391], freshly diluted with water and filtered before use. Then, sections were rinsed with isopropanol 60%, MQ water, PBS, glycerol 50% in PBS, and mounted in glycerol 50% in PBS right before imaging.

For Oil RedO staining on plated cells, wells were washed in PBS before fixation. Cells were then processed as tissue sections, and imaged after the last washing in PBS.

D.   Flow cytometry

1.   *Isolation of mouse mammary cells*

For each mouse, MGs #2, #3, #4 and #5 were collected and minced before an enzymatic digestion for 1h30 at 37°C, shaking 120rpm, in a solution containing 3mg/mL Collagenase A [Roche #10103586001]; 100U/mL Hyaluronidase [Sigma #H3884] in CO_2-independent medium [Gibco #18045-054], completed with 5% FBS, 2mM L-glutamine [Sigma Aldrich #G5792] and   100 U/mL of penicillin + 100 µg/mL of streptomycin [Gibco, #15140-122]. Digested tissues were centrifuged 5 min at 1100 rpm and the supernatant was discarded. After a wash with CO_2-independent medium and a centrifugation, each pellet was resuspended with 2mL of prewarmed PBS + 0.25% trypsin [Dutscher #P10-022100] and 0.1% EDTA Versen [Biochrom #L2113], for 1 min at RT. After a second wash in CO_2-independent medium + 5% FBS and a centrifugation, each pellet was resuspended in 2ml of CO_2-independent medium + 5% FBS containing 5mg/mL of dispase II [Roche #13752000] and 0.1mg/mL of DNAse I [Sigma Aldrich #D4527-40KU], and incubated 5 min at 37°C. After a third wash in CO_2-independent medium + 5% FBS and a centrifugation, pellets were resuspended in 2mL of cold ammonium chloride solution [Stem Cell Technologies #07800] and immediately centrifuged. After a resuspension in CO_2-independent medium

+ 5% FBS, cell solution was filtered through a nylon mesh cell strainer with 40μm pores before immunolabeling and cell sorting.

2. $C_{12}FDG$ staining

Following suppliers' guidelines, Bafilomycin A1 [Tebu #21910-2060] was resuspended in DMSO to a concentration of 0.1mM and stored at -20°C and $C_{12}FDG$ [Fisher #11590276] was resuspended in DMSO at a concentration of 20mM and stored at -20°C. After mammary cells dissociation, pellets of isolated cells were resuspended into 1mL of CO_2-independent medium [Gibco #18045-054]. To neutralize acidic pH of lysosomes, cells were treated with 100nM of Bafilomycin A1 for 1h at 37°C, 5% CO_2. Upon use, $C_{12}FDG$ 20mM stock was first diluted with DMSO to a temporary stock of 2mM in fresh culture media, and added to the cell solution at a concentration of 33μM. Cells were incubated 2h at 37°C, 5% CO_2 (eppendorf tubes were manually inverted every 30 min to homogenize the solution). After incubation, cells were washed twice with CO_2-independent medium and centrifuged 5 min at 1100 rpm. Resuspended pellets were then stained with antibodies compatible with the GFP-emitted signal from $C_{12}FDG$.

3. Stainings of isolated mammary cells for FACS

Freshly dissociated mammary cells were incubated at 4°C for 30min, out of direct light, with a combination of antibodies directly conjugated for flow cytometry. After incubation, cells were washed twice with CO_2-independent medium. Labeled cells were sorted using a MoFlo Astrios EQ [Beckman Coulter] and data were analyzed with FlowJo software.

Antibodies used for flow cytometry analysis: anti-CD45-APC 1:100 [Biolegend #103112, clone 30-F11]; anti-CD31-APC 1:100 [Biolegend #102510, clone MEC13.3]; anti-CD24-BV421 1:50 [Biolegend #101826, clone M1/69]; anti-α6-PE.Cy7 1:50 [Biolegend #313622, clone GoH3.

For immune cells, this mix of antibodies was kindly prepared from an immunology laboratory: anti-CD45-BUV395 1:100; anti-CD64-BV711 1:100; anti-F4/80-BV421 1:50; anti-MHCII-FITC 1:200; anti-SiglecF-PE 1:100; anti-CD11c-PE-Cy7 1:100; anti-CD206-APC 1:100; anti-CD11b-AF700 1:100.

E.   RNA extraction and RT-qPCR

Total RNAs were extracted from tissues using microbeads, two cycles of cell lysis [PreCellys24 Bertin] and TRIzol [Invitrogen #15596026] following provider's recommendations.

RNAs from sorted epithelial cells were extracted using the RNeasy Micro Kit [Qiagen #74004], following manufacturer's reference protocol.

RNA concentrations were measured on a Nanodrop and 1μg of RNAs were reverse transcribed into cDNA using the High Capacity cDNA Reverse Transcription Kit [Applied Biosystems #4368813] (RT program 25°C for 10 min, 37°C for 2h, 85°C for 5 min); diluted 1:5 in H2O and kept at -20°C until further use.

Gene	5'-3' Primer Forward	5'-3' Primer Reverse
ADIPOQ	TGTTCCTCTTAATCCTGCCCA	CCAACCTGCACAAGTTCCCTT
AMPHIREGULIN	GGTCTTAGGCTCAGGCCATTA	CGCTTATGGTGGAAACCTCTC
ARG1	CTCCAAGCCAAAGTCCTTAGAG	AGGAGCTGTCATTAGGGACATC
BAX	TGAAGACAGGGGCCTTTTTG	AATTCGCCGGAGACACTCG
BCL-2	AGTACCTGAACCGGCATCTG	GCTGAGCAGGGTCTTCAGAG
BCL-W	GGAAGGTAGTGTGTGTGG	ACTCCACTCTCTGGGTTCTTGG
BCL-X	TTCGGGATGGAGTAAACTGG	TGGATCCAAGGCTCTAGGTG
BCL-XL	CTAGAGCCTTGGATCCAGGAG	GTAGCAATGGTGGCTGAAGAG
BIM	GAGATACGGATTGCACAGGA	TCAGCCTCGCGGTAATCATT
CD14	ACAGGGGCTGCCAAATTGGTCG	AGCACACGCTCCATGGTCGGTA
CD68	CAGCACAGTGGACATTCATG	TAACTGTTGAGTCAGTGGC
COL1A1	CCC TGG TCC CTC TGG AAA TG	GGACCTTTGCCCCCTTCTTT
CSN2	CCTCTGAGACTGATAGTATTT	TGGATGCTGGAGTGAACTTTA
GAPDH	TTCACCACCATGGAGAAGGC	CCCTTTTGGCTCCACCCT
F4/80	CTTTGGCTATGGGCTTCCAGTC	GCAAGGAGGACAGAGTTTATCG

		TG
FABP4	AAGGTGAAGAGCATCATAACCCT	TCACGCCTTTCATAACACATTCC
IL1	TCCATAACCCATGATCTGGAA	TTGGTTGAGGGAATCATTCAT
IL6	TAGTCCTTCTACCCCAATTTCC	TTGGTCCTTAGCCACTCCTTC
INOS	GTTCTCAGCCCAACAATACAAGA	GTGGACGGGTCGATGTCAC
KRT5	GACCAGTCAACATCTCTGTC	TGCCAACACCAATGCTGCTG
KRT18	CCTTGCCGCCGATGACTTTA	CAGCCTTGTGATGTTGGTGT
MCL1	TAACAAACTGGGGCAGGATT	GTCCCGTTTCGTCCTTACAA
MMP2	TCTGGTGCTCCACCACATACAACT	CTGCATTGCCACCCATGGTAAACA
MMP3	ACATGGAGACTTTGTCCCTTTTG	TTGGCTGAGTGGTAGAGTCCC
MMP9	TGAGCTGGACAGCCAGACACTAAA	TCGCGGCAAGTCTTCAGAGTAGTT
MMP13	ACTTCTACCCATTTGATGGACCT	AAGCTCATGGGCAGCAACA
MMP14	CAGTATGGCTACCTACCTCCAG	GCCTTGCCTGTCACTTGTAAA
Noxa	GCAGAGCTACCACCTGAGTTC	CTTTTGCGACTTCCCAGGCA
p15	AGATCCCAACGCCCTGAAC	CCCATCATCATGACCTGGATT
p16	CGTACCCCGATTCAGGTGAT	TTGAGCAGAAGAGCTGCTACGT
p16-3MR HSV-TK	GGAGGCTGGGAGCTCACATG	GGAGGCTGGGAGCTCACATG
p16-3MR LUCIFERASE	CGAGCTGCTGAACCTTCCAAAG	TGGACGATGGCCTTGATCTTGT
p16-3MR mRFP	GACCTCGGCGTCGTAGTG	AAGGGCGAGATCAAGATGAG
p19	GCCGCACCGGAATCCT	TTGAGCAGAAGAGCTGCTACGT
p21	GTGGGTCTGACTCCAGCCC	CCTTCTCGTGAGACGCTTAC
p27	TCAAACGTGAGAGTGTCTAACG	CCGGGCCGAAGAGATTTCTG
PPARG	TCGCTGATGCACTGCCTATG	GAGAGGTCCACAGAGCTGATT
PU.1	ATGTTACAGGCGTGCAAAATGG	TGATCGCTATGGCTTTTCTCCA
PUMA	AGCAGCACTTAGAGTCGCC	CCTGGGTAAGGGGAGGAGT
TIMP1	GGTGGGTGGATGAGTAATGCG	TGCCAGAGATGCAAAGGGGG
TIMP3	CTTCTGCAACTCCGACATCGT	GGGGCATCTTACTGAAGCCTC
YM1	CAAAGAACAGTAGATCCTGGCAA	ATACCGTGTCCAGACCTTGGT
WAP	TTGAGGGCACAGAGTGTATC	TTTGCGGGTCCTACCACAG

Quantitative real-time PCR were performed using SYBR Green Master Mix [Roche #4309105] and run on a Light Cycler 480 II [Roche] with the standard program (Denaturation cycle of 10min at 95°C; 40 Amplification cycles (5 sec at 95°C; 15 sec at 60°C; 15 sec at 72°C); Melting cycle from 65°C to 95°C with increase rate of 0,11°C/s; Cooling to reach an end temperature of 40°C) and corresponding primers. For each sample, all values were obtained at least in duplicates and in a total of at least two independent assays. Calculations for the values were done as previously described using the ΔΔCt method ([Yuan et al. 2006](#)).

F.   Organoids

1.   *Organoids culture*

Mammary organoids isolation, culture, passage, process and time lapse imaging were extensively described in ([Charifou et al. 2021](#)).

2.   *Ex vivo treatment*

Drugs were resuspended in DMSO, at 50mg/ml for ganciclovir [Medchemexpress #HY-13637] and stored at -20°C in single-use aliquotes. After 6 days of 2.5nM FGF2 and 4 days of 1µg/ml prolactin + 1µg/ml hydrocortisone, organoids from p16-3MR mice were treated during involution-like process with either 50µg/ml ganciclovir in BOM (DMEM/F12, Glutamax, Pen/Strep, Insulin-Transferrin-Selenium) or BOM+DMSO, from Inv0 to Inv8, with refreshing of media every 2 days.

G.   RNA sequencing on isolated epithelial cells

1.   *RNA preparation*

Pieces of MG #2 were harvested from mice at Inv0, Inv3 and Inv7 in 4 biological replicates for each time point and were stored at -80°C until RNAs extraction using Trizol. 1000ng of each sample were sent to the Beijing Genomics Institute for RNA sequencing.

2.   *Bioinformatic analysis*

RNA-seq analysis was performed by the Beijing Genomics Institute. Co., Ltd. (Hong Kong, China). The potential biological pathways with differences between the experimental and the control group were investigated by GSEA (http://software.broadinstitute.org/gsea/downloads.jsp), which is a computational method that determines whether a previously-defined gene set shows significant differences between two biological phenotypes. Cellular senescence gene sets were defined and collected from the senequest website (https://senequest.net/genes). Hallmark gene sets and senescence gene sets were chosen as references. Enrichment plots were generated by GSEA. The normalized enrichment score (NES) reflected the degree to which a gene set was overrepresented in the groups, and the gene sets with false discovery rate (FDR)<0.05, and NES>1 were considered significant. The heat maps were also generated by GSEA and redrawn in Excel to make it clearer. The barplot, drawn by the R package ggplot, was used to show all the differentially hallmark gene sets from GSEA.

H.   Adipogenic differentiation

Mammary glands from Pdgfrα^{EGFP} mice were processed (see isolation of mammary cells) to isolate Pdgfrα-GFP$^+$ by FACS. GFP$^+$ cells were seeded after sorting in 12-well plates at a density of 200,000 cells in SVF medium (DMEM/F12 [Gibco #21331-020], Glutamax, Pen/Strep, and 10% FBS). SVF

medium was renewed the day after to remove dead cells. Attached cells were allowed to grow to confluence (approximately 1 day) and were held confluent for 2 days without changing of the media. Cells were then incubated with SVF medium supplemented with an adipogenic cocktail of 1µM dexamethasone [Sigma-Aldrich #D4902]; 0,5mM IBMX [Sigma-Aldrich #I7018]; and 1 µg/ml insulin [Sigma-Aldrich #I7018]; for 3 days ; before switching back to fresh SVF medium. Adipocytes were visible 2 days after withdrawal of the adipogenic cocktail, with a peak of differentiation between 2-4 days after adipogenic cocktail removal. Cells were either collected in RLT buffer for RNA extraction, or stained for OilRedO staining.

I.   *In vivo* experiments

1.   **In vivo sealing of mammary nipples**

After delivery, females were allowed to lactate for 10 days. Hair remover was applied to clean the nipple area from mammary glands #3L and #4L before sealing. After manually restraining the animal, a 200-300µl drop of veterinary tissue adhesive [3M Vetbond #1469C] was applied on the nipple and left to dry before the release of the mouse in the cage with the litter. The manipulation was repeated 3h later to ensure a full sealing of the nipple. Maintenance of lactation on counterpart open teats was checked everyday. MGs were harvested 2 or 3 days after teat closure.

2.   **In vivo treatment ABT-263**

ABT-263 [Tebu #T2101] was initially resuspended in DMSO at 100mg/ml, aliquoted for single doses of 12,5 µl and stored at -20°C. Each dose was then freshly resuspended by adding 112,5µl of vehicle (60%Phosal ; 30% PEG400 ; 10% pure EtOH) upon use. Mice were force-feeded daily with ABT-263 at 50mg/kg or vehicle + DMSO, for 3 consecutive days before MGs harvesting (125µl for a mouse of 25g).

J. Softwares and statistical analysis

Image quantifications were performed using ImageJ software. FACS profile analyses were performed using Flowjo software. Statistical analyses were performed using GraphPad Prism software; statistical tests and p-values are specified in figure legends. The number of independent biological replicates is indicated as n.

Annexes

I. <u>List of abbreviations</u>

AER: Apical Ectodermal Ridge

ARF: Alternative Reading Frame

ATTAC: Apoptosis Through Targeted Activation of Caspase

BCL-2: B-Cell Lymphoma 2

BCL-XL: B-Cell Lymphoma Extra Large

BCL-W: B-Cell Lymphoma W

BH3: BCL-2 homology domain 3

bFGF: basic Fibroblast Growth Factor

bp: base pair

CAR-T: Chimeric Antigen Receptor T

CC3: Cleaved-Caspase 3

CD: Cluster of Differentiation

CDK: Cyclin-Dependent Kinase

CDKN: Cyclin Dependent Kinase Inhibitor

C/EBPβ: CCAAT/enhancer-binding protein-β

CM: Conditioned Medium

COPD: Chronic Obstructive Pulmonary Disease

CRE: Cyclic Recombinase

CXCL1: C-X-C Motif Chemokine Ligand 1

DAPI: 4',6-DiAmidino-2-Phenyl-Indole

D+Q: Dasatinib + Quercetin

DDIS: DNA Damage-Induced Senescence

DDR: DNA Damage Response

DNA: Desoxyribonucleic Acid

ECM: Extracellular Matrix

EMT: Epithelial-Mesenchymal Transition

ER: Estrogen Receptor

FACS: Fluorescence-Activated Cell Sorting

FGF2: Fibroblast Growth Factor 2

γH2AX: gamma H2A Histone Family

H2B: Histone 2B

GCV: Ganciclovir

GFP: Green Fluorescent Protein

HSC: Hematopoietic Stem Cell

HSP: Heat Shock Protein

HSV-TK: truncated Herpes Simplex Virus-1 (HSV-1) Thymidine Kinase

IL-6: Interleukin 6

IL-8: Interleukin 8

Inv: Involution

kb: kilo bases

KO: Knockout

LAMP: Lysosome Associated Membrane Protein

LIF: Leukemia Inhibitory Factor

LMP: Lysosomal Membrane Permeabilization

MCP: Monocyte Chemoattractant Proteins

MEFs: Mouse Embryonic Fibroblasts

MiDAS: Mitochondria Dysfunction-Associated Senescence

MIP: Macrophage Inflammatory Proteins

MG: Mammary Gland

MMPs: Matrix Metalloproteinases

MMTV: Mouse Mammary Tumor Virus

mTOR: mechanistic Target Of Rapamycin

NF-κB: Nuclear Factor κB

NK: Natural Killer

OIS: Oncogene Induced Senescence

PDGFR-α: Platelet Derived Growth Factor Receptor alpha

PR: Progesterone Receptor

PRL: Prolactin

Rb: Retinoblastoma protein

RNA: Ribonucleic Acid

RT-qPCR: Retro-Transcriptase quantitative Poly Chain Reaction

ROS: Reactive Oxygen Species

SAβ-Gal: Senescence Associated beta Galactosidase

SAHF: Senescence Associated Heterochromatin Foci

SASP: Senescence Associated Secretory Phenotype

SMA: Smooth Muscle Actin

STAT: Signal Transducer and Activator of Transcription

TGF-β: Transforming Growth Factor Beta

TIMP: Tissue Inhibitor of Metalloproteinases

TUNEL: TdT-mediated dUTP Nick End Label

uPAR: Urokinase-type Plasminogen Activator Receptor

VEGF: Vascular Endothelial Growth Factor

WAP: Whey Acidic Protein

WT: Wild Type

3MR: Trimodality Reporter

II. <u>Articles</u>

1/ Sumbal, J., A. Chiche, E. Charifou, Z. Koledova, and H. Li. 2020. 'Primary Mammary Organoid Model of Lactation and Involution', *Front Cell Dev Biol*, 8: 68. ([Sumbal et al. 2020](#)).

2/ Charifou, E., J. Sumbal, Z. Koledova, H. Li, and A. Chiche. 2021. 'A Robust Mammary Organoid System to Model Lactation and Involution-like Processes', *Bio Protoc*, 11: e3996. ([Charifou et al. 2021](#)).

3/ Charifou, E., G. A. Traustadottir, M. Bentires-Alj, B. Howard, and A. Van Keymeulen. 2021. 'Twelfth Annual ENBDC Workshop: Methods in Mammary Gland Biology and Breast Cancer', *J Mammary Gland Biol Neoplasia*, 26: 221-26. ([Charifou, Traustadottir, et al. 2021](#)).

Primary Mammary Organoid Model of Lactation and Involution

Jakub Sumbal[1,2†], Aurelie Chiche[1†], Elsa Charifou[1], Zuzana Koledova[2*] and Han Li[1*]*

[1] *Department of Developmental and Stem Cell Biology, Cellular Plasticity and Disease Modelling, CNRS UMR 3738, Institut Pasteur, Paris, France,* [2] *Department of Histology and Embryology, Faculty of Medicine, Masaryk University, Brno, Czechia*

Mammary gland development occurs mainly after birth and is composed of three successive stages: puberty, pregnancy and lactation, and involution. These developmental stages are associated with major tissue remodeling, including extensive changes in mammary epithelium, as well as surrounding stroma. Three-dimensional (3D) mammary organoid culture has become an important tool in mammary gland biology and enabled invaluable discoveries on pubertal mammary branching morphogenesis and breast cancer. However, a suitable 3D organoid model recapitulating key aspects of lactation and involution has been missing. Here, we describe a robust and straightforward mouse mammary organoid system modeling lactation and involution-like process, which can be applied to study mechanisms of physiological mammary gland lactation and involution as well as pregnancy-associated breast cancer.

Keywords: 3D culture, fibroblast growth factor 2, involution, lactation, mammary gland, milk production, organoid, prolactin

INTRODUCTION

Lactation, the production of milk to feed progeny, is achieved by the mammary gland. This hallmark organ of mammals mainly develops postnatally and is highly dynamic (Macias and Hinck, 2012). With each pregnancy, mammary epithelium undergoes massive proliferation, tertiary branching of the mammary ductal system, and alveoli differentiation to prepare the epithelium for proper lactation (Brisken and Rajaram, 2006; Sternlicht, 2006). After parturition, mammary epithelium fully transforms into a milk-producing factory. Alveoli expand and take up space of regressing mammary stromal adipocytes, thereby multiplying epithelial volume many times (Macias and Hinck, 2012). After weaning, when milk production is no longer required, milk-producing epithelial cells are removed, and mammary gland is remodeled into a prepregnancy state. This process is called involution, which includes programmed cell death of the epithelium, ECM remodeling, and redifferentiation of adipocytes (Hughes and Watson, 2012; Macias and Hinck, 2012; Zwick et al., 2018; Jena et al., 2019). By the end of involution, mammary gland is ready for a new cycle of pregnancy-associated growth, lactation, and subsequent involution, which can be repeated throughout the reproductive lifespan. During these changes, mammary epithelium retains its bilayered architecture with lumen-facing luminal cells and basally situated myoepithelial cells, which is essential for proper function of the organ (Adriance et al., 2005; Haaksma et al., 2011; Macias and Hinck, 2012).

Abbreviations: BOM, basal organoid medium; Csn2, Casein2–β-casein gene; ECM, extracellular matrix; EGF, epidermal growth factor; FGF2, 7, or 10, fibroblast growth factor 2, 7, or 10; LM, lactation medium; Mmp, matrix metalloproteinase; TGFα, transforming growth factor-α; TGFβ, transforming growth factor-β; Wap, whey acidic protein.

Endocrine signaling is a crucial regulator of mammary morphogenesis during pregnancy. Ovarian hormones estrogen and especially progesterone govern growth and morphogenesis of epithelium via induction of paracrine signaling between mammary stroma and epithelium, involving members of several growth factor families (Hennighausen and Robinson, 2005; Brisken and O'Malley, 2010). Pituitary hormone prolactin, on the other hand, acts directly on prolactin receptor on luminal cells and triggers alveoli maturation and lactogenic differentiation (Hennighausen and Robinson, 2005; Brisken and Rajaram, 2006). Involution is linked to cessation of hormonal stimuli and increase in inflammatory cytokines (Watson, 2006; Stein et al., 2007).

To study various aspects of mammary gland biology, three-dimensional (3D) cell culture models have been widely used for decades (Koledova, 2017a). They combine the advantages of easy manipulation of 2D cellular systems with providing complex cell–cell and cell–ECM interactions, thereby mimicking physiological conditions of *in vivo* experiments more faithfully (Shamir and Ewald, 2014; Huch and Koo, 2015; Koledova, 2017a; Artegiani and Clevers, 2018). Among the 3D culture models, primary mammary organoids have played a major role in understanding mechanisms of mammary branching morphogenesis (Ewald et al., 2008; Huebner et al., 2016; Neumann et al., 2018), including the role of ECM (Simian et al., 2001) and stromal cells (Sumbal and Koledova, 2019). Furthermore, spheroids produced from mammary cell lines were used to study tissue response to growth factors (Xian et al., 2005); organoids grown from sorted single primary mammary epithelial cells were used to study developmental potential of mammary epithelial cells (Linnemann et al., 2015; Jamieson et al., 2017), and differentiation of mammary-like organoids was achieved from induced pluripotent stem cells (Qu et al., 2017).

Despite these advances in 3D cell culture models of mammary gland, systems faithfully modeling pregnancy-associated morphogenesis and lactation have been spare. In some studies, β-casein or milk protein expression was used as a read-out of mammary epithelial functionality (Mroue et al., 2015; Jamieson et al., 2017). Several aspects of lactation and involution were captured in a coculture of mammary epithelial and preadipocyte cell lines (Campbell et al., 2014) or in hormone-treated breast cancer cell spheroids (Ackland et al., 2003; Freestone et al., 2014). However, a system modeling lactation and involution in primary mammary organoids with proper architecture of bilayered epithelium with myoepithelial cell layer has not been characterized.

Here, we report on a mammary 3D culture system for studying induction and maintenance of lactation using easily accessible and physiologically relevant murine primary mammary organoids cultured in Matrigel. Upon prolactin stimulation, the organoids produce milk for at least 14 days and maintain a histologically normal architecture with a functional contractile myoepithelial layer. Moreover, upon prolactin signal withdrawal, our system recapitulates several aspects of involution. Altogether, we describe a robust, consistent, and easy-to-do system for modeling crucial aspects of pregnancy-associated mammary gland morphogenesis and lactation.

MATERIALS AND METHODS

Isolation of Primary Mammary Epithelial Organoids

Primary mammary organoids were prepared from 7- to 10-week-old female mice (ICR or C57/BL6) as previously described (Koledova, 2017b; **Supplementary Figure 1A**). ICR strain was used for the branching morphogenesis and time-lapse imaging, cell viability and replating assays, and confocal imaging. C57/BL6 strain was used for the rest of the experiments. The animals were obtained from the Central Animal Facility of the Institut Pasteur and the Laboratory Animal Breeding and Experimental Facility of the Faculty of Medicine, Masaryk University. Experiments involving animals were approved in accordance with French legislation in compliance with European Communities Council Directives (A 75-15-01-3), the regulations of Institut Pasteur Animal Care Committees (CETEA), the Ministry of Agriculture of the Czech Republic, and the Expert Committee for Laboratory Animal Welfare at the Faculty of Medicine, Masaryk University. The study was performed by certified individuals (AC, JS, EC, and ZK) and carried out in accordance with the principles of the Basel Declaration.

Briefly, the mice were euthanized by cervical dislocation, the thoracic and inguinal mammary glands were collected, visible lymph nodes were excised, and the pooled mammary glands were finely chopped to approximately 1-mm^3 pieces and digested in a solution of collagenase and trypsin [2 mg/mL collagenase (Roche, Switzerland or Sigma, United States), 2 mg/mL trypsin (*Dutscher Dominique, France or Sigma, United States), 5 μg/mL insulin (Sigma, United States), 50 μg/mL gentamicin (Sigma, United States), 5% fetal bovine serum (Hyclone/GE Healthcare, United States) Dulbecco's in modified Eagle medium (DMEM)/F12 (Thermo Fisher Scientific, United States)] for 30 min at 37°C with shaking at 100 rpm. Next, the tissue suspension was treated with 20 U/mL DNase I (Sigma, United States) and 0.5 mg/mL dispase II (Roche, Switzerland) and exposed to five rounds of differential centrifugation at $450 \times g$ for 10 s, which resulted in separation of epithelial (organoid) and stromal fractions (**Supplementary Figure 1A**). The organoids were resuspended in basal organoid medium [BOM; 1× insulin–transferrin–selenium supplement, 100 U/mL of penicillin, and 100 μg/mL of streptomycin, in DMEM/F12 (all from Thermo Fisher Scientific, United States)] and kept on ice up to 2 h before seeding for 3D culture.

3D Culture of Mammary Organoids

Freshly isolated primary mammary organoids were mixed with growth factor reduced Matrigel (Corning, United States) and plated in domes in 24-well culture plate (one dome per well, 70 μL of Matrigel per dome). 200, 400, or 1000 organoids per dome were seeded for histology, gene expression, and Western blot analysis, respectively. After setting the Matrigel for 45–60 min at 37°C, the 3D organoid cultures were overlaid with cell culture medium according to the experiment and incubated at 37°C in a humidified atmosphere with 5% CO_2 (**Supplementary Figure 1B**). The

media used were as follows: growth factor medium [BOM supplemented with different growth factors: 2.5 nM FGF2 (Peprotech, United States or Thermo Fisher Scientific, United States), 2.5 nM FGF7, 2.5 nM FGF10, 50 ng/mL EGF (all from Peprotech, United States), 5 nM TGFα (Sigma, United States), or a combination of 10 ng/mL WNT3A and 50 ng/mL R-spondin 1 (W3/R1, both from Peprotech, United States)] and lactation medium {LM; 1 μg/mL prolactin [mouse recombinant prolactin for quantitative polymerase chain reaction (qPCR), Western blot, immunohistochemistry and contraction experiments (Sigma, United States or Peprotech, United States), and sheep pituitary prolactin for confocal and time-lapse imaging, including contraction experiments (Sigma, United States)], and 1 μg/mL hydrocortisone (Sigma, United States) in BOM}. Media containing growth factors were changed every 3 days; LM was changed every 2 days. To induce contraction of lactation organoids grown with mouse recombinant prolactin, 40 μg/mL recombinant oxytocin (Sigma, United States) was used. For time-lapse imaging experiments, organoid cultures were incubated in a humidified atmosphere of 5% CO_2 at 37°C on Olympus IX81 microscope equipped with Hamamatsu camera and CellR system for time-lapse imaging. For morphological analysis of organoid development, the organoids were photographed from days 8 to 17 of culture; one image per organoid was taken every hour. The images were exported and analyzed using ImageJ (NIH, United States). For analysis of organoid contraction, the organoids were photographed from days 6 to 20 of culture. On each imaging day, the photographs were taken every second for 120 s. The images were exported to video at 10 frames per second using xCellence software (Olympus, Japan).

Replating of Organoids

To replate organoids, 3D cultures were rinsed with phosphate-buffered saline (PBS) and disintegrated by pipetting up and down in ice-cold PBS with a 1000 μL pipette. Successful disintegration of Matrigel was checked under a microscope. Organoid suspensions were centrifuged at 450 × g for 3 min. Organoid pellets were resuspended in fresh Matrigel and plated as described above. Organoids were maintained in BOM or in BOM supplemented with 2.5 nM FGF2; the medium was changed every 3 days. Organoid area was measured in ImageJ.

Cell Viability Assay

To asses cell viability in organoids treated with LM or LM-BOM, on the 20th day of culture, the media were changed with fresh BOM, and then resazurin (Merck, Germany) was added to the medium to the final concentration of 10 μg/mL. The plates were incubated for 6 h. Resorufin fluorescence (excitation at 560 nm, emission at 590 nm) was measured using Synergy H4 Hybrid multimode microplate reader (BioTek, United States) in technical triplicates. As a positive control of dying cells, organoids in LM-BOM conditions were treated from day 16 with 40 μM taxol (Sigma, United States) or killed on day 20 by treatment with 70% ethanol for 5 min.

Histology and Immunostaining Analysis

For histological analysis, organoids were fixed in 4% paraformaldehyde (Electron Microscopy Sciences, United States) for 30 min and embedded in 3% low gelling temperature agarose (**Supplementary Figure 1C**). After solidification, samples were dehydrated and paraffin embedded and cut in 5-μm sections, which were dewaxed for hematoxylin and eosin staining or immunostaining. For localization of prolactin receptor expressing cells, 10-μm cryosections of mammary glands from *Prlr-IRES-Cre;ROSA26-CAGS-GFP* mice (Aoki et al., 2019) were labeled with antibodies and counterstained with 0.5 μg/mL DAPI, mounted with Vectashield (Vector Labs, United States), and images were taken on LSM800 microscope (Zeiss, Germany). The following primary antibodies were used: goat anti-GFP (Origene, United States, R1091P, 1:200), rabbit polyclonal anti-keratin 5 (BioLegend, United States, 905501, 1:200), mouse monoclonal anti-keratin 8 (BioLegend, United States, 904801, 1:200), mouse monoclonal anti-β-casein (Santa Cruz, United States, sc-166530, 1:250), and rabbit anti-mouse milk proteins (*Accurate Chemical, United States, YNRMTM, 1:500). Corresponding secondary antibodies were used: donkey anti-rabbit Dylight 488 (Immuno Reagents, United States, DkxRb-003-D594NHSX, 1:200) and donkey anti-mouse Dylight 594 (Immuno Reagents, United States, DkxMu-003-D488NHSX, 1:200), together with 1 μg/mL of Hoechst-33342 (Thermo Fisher Scientific, United States) for immunofluorescence labeling, or anti-mouse/anti-rabbit horseradish peroxidase (HRP)-associated secondary antibodies (Dako, United States).

Whole Mount Staining of Mammary Organoids

Organoids were fixed with 10% formalin for 30 min, washed with PBS and 70% ethanol, and incubated with oil red O solution [0.3% (wt/vol) oil red O (Sigma, United States) in 70% (vol/vol) ethanol (Koopman et al., 2001; Kim et al., 2015)] for 30 min in the dark. Next, organoids were washed with 70% ethanol and PBS and incubated with 0.5 μg/mL DAPI and 2 units/sample phalloidin-AlexaFluor488 (Thermo Fisher Scientific, United States) in PBS for 1 h at room temperature (RT) in the dark. Subsequently, organoids were washed and transferred to coverslip-bottom 35-mm dishes (ibidi) covered with 1% low gelling temperature agarose (Sigma, United States) and overlaid with PBS. Images were acquired using LSM800 confocal microscope (Zeiss, Germany, **Supplementary Figure 1D**) and analyzed using ZEN blue software (Zeiss, Germany).

RNA Isolation and Real-Time qPCR

Total RNA was extracted from organoid samples using RNeasy Micro Kit (Qiagen, Germany) following the manufacturer's instructions. Reverse transcription was performed using high-capacity cDNA reverse transcription kit (Thermo Fisher Scientific, United States). Quantitative real-time PCR was performed using 5 ng cDNA, 5 pmol of the forward and reverse gene-specific primers each in Light Cycler SYBR Green I Master mix (Roche, Switzerland) on LightCycler 480 II (Roche, Switzerland). All reactions were performed at least in

duplicates and in a total of at least two independent assays. Relative gene expression was calculated using the $\Delta\Delta Ct$ method, and the values were normalized to housekeeping gene *Gapdh*. The primers of following sequences (5′–3′) were used: *Csn2*-forward (F): CCTCTGAGACTGATAGTATTT, *Csn2*-reverse (R): TGGATGCTGGAGTGAACTTTA; *Wap*-F: TT GAGGGCACAGAGTGTATC, *Wap*-R: TTTGCGGGTCCTACC ACAG; *Mmp3*-F: CCTGATGTTGGTGGCTTCA, *Mmp3*-R: TC CTGTAGGTGATGTGGGATTTC; *Mmp13*-F: ACTTCTACCCA TTTGATGGACCTT, *Mmp13*-R: AAGCTCATGGGCAGCAA CA; *Gapdh*-F: TTCACCACCATGGAGAAGGC, *Gapdh*-R: CC CTTTTGGCTCCACCCT. All primers were purchased from Sigma, United States.

Western Blot

Three-dimensional cultures were dissociated by repetitive pipetting in ice-cold PBS supplied with phosphatase inhibitor cocktail II (Merck, Germany; 2 mM imidazole, 1 mM sodium fluoride, 1.15 mM sodium molybdate, 1 mM sodium orthovanadate, 4 mM sodium tartrate dihydrate), followed by centrifugation at $450 \times g$ for 3 min at 4°C. Supernatant was discarded, and pellets were lysed in ready-to-use RIPA buffer [Merck, Germany; 150 mM NaCl, 1.0% IGEPAL® CA-630, 0.5% sodium deoxycholate, 0.1% sodium dodecyl sulfate (SDS), 50 mM Tris, pH 8.0] supplied with protease inhibitor cocktail I (Merck, Germany; 500 µM AEBSF hydrochloride, 150 nM aprotinin, 1 µM protease inhibitor E-64, 0.5 mM EDTA, 1 µM leupeptin hemisulfate) and phosphatase inhibitor cocktail II. After vortexing and sonication, protein lysates were cleared by centrifugation, and protein concentration was measured using Coomassie reagent (Merck, Germany). Denatured, reduced samples were resolved on 12.5% SDS–polyacrylamide electrophoresis (Bio-Rad, United States) and blotted onto nitrocellulose membranes by Trans-blot Turbo transfer system (Bio-Rad, United States). After blotting, the membranes were blocked with 2% bovine serum albumin in PBS with 0.1% Tween-20 (Merck, Germany; blocking buffer) and incubated with primary antibodies diluted in blocking buffer overnight at 4°C. After washing in PBS with 0.05% Tween-20, the membranes were incubated with HRP-conjugated secondary antibodies for 1 h at RT. Signal was developed using an ECL substrate (Thermo Fisher Scientific, United States) and imaged with ChemiDoc MP imaging system (Bio-Rad, United States), and band density was analyzed in ImageJ. The following antibodies were used for immunoblotting: mouse monoclonal anti-β-casein (Santa Cruz, United States, sc-166530, 1:1000), mouse monoclonal anti-α-tubulin (Santa Cruz, United States, sc-5286, 1:1000), and anti-mouse secondary antibody (Merck, NA931, 1:1000).

Statistical Analysis

Statistical analysis was performed using the Prism software (GraphPad, United States); statistical test used is specified in figure legends. $*p < 0.05$, $**p < 0.01$, $***p < 0.001$, $****p < 0.0001$. The number of independent biological replicates is indicated as *n*.

RESULTS

FGF2 Pretreatment Enhances Lactogenic Differentiation of Mammary Epithelium

During mammary gland morphogenesis, lactation is preceded by excessive branching of epithelial ducts. We hypothesized that epithelial expansion by branching morphogenesis might be required for lactogenic differentiation *in vitro*. Therefore, we first tested the impact of several growth factors on mammary epithelial morphogenesis. The primary mammary epithelial organoids were treated with FGF2, FGF7, FGF10, EGF, TGFα, or a combination of WNT3A and R-spondin 1 (W3/R1) for 7 days. Interestingly, only FGF2, a potent mammary epithelium branching-inducing factor (Ewald et al., 2008), induced extensively branched morphology (**Supplementary Figures 2A–D**).

Next, we tested if FGF2-induced epithelial expansion facilitated lactogenic differentiation. To this end, the primary mammary epithelial organoids were either treated only with LM (containing prolactin and hydrocortisone) for 4 days, or they were treated with FGF2 for 6 days and followed by 4 days of LM (**Figure 1A**). To detect lactogenic differentiation, we measured the expression of *Csn2* and *Wap* by RT-qPCR. Our results revealed that treatment of freshly isolated organoids with LM induced only expression of *Csn2* (**Figure 1B**). However, when organoids were pretreated with FGF2, the expressions of both *Csn2* and *Wap* were significantly increased (**Figure 1B**). These data suggest that mammary epithelial expansion, induced by branching morphogenesis, could enhance the lactogenic ability of mammary epithelium.

Lactation Medium Induces Production of Milk Proteins and Secretion of Lipid Droplets

Next, we compared the morphology of organoids treated with either FGF2 only or FGF2 and LM (FGF2-LM) to further characterize the phenotype of lactation organoids. On bright-field micrographs, we noticed that FGF2-LM organoids appeared to have a darker lumen, possibly due to the milk accumulation (**Figure 1C**). Interestingly, we also observed bubble-like structures at the apical site of epithelium in the same organoids, which potentially represented lipid droplets (**Figure 1C**). To further characterize these droplets, we stained the organoids for F-actin (with phalloidin), a cytoskeletal protein, or with oil red O. Confocal microscopy revealed that the droplets were negative for F-actin and strongly positive for oil red O, confirming the droplets were lipid (**Figures 1C,D**).

Next, we assessed the expression of milk proteins in the organoids. First, we detected a significant increase in *Csn2* by four orders in FGF2-LM-treated organoids compared to FGF2 alone by RT-qPCR (**Figure 1E**). Consistently, in FGF2-LM-treated organoids, we detected up-regulation of β-casein on the protein level by Western blot (**Figure 1F**) and a strong cytoplasmic signal by immunohistochemistry (**Figure 1G**), which was further confirmed by antibody against milk proteins (**Supplementary Figures 3A–C**). Taken together, these data demonstrate that
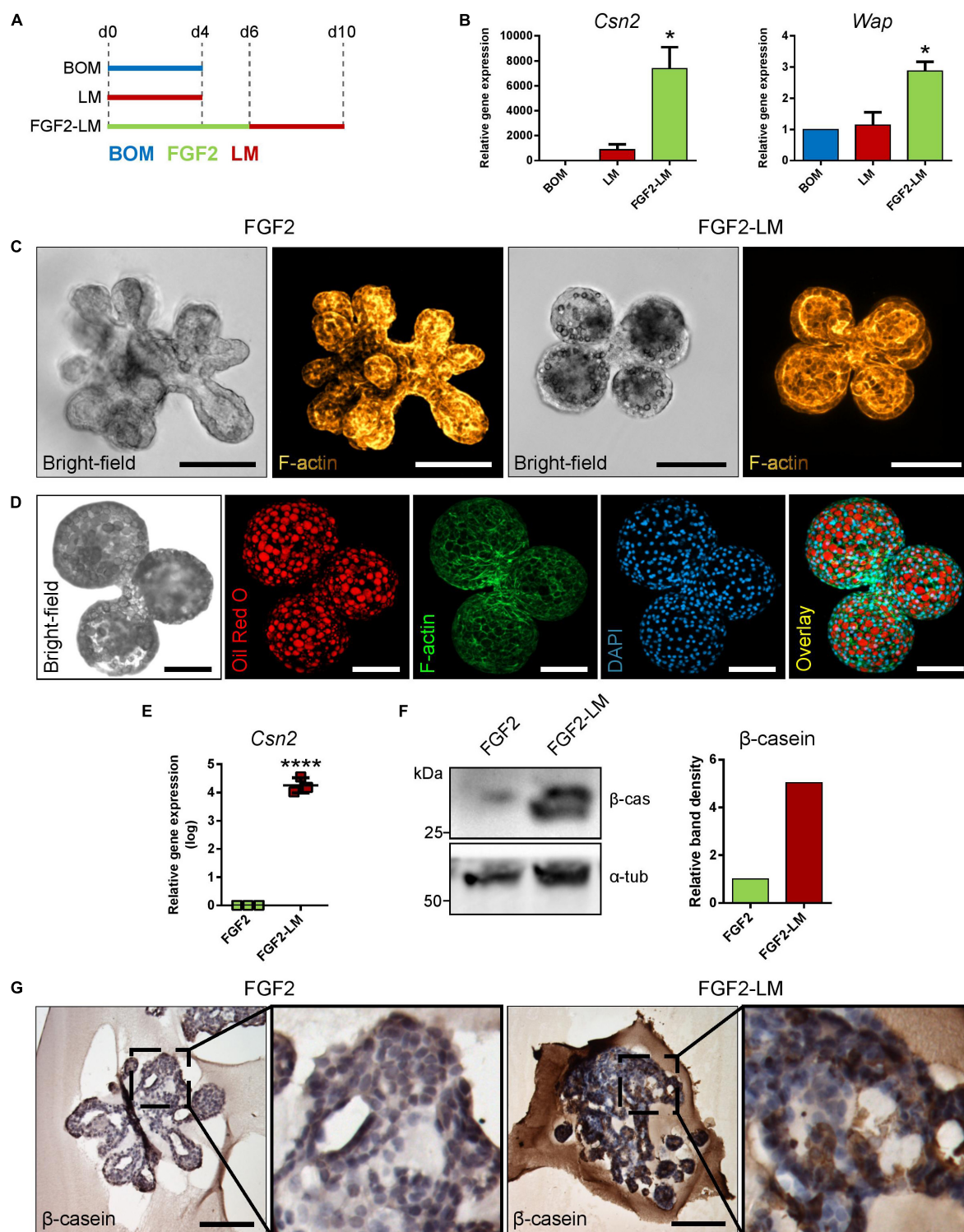
FIGURE 1 | Lactation induction in primary mammary organoids. **(A,B)** FGF2 pretreatment increases lactation capacity of primary mammary organoids. **(A)** Scheme depicting the experimental design. BOM, basal organoid medium; LM, lactation medium; FGF2, FGF2 medium. **(B)** Expression of milk genes *Csn2* and *Wap* in organoids treated with BOM, LM, or FGF2 followed by LM. The values are relative to BOM. The plot shows mean + SD; $n = 2$. One-way ANOVA, *$p < 0.05$. **(C)** Bright-field images and maximum intensity projection images from confocal imaging of whole-mount organoids after treatment with FGF2 only or with FGF2 followed by LM. Yellow-to-brown staining shows F-actin. Scale bars represent 100 μm. **(D)** Bright-field image and maximum intensity projection images from confocal imaging of whole-mount organoid treated with FGF2 followed by LM. Red, oil red O (lipids); green, F-actin; blue, DAPI (nuclei). Scale bars represent 100 μm.

(Continued)

mammary primary organoids are capable of milk production after prolactin treatment, which could be greatly enhanced by branching morphogenesis.

Morphology Maintenance in Long-Term Lactating Organoids

After successful induction of lactation in the primary mammary organoids with the FGF2-LM protocol, we went on to investigate the lactation-associated phenotype in long-term organoid culture. After 6 days of FGF2 treatment, the organoids were either cultured continuously with LM (FGF2-LM) or switched to BOM after 4 days of LM treatment (FGF2-LM-BOM) (**Figure 2A**). The morphogenesis of the organoids was recorded using time-lapse microscopy for 20 days. Interestingly, FGF2-LM-BOM cultured organoids regressed both in size and the complexity of the shape, whereas the organoids in FGF2-LM maintained the size and only partially lost the branched phenotype (**Figures 2B,C** and **Supplementary Figures 4A,B**). In contrast, continuous treatment with FGF2 for 20 days maintained the organoid branched morphology (**Supplementary Figures 4A,B**). In addition, unlike the organoids in FGF2-LM-BOM, the organoids in FGF2-LM retained the darker appearance, possibly due to the milk accumulation (**Figures 2B,D** and **Supplementary Figure 4A**). Morphologically, FGF2-LM-treated organoids exhibited complex architecture with multiple lumens filled with dense eosinophilic material, which was maintained throughout the experiment (**Figure 2E**, upper panel). However, upon LM withdrawal, the complex architecture was lost rapidly, and organoids involuted into small spheroids with much simpler structures (**Figure 2E**, lower panel).

Milk Production in Long-Term Lactating Organoids

Of note, we detected strong β-casein signal in the intraluminal of long-term lactating organoids by immunohistochemistry. Closer observation revealed that cytoplasmic β-casein signal was sustained in long-term LM culture (**Figure 3A**, upper panel), but lost after LM withdrawal (**Figure 3A**, lower panel). In addition, RT-qPCR revealed that FGF2-LM-treated organoids maintained a high level of *Csn2* expression, which was dramatically reduced by four to five orders of magnitude in FGF2-LM-BOM-treated organoids (**Figure 3B**). The same change was confirmed in the protein level by Western blot (**Figure 3C**). Therefore, the production of β-casein depended on the prolactin signaling.

Altogether, these data suggest that these organoids have a proper epithelial architecture and the capacity to maintain milk production over prolonged culture time in response to the prolactin signaling.

Lactating Organoids Retain Functional Myoepithelial Layer With Contractility

Next, we co-stained the lactating organoids for keratin 5 and keratin 8, markers of myoepithelial and luminal cells, respectively, to confirm that the organoids contain proper bilayer epithelial architecture. We found that FGF2-LM-treated organoids contained a continuous layer of myoepithelial cells, similar to FGF2-treated organoids (**Figure 4A**). Moreover, the myoepithelial cell layer was retained during the long-term culture in LM treatment, as well as after LM withdrawal (**Figure 4B**), suggesting the luminal–myoepithelial cell homeostasis was stable during long-term culture.

Importantly, FGF2 treatment induced stratification of the luminal layer, which is in agreement with published work (**Figure 4A**; Ewald et al., 2008). Upon LM treatment, the organoids showed resolution of the stratified epithelium to a predominantly bilayer structure, with luminal cells (keratin 8 positive) lining the luminal space (**Figures 4A,B**), which is important for producing milk. Remarkably, we observed the LM-treated organoids could contract periodically (**Supplementary Movie 2**). In comparison, organoids never treated with LM showed relatively static structures (**Supplementary Movie 1**). Of note, the contracting phenotype maintained during the long-term LM treatment and quickly ceased after LM withdrawal (**Figure 4C**). This result is somewhat puzzling because prolactin receptor is present only in the luminal cells (**Supplementary Figure 5A**). Of note, the prolactin used in our contraction experiments was isolated from sheep pituitary, which contains oxytocin (Vorherr et al., 1978). To test whether the contraction of myoepithelial cells is a direct effect of prolactin signaling, we compared contraction induction upon LM containing either sheep pituitary prolactin or mouse recombinant prolactin. Interestingly, only sheep pituitary prolactin induced organoid contraction; mouse recombinant prolactin did not induce contraction (**Supplementary Figure 5B** and **Supplementary Movie 3**). However, when the organoids cultured with mouse recombinant prolactin were treated with recombinant oxytocin, they did contract (**Supplementary Movie 4**), demonstrating that oxytocin is required for myoepithelial cell contraction. Taken together, these results demonstrate that myoepithelial layer is present in the lactating organoids. And more importantly, these myoepithelial cells can contract in response to LM treatment, suggesting they are functionally similar to the *in vivo* counterpart.

LM Withdrawal Triggers Involution-Like Phenotype in Lactating Organoids

Involution is characterized by the regression of the lactating epithelium through programmed cell death and remodeling of the mammary gland, which is induced upon weaning of the
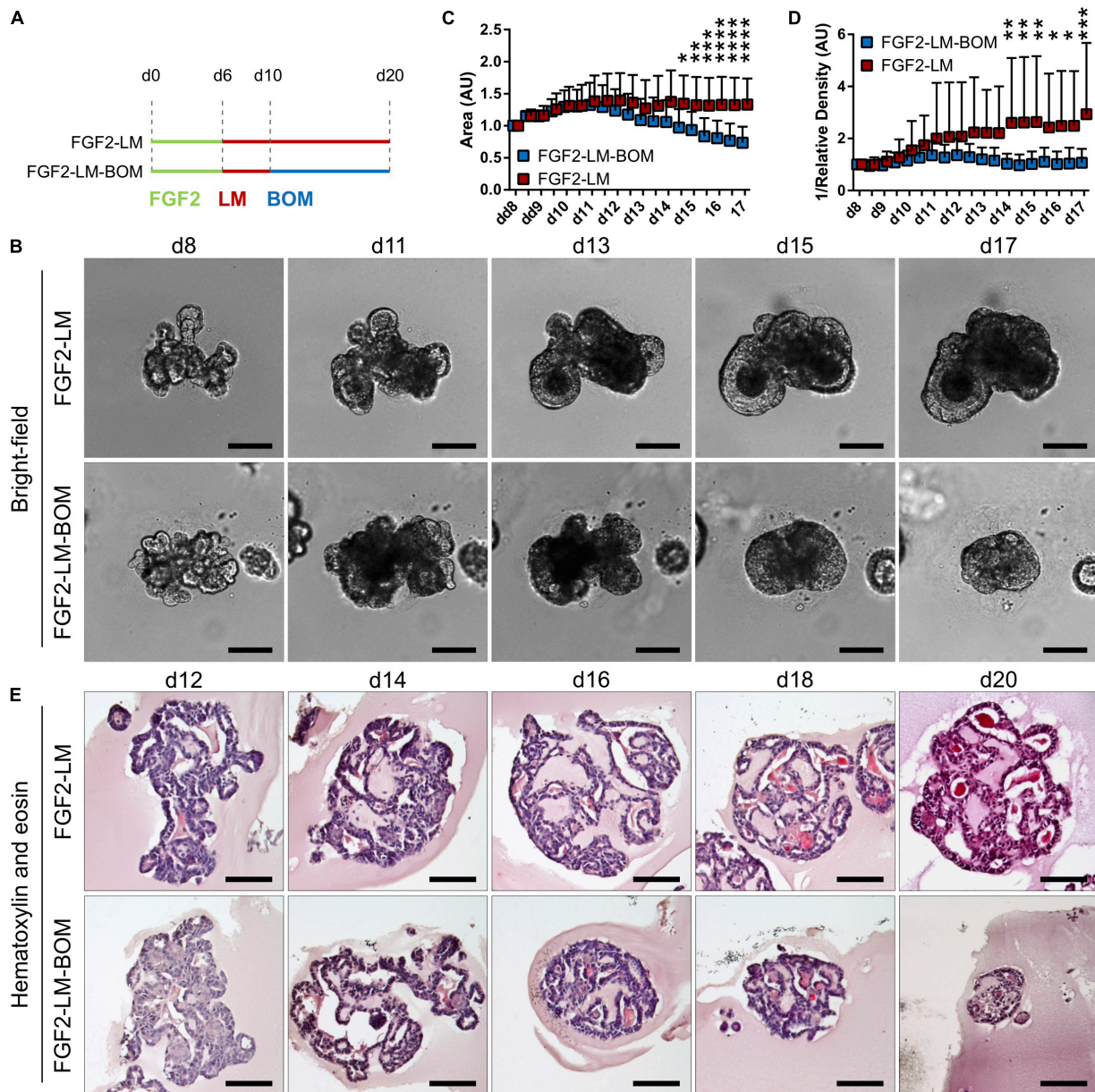
FIGURE 2 | Morphology of organoids undergoing long-term lactation. **(A)** Scheme depicting experimental design. FGF2, FGF2 medium; LM, lactation medium; BOM, basal organoid medium. **(B)** Bright-field images from time-lapse imaging of organoid morphogenesis under continuous LM treatment (FGF2-LM) or under LM withdrawal and replacement with BOM (FGF2-LM-BOM). Scale bars represent 100 μm. **(C,D)** Morphometric analysis of organoid area **(C)** and density **(D)** from the time-lapse experiment. The plots show mean + SD; $n = 2$, $N = 20$ organoids per condition. Two-way ANOVA, $*p < 0.05$, $**p < 0.01$, $***p < 0.001$, $****p < 0.0001$. **(E)** Hematoxylin and eosin staining of organoids at different time points of long-term lactation. Scale bars represent 100 μm.

pups (Jena et al., 2019). Interestingly, withdrawal of LM from lactating organoids also induced a size regression and loss of the branched morphology with luminal architecture (**Figures 2B–E**). Using cell viability assay that is based on conversion of non-fluorescent resazurin to fluorescent resorufin by viable cells, we found that lactating organoids upon LM withdrawal (FGF2-LM-BOM) showed reduced viability in comparison to lactating organoids in LM (FGF2-LM) (**Figure 5A**), most likely due to increased cell death in response to LM withdrawal, which is

a characteristic of involution. Yet the viability of organoids upon LM withdrawal was higher than that of organoids undergoing taxol- or ethanol-induced cell death (**Figure 5A**). Furthermore, replating of the involution-like organoids (FGF2-LM-BOM) to fresh Matrigel and FGF2 treatment reversed the size regression (**Figure 5B**) and, more importantly, induced branching morphogenesis (**Figures 5C,D**). This demonstrates that involuting organoids are viable and that the morphological changes induced upon LM withdrawal are reversible.
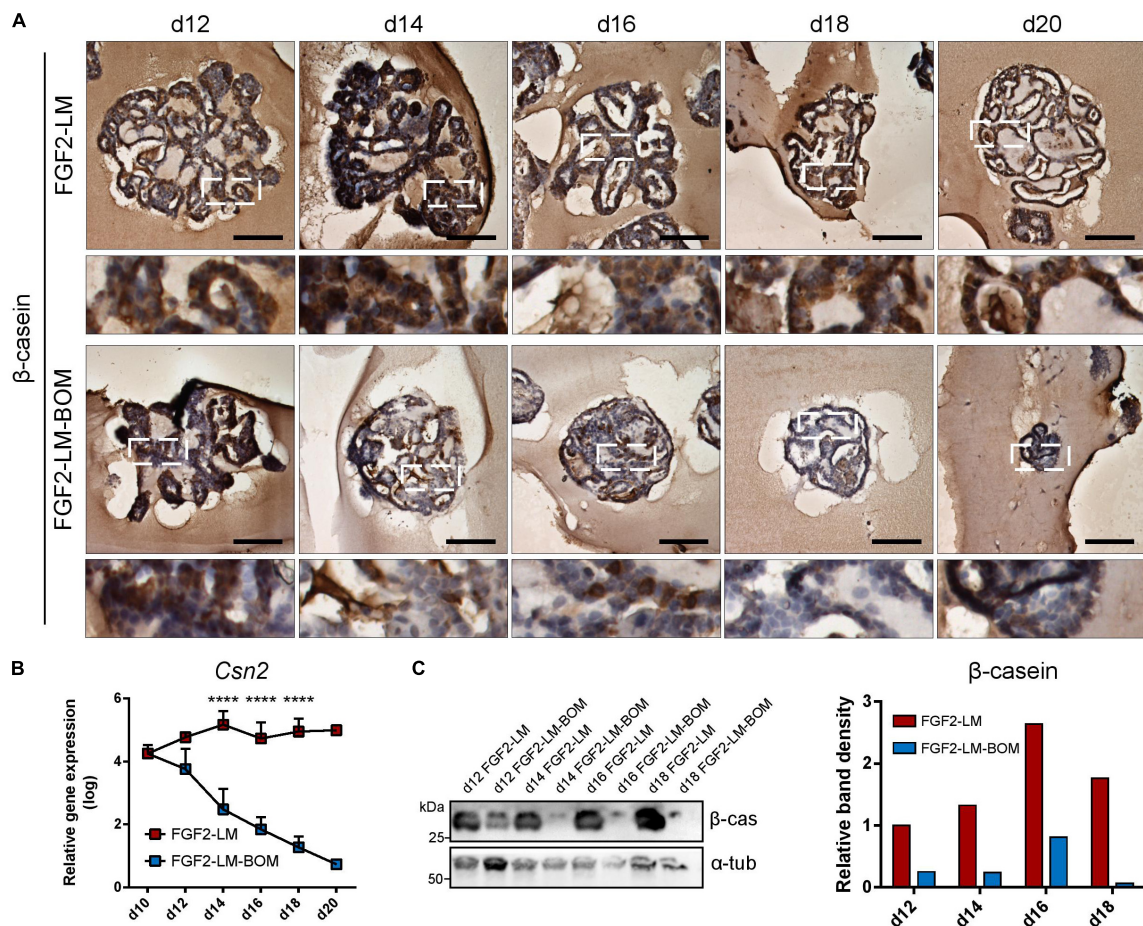
FIGURE 3 | Milk production during long-term lactation. **(A)** Immunohistochemical staining of β-casein in organoids during long-term LM treatment or after LM withdrawal (LM-BOM), according to experimental scheme in **Figure 2A**. Marked area is shown in higher magnification. Scale bars represent 100 μm. **(B)** Csn2 expression during long-term lactation with continuous lactation medium (FGF2-LM) or with hormonal withdrawal (FGF2-LM-BOM). The plot shows mean + SD; n = 3 for d12 to d18, n = 1 for d20. Two-way ANOVA, ****p < 0.0001. **(C)** Western blot analysis and band density quantification of β-casein expression in organoids during long-term lactation.

Furthermore, cessation of milk production and ECM remodeling are two hallmarks of involution. Consistently, we detected a reduced β-casein signal (**Figures 3A,C**) and Csn2 expression (**Figure 3B**) in the organoids upon LM withdrawal. Interestingly, we also found that the expression of Mmp2 and Mmp13, two important Mmps for the ECM remodeling process during involution, was up-regulated in organoids after LM withdrawal (**Figures 5E,F**). Together, these results demonstrate that upon withdrawal of hormonal stimulation lactating organoids stop milk production and enter an involution-like process, thereby mimicking the in vivo situation upon weaning.

DISCUSSION

In this work, we described the use of primary mammary epithelial organoids to model pregnancy-associated morphogenesis and lactation. In our 3D culture system, primary mammary organoids exposed to LM with prolactin recapitulated several aspects of lactation process. Upon LM withdrawal, organoids regressed in a manner similar to the involution process in vivo.

Our data showed that FGF2 primes mammary epithelium for lactation. This is consistent with in vivo studies that noted morphological abnormalities in pregnancy-associated tertiary branching of mammary epithelium with attenuated FGF receptor signaling (Lu et al., 2008; Parsa et al., 2008). However, it remains to be elucidated what of the FGF2-mediated processes, including epithelial expansion, branching, and maturation, are essential contributors to milk production efficiency.

While several previous studies reported lactation induction in mammary epithelial organoids in response to prolactin in vitro, they did so only at a single time point (Mroue et al., 2015; Jamieson et al., 2017). Long-term lactation in organoid cultures has not been reported before. In this study, we documented milk production maintenance and stable morphology of lactating organoids over 14 days' culture period. Physiological lactation in mouse lasts for circa 3 weeks (König and Markl, 1987),
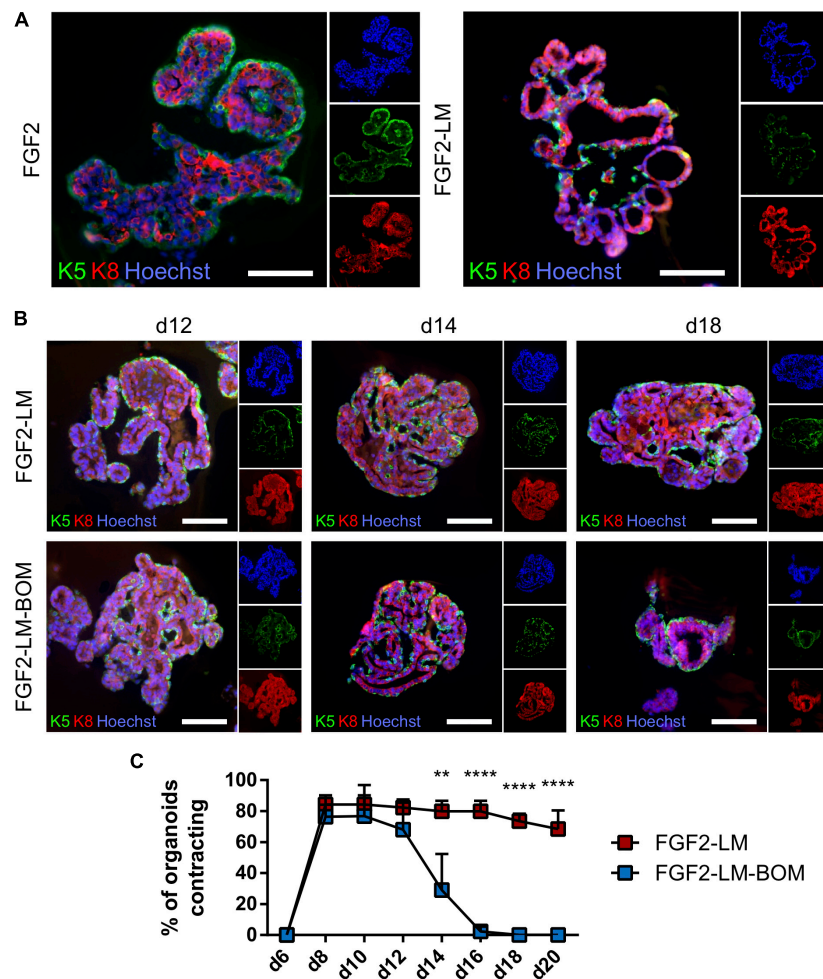
FIGURE 4 | Lactating organoids retain functional myoepithelial layer. **(A)** Immunofluorescent staining shows distribution of myoepithelial (keratin 5 positive, green) and luminal cells (keratin 8 positive, red) in organoids treated with FGF2 or FGF2 followed by LM. Hoechst, blue (nuclei). Scale bars represent 100 μm. **(B)** Immunofluorescent staining shows distribution of myoepithelial (keratin 5 positive, green) and luminal cells (keratin 8 positive, red) in organoids during long-term lactation. Hoechst, blue (nuclei). Scale bars represent 100 μm. **(C)** Quantification of contracting organoids from movies recorded at indicated time-points. The plot shows mean + SD; $n = 2$, $N = 50$ organoids per experiment. Two-way ANOVA, $**p < 0.01$, $****p < 0.0001$.

and milk composition and production rate vary during the lactation period to accommodate the needs of the offspring (Knight et al., 1986). We propose that our model would be suitable to study factors that influence dynamic changes in milk composition and quantity in the long term. Among others, insulin is used in our model to support cell survival and growth and has been implicated in milk production (Nommsen-Rivers, 2016) both in rodent and human. Our model could help to further elucidate how insulin signaling impacts on milk production. Moreover, while previous studies used sample-destructive methods to detect lactation, such as organoid fixation and immunodetection of milk proteins (Mroue et al., 2015; Jamieson et al., 2017), we propose approaches for observing changes in milk production in the same organoid over time. They include morphological changes accompanying lactation in organoids, namely, appearance of lipid droplets in luminal space, increase in organoid darkness (integrated density), and

the intriguing contraction of myoepithelial cells, which are easily observable by light microscopy and traceable by time-lapse imaging.

Myoepithelial cells form a layer of mammary epithelium that is situated basally to the luminal cells (Macias and Hinck, 2012). Besides the recently elucidated role in keeping epithelial homeostasis and integrity (Adriance et al., 2005; Goodwin and Nelson, 2018; Sirka et al., 2018), the key function of myoepithelial cells is to enable milk ejection by contraction when pups are suckling (Haaksma et al., 2011). In response to tactile stimuli, oxytocin is released from pituitary, and it binds to oxytocin receptor on myoepithelial cell to induce contraction (Nishimori et al., 1996; Froemke and Carcea, 2017). Therefore, oxytocin was used to induce myoepithelial contraction in single cells (Raymond et al., 2011), as well as in an organoid system (Mroue et al., 2015). However, organoid contraction was shown only as a decrease in organoid area
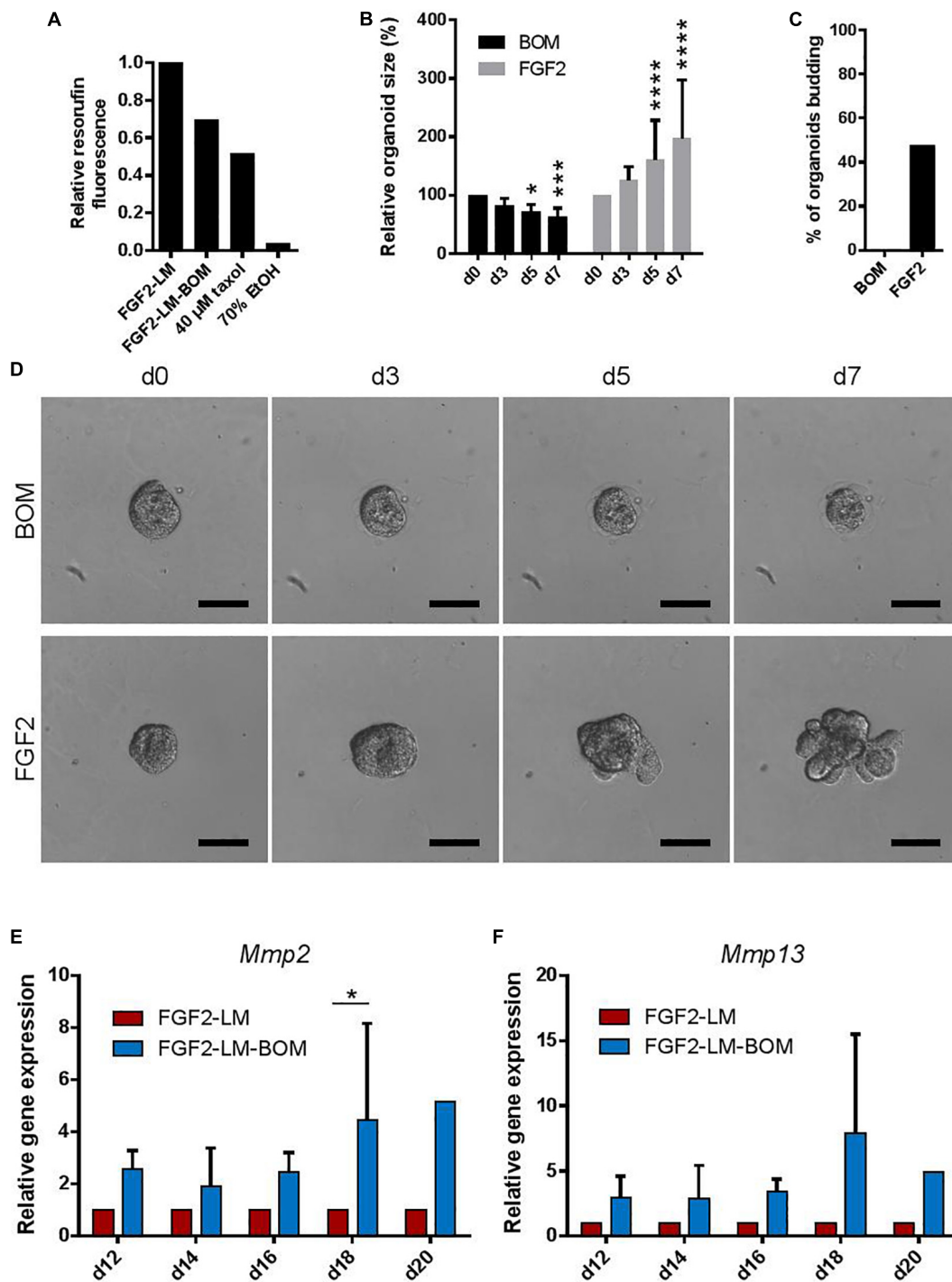
FIGURE 5 | Withdrawing hormones induces an involution-like phenotype in lactating organoids. **(A)** The viability of the lactating and involuting organoids using resazurin assay. The plot shows relative resorufin fluorescence of organoids with continuous LM treatment (FGF2-LM), LM withdrawal and replacement with BOM (FGF2-LM-BOM), and FGF2-LM-BOM organoids treated with 40 μM taxol for 4 days (40 μM taxol) or 70% ethanol for 5 min (70% EtOH) to induce cell death. Values are relative to FGF2-LM. **(B–D)** Analysis of FGF2-LM-BOM organoids after replating to BOM or FGF2 medium. **(B)** Quantification of the size of the FGF2-LM-BOM organoids that were replated and cultured with BOM or FGF2 for the number of days as indicated. The plot shows mean + SD; $n = 1$, $N = 25$ organoids per condition. Two-way ANOVA, asterisks indicate change in comparison to d0; *$p < 0.5$, ***$p < 0.001$, ****$p < 0.0001$. **(C)** Quantification of the number of budding FGF2-LM-BOM organoids after replating and culture with BOM or FGF2 for 7 days. **(D)** Bright-field images showing morphogenesis of FGF2-LM-BOM organoids after replating and culture with BOM or FGF2 for 7 days. Scale bars represent 100 μm. **(E,F)** RT-qPCR analysis of *Mmp2* and *Mmp13* expression in organoids during long-term lactation with continuous lactation medium (LM) treatment or with hormonal/LM withdrawal (LM-BOM). The values are relative to FGF2-LM at each time point. The plots show mean + SD; $n = 3$ for d12–d18, $n = 1$ for d20. Two-way ANOVA, *$p < 0.05$.

over 20 min (Mroue et al., 2015). In contrary, we observed that contraction of a lactating organoid is a very fast process, and the dynamic changes in organoid shape and size are visible to human eye. From videos of contracting organoids, recorded at the rate of one frame per second, we calculated that the frequency is about one contraction per 10 s, which is very similar to the recently reported alveoli warping frequency of lactating mammary tissue upon oxytocin stimulation (Stewart et al., 2019). Therefore, our model provides a suitable *in vitro* system for studying the regulation of the contractile function of myoepithelial cells.

Upon LM withdrawal, lactating organoids underwent involution-like process: regression in size and complexity, which is reversible by FGF2 treatment upon reseeding; and up-regulation of the expression of MMPs, the proteases typically found in mammary gland during involution (Lund et al., 1996; Green and Lund, 2005). Involution-like morphological changes upon prolactin withdrawal were documented also in the 3D coculture model of lactation using mammary epithelial and preadipocyte cell lines. However, epithelial cells cultured without preadipocytes were not reported (Campbell et al., 2014). Thus, for the first time in organoid culture, we show that involution-like regression of epithelium occurs, at least in part, in an epithelium-intrinsic manner. Our observations do not contradict the crucial role of paracrine signaling required for proper involution, including the leukemia inhibitory factor and TGFβ signaling that activate STAT3-mediated regression of epithelium (Nguyen and Pollard, 2000; Kritikou et al., 2003; Hughes and Watson, 2012). Our results point to the existence of epithelial-intrinsic mechanisms of involution, for study of which our epithelial-only organoid model could be advantageous. Certainly, more work is required to establish this model as a valid system for studying physiological involution. In this study, we did not evaluate the onset of programmed cell death and its regulation. In addition, optimization of the culture conditions with cytokine cocktail would be required to further mimic physiological involution.

Several human diseases, developmental defects, or insufficiencies in mammary epithelial tissue are linked to lactation and involution period. Among others, inadequate milk production affects many women after giving birth, especially after premature deliveries and with obese mothers (Olsen and Gordon, 1990; Kent et al., 2012; Nommsen-Rivers, 2016). We propose that human breast tissue, gained from reduction mammoplasties, could be utilized to isolate primary human breast organoids for an analogous lactation assay. Furthermore, findings from murine organoids could be translated into human organoids to identify physiological barriers for lactation, which will provide valuable information for developing novel interventions to support lactation success and provide health benefit across two generations. Moreover, our organoid model could be used to investigate mechanisms of pregnancy-associated breast cancer, an aggressive form of breast cancer with peak of incidence within 5 years after delivery (Schedin, 2006). Mammary organoids isolated from genetic mouse models, such as animals carrying mutations in oncogenes or tumor suppressors, or organoids exposed to carcinogens could be used in our lactation model to unveil mechanisms and signaling pathways leading to epithelial cell carcinogenesis.

DATA AVAILABILITY STATEMENT

The raw data supporting the conclusions of this article will be made available by the authors, without undue reservation, to any qualified researcher.

ETHICS STATEMENT

The animal study was reviewed and approved by the French legislation in compliance with European Communities Council Directives (A 75-15-01-3), the regulations of Institut Pasteur Animal Care Committees (CETEA),the Ministry of Agriculture of the Czech Republic, and the Expert Committee for Laboratory Animal Welfare at the Faculty of Medicine, Masaryk University.

AUTHOR CONTRIBUTIONS

JS, AC, EC, and ZK performed the experimental work. AC, JS, ZK, and HL contributed to the experimental design and data analysis. AC, ZK, and HL supervised the study. All the authors interpreted the data. ZK and HL acquired funding for the study. AC, JS, and ZK wrote the manuscript. All authors discussed the results and approved the final version of the manuscript.

FUNDING

ACKNOWLEDGMENTS

Masaryk University. We also thank the Revive Consortium for funding the exchange program. We acknowledge the core facility CELLIM of CEITEC supported by the Czech-BioImaging large RI project (LM2015062 funded by MEYS CR) for their support with obtaining scientific data presented in this manuscript.

SUPPLEMENTARY MATERIAL

The Supplementary Material for this article can be found online at: https://www.frontiersin.org/articles/10.3389/fcell.2020.00068/full#supplementary-material

REFERENCES

Ackland, M. L., Ward, J., Ackland, C. M., Greaves, M., and Walker, M. (2003). Extracellular matrix induces formation of organoids and changes in cell surface morphology in cultured human breast carcinoma cells PMC42-LA. *In Vitro Cell. Dev. Biol. Anim.* 39, 428–433. doi: 10.1290/1543-706X2003039

Adriance, M. C., Inman, J. L., Petersen, O. W., and Bissell, M. J. (2005). Myoepithelial cells: good fences make good neighbors. *Breast Cancer Res.* 7, 190–197. doi: 10.1186/bcr1286

Aoki, M., Wartenberg, P., Grünewald, R., Phillipps, H. R., Wyatt, A., Grattan, D. R., et al. (2019). Widespread Cell-specific prolactin receptor expression in multiple murine organs. *Endocrinology* 160, 2587–2599. doi: 10.1210/en.2019-2234

Artegiani, B., and Clevers, H. (2018). Use and application of 3D-organoid technology. *Hum. Mol. Genet.* 27, R99–R107. doi: 10.1093/hmg/ddy187

Brisken, C., and O'Malley, B. (2010). Hormone action in the mammary gland. *Cold Spring Harb. Perspect. Biol.* 2:a003178. doi: 10.1101/cshperspect.a003178

Brisken, C., and Rajaram, R. D. (2006). Alveolar and lactogenic differentiation. *J. Mammary Gland Biol. Neoplasia* 11, 239–248. doi: 10.1007/s10911-006-9026-9020

Campbell, J. J., Botos, L.-A., Sargeant, T. J., Davidenko, N., Cameron, R. E., and Watson, C. J. (2014). A 3-D in vitro co-culture model of mammary gland involution. *Integr. Biol. Quant. Biosci. Nano Macro.* 6, 618–626. doi: 10.1039/c3ib40257f

Ewald, A. J., Brenot, A., Duong, M., Chan, B. S., and Werb, Z. (2008). Collective epithelial migration and cell rearrangements drive mammary branching morphogenesis. *Dev. Cell* 14, 570–581. doi: 10.1016/j.devcel.2008.03.003

Freestone, D., Cater, M. A., Ackland, M. L., Paterson, D., Howard, D. L., de Jonge, M. D., et al. (2014). Copper and lactational hormones influence the CTR1 copper transporter in PMC42-LA mammary epithelial cell culture models. *J. Nutr. Biochem.* 25, 377–387. doi: 10.1016/j.jnutbio.2013.11.011

Froemke, R. C., and Carcea, I. (2017). "Chapter 13 - oxytocin and brain plasticity," in *Principles of Gender-Specific Medicine*, ed. M. J. Legato (San Diego: Academic Press), 161–182. doi: 10.1016/B978-0-12-803506-1.00037-1

Goodwin, K., and Nelson, C. M. (2018). Myoepithelial crowd control of cancer cells. *J. Cell Biol.* 217, 3319–3321. doi: 10.1083/jcb.201808097

Green, K. A., and Lund, L. R. (2005). ECM degrading proteases and tissue remodelling in the mammary gland. *Bioessays News Rev. Mol. Cell. Dev. Biol.* 27, 894–903. doi: 10.1002/bies.20281

Haaksma, C. J., Schwartz, R. J., and Tomasek, J. J. (2011). Myoepithelial cell contraction and milk ejection are impaired in mammary glands of mice lacking smooth muscle alpha-actin. *Biol. Reprod.* 85, 13–21. doi: 10.1095/biolreprod.110.090639

Hennighausen, L., and Robinson, G. W. (2005). Information networks in the mammary gland. *Nat. Rev. Mol. Cell Biol.* 6, 715–725. doi: 10.1038/nrm1714

Huch, M., and Koo, B.-K. (2015). Modeling mouse and human development using organoid cultures. *Development* 142, 3113–3125. doi: 10.1242/dev.118570

Huebner, R. J., Neumann, N. M., and Ewald, A. J. (2016). Mammary epithelial tubes elongate through MAPK-dependent coordination of cell migration. *Development* 143, 983–993. doi: 10.1242/dev.127944

Hughes, K., and Watson, C. J. (2012). The spectrum of STAT functions in mammary gland development. *JAKSTAT* 1, 151–158. doi: 10.4161/jkst.19691

Jamieson, P. R., Dekkers, J. F., Rios, A. C., Fu, N. Y., Lindeman, G. J., and Visvader, J. E. (2017). Derivation of a robust mouse mammary organoid system for studying tissue dynamics. *Development* 144, 1065–1071. doi: 10.1242/dev.145045

Jena, M. K., Jaswal, S., Kumar, S., and Mohanty, A. K. (2019). Molecular mechanism of mammary gland involution: an update. *Dev. Biol.* 445, 145–155. doi: 10.1016/j.ydbio.2018.11.002

Kent, J. C., Prime, D. K., and Garbin, C. P. (2012). Principles for Maintaining or Increasing Breast Milk Production. *J. Obstet. Gynecol. Neonatal Nurs.* 41, 114–121. doi: 10.1111/j.1552-6909.2011.01313.x

Kim, S.-H., Wu, S.-Y., Baek, J.-I., Choi, S. Y., Su, Y., Flynn, C. R., et al. (2015). A post-developmental genetic screen for zebrafish models of inherited liver disease. *PLoS One* 10:e0125980. doi: 10.1371/journal.pone.0125980

Knight, C. H., Maltz, E., and Docherty, A. H. (1986). Milk yield and composition in mice: effects of litter size and lactation number. *Comp. Biochem. Physiol. A* 84, 127–133. doi: 10.1016/0300-9629(86)90054-x

Koledova, Z. (2017a). 3D cell culture: an introduction. *Methods Mol. Biol.* 1612, 1–11. doi: 10.1007/978-1-4939-7021-6-1

Koledova, Z. (2017b). 3D coculture of mammary organoids with fibrospheres: a model for studying epithelial-stromal interactions during mammary branching morphogenesis. *Methods Mol. Biol.* 1612, 107–124. doi: 10.1007/978-1-4939-7021-6-8

König, B., and Markl, H. (1987). Maternal care in house mice. *Behav. Ecol. Sociobiol.* 20, 1–9. doi: 10.1007/BF00292161

Koopman, R., Schaart, G., and Hesselink, M. K. (2001). Optimisation of oil red O staining permits combination with immunofluorescence and automated quantification of lipids. *Histochem. Cell Biol.* 116, 63–68. doi: 10.1007/s004180100297

Kritikou, E. A., Sharkey, A., Abell, K., Came, P. J., Anderson, E., Clarkson, R. W. E., et al. (2003). A dual, non-redundant, role for LIF as a regulator of development and STAT3-mediated cell death in mammary gland. *Development* 130, 3459–3468. doi: 10.1242/dev.00578

Linnemann, J. R., Miura, H., Meixner, L. K., Irmler, M., Kloos, U. J., Hirschi, B., et al. (2015). Quantification of regenerative potential in primary human mammary epithelial cells. *Development* 142, 3239–3251. doi: 10.1242/dev.123554

Lu, P., Ewald, A. J., Martin, G. R., and Werb, Z. (2008). Genetic mosaic analysis reveals FGF receptor 2 function in terminal end buds during mammary gland branching morphogenesis. *Dev. Biol.* 321, 77–87. doi: 10.1016/j.ydbio.2008.06.005

Lund, L. R., Rømer, J., Thomasset, N., Solberg, H., Pyke, C., Bissell, M. J., et al. (1996). Two distinct phases of apoptosis in mammary gland involution: proteinase-independent and -dependent pathways. *Dev. Camb. Engl.* 122, 181–193.

Macias, H., and Hinck, L. (2012). Mammary gland development. *Wiley Interdiscip. Rev. Dev. Biol.* 1, 533–557. doi: 10.1002/wdev.35

Mroue, R., Inman, J., Mott, J., Budunova, I., and Bissell, M. J. (2015). Asymmetric expression of connexins between luminal epithelial- and myoepithelial- cells is essential for contractile function of the mammary gland. *Dev. Biol.* 399, 15–26. doi: 10.1016/j.ydbio.2014.11.026

Neumann, N. M., Perrone, M. C., Veldhuis, J. H., Huebner, R. J., Zhan, H., Devreotes, P. N., et al. (2018). Coordination of receptor tyrosine kinase signaling and interfacial tension dynamics drives radial intercalation and tube elongation. *Dev. Cell* 45, 67–82.e6. doi: 10.1016/j.devcel.2018.03.011

Nguyen, A. V., and Pollard, J. W. (2000). Transforming growth factor beta3 induces cell death during the first stage of mammary gland involution. *Development* 127, 3107–3118.

Nishimori, K., Young, L. J., Guo, Q., Wang, Z., Insel, T. R., and Matzuk, M. M. (1996). Oxytocin is required for nursing but is not essential for parturition or reproductive behavior. *Proc. Natl. Acad. Sci. U.S.A.* 93, 11699–11704. doi: 10.1073/pnas.93.21.11699

Nommsen-Rivers, L. A. (2016). Does insulin explain the relation between maternal obesity and poor lactation outcomes? an overview of the literature. *Adv. Nutr.* 7, 407–414. doi: 10.3945/an.115.011007

Olsen, C. G., and Gordon, R. E. (1990). Breast disorders in nursing mothers. *Am. Fam. Phys.* 41, 1509–1516.

Parsa, S., Ramasamy, S. K., De Langhe, S., Gupte, V. V., Haigh, J. J., Medina, D., et al. (2008). Terminal end bud maintenance in mammary gland is dependent upon FGFR2b signaling. *Dev. Biol.* 317, 121–131. doi: 10.1016/j.ydbio.2008.02.014

Qu, Y., Han, B., Gao, B., Bose, S., Gong, Y., Wawrowsky, K., et al. (2017). Differentiation of human induced pluripotent stem cells to mammary-like organoids. *Stem Cell Rep.* 8, 205–215. doi: 10.1016/j.stemcr.2016.12.023

Raymond, K., Cagnet, S., Kreft, M., Janssen, H., Sonnenberg, A., and Glukhova, M. A. (2011). Control of mammary myoepithelial cell contractile function by α3β1 integrin signalling. *EMBO J.* 30, 1896–1906. doi: 10.1038/emboj.2011.113

Schedin, P. (2006). Pregnancy-associated breast cancer and metastasis. *Nat. Rev. Cancer* 6, 281–291. doi: 10.1038/nrc1839

Shamir, E. R., and Ewald, A. J. (2014). Three-dimensional organotypic culture: experimental models of mammalian biology and disease. *Nat. Rev. Mol. Cell Biol.* 15, 647–664. doi: 10.1038/nrm3873

Simian, M., Hirai, Y., Navre, M., Werb, Z., Lochter, A., and Bissell, M. J. (2001). The interplay of matrix metalloproteinases, morphogens and growth factors is necessary for branching of mammary epithelial cells. *Development* 128, 3117–3131.

Sirka, O. K., Shamir, E. R., and Ewald, A. J. (2018). Myoepithelial cells are a dynamic barrier to epithelial dissemination. *J. Cell Biol.* 217, 3368–3381. doi: 10.1083/jcb.201802144

Stein, T., Salomonis, N., and Gusterson, B. A. (2007). Mammary gland involution as a multi-step process. *J. Mammary Gland Biol. Neoplasia* 12, 25–35. doi: 10.1007/s10911-007-9035-9037

Sternlicht, M. D. (2006). Key stages in mammary gland development: the cues that regulate ductal branching morphogenesis. *Breast Cancer Res.* 8:201. doi: 10.1186/bcr1368

Stewart, T. A., Hughes, K., Stevenson, A. J., Marino, N., Ju, A. L., Morehead, M., et al. (2019). Mammary mechanobiology: PIEZO1 mechanically-activated ion channels in lactation and involution. *bioRxiv* [Preprint], doi: 10.1101/649038

Sumbal, J., and Koledova, Z. (2019). FGF signaling in mammary gland fibroblasts regulates multiple fibroblast functions and mammary epithelial morphogenesis. *Development* 146:dev185306. doi: 10.1242/dev.185306

Vorherr, H., Vorherr, U. F., and Solomon, S. (1978). Contamination of prolactin preparations by antidiuretic hormone and oxytocin. *Am. J. Physiol.* 234, F318–F324. doi: 10.1152/ajprenal.1978.234.4.F318

Watson, C. J. (2006). Key stages in mammary gland development - involution: apoptosis and tissue remodelling that convert the mammary gland from milk factory to a quiescent organ. *Breast Cancer Res.* 8:203. doi: 10.1186/bcr1401

Xian, W., Schwertfeger, K. L., Vargo-Gogola, T., and Rosen, J. M. (2005). Pleiotropic effects of FGFR1 on cell proliferation, survival, and migration in a 3D mammary epithelial cell model. *J. Cell Biol.* 171, 663–673. doi: 10.1083/jcb.200505098

Zwick, R. K., Rudolph, M. C., Shook, B. A., Holtrup, B., Roth, E., Lei, V., et al. (2018). Adipocyte hypertrophy and lipid dynamics underlie mammary gland remodeling after lactation. *Nat. Commun.* 9:3592. doi: 10.1038/s41467-018-05911-5910

A Robust Mammary Organoid System to Model Lactation and Involution-like Processes

Elsa Charifou[1], Jakub Sumbal[1, 2], Zuzana Koledova[2], Han Li[1] and Aurélie Chiche[1, *]

[1]Cellular Plasticity & Disease Modeling - Department of Developmental & Stem Cell Biology, CNRS UMR3738 - Institut Pasteur, 25 rue du Dr Roux, Paris 75015, France; [2]Department of Histology and Embryology, Faculty of Medicine, Masaryk University, Kamenice 3, Brno 625 00, Czech Republic

*For correspondence: aurelie.chiche@pasteur.fr

[Abstract] The mammary gland is a highly dynamic tissue that changes throughout reproductive life, including growth during puberty and repetitive cycles of pregnancy and involution. Mammary gland tumors represent the most common cancer diagnosed in women worldwide. Studying the regulatory mechanisms of mammary gland development is essential for understanding how dysregulation can lead to breast cancer initiation and progression. Three-dimensional (3D) mammary organoids offer many exciting possibilities for the study of tissue development and breast cancer. In the present protocol derived from Sumbal et al., we describe a straightforward 3D organoid system for the study of lactation and involution *ex vivo*. We use primary and passaged mouse mammary organoids stimulated with fibroblast growth factor 2 (FGF2) and prolactin to model ~~the~~ three cycles of mouse mammary gland lactation and involution processes. This 3D organoid model represents a valuable tool to study late postnatal mammary gland development and breast cancer, in particular postpartum-associated breast cancer.

Graphic abstract:
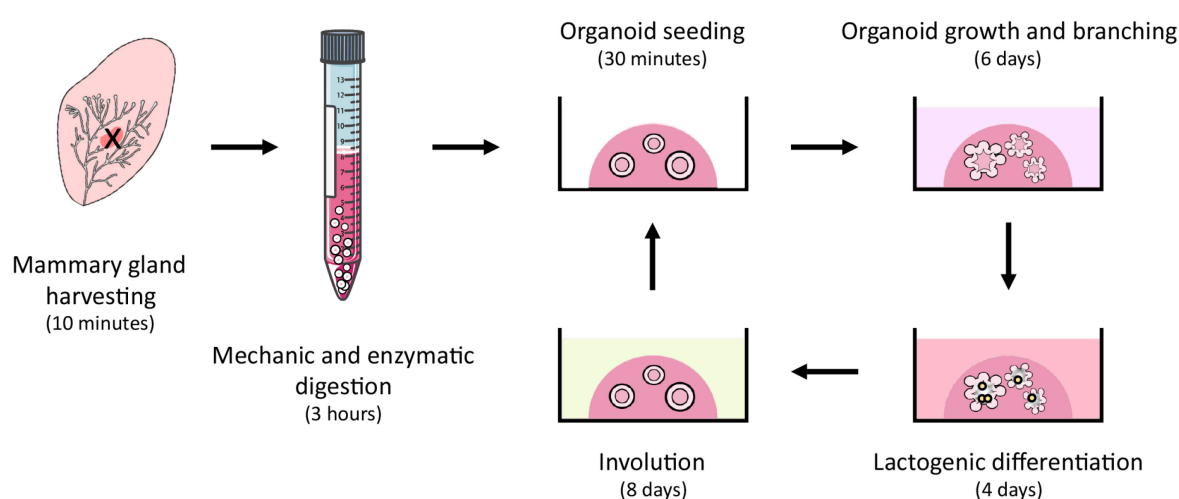
Mammary gland organoid isolation and culture procedures

Keywords: Mouse, Mammary gland, 3D organoid, *Ex vivo*, Lactation, Involution

[Background] The primary function of the mammary gland is to provide nutrition to newborns via milk production. The development of the mammary gland is a highly dynamic process that occurs mainly after birth and is regulated by several factors including hormones and growth factors (Brisken and Rajaram, 2006; Sternlicht, 2006). During puberty, hormones and growth factors regulate ductal morphogenesis from a rudimentary embryonic ductal tree (Brisken and O'Malley, 2010). During each pregnancy, the mammary gland begins a new morphogenetic step initiated by hormonal stimulation, which is characterized by massive proliferation for epithelial expansion and alveolar development accompanied by adipocyte regression (Brisken and O'Malley, 2010). Importantly, prolactin signaling plays a crucial role in the terminal differentiation of luminal cells to enable milk production (Ormandy *et al.*, 1997). At the end of lactation after weaning of the progeny, the mammary gland enters the involution stage characterized by programmed cell death, tissue remodeling, and redifferentiation of adipocytes (Hughes and Watson, 2012; Macias and Hinck, 2012; Zwick *et al.*, 2018; Jena *et al.*, 2019).

Histologically, the mammary gland is composed of a bilayered epithelium consisting of an inner layer of luminal cells (keratin 8+) and an outer layer of contractile basal cells (keratin 5+). Luminal cells are responsible for milk production during lactation, while basal cells aid milk ejection. The epithelium is surrounded by a stromal fat pad that comprises fibroblasts, nerves, vasculature, lymphatics, immune cells, adipocytes, and extracellular matrix (ECM) (Richert *et al.*, 2000).

Over the past decade, organoids of various tissues, such as stomach, colon, lung, and pancreas, have been developed (Huch and Koo, 2015), offering many exciting possibilities for the study of tissue development and disease. The organoid system is a powerful tool that combines the advantages of a 2D culture (easy manipulation, precise control of cell composition and microenvironment, live imaging) with the opportunity to study complex cell–cell and cell–ECM interactions in a more controlled *ex vivo* manner (Huch and Koo, 2015; Shamir and Ewald, 2015; Koledova, 2017; Artegiani and Clevers, 2018).

Several models have been developed to study the mechanisms of mammary branching morphogenesis in primary mammary epithelium using different protocols (Ewald *et al.*, 2008; Huebner *et al.*, 2016; Neumann *et al.*, 2018), cell lines (Xian *et al.*, 2005), sorted cells *(*Jamieson *et al.,* 2017*;* Linnemann *et al.*, *2015*), or induced pluripotent stem cells (Qu *et al.*, 2017). However, an organoid system modeling key aspects of the late postnatal developmental stages of the mammary gland has remained challenging to establish.

Previously, there have been several attempts to model lactation in 3D culture: spheroids of a breast adenoma cell line were used to study copper secretion into milk (Freestone *et al.*, 2014); organoids of primary epithelium were shown to produce milk following the administration of a lactogenic stimulus (Mroue *et al.*, 2015; Jamieson *et al.*, 2017); and co-culture of breast epithelium and pre-adipocyte cell lines was shown to initiate an involution-like process (Campbell *et al.*, 2014). However, in-depth characterization of milk production and involution or the proper bilayered architecture of mammary epithelium remained to be carried out.

Recently, we developed a model of lactation and involution of mammary epithelium based on organoids of primary mammary gland tissue cultured in 3D Matrigel® (Sumbal *et al.*, 2020b). Under lactogenic stimuli, primary organoids maintain long-term milk production, retain the contractile

myoepithelial layer, and enter involution following hormone withdrawal. Moreover, after involution, the organoids remain hormonally sensitive and are able to enter another round of lactation (Sumbal *et al.*, 2020b). Here, we present a methodological guideline to establish the primary mammary organoid-based *ex vivo* model of lactation and involution, with detailed procedures for obtaining tissue, isolating organoids, establishing and maintaining 3D culture, and preparing organoid samples for subsequent RNA or protein expression analysis or histological examination. This model can be used for studies on lactation biology, mammary stem cell plasticity, regulatory mechanisms of mammary epithelial cell differentiation and death, or other interesting biological phenomena. We believe that this model will initiate the further development of organoid technology, including creative applications in biotechnology and regenerative medicine (Sumbal *et al.*, 2020a).

Materials and Reagents

1. 100-mm tissue culture Petri dish (*e.g.*, Corning, catalog number: 353003)
2. 0.2-µm filters and 50 ml syringes (*e.g.*, GVS, catalog number: FJ25ASCCA002DL01)
3. No. 22 disposable scalpel blades (*e.g.*, Swann-Morton, catalog number: 0508)
4. 50-ml tubes (*e.g.*, Corning, catalog number: 352070)
5. 15-ml tubes (*e.g.*, Corning, catalog number: 352096)
6. 10-ml disposable plastic pipettes (*e.g.*, Corning, catalog number: 357551)
7. 25-ml disposable plastic pipettes (*e.g.*, Corning, catalog number: 357535)
8. 24-well tissue culture plates (*e.g.*, Corning, catalog number: 353047)
9. 30 G insulin syringes (*e.g.*, BD Microfine, catalog number: 324826)
10. Plastic histology molds (*e.g.*, Thermo Scientific, catalog number: 1830)
11. Plastic embedding cassettes (*e.g.*, Simport, catalog number: M492-2)
12. Histology tissue molds (*e.g.*, Simport, catalog number: M474-3)
13. Microscope slides for histology (*e.g.*, Thermo Scientific, catalog number: J1800AMNZ)
14. Mice: virgin females, 7–10 weeks old, inbred strain C57BL/6J (*e.g.*, The Jackson Laboratory, catalog number: 000664)
15. Ethanol (EtOH), 70%, 95%, and 100% (*e.g.*, VWR, catalog number: 83813)
16. Phosphate-buffered saline (PBS) (*e.g.*, Sigma-Aldrich, catalog number: D1408)
17. Dulbecco's modified Eagle medium (DMEM)/F12 (*e.g.,* Gibco, catalog number: 21331-020)
18. Bovine serum albumin (BSA) (*e.g.*, Sigma-Aldrich, catalog number: A3608)
19. Fetal bovine serum (FBS) (*e.g.*, Sigma-Aldrich, catalog number: F0804)
20. Collagenase A (*e.g.*, Roche, catalog number:11088793001)
21. Trypsin (*e.g.,* Dutcher Dominique, catalog number: P10-022100)
22. Insulin (*e.g.*, Sigma-Aldrich, catalog number: I6634-100MG)
23. Gentamicin (*e.g.*, Sigma-Aldrich, catalog number: G1397)
24. Glutamine (*e.g.*, Gibco, catalog number: 35050-061)
25. DNase I (*e.g.*, Sigma-Aldrich, catalog number: D4527-40KU)

26. Dispase II (*e.g.*, Roche, catalog number: 13 75 2000)

27. Growth factor-reduced Matrigel® (*e.g.*, Corning, catalog number: 354230)

28. Insulin-transferrin-selenium (ITS) (*e.g.*, Gibco, catalog number: 41400-045)

29. Penicillin/Streptomycin (*e.g.*, Gibco, catalog number: 15140-122)

30. FGF2 (*e.g.*, Gibco, catalog number: PM60034)

31. Prolactin (*e.g.*, Sigma-Aldrich, catalog number: SRP4688)

32. Hydrocortisone (*e.g.*, Sigma-Aldrich, catalog number: S H6909)

33. Oxytocin (*e.g.*, Sigma-Aldrich, catalog number: O3251)

34. RNeasy Micro Kit (*e.g.*, Qiagen, catalog number: 74004)

35. β-Mercaptoethanol (*e.g.*, Sigma-Aldrich, catalog number: M6250)

36. Phosphatase inhibitor cocktail II (*e.g.*, Millipore, catalog number: 524625)

37. RIPA buffer (*e.g.*, Sigma-Aldrich, catalog number: R0278)

38. Protease inhibitor cocktail I (*e.g.*, Sigma-Aldrich, catalog number: 539131)

39. Pierce Coomassie (Bradford) Protein Assay Kit (*e.g.*, Thermo Scientific, catalog number: 23200)

40. Paraformaldehyde (PFA), 32% (*e.g.*, Electron Microscopy Sciences, catalog number: 15714)

41. Low gelling temperature agarose (*e.g.*, Sigma-Aldrich, catalog number: A9414)

42. Xylene (*e.g.*, Sigma-Aldrich, catalog number: 534056)

43. Paraffin (*e.g.*, Sigma-Aldrich, catalog number: 1071642504)

44. Dissociation solution (see Recipes)

45. BSA solution (see Recipes)

46. Basal organoid medium (BOM) (see Recipes)

47. Morphogenesis medium (see Recipes)

48. Lactation medium (see Recipes)

49. 4% PFA (see Recipes)

50. RNA lysis buffer (see Recipes)

Equipment

1. Surgical tools

   Forceps (*e.g.*, Phymep, catalog numbers: 11050-10 and 11051-10)

   Scissors (*e.g.*, Phymep, catalog number: 14088-10)

2. Dissection board (*e.g.*, Thermo Scientific, catalog number: 36-119)

3. P1000 pipette

4. Laminar flow hood

5. Fridge 4°C (*e.g.*, Liebherr, catalog number: 7083 001-01)

6. Freezer –80 °C (*e.g.*, Thermo Scientific, catalog number: 88400V)

7. Liquid nitrogen tank (*e.g.*, Air Liquide Espace 151, catalog number: 2433867)

8. Shaking incubator at 37°C (*e.g.*, Infors HT Multitron)

9. Centrifuge (*e.g.*, Thermo Scientific, model: Sorvall ST40)

10. Incubator for cell culture, 37°C, 5% CO_2 (*e.g.*, Thermo Scientific, model: HERAcell 150i)

11. Heating plate at 37°C (*e.g.*, Techne DRI-Block DB-2A)

12. Microscope and camera (*e.g.*, Olympus model: CKX41)

13. NanoDrop™ (*e.g.*, Implen Nanophotomoter NP80)

14. Sonicator (*e.g.*, Diagenode Bioruptor Pico)

15. Incubator at 65°C (*e.g.*, Memmert Incubator I)

16. Embedding workstation (*e.g.*, Leica EG1150C)

Procedure

A. Isolation of mammary primary organoids

   1. Dissection of a virgin mouse to harvest mammary glands (see Video 1).

Video 1. Mammary gland harvesting. This video was made at Pasteur Institute. according to guidelines from the regulations of Institut Pasteur Animal Care Committees (CETEA). on Animal Care and approved by the French legislation in compliance with European Communities Council Directives (A 75-15-01-3).

   a. Euthanize the donor mouse using an ethically approved method (*e.g.*, cervical dislocation) and immediately proceed to mammary gland collection.
   Notes:
   i. *Cervical dislocation is a common method for animal euthanasia and provides a fast and painless death. With this method, cell/tissue survival in culture is not altered if collected immediately.*
   ii. *In the case of processing multiple mice, euthanize one animal and collect the glands immediately, then proceed to the next animal.*

   b. Sanitize the ventral side of the animal by spraying 70% EtOH on the skin.
   Note: After disinfection, work inside a laminar flow hood to maintain aseptic conditions. Application of aseptic work procedures, together with the presence of antimycotic and

antibiotic supplements (gentamicin in digestion solution; penicillin and streptomycin in culture medium) will prevent the occurrence of contamination.

c. Pin the mouse by its four paws to a dissection board, with the abdomen facing upward (see Figure 1A, pins 1–4).

d. Using forceps, tightly grasp the skin of the lower part of the abdomen at half the width (see Figure 1A, point A).

e. Using surgical scissors, make the first incision in the skin at point A.
Note: Be careful to incise only the skin and not rupture the underlying peritoneum.

f. Continue to incise the skin cranially to the throat of the animal (see Figure 1A, from point A to point B).

g. From this median line, use forceps to grasp the skin and cut toward each of the four paws (see Figure 1A, incise to join the middle line to points C, D, E or F, respectively).

h. Using forceps and a cotton swab, gently separate the skin from the peritoneum on one side of the animal. Attach the skin to the dissection board with three pins (see Figure 1B, pins 5–7).

i. Repeat step 8 on the other side of the animal (see Figure 1B, pins 8–10). The mammary glands are now exposed.

j. Identify the lymph node of the mammary gland #4 (a small dense structure, round in shape; see Figure 1B, surrounded). Remove the lymph node from both glands using forceps and scissors and discard.

k. Proceed to the harvest of the mammary glands #3 and #4. Using curved forceps, grasp the mammary glands and gently separate them from the skin and other tissues with scissors.
Note: Carefully separate the mammary glands #3 (whitish and shiny) from the muscles (light brown ribbed structure) since this protocol does not prevent muscle contamination.

l. Place all the collected glands in the same sterile Petri dish containing cold PBS (approximately 3 ml, previously stored at 4°C) for washing prior to tissue processing.

m. Properly dispose of the animal corpse and continue with mechanical and enzymatic dissociation of the mammary glands.

2. Mechanical and enzymatic dissociation
Reminder: Work inside a laminar flow hood to maintain aseptic conditions.

a. Freshly prepare 10 ml dissociation solution for the four glands collected from one mouse, pass through a 0.2-μm filter, and pre-heat at 37°C.
Note: Do not exceed the maximum 30 ml dissociation solution in a 50-ml tube to ensure correct dissociation.

b. Transfer the freshly collected mammary glands to a new sterile Petri dish.

c. Use three scalpels to finely chop the mammary glands and obtain a homogeneous mince of 1-mm^3 mammary fragments (see Figure 1C).

d. Transfer the mince to a 50-ml tube containing the pre-warmed dissociation solution.

e. Place the tube in a shaking incubator for 30 min at 37°C, 100 rpm.

Notes:

i.   All the following steps are performed at room temperature except incubation with dispase.

ii.   From here on, pre-coat all the pipettes, tips, and tubes with 2.5% BSA solution. Prepare the BSA solution in a 50-ml tube and aspirate/remove from every consumable following coating; this will prevent stickiness and loss of organoids. The BSA solution can then be filtered, stored at 4°C, and re-used.

f.   After incubation, resuspend the dissociated mammary glands by performing ten up-and-down motions with a 10-ml pipette. Centrifuge for 10 min at 400 × *g*.

g.   After centrifugation, handle the 50-ml tube carefully to prevent disturbance of the three separated layers (see Figure 1C). Keep the epithelial pellet intact and transfer the middle aqueous phase and the top fatty layer into a clean 15-ml tube.

h.   Resuspend the epithelial pellet in 5 ml DMEM/F12 and set it aside.

i.   Focus on the fatty and aqueous solutions in the 15-ml tube: resuspend by performing ten up-and-down motions with a 10-ml pipette. Centrifuge for 10 min at 400 × *g*.
     Note: This step allows recovery of epithelial fragments trapped in the fatty layer.

j.   Again, handle the 15-ml tube carefully to avoid disturbing the three separated layers. Discard the fatty and aqueous layers.

k.   Take the 5 ml resuspended pellet from the 50-ml tube to resuspend the pellet in the 15-ml tube.

l.   Wash the 50-ml tube with 5 ml DMEM/F12, pool with the suspension in the 15-ml tube, and mix.

m.   Centrifuge for 10 min at 400 × *g*.

n.   Discard the supernatant. Use 4 ml DMEM/F12 to resuspend the pellet. Subsequently, add 80 µl DNAse I at 100 µg/ml and agitate for 5 min by hand or on an orbital shaker at 100 rpm.

o.   Add 6 ml DMEM/F12 and resuspend the solution by performing 5 up-and-down motions with a 10-ml pipette.

p.   Centrifuge for 10 min at 400 × *g*.

q.   Discard the supernatant. Use 4 ml DMEM/F12 to resuspend the pellet. Subsequently, add 150 µl dispase II at 0.5 mg/ml and incubate for 5 min at 37°C.

r.   Add 6 ml DMEM/F12 and resuspend the solution by performing 5 up-and-down motions with a 10-ml pipette.

s.   Centrifuge for 10 min at 400 × *g*.

t.   Discard the supernatant. Resuspend the pellet in 9 ml DMEM/F12.

u.   Perform differential centrifugation to separate the mammary epithelium from the stromal fraction: centrifuge the suspension for 15 s at room temperature, 400 × *g*. Discard the supernatant containing the stromal fraction and resuspend the epithelial pellet in 9 ml DMEM/F12.

Note: Set the time on the centrifuge to 1 min. Once a speed of 400 × g is reached, time 15 s precisely and stop the centrifuge manually.

v.   Repeat the previous step (t) 4 times, for a total of 5 differential centrifugations, to efficiently remove stromal contamination.

w.   Resuspend the final pellet in 1 ml basal organoid medium (BOM) and place on ice. The organoids are now ready to be counted and cultured.

Note: Adjust the volume of resuspension according to pellet size. From a pool of 2–3 mice, the final pellet was resuspended in 1 ml basal organoid medium, for an expected range of 3,000–6,000 organoids. Adjust the volume of BOM for resuspension of the pellet according to the number of mice pooled.
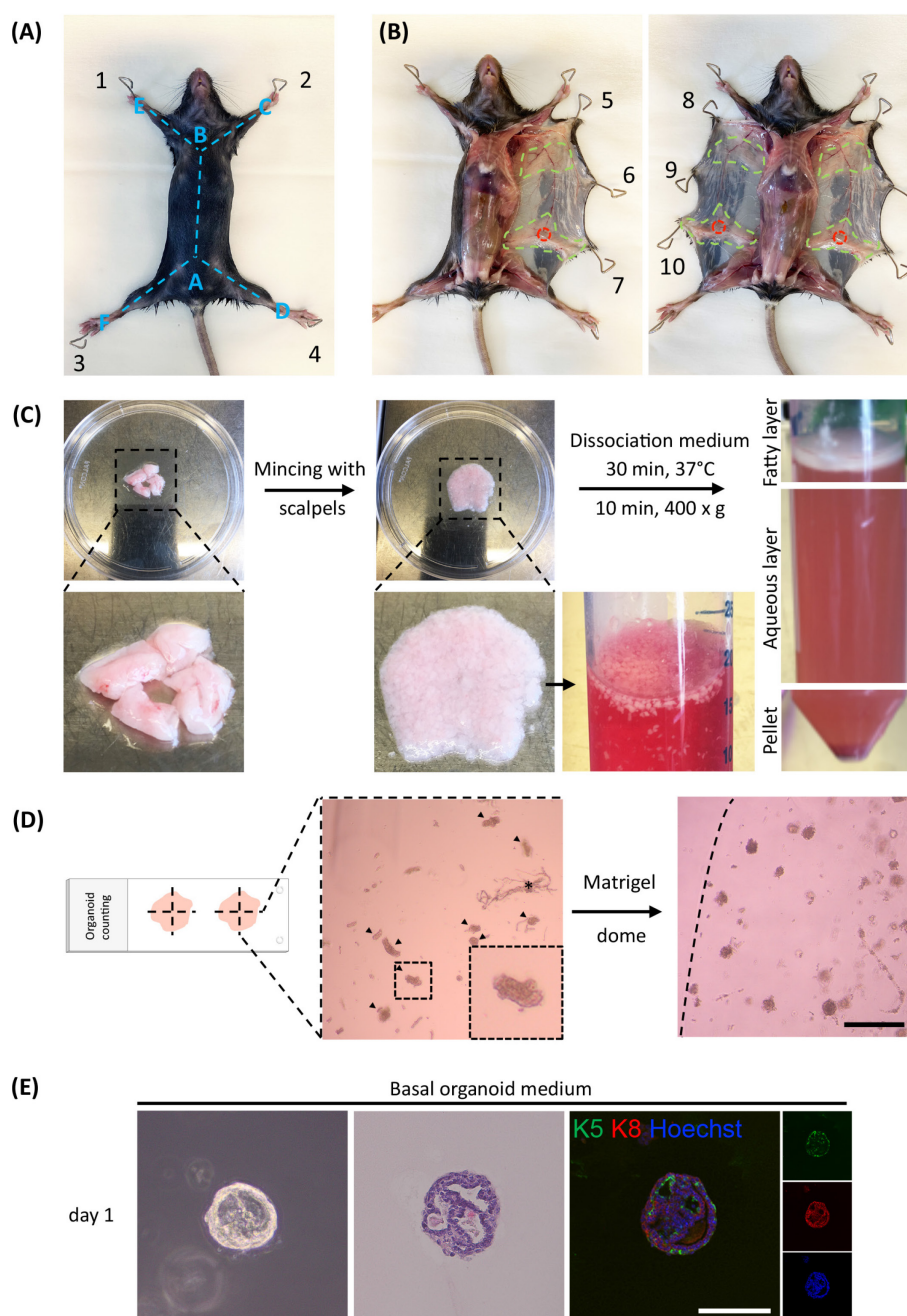
Figure 1. Key steps of mammary gland collection for organoid isolation and 3D culture. A,B. Images of mouse dissection to access the mammary gland. A. Needles 1–4 represent the points at which to pin the mouse. Needles 5–7 and 8–10 represent the points at which to pin the skin of the mouse. Letters A–F with the blue dotted lines indicate the cuts. B. Green dotted lines denote the mammary gland. The lymph node is denoted in red and must be removed. C. Mammary gland before (left panel) and after (middle panel) mincing with a scalpel. Mammary organoids after transfer to dissociation medium (right panel). D. Example of mammary organoid counting. Left panel: organoids are surrounded by dotted lines. Star represents nerves. Right panel: organoids after embedding in Matrigel®. Arrow represents the edge of the Matrigel® dome. Scale bar = 500 μm. E. Freshly isolated primary organoid. Left panel: image of a mammary

organoid on day 1 post-isolation. Middle panel: Hematoxylin & eosin staining of an organoid on day 1 post-isolation. Right panel: immunofluorescence staining showing the distribution of myoepithelial (keratin 5+, green) and luminal cells (keratin 8+, red) in organoids on day 1 post-isolation. Hoechst, blue (nuclei). Scale bar = 100 μm.

3. Organoid counting

   Reminder: Work inside a laminar flow hood to maintain aseptic conditions.

   a. Draw two large crosses with a marker on a microscope slide.

   b. Take the organoid suspension and homogenize by performing five up-and-down motions with a P1000 pipette.

   c. On the reverse side of the slide, spread 10 μl solution around the center of each cross.
      Note: Use a 20-μl tip or cut the extremity of a 10-μl tip to avoid large organoids becoming trapped.

   d. Count the organoids under the microscope at 4× magnification (see Figure 1D).
      Notes:
      i. *Take each quarter of the cross as a landmark to avoid double-counting of the same organoid.*
      ii. *Organoids appear as rounded structures with a smooth perimeter. Occasionally and unavoidably, nerves and endothelium are also present. The nerves appear as rope-like structures and can be organized in bundles (see Figure 1D). The endothelium has a somewhat ragged look in comparison with the smooth-looking organoids. The minor presence of primary nerves and endothelium does not interfere with organoid lactation or involution.*
      iii. *Count only the organoids with a diameter greater than 30–50 μm since the smaller ones may not develop properly.*

   e. Calculate the average of the two counts in 10 μl solution and multiply according to the volume of BOM used to resuspend the pellet to obtain the total number of organoids.
      Note: Freshly isolated organoids can be viably frozen in a solution of FBS containing 10% DMSO for long-term storage in liquid nitrogen and later use.

B. 3D culture of mammary organoids

   1. Embedding in Matrigel®

      Reminder: Work inside a laminar flow hood to maintain aseptic conditions. Wash the ice bucket and heating plate thoroughly with 70% EtOH prior to placement in the laminar flow hood.

      a. Thaw the Matrigel® on ice or at 4°C.
         Notes:
         i. *Matrigel® solidifies really fast at room temperature. Always keep it on ice before use and during the plating procedure.*

www.bio-protocol.org/e3996

Bio-protocol 11(08): e3996.
DOI:10.21769/BioProtoc.3996

    ii. *Keep in mind that Matrigel® thawing takes time; therefore, begin thawing prior to the procedure (2 h for a 1-ml aliquot, 6 h for a 10-ml bottle).*

b. Place a 24-well plate on ice. Calculate the number of wells needed and spread 20-μl Matrigel® in a round patch on the bottom of each well.

    Note: Start by placing the tip containing Matrigel® at the center of a well and expand circularly towards the edges of the well, without touching them.

c. Incubate the 24-well plate in a cell incubator (5% CO_2) for 15 min at 37°C.

d. In the meantime, pre-heat a heating plate to 37°C.

e. Prepare the organoid suspension in the Matrigel®: calculate the volume of organoid suspension required to obtain the desired number of organoids. Pipette this volume of suspension into a fresh 1.5-ml tube and centrifuge for 3 min at 400 × *g*.

    Note: Adjust the number of organoids per well depending on the type of experiment: 200 organoids per well for morphology and histology, 400 for gene expression, and 1000 for western blotting analysis.

f. Carefully remove the supernatant and place the tube on ice. Subsequently, carefully resuspend the pellet in the required volume of cold Matrigel® (50 μl per well), avoiding bubble formation. Keep on ice.

g. Remove the 24-well plate from the cell incubator and place on the 37°C heating plate.

h. In each Matrigel®-precoated well, cautiously seed the suspension of organoids (in Matrigel®) as a dome on top of the solidified Matrigel® patch.

i. Place the 24-well plate back in the cell incubator (5% CO_2) for 30 min at 37°C to solidify the Matrigel® (see Figure 1D).

j. In the meantime, pre-warm BOM at 37°C.

k. Following incubation, carefully add 1 ml pre-heated BOM to each well and culture in the cell incubator at 37°C, 5% CO_2.

    Notes:

    i. *Add medium against the edges of the well to avoid disruption of the dome.*

    ii. *Characterization of the organoids can be performed using regular histological stains (e.g., hematoxylin & eosin) or immunostaining on day 1 post-recovery in BOM (see Figure 1E and Step B2 of the procedure).*

2. Morphogenesis with FGF2

Reminder: Work inside a laminar flow hood to maintain aseptic conditions.

Note: Overnight recovery is optimal for organoid culture; however, FGF2 treatment can be administered immediately after plating the organoids.

a. Pre-heat the BOM at 37°C.

b. Add fresh FGF2 at a final concentration of 2.5 nM to pre-heated BOM to obtain the morphogenesis medium.

c. Aspirate the medium from the wells without touching the Matrigel® dome and replace with 800 μl fresh morphogenesis medium.

    d. Renew all medium with fresh morphogenesis medium every 3 days, for a total of 6 days of treatment.

3.   Lactogenic differentiation with prolactin

    a. Pre-heat the BOM at 37°C.

    b. Add 1 µg/ml prolactin and 1 µg/ml hydrocortisone to the pre-heated BOM to obtain the lactation medium.

    c. Aspirate the medium from the wells without touching the Matrigel® dome and replace with 800 µl fresh lactation medium.

    d. Renew all medium with fresh lactation medium every two days, for a total of 4 days of treatment.

4. Myoepithelial cell contraction with oxytocin

    a. Prepare fresh lactation medium, filter, and pre-heat at 37°C.

    b. Add 40 µg/ml recombinant oxytocin to the lactation medium.

    c. Aspirate the medium from the wells without touching the Matrigel® dome and replace with 800 µl fresh lactation medium supplemented with oxytocin.

    d. Using live cell imaging, record contraction images every second for 120 s.

5. Mimicking involution by hormonal withdrawal

    a. Pre-heat the BOM at 37°C.

    b. Aspirate the medium from the wells without touching the Matrigel® dome and replace with 800 µl fresh BOM.

    c. Renew all medium with BOM every two days, for a total of 8 days of treatment.

6. Replating

   Note: Use tips pre-coated with 2.5% BSA.

    a. Aspirate the supernatant and wash the wells twice with 800 µl cold PBS.

    b. Add 1 ml cold PBS and disrupt the Matrigel® dome using an up-and-down motion with a P1000 pipette.

    c. Check for successful disintegration of the Matrigel® under a microscope.

    d. Transfer the suspension to a 15-ml tube and add cold PBS to a total volume of 10 ml.

    e. Centrifuge for 3 min at 400 × *g*.

    f. Carefully remove the supernatant, resuspend the organoid pellet in fresh Matrigel® and plate as described in B1.

C. Organoid processing for further analysis

Note: We suggest carefully following organoid development under the microscope before renewing the media. Morphogenesis with FGF2 should induce branching after 3–4 days of treatment, while organoids in culture with BOM only, as the negative control, should remain round. Lactogenic differentiation can be confirmed by analysis of Csn2 mRNA using qPCR, comparing organoids before and after prolactin treatment (d6 versus d10). The involution process can also be confirmed using qPCR by detecting decreased expression of Csn2 mRNA following prolactin withdrawal (d10

www.bio-protocol.org/e3996

versus d18), or at the morphological level by the progressive disappearance of branching (see Figure 2B and Figure 3B).
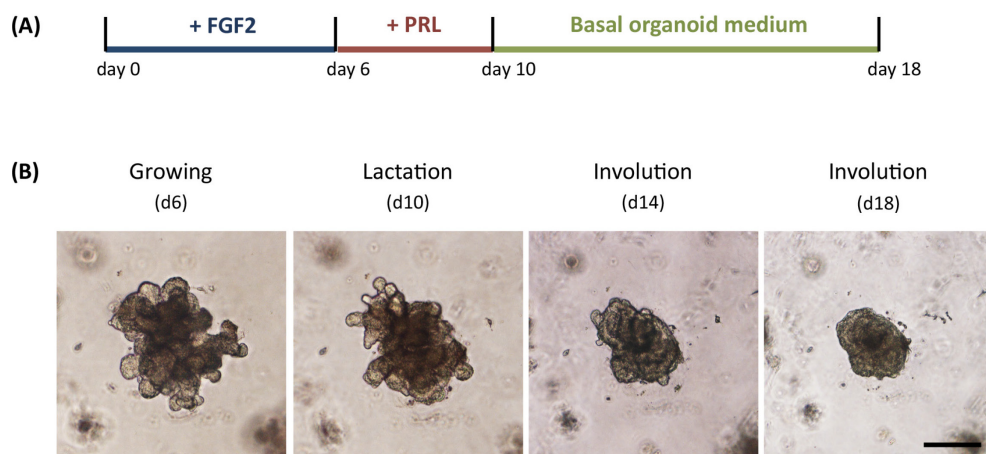

Figure 2. Modeling lactation and involution-like processes in primary mammary organoids. A. Scheme depicting the experimental design. B. Morphology of primary mammary organoids during lactation and involution-like processes. Bright-field images of organoid morphology following morphogenic and lactogenic stimulation and on days 4 or 8 after hormonal withdrawal. Scale bar = 100 μm.
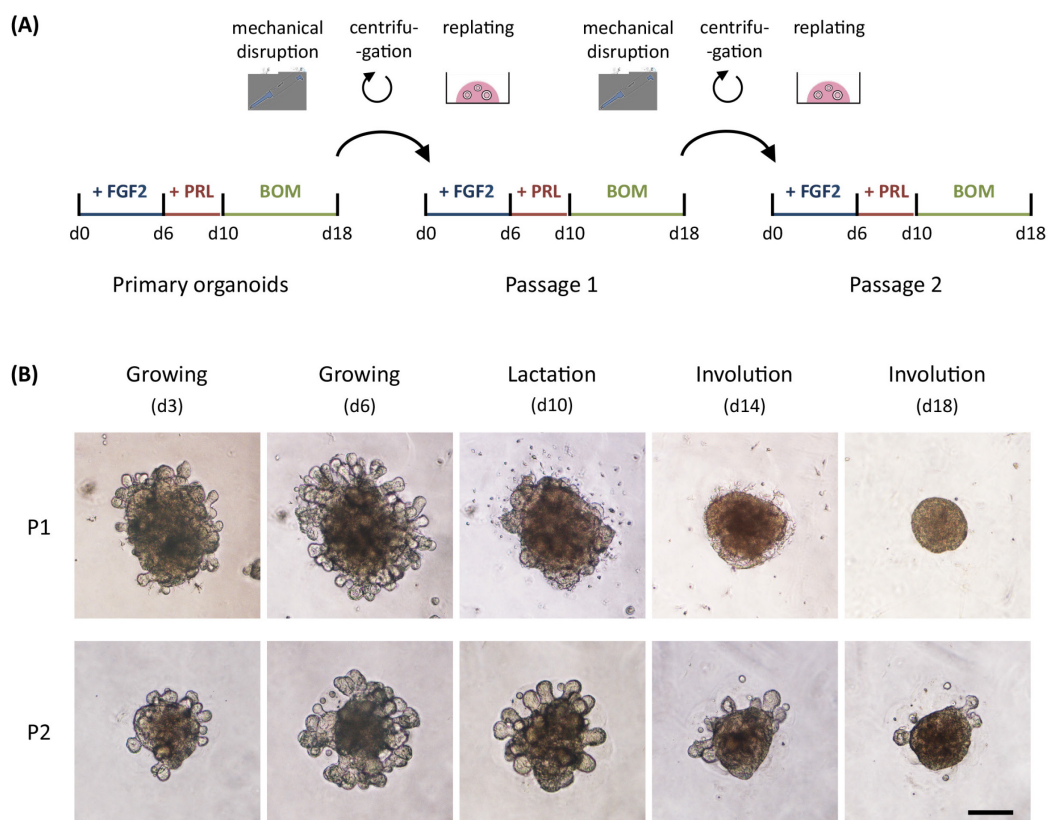
Figure 3. Passage of involution-like organoids. A. Scheme depicting the experimental design. PRL: Prolactin; BOM: basal organoid medium. B. Morphology of passaged organoids during the lactation and involution-like processes. Brightfield images of passage 1 (upper panel) and passage 2 (lower panel) organoids following morphogenic and lactogenic stimulation and on days 4 or 8 after hormonal withdrawal. Scale bar = 100 µm.

1. RNA isolation

    Note: Embedding in Matrigel® does not interfere with the quality of extracted RNA.

    a. Aspirate the culture medium.

    b. Add 350 µl RLT buffer (RNeasy Micro Kit) contiaining 3.5 µl β-mercaptoethanol to each well.

    c. Disintegrate the organoid culture in lysis buffer by performing ten up-and-down motions with a P1000 pipette.

    d. Transfer the solution to a fresh 1.5-ml tube and vortex well.

        Note: Samples can be stored at –80°C until RNA extraction. To perform RNA extraction, thaw samples on ice and proceed according to the following instructions.

    e. Homogenize RNA lysates by performing ten up-and-down motions with a single-use 30 G insulin syringe.

    f. Process samples as described in the RNeasy Micro Kit booklet, starting from Step C1b.

    g. Measure the RNA concentration using a NanoDrop™.

2. Protein extraction

    Note: Embedding in Matrigel® interferes with western blotting analysis. Follow these steps to remove the Matrigel® prior to protein extraction.

    a. Aspirate the culture medium and dissociate the 3D culture with 800 µl cold PBS supplemented with phosphatase inhibitor cocktail II.

    b. Transfer the suspension to a clean 1.5-ml tube and centrifuge for 3 min at 400 × *g*, 4°C.

    c. Rinse twice with PBS supplemented with phosphatase inhibitor cocktail II.

    d. Discard the supernatant and resuspend the pellet in 100 µl ice-cold ready-to-use RIPA buffer supplemented with protease inhibitor cocktail I and phosphatase inhibitor cocktail II.

        Note: Samples can be stored at –80°C until protein extraction. To perform protein extraction, thaw samples on ice and proceed according to the following instructions.

    e. Sonicate the samples twice at 4°C using a 60-kHz ultrasonic wave frequency program (30 s ON/30 s OFF).

    f. Vortex the samples, cool on ice, and repeat the sonication according to Step C2e.

    g. Centrifuge for 20 min at >10,000 × *g*, 4°C.

    h. Transfer the supernatant to a clean 1.5-ml tube.

    i. Measure the protein concentration using a Coomassie Protein Assay Kit.

3. Fixation and embedding for histology

    a. Aspirate the culture medium and rinse the culture twice with 800 µl cold PBS.

b. Incubate with 800 µl 4% PFA for 30 min. Following removal of the 4% PFA, wash twice with PBS.

   Notes:

   i. *Domes should be entirely covered with the solution. Add a greater volume if required.*

   ii. *The fixed cultures can be stored in PBS at 4°C until embedding.*

c. Prepare 3% low gelling temperature agarose in PBS and melt slowly in a microwave for 1.5–2 min at 1000 W (homogenize every 30 s by hand rotation).

d. Detach the fixed culture using the flat side of a spatula and transfer to a plastic histology mold containing melted agarose. Overlay with more agarose.

e. After solidification of the agarose, unmold the block. Use a scalpel to remove the excess agarose surrounding the Matrigel® dome and place in a plastic embedding cassette for histology.

f. Proceed to sample dehydration: incubate the embedding cassettes in successive 1-h baths of 70% EtOH, 95% EtOH, 100% EtOH (twice), xylene (twice), 50% xylene-50% melted paraffin, and 100% melted paraffin.

g. Incubate overnight at 65°C in a second bath of 100% melted paraffin.

h. Embed in a histology tissue mold using an embedding workstation.

i. Unmold the paraffin blocks after 24 h of solidification.

j. Cut 5-µm sections and spread on microscope slides. Keep the slides at room temperature until further analysis.

k. Remove the paraffin prior to any staining by successive 5-min baths of xylene (twice), 100% EtOH (twice), 95% EtOH, 70% EtOH, and H_2O.

Recipes

1. Dissociation solution

   Note: This solution is prepared inside a laminar flow hood under aseptic conditions and does not need to be filter-sterilized.

   2 mg/ml collagenase

   2 mg/ml trypsin

   5 µg/ml insulin

   50 µg/ml gentamicin

   5% FBS

   2 mM glutamine

   in DMEM/F12

2. BSA solution

   Note: This solution can be filter-sterilized and reused several times when stored at 4°C.

   2.5% BSA in PBS

3. Basal organoid medium (BOM)

Note: This solution is prepared inside a laminar flow hood under aseptic conditions and does not need to be filter-sterilized.

1× insulin-transferrin-selenium (ITS)

100 U/ml penicillin

100 µg/ml streptomycin

2 mM glutamine

in DMEM/F12

4. Morphogenesis medium

Note: This solution is prepared inside a laminar flow hood under aseptic conditions and does not need to be filter-sterilized.

2.5 nM FGF2 in BOM

5. Lactation medium

Note: This solution is prepared inside a laminar flow hood under aseptic conditions and does not need to be filter-sterilized.

1 µg/ml prolactin

1 µg/ml hydrocortisone

in BOM

6. 4% PFA

Note: This solution is prepared inside a chemical hood and does not need to be filter-sterilized.

4% paraformaldehyde in PBS

7. RNA lysis buffer

Note: This solution is prepared inside a chemical hood and does not need to be filter-sterilized.

10 µl β-mercaptoethanol per 1 ml RLT lysis buffer (from the RNeasy Micro Kit; this solution can be stored for up to one month at room temperature).

8. Phosphatase inhibitor cocktail II

Note: This solution is prepared inside a chemical hood or on a bench and does not need to be filter-sterilized.

2 mM imidazole

1 mM sodium fluoride

1.15 mM sodium molybdate

1 mM sodium orthovanadate

4 mM sodium tartrate dihydrate

in RIPA buffer

9. Protease inhibitor cocktail I

Note: This solution is prepared inside a chemical hood or on a bench and does not need to be filter-sterilized.

500 µM AEBSF hydrochloride

150 nM aprotinin

1 µM protease inhibitor E-64

0.5 mM EDTA

1 µM leupeptin hemisulfate

in RIPA buffer

Acknowledgments

This protocol was derived from the original research paper "Primary Mammary Organoid Model of Lactation and Involution" (Sumbal *et al.*, 2020b).

Competing interests

The authors declare that they have no competing interests.

Ethics

The animal study was reviewed and approved by French legislation in compliance with European Communities Council Directives (A 75-15-01-3) and the regulations of the Institut Pasteur Animal Care Committees (CETEA).

References

1. Artegiani, B., and Clevers, H. (2018). Use and application of 3D-organoid technology. *Hum Mol Genet* 27: R99-R107.
2. Brisken, C. and O'Malley, B. (2010). Hormone action in the mammary gland. *Cold Spring Harb Perspect Biol* 2(12): a003178.
3. Brisken, C. and Rajaram, R. D. (2006). Alveolar and lactogenic differentiation. *J Mammary Gland Biol Neoplasia* 11(3-4): 239-248.
4. Campbell, J. J., Botos, L. A., Sargeant, T. J., Davidenko, N., Cameron, R. E. and Watson, C. J. (2014). A 3-D *in vitro* co-culture model of mammary gland involution. *Integr Biol (Camb)* 6(6): 618-626.

5. Ewald, A. J., Brenot, A., Duong, M., Chan, B. S. and Werb, Z. (2008). Collective epithelial migration and cell rearrangements drive mammary branching morphogenesis. *Dev Cell* 14(4): 570-581.

6. Freestone, D., Cater, M. A., Ackland, M. L., Paterson, D., Howard, D. L., de Jonge, M. D. and Michalczyk, A. (2014). Copper and lactational hormones influence the CTR1 copper transporter in PMC42-LA mammary epithelial cell culture models. *J Nutr Biochem* 25(4): 377-387.

7. Huch, M. and Koo, B. K. (2015). Modeling mouse and human development using organoid cultures. *Development* 142(18): 3113-3125.

8. Huebner, R. J., Neumann, N. M. and Ewald, A. J. (2016). Mammary epithelial tubes elongate through MAPK-dependent coordination of cell migration. *Development* 143: 983-993.

9. Hughes, K. and Watson, C. J. (2012). The spectrum of STAT functions in mammary gland development. *JAKSTAT* 1(3): 151-158.

10. Jamieson, P. R., Dekkers, J. F., Rios, A. C., Fu, N. Y., Lindeman, G. J. and Visvader, J. E. (2017). Derivation of a robust mouse mammary organoid system for studying tissue dynamics. *Development* 144(6): 1065-1071.

11. Jena, M. K., Jaswal, S., Kumar, S. and Mohanty, A. K. (2019). Molecular mechanism of mammary gland involution: An update. *Dev Biol* 445(2): 145-155.

12. Koledova, Z. (2017). 3D Cell Culture: An Introduction. *Methods Mol Biol* 1612: 1-11.

13. Linnemann, J. R., Miura, H., Meixner, L. K., Irmler, M., Kloos, U. J., Hirschi, B., Bartsch, H. S., Sass, S., Beckers, J., Theis, F. J., Gabka, C., Sotlar, K. and Scheel, C. H. (2015). Quantification of regenerative potential in primary human mammary epithelial cells. *Development* 142(18): 3239-3251.

14. Macias, H. and Hinck, L. (2012). Mammary gland development. *Wiley Interdiscip Rev Dev Biol* 1(4): 533-557.

15. Mroue, R., Inman, J., Mott, J., Budunova, I., and Bissell, M.J. (2015). Asymmetric expression of connexins between luminal epithelial- and myoepithelial- cells is essential for contractile function of the mammary gland. *Dev Biol* 399(1): 15-26.

16. Neumann, N. M., Perrone, M. C., Veldhuis, J. H., Huebner, R. J., Zhan, H., Devreotes, P. N., Brodland, G. W. and Ewald, A. J. (2018). Coordination of Receptor Tyrosine Kinase Signaling and Interfacial Tension Dynamics Drives Radial Intercalation and Tube Elongation. *Dev Cell* 45(1): 67-82 e66.

17. Ormandy, C. J., Camus, A., Barra, J., Damotte, D., Lucas, B., Buteau, H., Edery, M., Brousse, N., Babinet, C., Binart, N. and Kelly, P. A. (1997). Null mutation of the prolactin receptor gene produces multiple reproductive defects in the mouse. *Genes Dev* 11(2): 167-178.

18. Qu, Y., Han, B., Gao, B., Bose, S., Gong, Y., Wawrowsky, K., Giuliano, A. E., Sareen, D. and Cui, X. (2017). Differentiation of Human Induced Pluripotent Stem Cells to Mammary-like Organoids. *Stem Cell Reports* 8(2): 205-215.

19. Richert, M. M., Schwertfeger, K. L., Ryder, J. W. and Anderson, S. M. (2000). An atlas of mouse mammary gland development. *J Mammary Gland Biol Neoplasia* 5(2): 227-241.

20. Shamir, E. R. and Ewald, A. J. (2015). Adhesion in mammary development: novel roles for E-cadherin in individual and collective cell migration. *Curr Top Dev Biol* 112: 353-382.

21. Sternlicht, M. D. (2006). Key stages in mammary gland development: the cues that regulate ductal branching morphogenesis. *Breast Cancer Res* 8(1): 201.

22. Sumbal, J., Budkova, Z., Traustadottir, G. A. and Koledova, Z. (2020a). Mammary Organoids and 3D Cell Cultures: Old Dogs with New Tricks. *J Mammary Gland Biol Neoplasia*. doi: 10.1007/s10911-020-09468-x.

23. Sumbal, J., Chiche, A., Charifou, E., Koledova, Z. and Li, H. (2020b). Primary Mammary Organoid Model of Lactation and Involution. *Front Cell Dev Biol* 8: 68.

24. Xian, W., Schwertfeger, K. L., Vargo-Gogola, T. and Rosen, J. M. (2005). Pleiotropic effects of FGFR1 on cell proliferation, survival, and migration in a 3D mammary epithelial cell model. *J Cell Biol* 171(4): 663-673.

25. Zwick, R. K., Rudolph, M. C., Shook, B. A., Holtrup, B., Roth, E., Lei, V., Van Keymeulen, A., Seewaldt, V., Kwei, S., Wysolmerski, J., Rodeheffer, M. S. and Horsley, V. (2018). Adipocyte hypertrophy and lipid dynamics underlie mammary gland remodeling after lactation. *Nat Commun* 9(1): 3592.

EDITORIAL

Twelfth Annual ENBDC Workshop: Methods in Mammary Gland Biology and Breast Cancer

Elsa Charifou[1] · Gunnhildur Asta Traustadottir[2] · Mohamed Bentires-Alj[3] · Beatrice Howard[4] ·
Alexandra Van Keymeulen[5]

Abstract

The twelfth annual workshop of the European Network for Breast Development and Cancer focused on methods in mammary gland biology and breast cancer, was scheduled to take place on March 26–28, 2020, in Weggis, Switzerland. Due to the COVID-19 pandemic, the meeting was rescheduled twice and eventually happened as a virtual meeting on April 22 and 23, 2021. The main topics of the meeting were branching and development of the mammary gland, tumor microenvironment, circulating tumor cells, tumor dormancy and breast cancer metastasis. Novel and unpublished findings related to these topics were presented, with a particular focus on the methods used to obtain them. Virtual poster sessions were a success, with many constructive and fruitful interactions between researchers and covered many areas of mammary gland biology and breast cancer.

Keywords Mammary gland · Breast cancer · Breast development · Branching · Organoids · Patient-derived xenografts · Circulating tumor cells · Metastasis · Tumor dormancy · Tumor microenvironment · Signaling · Premetastatic niche · In vivo live imaging · Lineage tracing · Transcriptomics · Resistance to therapy

Introduction

The European network of breast development and cancer (ENBDC) organizes an annual workshop on methods in mammary gland biology and breast cancer. This three-day meeting has been hosted every year until now in the

---

Elsa Charifou and Gunnhildur Asta Traustadottir are contributed equally to this work.

✉ Alexandra Van Keymeulen
Alexandra.van.keymeulen@ulb.be

1   Cellular Plasticity and Disease Modeling, Department of Developmental & Stem Cell Biology, CNRS UMR3738 - Institut Pasteur, 25 rue du Dr Roux, 75015 Paris, France

2   Stem Cell Research Unit, Department of Anatomy, Faculty of Medicine, School of Health Sciences, Biomedical Center, University of Iceland, Reykjavík, Iceland

3   Department of Biomedicine, University of Basel, University Hospital Basel, Basel, Switzerland

4   The Breast Cancer Now Toby Robins Research Centre, The Institute of Cancer Research, London, UK

5   Laboratory of Stem Cells and Cancer, Université Libre de Bruxelles (ULB), Brussels, Belgium

charming small town Weggis in Switzerland [1], but the twelfth annual meeting took place virtually on April 22 and 23, 2021. The virtual format allowed many more scientists to attend the meeting and we reached over 100 participants from many different countries, while the ENBDC meeting on site usually gathers around 65 participants [1]. The meeting schedule was rearranged to fit in two full days, with regular breaks, and more relaxed poster sessions in the afternoon. This first virtual meeting was a great success, with high quality talks on very hot topics and discussions after each talk. Poster sessions enabled all attendees to present their work to a smaller audience. The conviviality and friendly interactions we usually enjoy during breaks and meals in Weggis were however missed by most of us, and we are all looking forward to gather next year in Weggis on April 28–30, 2022.

Meeting Report

The meeting started with the Keynote speaker Nicola Aceto, from the Swiss Federal Institute of Technology Zürich (ETH) in Switzerland. Nicola Aceto's work focuses on

circulating tumor cells (CTC), some of which will eventually lead to metastasis. He started his presentation by explaining the size-based, antigen-independent microfluidic technique used to trap CTC which are bigger and less deformable than blood cells [2]. Nicola Aceto then described the presence of CTC clusters [3] and their characteristics and showed how these CTC clusters in patients are associated with a worse prognosis. Using mice engrafted with tagged mammary tumor cells, he demonstrated that these CTC clusters had a 50-fold increased metastatic potential compared to single CTC [4–6]. He went further in the comparison of single and clustered CTC and showed that the latter bear hypomethylated DNA regions and featured stem and proliferative-like programs, expressing *OCT4*, *SOX2* and *NANOG*. He then presented an elegant idea to screen for drugs able to dissociate clustered CTC without killing the cells, and found that a Na + K + ATPase inhibitor presented these characteristics. Validation in vivo in mice showed that this inhibitor dissociated CTC clusters without killing single CTC and decreased the metastatic index [7]. Ongoing effort is focused on translating this work to human patients in ongoing clinical trials. Another characteristic of clustered CTC is that some of them include immune cells. He showed that breast cancer patient survival was worst when they present CTC white blood cell (WBC) clusters. Using single cell RNA sequencing of patient samples, he found that in 90% of the cases these WBC were neutrophils. In mice, he showed that CTC-neutrophil clusters were the most metastasis-competent CTC subpopulation [8]. He concluded this talk presenting his work on hypoxia, which he showed is not restricted to the center of the tumor. Intratumor hypoxia leads to cell–cell junction upregulation. Clustered CTC were usually hypoxic, while single CTC were normoxic. Anti-angiogenic therapy reduced tumor size, but increases hypoxia, CTC clusters and metastasis [9]. This observation will be important to keep in mind when testing anti-cancer therapies.

The first session focused on breast cancer metastasis and was chaired by Mohamed Bentires-Alj from University of Basel, Switzerland. The first speaker of the session was Ilaria Malanchi form the Francis Crick Institute in London, UK. Her work focuses on the local interaction of metastatic cells within the tissue. To study this technically challenging question, she set up a new method called Cherry-niche which enables cells expressing a fluorescent protein to label surrounding cells [10, 11]. In particular, she focused her study on the metastatic niche in the mouse lung, using injection of 4T1 mouse mammary metastatic cells. Using the Cherry-niche system, cancer cells express *GFP* and a liposoluble red fluorescent tag and appear yellow, while neighboring cells, which constitute the niche, are tagged with the red fluorescent compound and the rest of the lung is not labelled. With this elegant approach, she showed the presence of cancer associated parenchymal cells with stem

cell-like features and expression of lung progenitor markers, as well as self-renewal and differentiation potential [10].

Eva Gonzalez-Suarez, from the Spanish National Cancer Research Center (CNIO) in Spain, was the second speaker of this session, and presented her work on *RANK* and *RANKL*. She showed that loss of *RANK* signaling in *MMTV-PyMT* mouse tumor cells increased the number of lymphocytes, leukocytes and CD8 + T cells, and reduced macrophage and neutrophil infiltration, clearly demonstrating an effect of *RANK* pathway on mammary tumor immune surveillance. She showed that *RANKL* inhibition increased the effect of immunotherapy in mammary gland tumors. This immune-modulatory effect of *RANK* signaling (increased TILS and CD8 + T cells) was confirmed in pre-menopausal early breast cancer patients treated with denosumab in the D-BEYOND trial and is being further investigated in an ongoing clinical trial (D-BIOMARK) treating pre- and post-menopausal women with early breast cancer with neoadjuvant denosumab. Her findings indicate that tumor cells use *RANK* pathway to evade immune surveillance and support the use of *RANK* pathway inhibitors to increase response to immunotherapy in luminal breast cancer [12]. She presented new results showing that *RANK* expression unexpectedly delayed mammary tumor latency in two oncogene-driven mouse models, (*MMTV-PyMT* and *MMTV-Neu*). The mechanism behind this observation is that activation of *RANK* signaling induced senescence through *P16/P19*. This *RANK*-induced senescence increased stemness properties and promoted tumor growth and metastasis. This work shows that while *RANK* induces senescence and stemness, which delays tumor initiation, it eventually increases tumor aggressiveness [13].

Roger Gomis, from the Institute for Research in Biomedicine (IRB) Barcelona in Spain, presented a short talk on metastasis latency and bone metastasis in breast cancer. His work demonstrated that gain in a chromosomal region coding for the transcription factor *MAF* in primary breast tumors is associated with metastasis in bone but not to other organs [14]. *MAF* is therefore a potential biomarker to select patients at risk of bone metastasis for bisphosphonate adjuvant therapy. To go further on this important observation, a clinical trial was performed and concluded that *MAF* amplification status predicts likelihood of benefit from adjuvant zoledronic acid [14, 15]. Roger Gomis is now focusing on the *MAF*-mediated metastasis mechanisms and is studying *MAF* interactome as well as the *MAF*-mediated chromatin opening and transcriptional program.

Ana Luisa Correia, a postdoc from Mohamed Bentires-Alj lab at the University of Basel in Switzerland, closed this session on breast tumor dormancy and metastasis with a short talk on her recent findings. Her work focuses on dormant disseminated tumor cells (DTC). In order to study the differences between cycling and quiescent DTCs, she used mouse models of metastasis consisting of xenografting

human MDA-MB-231 cells into the mammary glands of immunocompromised *NOD-SCID* mice, followed by primary tumor resection. The novelty of her experimental approach is in using tumor cells co-expressing a *Tomato* reporter and a mutant reporter of *P27* which identifies quiescent cells. Analysis of the distribution of DTCs amongst different metastatic organs showed that the liver, often associated with poor prognosis, mainly harbored DTCs in dormant state. She showed that there was a selective increase in natural killer (NK) cells in the dormant microenvironment. She then showed in mice that immunotherapy ensured a pool of NK cells that sustained dormancy through interferon gamma signaling, which appeared to be a master switch between dormancy and metastasis in the liver. Lastly, Ana found that liver injury limits NK cell expansion. Using a model of chemically-induced liver injury, she showed that hepatic stellate cells become activated and secrete an inhibitor of NK cell proliferation, *CXCL12*, through its cognate receptor *CXCR4*. This study is very promising as it suggests that therapies aiming at normalizing NK cell density could halt dormant DTCs from awakening and prevent metastatic disease [16].

We were pleased to listen to John Stingl next, a former member of the ENBDC committee now working at STEMCELL Technologies Inc. in Canada, for the Meet the Expert session. STEMCELL is commercializing media for growing organoids from a wide variety of tissues, including the mouse mammary gland. John shared with us his protocols and advice on how to culture mammary gland organoids in Matrigel domes with the MammoCult Organoid Growth Medium (OGM) developed at STEMCELL. An important trait of the MammoCult OGM is that it is serum-, estrogen-, progesterone- and phenol red-free. Different combinations of supplements are used, depending on whether branched multilineage or luminal-restricted organoids are desired. John recommended that for maintaining organoid lines they were passaged as fragments since this would help maintain a normal karyotype, however seeding cells as single cells was recommended for quantitative experiments since there would be less variability in organoid numbers between technical replicates. Branched organoids are multilineage, with basal cells expressing *K14* and *SMA*, and luminal cells expressing *K8* and *PR*. These organoids were able to synthesize casein in response to lactogenic stimulation. He also presented data on EpiCult Plus Medium, which is a serum-free medium that promotes robust long-term expansion of mouse mammary cells in 2D culture in the absence of feeders, while still retaining organoid-forming potential. This medium could be useful for gene editing prior to organoid culture.

The second day, we moved on with the branching and mammary development session, chaired by Beatrice Howard from The Institute of Cancer Research, UK. Our first speaker was Thorarinn Gudjonsson from the University of Iceland,

Iceland, with his talk on epithelial to mesenchymal transition (EMT) in breast morphogenesis and cancer. He presented the generation of the D492 cell line by isolating MUCIN 1 negative, EPCAM positive cells from primary cultures of breast cells obtained from reduction mammoplasties. This cell line has epithelial characteristics as well as stem cell properties and is able to form branched 3D structures resembling terminal duct lobular units [17, 18]. By co-culturing D492 cells and primary breast endothelial cells in Matrigel, he showed that endothelial cells induced branching morphogenesis, highlighting the importance of endothelial cells in branching morphogenesis, but also that some colonies showed spindle shape with EMT characteristics. A new cell line, named D492M, was derived from these spindle colonies, and showed mesenchymal traits [19]. The two cell lines, D492 with epithelial properties and D492M with mesenchymal properties, allowed to study EMT and mesenchymal to epithelial transition (MET). Comparison of microRNA profiling of the two cell lines indicated that *miRNA 200c/miRNA 141* and *miRNA 203* were down-regulated in D492 cells and that overexpression of these miRNA in D492M cell line reinduced epithelial traits, demonstrating their role in EMT and MET. In particular, overexpression of *miRNA 200c/miRNA 141* combined with *p63* was able to completely reverse the mesenchymal phenotype to a fully branched epithelial phenotype [20]. The D492 cell line was also used to generate a tumorigenic cell line expressing *HER2* for use in breast cancer studies [21].

The next speaker was Bethan Lloyd-Lewis, who recently established her lab at the University of Bristol, UK. She presented her previous postdoctoral work where she used intravital imaging to investigate mammary epithelial cell fate dynamics during normal and pathological mammary morphogenesis, alongside developing a flexible and suture-less, silicone-based imaging window for rodent intravital microscopy. This low-cost, suture-less device is suitable for many anatomical locations, representing a substantial advance the field [22]. Using intravital imaging in *NOTCH1-CREERT2* and *SMA-CREERT2* lines crossed to *mT/mG* fluorescent reporter mice, she traced luminal and basal mammary cell behaviors during ductal development, and in response to mutagenic beta-catenin activation. This approach revealed that, regardless of the mammary lineage targeted, mutant beta-catenin stabilisation leads to cellular rearrangements that precipitate the formation of hyperplastic lesions that undergo squamous transdifferentiation [23].

Satu-Marja Myllymäki, a postdoc from Marja Mikkola's lab in Helsinki Institute of Life Science (HiLIFE), Institute of Biotechnology in Helsinki, Finland, presented a short talk entitled "From cells to branches- Insights into mammary branch formation". While there are two mechanisms leading to branching: tip bifurcation and side branching, there are many behaviors that can drive branching like localized cell

proliferation, oriented cell division, directional migration, cell rearrangement, cell shape change or adhesion remodeling. She focused her work on the contribution of localized cell proliferation and directional migration. Using the *Fucci2a* mice [24], in which cells in M/G2/S phase are green and cells in G1/G0 are red, she showed that luminal cells were more frequently detected in M/G2/S phase than basal cells, and that luminal cells in tips were more frequently detected in M/G2/S phase than luminal cells in duct and branch points. Mikkola lab used an ex vivo culture system of embryonic mammary glands to study branching events and quantified the proportion of lateral branching, bifurcations and trifurcations. She presented her data on how cell proliferation and cell motility contributed to branching. Her data suggest that establishment of a new branch point during bifurcation may require cell immobilization and inhibition of cell cycle activity and that proliferation becomes restricted to the daughter tips and cells assume a new direction of movement.

Zuzana Koledova from Masaryk University in Czech Republic closed this session with a short talk on her current work on the role of fibroblasts on mammary gland morphogenesis. Fibroblasts are known to interact with the mammary gland epithelium through paracrine signaling as well as through extracellular matrix production and remodeling [25]. Zuzana Koledova team currently investigates the potential involvement of mechanical forces exerted by fibroblasts in mammary epithelial branching using mouse models, co-cultures of fibroblast and mammary gland epithelium [26] and time lapse visualization of organoid dynamics and branching.

The student/postdoc session chairs of this year were Elsa Charifou from Institut Pasteur in France and Gunnhildur Asta Traustadottir from University of Iceland in Iceland. They chose the topic of the session, tumor microenvironment, as well as the speakers for their session.

The first talk was given by Jayakumar Vadakekolathu from Nottingham Trent University in UK. His work is focused on the EMT as one of the key steps in the metastatic process. He modelled EMT transition in a cell line model from which clonal progenies with different epithelial and mesenchymal characteristics have been derived [27]. Comparison of expression profiles and proteomics between the different clonal progenies revealed that *NNMT* is the most upregulated gene in the most mesenchymal clone. Data mining and analysis as well as in vitro experiments showed that *NNMT* seemed to be a key regulator of EMT and that *NNMT* expression was associated with tumor grade level in breast cancer. High expression of *NNMT* was correlated with poor relapse free survival, indicating its probable role in promoting metastatic spreading. His findings suggest that inhibition of *NNMT* might be an ideal candidate to target to reduce triple negative breast cancer progression.

The last talk of this session, presented by Ingunn Holen from the University of Sheffield, UK, was focused on the role of the bone microenvironment in regulating breast cancer metastasis. Studies have shown that up to 60% of patients with detectable disseminated tumor cells (DTC) in bone marrow remain relapse-free 6 years later. This implies that tumor cells reaching bone is not in itself sufficient to develop metastasis and that events at the secondary site are key to tumor progression. To study the effect of the bone microenvironment on DTC and metastasis, her team used a mouse model where intracardiac injection of labelled human breast cancer MDA-MB-231 cells formed tumors in the bone and DTCs in bone can then be studied using 2-photon microscopy. She showed that tumor cell homing was not uniform, with the majority of breast cancer cells located in the trabecular areas of the bone. Her work also showed that there may be a limited number of suitable niches available in bone for DTCs to colonise. When hematopoietic stem cells (HSC) were mobilized from their bone niches to the circulation (via injection of AMD3100, an inhibitor of *CXCR4*) prior to the injection of tumor cells, the number of DTC in trabecular regions increased, suggesting that the HSC and the bone metastatic niche overlap [28]. She presented a model of tumor dormancy in bone, allowing comparison of conditions in which DTC will develop in metastasis or remain dormant based simply on the age of mice (which impacts the bone microenvironment) at the onset of the experiment. By expanding the osteoblast number with parathyroid hormone prior to tumor cell injection, she showed that the osteoblasts were important for tumor cell survival and progression but not for DTC homing [29]. She also described studies of the effect of osteoclast activity on DTC by ovariectomizing (OVX) mice. OVX induced rapid bone loss and increased osteoclast activity, which triggered a large increase in growth of DTC to form new colonies in bone, compared to a sham operation. The OVX-induced growth of DTCs was inhibited with anti-resorptive agents, demonstrating tumor growth is driven by osteoclast-mediated mechanisms [30].

In conclusion, the virtual 2021 workshop was a success, with a very wide range of techniques described to obtain highly relevant new observations for breast cancer patient benefit and mammary gland fundamental comprehension. The DeOme prize for the best short talk presentation was awarded to Ana Luisa Correia from Mohamed Bentires-Alj lab in University of Basel, Switzerland. The three poster prizes were awarded to Johanna Englund, from the University of Helsinki, for her study of the role of laminin alpha 5 in the mammary gland, Guillaume Jacquemin, from Silvia Fre's lab in Institut Curie in Paris, for his work on improving windows for in vivo imaging of the mouse mammary gland, and Hannah Harrison, from University of Manchester, for her work describing a novel explant culture model for studying normal human breast tissue.

The next ENBDC workshop will take place in Weggis, Switzerland on April 28–30, 2022 and will be chaired by Beatrice Howard from the Institute of Cancer Research in London, UK, co-chaired by Jos Jonkers, from the Netherlands Cancer Institute in Amsterdam. The student/postdoc chairs will be Jakub Sumbal, from Masaryk University in Czech Republic, and Hannah Harrison, from University of Manchester.

Declarations

Ethics MB-A, BH and AVK are Editorial board members of the Journal of Mammary Gland Biology and Neoplasia.

References

1. Vafaizadeh V, Peuhu E, Mikkola ML, Khaled WT, Bentires-Alj M, Koledova Z. The eleventh ENBDC workshop: advances in technology help to unveil mechanisms of mammary gland development and cancerogenesis. J Mammary Gland Biol Neoplasia. 2019;24(3):201–6.

2. Cho H, Kim J, Song H, Sohn KY, Jeon M, Han KH. Microfluidic technologies for circulating tumor cell isolation. Analyst. 2018;143(13):2936–70.

3. Stott SL, Lee RJ, Nagrath S, Yu M, Miyamoto DT, Ulkus L, Inserra EJ, Ulman M, Springer S, Nakamura Z, Moore AL, Tsukrov DI, Kempner ME, Dahl DM, Wu CL, Iafrate AJ, Smith MR, Tompkins RG, Sequist LV, Toner M, Haber DA, Maheswaran S. Isolation and characterization of circulating tumor cells from patients with localized and metastatic prostate cancer. Sci Transl Med. 2010;2(25):25ra23.

4. Aceto N, Bardia A, Miyamoto DT, Donaldson MC, Wittner BS, Spencer JA, Yu M, Pely A, Engstrom A, Zhu H, Brannigan BW, Kapur R, Stott SL, Shioda T, Ramaswamy S, Ting DT, Lin CP, Toner M, Haber DA, Maheswaran S. Circulating tumor cell

5. Sarioglu AF, Aceto N, Kojic N, Donaldson MC, Zeinali M, Hamza B, Engstrom A, Zhu H, Sundaresan TK, Miyamoto DT, Luo X, Bardia A, Wittner BS, Ramaswamy S, Shioda T, Ting DT, Stott SL, Kapur R, Maheswaran S, Haber DA, Toner M. A microfluidic device for label-free, physical capture of circulating tumor cell clusters. Nat Methods. 2015;12(7):685–91.

6. Aceto N, Toner M, Maheswaran S, Haber DA. En route to metastasis: circulating tumor cell clusters and epithelial-to-mesenchymal transition. Trends Cancer. 2015;1(1):44–52.

7. Gkountela S, Castro-Giner F, Szczerba BM, Vetter M, Landin J, Scherrer R, Krol I, Scheidmann MC, Beisel C, Stirnimann CU, Kurzeder C, Heinzelmann-Schwarz V, Rochlitz C, Weber WP, Aceto N. Circulating tumor cell clustering shapes dna methylation to enable metastasis seeding. Cell. 2019;176(1–2):98-112.e14.

8. Szczerba BM, Castro-Giner F, Vetter M, Krol I, Gkountela S, Landin J, Scheidmann MC, Donato C, Scherrer R, Singer J, Beisel C, Kurzeder C, Heinzelmann-Schwarz V, Rochlitz C, Weber WP, Beerenwinkel N, Aceto N. Neutrophils escort circulating tumour cells to enable cell cycle progression. Nature. 2019;566(7745):553–7.

9. Donato C, Kunz L, Castro-Giner F, Paasinen-Sohns A, Strittmatter K, Szczerba BM, Scherrer R, Di Maggio N, Heusermann W, Biehlmaier O, Beisel C, Vetter M, Rochlitz C, Weber WP, Banfi A, Schroeder T, Aceto N. Hypoxia triggers the intravasation of clustered circulating tumor cells. Cell Rep. 2020;32(10):108105.

10. Ombrato L, Nolan E, Kurelac I, Mavousian A, Bridgeman VL, Heinze I, Chakravarty P, Horswell S, Gonzalez-Gualda E, Matacchione G, Weston A, Kirkpatrick J, Husain E, Speirs V, Collinson L, Ori A, Lee JH, Malanchi I. Metastatic-niche labelling reveals parenchymal cells with stem features. Nature. 2019;572(7771):603–8.

11. Ombrato L, Nolan E, Passaro D, Kurelac I, Bridgeman VL, Waclawiczek A, Duarte D, Lo Celso C, Bonnet D, Malanchi I. Generation of neighbor-labeling cells to study intercellular interactions in vivo. Nat Protoc. 2021;16(2):872–92.

12. Gómez-Aleza C, Nguyen B, Yoldi G, Ciscar M, Barranco A, Hernández-Jiménez E, Maetens M, Salgado R, Zafeiroglou M, Pellegrini P, Venet D, Garaud S, Trinidad EM, Benítez S, Vuylsteke P, Polastro L, Wildiers H, Simon P, Lindeman G, Larsimont D, Van den Eynden G, Velghe C, Rothé F, Willard-Gallo K, Michiels S, Muñoz P, Walzer T, Planelles L, Penninger J, Azim HA Jr, Loi S, Piccart M, Sotiriou C, González-Suárez E. Inhibition of RANK signaling in breast cancer induces an anti-tumor immune response orchestrated by CD8+ T cells. Nat Commun. 2020;11(1):6335.

13. Benítez S, Cordero A, Santamaría PG, Redondo-Pedraza J, Rocha AS, Collado-Solé A, Jimenez M, Sanz-Moreno A, Yoldi G, Santos JC, De Benedictis I, Gómez-Aleza C, Da Silva-Álvarez S, Troulé K, Gómez-López G, Alcazar N, Palmero I, Collado M, Serrano M, Gonzalez-Suarez E. RANK links senescence to stemness in the mammary epithelia, delaying tumor onset but increasing tumor aggressiveness. Dev Cell. 2021;56(12):1727-41.e7.

14. Pavlovic M, Arnal-Estapé A, Rojo F, Bellmunt A, Tarragona M, Guiu M, Planet E, Garcia-Albéniz X, Morales M, Urosevic J, Gawrzak S, Rovira A, Prat A, Nonell L, Lluch A, Jean-Mairet J, Coleman R, Albanell J, Gomis RR. Enhanced MAF oncogene expression and breast cancer bone metastasis. J Natl Cancer Inst. 2015;107(12):djv256.

15. Coleman RE, Collinson M, Gregory W, Marshall H, Bell R, Dodwell D, Keane M, Gil M, Barrett-Lee P, Ritchie D, Bowman A, Liversedge V, De Boer RH, Passos-Coelho JL, O'Reilly S, Bertelli G, Joffe J, Brown JE, Wilson C, Tercero JC, Jean-Mairet J, Gomis R, Cameron D. Benefits and risks of adjuvant treatment with zoledronic acid in stage II/III breast cancer. 10 years

follow-up of the AZURE randomized clinical trial (BIG 01/04). J Bone Oncol. 2018;13:123–35.

16. Correia AL, Guimaraes JC, Auf der Maur P, De Silva D, Trefny MP, Okamoto R, Bruno S, Schmidt A, Mertz K, Volkmann K, Terracciano L, Zippelius A, Vetter M, Kurzeder C, Weber WP, Bentires-Alj M. Hepatic stellate cells suppress NK cell-sustained breast cancer dormancy. Nature. 2021;594(7864):566–71.

17. Gudjonsson T, Villadsen R, Nielsen HL, Rønnov-Jessen L, Bissell MJ, Petersen OW. Isolation, immortalization, and characterization of a human breast epithelial cell line with stem cell properties. Genes Dev. 2002;16(6):693–706.

18. Briem E, Ingthorsson S, Traustadottir GA, Hilmarsdottir B, Gudjonsson T. Application of the D492 cell lines to explore breast morphogenesis, EMT and cancer progression in 3D culture. J Mammary Gland Biol Neoplasia. 2019;24(2):139–47.

19. Sigurdsson V, Hilmarsdottir B, Sigmundsdottir H, Fridriksdottir AJ, Ringnér M, Villadsen R, Borg A, Agnarsson BA, Petersen OW, Magnusson MK, Gudjonsson T. Endothelial induced EMT in breast epithelial cells with stem cell properties. PLoS One. 2011;6(9):e23833.

20. Hilmarsdóttir B, Briem E, Sigurdsson V, Franzdóttir SR, Ringnér M, Arason AJ, Bergthorsson JT, Magnusson MK, Gudjonsson T. MicroRNA-200c-141 and ΔNp63 are required for breast epithelial differentiation and branching morphogenesis. Dev Biol. 2015;403(2):150–61.

21. Ingthorsson S, Andersen K, Hilmarsdottir B, Maelandsmo GM, Magnusson MK, Gudjonsson T. HER2 induced EMT and tumorigenicity in breast epithelial progenitor cells is inhibited by coexpression of EGFR. Oncogene. 2016;35(32):4244–55.

22. Jacquemin G, Benavente-Diaz M, Djaber S, Bore A, Dangles-Marie V, Surdez D, Tajbakhsh S, Fre S, Lloyd-Lewis B. Longitudinal high-resolution imaging through a flexible intravital imaging window. Sci Adv. 2021;7(25).

23. Lloyd-Lewis B, Gobbo F, Perkins M, Jacquemin G, Faraldo MF, Fre S. In vivo imaging of mammary epithelial cell dynamics in response to lineage-biased Wnt/b-catenin activation. bioRxiv. 2021.

24. Mort RL, Ford MJ, Sakaue-Sawano A, Lindstrom NO, Casadio A, Douglas AT, Keighren MA, Hohenstein P, Miyawaki A, Jackson IJ. Fucci2a: a bicistronic cell cycle reporter that allows Cre mediated tissue specific expression in mice. Cell Cycle. 2014;13(17):2681–96.

25. Sumbal J, Belisova D, Koledova Z. Fibroblasts: The grey eminence of mammary gland development. Semin Cell Dev Biol. 2021;114:134–42.

26. Koledova Z, Lu P. A 3D fibroblast-epithelium co-culture model for understanding microenvironmental role in branching morphogenesis of the mammary gland. Methods Mol Biol. 2017;1501:217–31.

27. Harner-Foreman N, Vadakekolathu J, Laversin SA, Mathieu MG, Reeder S, Pockley AG, Rees RC, Boocock DJ. A novel spontaneous model of epithelial-mesenchymal transition (EMT) using a primary prostate cancer derived cell line demonstrating distinct stem-like characteristics. Sci Rep. 2017;7:40633.

28. Allocca G, Hughes R, Wang N, Brown HK, Ottewell PD, Brown NJ, Holen I. The bone metastasis niche in breast cancer-potential overlap with the haematopoietic stem cell niche in vivo. J Bone Oncol. 2019;17:100244.

29. Hughes R, Chen X, Cowley N, Ottewell PD, Hawkins RJ, Hunter KD, Hobbs JK, Brown NJ, Holen I. Osteoblast-derived paracrine and juxtacrine signals protect disseminated breast cancer cells from stress cancers. (Basel). 2021;13(6).

30. Ottewell PD, Wang N, Brown HK, Reeves KJ, Fowles CA, Croucher PI, Eaton CL, Holen I. Zoledronic acid has differential antitumor activity in the pre- and postmenopausal bone microenvironment in vivo. Clin Cancer Res. 2014;20(11):2922–32.

Publisher's Note Springer Nature remains neutral with regard to jurisdictional claims in published maps and institutional affiliations.

References

References

Acconcia, F., and R. Kumar. 2006. 'Signaling regulation of genomic and nongenomic functions of estrogen receptors', *Cancer Lett*, 238: 1-14.

Acosta, J. C., A. Banito, T. Wuestefeld, A. Georgilis, P. Janich, J. P. Morton, D. Athineos, T. W. Kang, F. Lasitschka, M. Andrulis, G. Pascual, K. J. Morris, S. Khan, H. Jin, G. Dharmalingam, A. P. Snijders, T. Carroll, D. Capper, C. Pritchard, G. J. Inman, T. Longerich, O. J. Sansom, S. A. Benitah, L. Zender, and J. Gil. 2013. 'A complex secretory program orchestrated by the inflammasome controls paracrine senescence', *Nat Cell Biol*, 15: 978-90.

Adnot, S., V. Amsellem, L. Boyer, E. Marcos, M. Saker, A. Houssaini, K. Kebe, M. Dagouassat, L. Lipskaia, and J. Boczkowski. 2015. 'Telomere Dysfunction and Cell Senescence in Chronic Lung Diseases: Therapeutic Potential', *Pharmacol Ther*, 153: 125-34.

Albrektsen, G., I. Heuch, S. Hansen, and G. Kvale. 2005. 'Breast cancer risk by age at birth, time since birth and time intervals between births: exploring interaction effects', *Br J Cancer*, 92: 167-75.

Alexander, C. M., S. Selvarajan, J. Mudgett, and Z. Werb. 2001. 'Stromelysin-1 regulates adipogenesis during mammary gland involution', *Journal of Cell Biology*, 152: 693-703.

Allsopp, R. C., H. Vaziri, C. Patterson, S. Goldstein, E. V. Younglai, A. B. Futcher, C. W. Greider, and C. B. Harley. 1992. 'Telomere length predicts replicative capacity of human fibroblasts', *Proc Natl Acad Sci U S A*, 89: 10114-8.

Althubiti, M., L. Lezina, S. Carrera, R. Jukes-Jones, S. M. Giblett, A. Antonov, N. Barlev, G. S. Saldanha, C. A. Pritchard, K. Cain, and S. Macip. 2014. 'Characterization of novel markers of senescence and their prognostic potential in cancer', *Cell Death Dis*, 5: e1528.

Amor, C., J. Feucht, J. Leibold, Y. J. Ho, C. Zhu, D. Alonso-Curbelo, J. Mansilla-Soto, J. A. Boyer, X. Li, T. Giavridis, A. Kulick, S. Houlihan, E. Peerschke, S. L. Friedman, V. Ponomarev, A. Piersigilli, M. Sadelain, and S. W. Lowe. 2020. 'Senolytic CAR T cells reverse senescence-associated pathologies', *Nature*, 583: 127-32.

Araujo, J., and C. Logothetis. 2010. 'Dasatinib: a potent SRC inhibitor in clinical development for the treatment of solid tumors', *Cancer Treat Rev*, 36: 492-500.

Asselin-Labat, M. L., M. Shackleton, J. Stingl, F. Vaillant, N. C. Forrest, C. J. Eaves, J. E. Visvader, and G. J. Lindeman. 2006. 'Steroid hormone receptor status of mouse mammary stem cells', *J Natl Cancer Inst*, 98: 1011-4.

Baker, D. J., B. G. Childs, M. Durik, M. E. Wijers, C. J. Sieben, J. Zhong, R. A. Saltness, K. B. Jeganathan, G. C. Verzosa, A. Pezeshki, K. Khazaie, J. D. Miller, and J. M. van Deursen. 2016. 'Naturally occurring p16(Ink4a)-positive cells shorten healthy lifespan', *Nature*, 530: 184-9.

Baker, D. J., T. Wijshake, T. Tchkonia, N. K. LeBrasseur, B. G. Childs, B. van de Sluis, J. L. Kirkland, and J. M. van Deursen. 2011. 'Clearance of p16Ink4a-positive senescent cells delays ageing-associated disorders', *Nature*, 479: 232-6.

Barash, I. 2006. 'Stat5 in the mammary gland: controlling normal development and cancer', *J Cell Physiol*, 209: 305-13.

Basisty, N., A. Kale, O. H. Jeon, C. Kuehnemann, T. Payne, C. Rao, A. Holtz, S. Shah, V. Sharma, L. Ferrucci, J. Campisi, and B. Schilling. 2020. 'A proteomic atlas of senescence-associated secretomes for aging biomarker development', *PLoS Biol*, 18: e3000599.

Benitez, S., A. Cordero, P. G. Santamaria, J. Redondo-Pedraza, A. S. Rocha, A. Collado-Sole, M. Jimenez, A. Sanz-Moreno, G. Yoldi, J. C. Santos, I. De Benedictis, C. Gomez-Aleza, S. Da Silva-Alvarez, K. Troule, G. Gomez-Lopez, N. Alcazar, I. Palmero, M. Collado, M. Serrano, and E. Gonzalez-Suarez. 2021. 'RANK links senescence to stemness in the mammary epithelia, delaying tumor onset but increasing tumor aggressiveness', *Dev Cell*, 56: 1727-41 e7.

Bettelli, E., Y. Carrier, W. Gao, T. Korn, T. B. Strom, M. Oukka, H. L. Weiner, and V. K. Kuchroo. 2006. 'Reciprocal developmental pathways for the generation of pathogenic effector TH17 and regulatory T cells', *Nature*, 441: 235-8.

Bhat, R., E. P. Crowe, A. Bitto, M. Moh, C. D. Katsetos, F. U. Garcia, F. B. Johnson, J. Q. Trojanowski, C. Sell, and C. Torres. 2012. 'Astrocyte senescence as a component of Alzheimer's disease', *PLoS One*, 7: e45069.

Brighton, P. J., Y. Maruyama, K. Fishwick, P. Vrljicak, S. Tewary, R. Fujihara, J. Muter, E. S. Lucas, T. Yamada, L. Woods, R. Lucciola, Y. Hou Lee, S. Takeda, S. Ott, M. Hemberger, S. Quenby, and J. J. Brosens. 2017. 'Clearance of senescent decidual cells by uterine natural killer cells in cycling human endometrium', *Elife*, 6.

Brisken, C., and B. O'Malley. 2010. 'Hormone action in the mammary gland', *Cold Spring Harb Perspect Biol*, 2: a003178.

Brisken, C., S. Park, T. Vass, J. P. Lydon, B. W. O'Malley, and R. A. Weinberg. 1998. 'A paracrine role for the epithelial progesterone receptor in mammary gland development', *Proc Natl Acad Sci U S A*, 95: 5076-81.

Bursuker, I., J. M. Rhodes, and R. Goldman. 1982. 'Beta-galactosidase--an indicator of the maturational stage of mouse and human mononuclear phagocytes', *J Cell Physiol*, 112: 385-90.

Busuttil, R. A., M. Rubio, M. E. Dolle, J. Campisi, and J. Vijg. 2003. 'Oxygen accelerates the accumulation of mutations during the senescence and immortalization of murine cells in culture', *Aging Cell*, 2: 287-94.

Cahu, J., and B. Sola. 2013. 'A sensitive method to quantify senescent cancer cells', *J Vis Exp*.

Camacho-Morales, A., M. Caba, M. Garcia-Juarez, M. D. Caba-Flores, R. Viveros-Contreras, and C. Martinez-Valenzuela. 2021. 'Breastfeeding Contributes to Physiological Immune Programming in the Newborn', *Front Pediatr*, 9: 744104.

Campisi, J., and F. d'Adda di Fagagna. 2007. 'Cellular senescence: when bad things happen to good cells', *Nat Rev Mol Cell Biol*, 8: 729-40.

Carrel, A. 1912. 'On the Permanent Life of Tissues Outside of the Organism', *J Exp Med*, 15: 516-28.

Carroll, J. S., T. E. Hickey, G. A. Tarulli, M. Williams, and W. D. Tilley. 2017. 'Deciphering the divergent roles of progestogens in breast cancer', *Nat Rev Cancer*, 17: 54-64.

Chandra, T., and K. Kirschner. 2016. 'Chromosome organisation during ageing and senescence', *Curr Opin Cell Biol*, 40: 161-67.

Chang, J., Y. Wang, L. Shao, R. M. Laberge, M. Demaria, J. Campisi, K. Janakiraman, N. E. Sharpless, S. Ding, W. Feng, Y. Luo, X. Wang, N. Aykin-Burns, K. Krager, U. Ponnappan, M. Hauer-Jensen, A. Meng, and D. Zhou. 2016. 'Clearance of senescent cells by ABT263 rejuvenates aged hematopoietic stem cells in mice', *Nat Med*, 22: 78-83.

Charifou, E., J. Sumbal, Z. Koledova, H. Li, and A. Chiche. 2021. 'A Robust Mammary Organoid System to Model Lactation and Involution-like Processes', *Bio Protoc*, 11: e3996.

Charifou, E., G. A. Traustadottir, M. Bentires-Alj, B. Howard, and A. Van Keymeulen. 2021. 'Twelfth Annual ENBDC Workshop: Methods in Mammary Gland Biology and Breast Cancer', *J Mammary Gland Biol Neoplasia*, 26: 221-26.

Chien, Y., C. Scuoppo, X. Wang, X. Fang, B. Balgley, J. E. Bolden, P. Premsrirut, W. Luo, A. Chicas, C. S. Lee, S. C. Kogan, and S. W. Lowe. 2011. 'Control of the senescence-associated secretory phenotype by NF-kappaB promotes senescence and enhances chemosensitivity', *Genes Dev*, 25: 2125-36.

Childs, B. G., D. J. Baker, J. L. Kirkland, J. Campisi, and J. M. van Deursen. 2014. 'Senescence and apoptosis: dueling or complementary cell fates?', *EMBO Rep*, 15: 1139-53.

Childs, B. G., M. Gluscevic, D. J. Baker, R. M. Laberge, D. Marquess, J. Dananberg, and J. M. van Deursen. 2017. 'Senescent cells: an emerging target for diseases of ageing', *Nat Rev Drug Discov*, 16: 718-35.

Chuprin, A., H. Gal, T. Biron-Shental, A. Biran, A. Amiel, S. Rozenblatt, and V. Krizhanovsky. 2013. 'Cell fusion induced by ERVWE1 or measles virus causes cellular senescence', *Genes Dev*, 27: 2356-66.

Clarke, R. B., A. Howell, C. S. Potten, and E. Anderson. 1997. 'Dissociation between steroid receptor expression and cell proliferation in the human breast', *Cancer Res*, 57: 4987-91.

Collado, M., and M. Serrano. 2006. 'The power and the promise of oncogene-induced senescence markers', *Nat Rev Cancer*, 6: 472-6.

Colleluori, G., J. Perugini, G. Barbatelli, and S. Cinti. 2021. 'Mammary gland adipocytes in lactation cycle, obesity and breast cancer', *Rev Endocr Metab Disord*, 22: 241-55.

Coppe, J. P., P. Y. Desprez, A. Krtolica, and J. Campisi. 2010. 'The senescence-associated secretory phenotype: the dark side of tumor suppression', *Annu Rev Pathol*, 5: 99-118.

Coppe, J. P., K. Kauser, J. Campisi, and C. M. Beausejour. 2006. 'Secretion of vascular endothelial growth factor by primary human fibroblasts at senescence', *J Biol Chem*, 281: 29568-74.

Coppe, J. P., C. K. Patil, F. Rodier, Y. Sun, D. P. Munoz, J. Goldstein, P. S. Nelson, P. Y. Desprez, and J. Campisi. 2008. 'Senescence-associated secretory phenotypes reveal cell-nonautonomous functions of oncogenic RAS and the p53 tumor suppressor', *PLoS Biol*, 6: 2853-68.

Daling, J. R., K. E. Malone, D. R. Doody, B. O. Anderson, and P. L. Porter. 2002. 'The relation of reproductive factors to mortality from breast cancer', *Cancer Epidemiol Biomarkers Prev*, 11: 235-41.

Daniel, C. W., K. B. De Ome, J. T. Young, P. B. Blair, and L. J. Faulkin, Jr. 1968. 'The in vivo life span of normal and preneoplastic mouse mammary glands: a serial transplantation study', *Proc Natl Acad Sci U S A*, 61: 53-60.

Davis, F. M., B. Lloyd-Lewis, O. B. Harris, S. Kozar, D. J. Winton, L. Muresan, and C. J. Watson. 2016. 'Single-cell lineage tracing in the mammary gland reveals

stochastic clonal dispersion of stem/progenitor cell progeny', *Nat Commun*, 7: 13053.

Dawson, C. A., B. Pal, F. Vaillant, L. C. Gandolfo, Z. Liu, C. Bleriot, F. Ginhoux, G. K. Smyth, G. J. Lindeman, S. N. Mueller, A. C. Rios, and J. E. Visvader. 2020. 'Tissue-resident ductal macrophages survey the mammary epithelium and facilitate tissue remodelling', *Nat Cell Biol*, 22: 546-58.

Demaria, M., N. Ohtani, S. A. Youssef, F. Rodier, W. Toussaint, J. R. Mitchell, R. M. Laberge, J. Vijg, H. Van Steeg, M. E. Dolle, J. H. Hoeijmakers, A. de Bruin, E. Hara, and J. Campisi. 2014. 'An essential role for senescent cells in optimal wound healing through secretion of PDGF-AA', *Dev Cell*, 31: 722-33.

Deng, C., P. Zhang, J. W. Harper, S. J. Elledge, and P. Leder. 1995. 'Mice lacking p21CIP1/WAF1 undergo normal development, but are defective in G1 checkpoint control', *Cell*, 82: 675-84.

Deome, K. B., L. J. Faulkin, Jr., H. A. Bern, and P. B. Blair. 1959. 'Development of mammary tumors from hyperplastic alveolar nodules transplanted into gland-free mammary fat pads of female C3H mice', *Cancer Res*, 19: 515-20.

Deugnier, M. A., E. P. Moiseyeva, J. P. Thiery, and M. Glukhova. 1995. 'Myoepithelial cell differentiation in the developing mammary gland: progressive acquisition of smooth muscle phenotype', *Dev Dyn*, 204: 107-17.

Deugnier, M. A., J. Teuliere, M. M. Faraldo, J. P. Thiery, and M. A. Glukhova. 2002. 'The importance of being a myoepithelial cell', *Breast Cancer Res*, 4: 224-30.

Di Micco, R., V. Krizhanovsky, D. Baker, and F. d'Adda di Fagagna. 2021. 'Cellular senescence in ageing: from mechanisms to therapeutic opportunities', *Nat Rev Mol Cell Biol*, 22: 75-95.

Dimri, G. P., X. Lee, G. Basile, M. Acosta, G. Scott, C. Roskelley, E. E. Medrano, M. Linskens, I. Rubelj, O. Pereira-Smith, and et al. 1995. 'A biomarker that identifies senescent human cells in culture and in aging skin in vivo', *Proc Natl Acad Sci U S A*, 92: 9363-7.

Egashira, M., Y. Hirota, R. Shimizu-Hirota, T. Saito-Fujita, H. Haraguchi, L. Matsumoto, M. Matsuo, T. Hiraoka, T. Tanaka, S. Akaeda, C. Takehisa, M. Saito-Kanatani, K. I. Maeda, T. Fujii, and Y. Osuga. 2017. 'F4/80+ Macrophages Contribute to Clearance of Senescent Cells in the Mouse Postpartum Uterus', *Endocrinology*, 158: 2344-53.

Ewald, A. J., A. Brenot, M. Duong, B. S. Chan, and Z. Werb. 2008. 'Collective epithelial migration and cell rearrangements drive mammary branching morphogenesis', *Dev Cell*, 14: 570-81.

Faget, D. V., Q. Ren, and S. A. Stewart. 2019. 'Unmasking senescence: context-dependent effects of SASP in cancer', *Nat Rev Cancer*, 19: 439-53.

Fata, J. E., V. Chaudhary, and R. Khokha. 2001. 'Cellular turnover in the mammary gland is correlated with systemic levels of progesterone and not 17beta-estradiol during the estrous cycle', *Biol Reprod*, 65: 680-8.

Fata, J. E., K. J. Leco, E. B. Voura, H. Y. Yu, P. Waterhouse, G. Murphy, R. A. Moorehead, and R. Khokha. 2001. 'Accelerated apoptosis in the Timp-3-deficient mammary gland', *J Clin Invest*, 108: 831-41.

Feng, Z., A. Marti, B. Jehn, H. J. Altermatt, G. Chicaiza, and R. Jaggi. 1995. 'Glucocorticoid and progesterone inhibit involution and programmed cell death in the mouse mammary gland', *Journal of Cell Biology*, 131: 1095-103.

Freund, A., R. M. Laberge, M. Demaria, and J. Campisi. 2012. 'Lamin B1 loss is a senescence-associated biomarker', *Mol Biol Cell*, 23: 2066-75.

Fu, N. Y., E. Nolan, G. J. Lindeman, and J. E. Visvader. 2020. 'Stem Cells and the Differentiation Hierarchy in Mammary Gland Development', *Physiol Rev*, 100: 489-523.

Fujita, K., and N. Tsumaki. 2013. '[Stem cell aging and the implications for stem cell-based therapies for aging-related diseases and aged tissues]', *Clin Calcium*, 23: 65-73.

Gerace, L., A. Blum, and G. Blobel. 1978. 'Immunocytochemical localization of the major polypeptides of the nuclear pore complex-lamina fraction. Interphase and mitotic distribution', *Journal of Cell Biology*, 79: 546-66.

Ghebranious, N., and L. A. Donehower. 1998. 'Mouse models in tumor suppression', *Oncogene*, 17: 3385-400.

Gieniec, K. A., and F. M. Davis. 2022. 'Mammary basal cells: Stars of the show', *Biochim Biophys Acta Mol Cell Res*, 1869: 119159.

Gil, J., and G. Peters. 2006. 'Regulation of the INK4b-ARF-INK4a tumour suppressor locus: all for one or one for all', *Nat Rev Mol Cell Biol*, 7: 667-77.

Gilazieva, Z., A. Ponomarev, C. Rutland, A. Rizvanov, and V. Solovyeva. 2020. 'Promising Applications of Tumor Spheroids and Organoids for Personalized Medicine', *Cancers (Basel)*, 12.

Gimpl, G., and F. Fahrenholz. 2001. 'The oxytocin receptor system: structure, function, and regulation', *Physiol Rev*, 81: 629-83.

Gonzalez-Gualda, E., M. Paez-Ribes, B. Lozano-Torres, D. Macias, J. R. Wilson, 3rd, C. Gonzalez-Lopez, H. L. Ou, S. Miron-Barroso, Z. Zhang, A. Lerida-Viso, J. F. Blandez, A. Bernardos, F. Sancenon, M. Rovira, L. Fruk, C. P. Martins, M. Serrano, G. J. Doherty, R. Martinez-Manez, and D. Munoz-Espin. 2020. 'Galacto-conjugation of Navitoclax as an efficient strategy to increase senolytic specificity and reduce platelet toxicity', *Aging Cell*, 19: e13142.

Gorgoulis, V., P. D. Adams, A. Alimonti, D. C. Bennett, O. Bischof, C. Bishop, J. Campisi, M. Collado, K. Evangelou, G. Ferbeyre, J. Gil, E. Hara, V. Krizhanovsky, D. Jurk, A. B. Maier, M. Narita, L. Niedernhofer, J. F. Passos, P. D. Robbins, C. A. Schmitt, J. Sedivy, K. Vougas, T. von Zglinicki, D. Zhou, M. Serrano, and M. Demaria. 2019. 'Cellular Senescence: Defining a Path Forward', *Cell*, 179: 813-27.

Gorgoulis, V. G., and T. D. Halazonetis. 2010. 'Oncogene-induced senescence: the bright and dark side of the response', *Curr Opin Cell Biol*, 22: 816-27.

Gosain, A., and L. A. DiPietro. 2004. 'Aging and wound healing', *World J Surg*, 28: 321-6.

Gouon-Evans, V., M. E. Rothenberg, and J. W. Pollard. 2000. 'Postnatal mammary gland development requires macrophages and eosinophils', *Development*, 127: 2269-82.

Grosse, L., N. Wagner, A. Emelyanov, C. Molina, S. Lacas-Gervais, K. D. Wagner, and D. V. Bulavin. 2020. 'Defined p16(High) Senescent Cell Types Are Indispensable for Mouse Healthspan', *Cell Metab*, 32: 87-99 e6.

Hardwick, J. M., and L. Soane. 2013. 'Multiple functions of BCL-2 family proteins', *Cold Spring Harb Perspect Biol*, 5.

Hayflick, L., and P. S. Moorhead. 1961. 'The serial cultivation of human diploid cell strains', *Exp Cell Res*, 25: 585-621.

He, S., and N. E. Sharpless. 2017. 'Senescence in Health and Disease', *Cell*, 169: 1000-11.

Hennighausen, L., and G. W. Robinson. 2005. 'Information networks in the mammary gland', *Nat Rev Mol Cell Biol*, 6: 715-25.

Herbig, U., M. Ferreira, L. Condel, D. Carey, and J. M. Sedivy. 2006. 'Cellular senescence in aging primates', *Science*, 311: 1257.

Hernandez-Segura, A., T. V. de Jong, S. Melov, V. Guryev, J. Campisi, and M. Demaria. 2017. 'Unmasking Transcriptional Heterogeneity in Senescent Cells', *Curr Biol*, 27: 2652-60 e4.

Hernandez-Segura, A., J. Nehme, and M. Demaria. 2018. 'Hallmarks of Cellular Senescence', *Trends Cell Biol*, 28: 436-53.

Herranz, N., and J. Gil. 2018. 'Mechanisms and functions of cellular senescence', *J Clin Invest*, 128: 1238-46.

Hickson, L. J., L. G. P. Langhi Prata, S. A. Bobart, T. K. Evans, N. Giorgadze, S. K. Hashmi, S. M. Herrmann, M. D. Jensen, Q. Jia, K. L. Jordan, T. A. Kellogg, S. Khosla, D. M. Koerber, A. B. Lagnado, D. K. Lawson, N. K. LeBrasseur, L. O. Lerman, K. M. McDonald, T. J. McKenzie, J. F. Passos, R. J. Pignolo, T. Pirtskhalava, I. M. Saadiq, K. K. Schaefer, S. C. Textor, S. G. Victorelli, T. L. Volkman, A. Xue, M. A. Wentworth, E. O. Wissler Gerdes, Y. Zhu, T. Tchkonia, and J. L. Kirkland. 2019. 'Senolytics decrease senescent cells in humans: Preliminary report from a clinical trial of Dasatinib plus Quercetin in individuals with diabetic kidney disease', *EBioMedicine*, 47: 446-56.

Hitchcock, J. R., K. Hughes, O. B. Harris, and C. J. Watson. 2020. 'Dynamic architectural interplay between leucocytes and mammary epithelial cells', *FEBS J*, 287: 250-66.

Hovey, R. C., and L. Aimo. 2010. 'Diverse and active roles for adipocytes during mammary gland growth and function', *J Mammary Gland Biol Neoplasia*, 15: 279-90.

Howlin, J., J. McBryan, and F. Martin. 2006. 'Pubertal mammary gland development: insights from mouse models', *J Mammary Gland Biol Neoplasia*, 11: 283-97.

Hu, J., I. S. Batth, X. Xia, and S. Li. 2016. 'Regulation of NKG2D(+)CD8(+) T-cell-mediated antitumor immune surveillance: Identification of a novel CD28 activation-mediated, STAT3 phosphorylation-dependent mechanism', *Oncoimmunology*, 5: e1252012.

Humphreys, R. C., B. Bierie, L. Zhao, R. Raz, D. Levy, and L. Hennighausen. 2002. 'Deletion of Stat3 blocks mammary gland involution and extends functional competence of the secretory epithelium in the absence of lactogenic stimuli', *Endocrinology*, 143: 3641-50.

Iavnilovitch, E., B. Groner, and I. Barash. 2002. 'Overexpression and forced activation of stat5 in mammary gland of transgenic mice promotes cellular proliferation, enhances differentiation, and delays postlactational apoptosis', *Mol Cancer Res*, 1: 32-47.

Ingthorsson, S., E. Briem, J. T. Bergthorsson, and T. Gudjonsson. 2016. 'Epithelial Plasticity During Human Breast Morphogenesis and Cancer Progression', *J Mammary Gland Biol Neoplasia*, 21: 139-48.

Inman, J. L., C. Robertson, J. D. Mott, and M. J. Bissell. 2015. 'Mammary gland development: cell fate specification, stem cells and the microenvironment', *Development*, 142: 1028-42.

Jackson, S. P., and J. Bartek. 2009. 'The DNA-damage response in human biology and disease', *Nature*, 461: 1071-8.

Jager, R., U. Herzer, J. Schenkel, and H. Weiher. 1997. 'Overexpression of Bcl-2 inhibits alveolar cell apoptosis during involution and accelerates c-myc-induced tumorigenesis of the mammary gland in transgenic mice', *Oncogene*, 15: 1787-95.

Jamieson, P. R., J. F. Dekkers, A. C. Rios, N. Y. Fu, G. J. Lindeman, and J. E. Visvader. 2017. 'Derivation of a robust mouse mammary organoid system for studying tissue dynamics', *Development*, 144: 1065-71.

Joshi, P. A., P. D. Waterhouse, K. Kasaian, H. Fang, O. Gulyaeva, H. S. Sul, P. C. Boutros, and R. Khokha. 2019. 'PDGFRalpha(+) stromal adipocyte progenitors transition into epithelial cells during lobulo-alveologenesis in the murine mammary gland', *Nat Commun*, 10: 1760.

Joven, A., A. Elewa, and A. Simon. 2019. 'Model systems for regeneration: salamanders', *Development*, 146.

Jun, J. I., and L. F. Lau. 2010. 'The matricellular protein CCN1 induces fibroblast senescence and restricts fibrosis in cutaneous wound healing', *Nat Cell Biol*, 12: 676-85.

Kaefer, A., J. Yang, P. Noertersheuser, S. Mensing, R. Humerickhouse, W. Awni, and H. Xiong. 2014. 'Mechanism-based pharmacokinetic/pharmacodynamic meta-analysis of navitoclax (ABT-263) induced thrombocytopenia', *Cancer Chemother Pharmacol*, 74: 593-602.

Kang, T. W., T. Yevsa, N. Woller, L. Hoenicke, T. Wuestefeld, D. Dauch, A. Hohmeyer, M. Gereke, R. Rudalska, A. Potapova, M. Iken, M. Vucur, S. Weiss, M. Heikenwalder, S. Khan, J. Gil, D. Bruder, M. Manns, P. Schirmacher, F. Tacke, M. Ott, T. Luedde, T. Longerich, S. Kubicka, and L. Zender. 2011. 'Senescence surveillance of pre-malignant hepatocytes limits liver cancer development', *Nature*, 479: 547-51.

Kerr, J. F., A. H. Wyllie, and A. R. Currie. 1972. 'Apoptosis: a basic biological phenomenon with wide-ranging implications in tissue kinetics', *Br J Cancer*, 26: 239-57.

Kirkland, J. L., and T. Tchkonia. 2020. 'Senolytic drugs: from discovery to translation', *J Intern Med*, 288: 518-36.

Kirschner, K., N. Rattanavirotkul, M. F. Quince, and T. Chandra. 2020. 'Functional heterogeneity in senescence', *Biochem Soc Trans*, 48: 765-73.

Kralisch, S., and M. Fasshauer. 2013. 'Adipocyte fatty acid binding protein: a novel adipokine involved in the pathogenesis of metabolic and vascular disease?', *Diabetologia*, 56: 10-21.

Kreuzaler, P. A., A. D. Staniszewska, W. Li, N. Omidvar, B. Kedjouar, J. Turkson, V. Poli, R. A. Flavell, R. W. Clarkson, and C. J. Watson. 2011. 'Stat3 controls lysosomal-mediated cell death in vivo', *Nat Cell Biol*, 13: 303-9.

Krishnamurthy, J., C. Torrice, M. R. Ramsey, G. I. Kovalev, K. Al-Regaiey, L. Su, and N. E. Sharpless. 2004. 'Ink4a/Arf expression is a biomarker of aging', *J Clin Invest*, 114: 1299-307.

Kritikou, E. A., A. Sharkey, K. Abell, P. J. Came, E. Anderson, R. W. Clarkson, and C. J. Watson. 2003. 'A dual, non-redundant, role for LIF as a regulator of development and STAT3-mediated cell death in mammary gland', *Development*, 130: 3459-68.

Krizhanovsky, V., M. Yon, R. A. Dickins, S. Hearn, J. Simon, C. Miething, H. Yee, L. Zender, and S. W. Lowe. 2008. 'Senescence of activated stellate cells limits liver fibrosis', *Cell*, 134: 657-67.

Krtolica, A., S. Parrinello, S. Lockett, P. Y. Desprez, and J. Campisi. 2001. 'Senescent fibroblasts promote epithelial cell growth and tumorigenesis: a link between cancer and aging', *Proc Natl Acad Sci U S A*, 98: 12072-7.

Kuilman, T., C. Michaloglou, L. C. Vredeveld, S. Douma, R. van Doorn, C. J. Desmet, L. A. Aarden, W. J. Mooi, and D. S. Peeper. 2008. 'Oncogene-induced senescence relayed by an interleukin-dependent inflammatory network', *Cell*, 133: 1019-31.

Kumari, R., and P. Jat. 2021. 'Mechanisms of Cellular Senescence: Cell Cycle Arrest and Senescence Associated Secretory Phenotype', *Front Cell Dev Biol*, 9: 645593.

Kurz, D. J., S. Decary, Y. Hong, and J. D. Erusalimsky. 2000. 'Senescence-associated (beta)-galactosidase reflects an increase in lysosomal mass during replicative ageing of human endothelial cells', *J Cell Sci*, 113 (Pt 20): 3613-22.

Kuwana, Y., Y. Asakura, N. Utsunomiya, M. Nakanishi, Y. Arata, S. Itoh, F. Nagase, and Y. Kurosawa. 1987. 'Expression of chimeric receptor composed of immunoglobulin-derived V regions and T-cell receptor-derived C regions', *Biochem Biophys Res Commun*, 149: 960-8.

Lee, B. Y., J. A. Han, J. S. Im, A. Morrone, K. Johung, E. C. Goodwin, W. J. Kleijer, D. DiMaio, and E. S. Hwang. 2006. 'Senescence-associated beta-galactosidase is lysosomal beta-galactosidase', *Aging Cell*, 5: 187-95.

Lewis, D. A., Q. Yi, J. B. Travers, and D. F. Spandau. 2008. 'UVB-induced senescence in human keratinocytes requires a functional insulin-like growth factor-1 receptor and p53', *Mol Biol Cell*, 19: 1346-53.

Li, M., X. Liu, G. Robinson, U. Bar-Peled, K. U. Wagner, W. S. Young, L. Hennighausen, and P. A. Furth. 1997. 'Mammary-derived signals activate programmed cell death during the first stage of mammary gland involution', *Proc Natl Acad Sci U S A*, 94: 3425-30.

Lilla, J. N., R. V. Joshi, C. S. Craik, and Z. Werb. 2009. 'Active plasma kallikrein localizes to mast cells and regulates epithelial cell apoptosis, adipocyte differentiation, and stromal remodeling during mammary gland involution', *J Biol Chem*, 284: 13792-803.

Lloyd-Lewis, B., O. B. Harris, C. J. Watson, and F. M. Davis. 2017. 'Mammary Stem Cells: Premise, Properties, and Perspectives', *Trends Cell Biol*, 27: 556-67.

Lloyd-Lewis, B., T. J. Sargeant, P. A. Kreuzaler, H. K. Resemann, S. Pensa, and C. J. Watson. 2017. 'Analysis of the Involuting Mouse Mammary Gland: An In Vivo Model for Cell Death', *Methods Mol Biol*, 1501: 165-86.

Lund, L. R., J. Romer, N. Thomasset, H. Solberg, C. Pyke, M. J. Bissell, K. Dano, and Z. Werb. 1996. 'Two distinct phases of apoptosis in mammary gland involution: proteinase-independent and -dependent pathways', *Development*, 122: 181-93.

Marti, A., P. M. Ritter, R. Jager, H. Lazar, A. Baltzer, J. Schenkel, W. Declercq, P. Vandenabeele, and R. Jaggi. 2001. 'Mouse mammary gland involution is associated with cytochrome c release and caspase activation', *Mech Dev*, 104: 89-98.

Mavrogonatou, E., H. Pratsinis, A. Papadopoulou, N. K. Karamanos, and D. Kletsas. 2019. 'Extracellular matrix alterations in senescent cells and their significance in tissue homeostasis', *Matrix Biol*, 75-76: 27-42.

McDaniel, S. M., K. K. Rumer, S. L. Biroc, R. P. Metz, M. Singh, W. Porter, and P. Schedin. 2006. 'Remodeling of the mammary microenvironment after lactation promotes breast tumor cell metastasis', *Am J Pathol*, 168: 608-20.

McHugh, D., and J. Gil. 2018. 'Senescence and aging: Causes, consequences, and therapeutic avenues', *Journal of Cell Biology*, 217: 65-77.

McNally, S., and T. Stein. 2017. 'Overview of Mammary Gland Development: A Comparison of Mouse and Human', *Methods Mol Biol*, 1501: 1-17.

Metcalfe, A. D., A. Gilmore, T. Klinowska, J. Oliver, A. J. Valentijn, R. Brown, A. Ross, G. MacGregor, J. A. Hickman, and C. H. Streuli. 1999. 'Developmental regulation of Bcl-2 family protein expression in the involuting mammary gland', *J Cell Sci*, 112 (Pt 11): 1771-83.

Mikaelian, I., M. Hovick, K. A. Silva, L. M. Burzenski, L. D. Shultz, C. L. Ackert-Bicknell, G. A. Cox, and J. P. Sundberg. 2006. 'Expression of terminal differentiation proteins defines stages of mouse mammary gland development', *Vet Pathol*, 43: 36-49.

Milanese, T. R., L. C. Hartmann, T. A. Sellers, M. H. Frost, R. A. Vierkant, S. D. Maloney, V. S. Pankratz, A. C. Degnim, C. M. Vachon, C. A. Reynolds, R. A. Thompson, L. J. Melton, 3rd, E. L. Goode, and D. W. Visscher. 2006. 'Age-related lobular involution and risk of breast cancer', *J Natl Cancer Inst*, 98: 1600-7.

Monks, J., C. Smith-Steinhart, E. R. Kruk, V. A. Fadok, and P. M. Henson. 2008. 'Epithelial cells remove apoptotic epithelial cells during post-lactation involution of the mouse mammary gland', *Biol Reprod*, 78: 586-94.

Morroni, M., A. Giordano, M. C. Zingaretti, R. Boiani, R. De Matteis, B. B. Kahn, E. Nisoli, C. Tonello, C. Pisoschi, M. M. Luchetti, M. Marelli, and S. Cinti. 2004. 'Reversible transdifferentiation of secretory epithelial cells into adipocytes in the mammary gland', *Proc Natl Acad Sci U S A*, 101: 16801-6.

Mouraret, N., E. Marcos, S. Abid, G. Gary-Bobo, M. Saker, A. Houssaini, J. L. Dubois-Rande, L. Boyer, J. Boczkowski, G. Derumeaux, V. Amsellem, and S. Adnot. 2013. 'Activation of lung p53 by Nutlin-3a prevents and reverses experimental pulmonary hypertension', *Circulation*, 127: 1664-76.

Munoz-Espin, D., M. Canamero, A. Maraver, G. Gomez-Lopez, J. Contreras, S. Murillo-Cuesta, A. Rodriguez-Baeza, I. Varela-Nieto, J. Ruberte, M. Collado, and M. Serrano. 2013. 'Programmed cell senescence during mammalian embryonic development', *Cell*, 155: 1104-18.

Munoz-Espin, D., M. Rovira, I. Galiana, C. Gimenez, B. Lozano-Torres, M. Paez-Ribes, S. Llanos, S. Chaib, M. Munoz-Martin, A. C. Ucero, G. Garaulet, F. Mulero, S. G. Dann, T. VanArsdale, D. J. Shields, A. Bernardos, J. R. Murguia, R. Martinez-Manez, and M. Serrano. 2018. 'A versatile drug delivery system targeting senescent cells', *EMBO Mol Med*, 10.

Munoz-Espin, D., and M. Serrano. 2014. 'Cellular senescence: from physiology to pathology', *Nat Rev Mol Cell Biol*, 15: 482-96.

Nagasawa, M., S. Okabe, K. Mogi, and T. Kikusui. 2012. 'Oxytocin and mutual communication in mother-infant bonding', *Front Hum Neurosci*, 6: 31.

Narita, M., S. Nunez, E. Heard, M. Narita, A. W. Lin, S. A. Hearn, D. L. Spector, G. J. Hannon, and S. W. Lowe. 2003. 'Rb-mediated heterochromatin formation and silencing of E2F target genes during cellular senescence', *Cell*, 113: 703-16.

Neville, M. C., T. B. McFadden, and I. Forsyth. 2002. 'Hormonal regulation of mammary differentiation and milk secretion', *J Mammary Gland Biol Neoplasia*, 7: 49-66.

Ngoi, N. Y., A. Q. Liew, S. J. F. Chong, M. S. Davids, M. V. Clement, and S. Pervaiz. 2021. 'The redox-senescence axis and its therapeutic targeting', *Redox Biol*, 45: 102032.

Nguyen, A. V., and J. W. Pollard. 2000. 'Transforming growth factor beta3 induces cell death during the first stage of mammary gland involution', *Development*, 127: 3107-18.

O'Brien, J., T. Lyons, J. Monks, M. S. Lucia, R. S. Wilson, L. Hines, Y. G. Man, V. Borges, and P. Schedin. 2010. 'Alternatively activated macrophages and collagen remodeling characterize the postpartum involuting mammary gland across species', *Am J Pathol*, 176: 1241-55.

O'Brien, J., H. Martinson, C. Durand-Rougely, and P. Schedin. 2012. 'Macrophages are crucial for epithelial cell death and adipocyte repopulation during mammary gland involution', *Development*, 139: 269-75.

O'Brien, W., G. Stenman, and R. Sager. 1986. 'Suppression of tumor growth by senescence in virally transformed human fibroblasts', *Proc Natl Acad Sci U S A*, 83: 8659-63.

Oftedal, O. T. 2002. 'The mammary gland and its origin during synapsid evolution', *J Mammary Gland Biol Neoplasia*, 7: 225-52.

Oh, J., Y. D. Lee, and A. J. Wagers. 2014. 'Stem cell aging: mechanisms, regulators and therapeutic opportunities', *Nat Med*, 20: 870-80.

Orjalo, A. V., D. Bhaumik, B. K. Gengler, G. K. Scott, and J. Campisi. 2009. 'Cell surface-bound IL-1alpha is an upstream regulator of the senescence-associated IL-6/IL-8 cytokine network', *Proc Natl Acad Sci U S A*, 106: 17031-6.

Ormandy, C. J., A. Camus, J. Barra, D. Damotte, B. Lucas, H. Buteau, M. Edery, N. Brousse, C. Babinet, N. Binart, and P. A. Kelly. 1997. 'Null mutation of the prolactin receptor gene produces multiple reproductive defects in the mouse', *Genes Dev*, 11: 167-78.

Pajvani, U. B., M. E. Trujillo, T. P. Combs, P. Iyengar, L. Jelicks, K. A. Roth, R. N. Kitsis, and P. E. Scherer. 2005. 'Fat apoptosis through targeted activation of caspase 8: a new mouse model of inducible and reversible lipoatrophy', *Nat Med*, 11: 797-803.

Paramos-de-Carvalho, D., A. Jacinto, and L. Saude. 2021. 'The right time for senescence', *Elife*, 10.

Pardee, A. B. 1989. 'G1 events and regulation of cell proliferation', *Science*, 246: 603-8.

Perez-Mancera, P. A., A. R. Young, and M. Narita. 2014. 'Inside and out: the activities of senescence in cancer', *Nat Rev Cancer*, 14: 547-58.

Petrova, N. V., A. K. Velichko, S. V. Razin, and O. L. Kantidze. 2016. 'Small molecule compounds that induce cellular senescence', *Aging Cell*, 15: 999-1017.

Poblocka, M., A. L. Bassey, V. M. Smith, M. Falcicchio, A. S. Manso, M. Althubiti, X. Sheng, A. Kyle, R. Barber, M. Frigerio, and S. Macip. 2021. 'Targeted clearance of senescent cells using an antibody-drug conjugate against a specific membrane marker', *Sci Rep*, 11: 20358.

Prata, Lgpl, I. G. Ovsyannikova, T. Tchkonia, and J. L. Kirkland. 2018. 'Senescent cell clearance by the immune system: Emerging therapeutic opportunities', *Semin Immunol*, 40: 101275.

Primikyri, A., M. V. Chatziathanasiadou, E. Karali, E. Kostaras, M. D. Mantzaris, E. Hatzimichael, J. S. Shin, S. W. Chi, E. Briasoulis, E. Kolettas, I. P. Gerothanassis, and A. G. Tzakos. 2014. 'Direct binding of Bcl-2 family proteins by quercetin triggers its pro-apoptotic activity', *ACS Chem Biol*, 9: 2737-41.

Quaglino, A., M. Salierno, J. Pellegrotti, N. Rubinstein, and E. C. Kordon. 2009. 'Mechanical strain induces involution-associated events in mammary epithelial cells', *BMC Cell Biol*, 10: 55.

Radisky, D. C., and L. C. Hartmann. 2009. 'Mammary involution and breast cancer risk: transgenic models and clinical studies', *J Mammary Gland Biol Neoplasia*, 14: 181-91.

Ray, P., A. De, J. J. Min, R. Y. Tsien, and S. S. Gambhir. 2004. 'Imaging tri-fusion multimodality reporter gene expression in living subjects', *Cancer Res*, 64: 1323-30.

Rhinn, M., B. Ritschka, and W. M. Keyes. 2019. 'Cellular senescence in development, regeneration and disease', *Development*, 146.

Richert, M. M., K. L. Schwertfeger, J. W. Ryder, and S. M. Anderson. 2000. 'An atlas of mouse mammary gland development', *J Mammary Gland Biol Neoplasia*, 5: 227-41.

Rios, A. C., N. Y. Fu, G. J. Lindeman, and J. E. Visvader. 2014. 'In situ identification of bipotent stem cells in the mammary gland', *Nature*, 506: 322-7.

Roberson, R. S., S. J. Kussick, E. Vallieres, S. Y. Chen, and D. Y. Wu. 2005. 'Escape from therapy-induced accelerated cellular senescence in p53-null lung cancer cells and in human lung cancers', *Cancer Res*, 65: 2795-803.

Rodier, F., and J. Campisi. 2011. 'Four faces of cellular senescence', *Journal of Cell Biology*, 192: 547-56.

Rosner, B., G. A. Colditz, and W. C. Willett. 1994. 'Reproductive risk factors in a prospective study of breast cancer: the Nurses' Health Study', *Am J Epidemiol*, 139: 819-35.

Ryu, S. J., Y. S. Oh, and S. C. Park. 2007. 'Failure of stress-induced downregulation of Bcl-2 contributes to apoptosis resistance in senescent human diploid fibroblasts', *Cell Death Differ*, 14: 1020-8.

Sagiv, A., D. G. Burton, Z. Moshayev, E. Vadai, F. Wensveen, S. Ben-Dor, O. Golani, B. Polic, and V. Krizhanovsky. 2016. 'NKG2D ligands mediate immunosurveillance of senescent cells', *Aging (Albany NY)*, 8: 328-44.

Sahai, E., I. Astsaturov, E. Cukierman, D. G. DeNardo, M. Egeblad, R. M. Evans, D. Fearon, F. R. Greten, S. R. Hingorani, T. Hunter, R. O. Hynes, R. K. Jain, T. Janowitz, C. Jorgensen, A. C. Kimmelman, M. G. Kolonin, R. G. Maki, R. S. Powers, E. Pure, D. C. Ramirez, R. Scherz-Shouval, M. H. Sherman, S. Stewart, T. D. Tlsty, D. A. Tuveson, F. M. Watt, V. Weaver, A. T. Weeraratna, and Z. Werb. 2020. 'A framework for advancing our understanding of cancer-associated fibroblasts', *Nat Rev Cancer*, 20: 174-86.

Sanders, Y. Y., H. Liu, X. Zhang, L. Hecker, K. Bernard, L. Desai, G. Liu, and V. J. Thannickal. 2013. 'Histone modifications in senescence-associated resistance to apoptosis by oxidative stress', *Redox Biol*, 1: 8-16.

Saraste, A., and K. Pulkki. 2000. 'Morphologic and biochemical hallmarks of apoptosis', *Cardiovasc Res*, 45: 528-37.

Schedin, P. 2006. 'Pregnancy-associated breast cancer and metastasis', *Nat Rev Cancer*, 6: 281-91.

Schedin, P., T. Mitrenga, S. McDaniel, and M. Kaeck. 2004. 'Mammary ECM composition and function are altered by reproductive state', *Mol Carcinog*, 41: 207-20.

Serrano, M. 1997. 'The tumor suppressor protein p16INK4a', *Exp Cell Res*, 237: 7-13.

Serrano, M., H. Lee, L. Chin, C. Cordon-Cardo, D. Beach, and R. A. DePinho. 1996. 'Role of the INK4a locus in tumor suppression and cell mortality', *Cell*, 85: 27-37.

Serrano, M., A. W. Lin, M. E. McCurrach, D. Beach, and S. W. Lowe. 1997. 'Oncogenic ras provokes premature cell senescence associated with accumulation of p53 and p16INK4a', *Cell*, 88: 593-602.

Shackleton, M., F. Vaillant, K. J. Simpson, J. Stingl, G. K. Smyth, M. L. Asselin-Labat, L. Wu, G. J. Lindeman, and J. E. Visvader. 2006. 'Generation of a functional mammary gland from a single stem cell', *Nature*, 439: 84-8.

Shamir, E. R., and A. J. Ewald. 2014. 'Three-dimensional organotypic culture: experimental models of mammalian biology and disease', *Nat Rev Mol Cell Biol*, 15: 647-64.

Sharpless, N. E., and C. J. Sherr. 2015. 'Forging a signature of in vivo senescence', *Nat Rev Cancer*, 15: 397-408.

Shaw, F. L., H. Harrison, K. Spence, M. P. Ablett, B. M. Simoes, G. Farnie, and R. B. Clarke. 2012. 'A detailed mammosphere assay protocol for the quantification of breast stem cell activity', *J Mammary Gland Biol Neoplasia*, 17: 111-7.

Sherr, C. J. 2001. 'The INK4a/ARF network in tumour suppression', *Nat Rev Mol Cell Biol*, 2: 731-7.

Simian, M., Y. Hirai, M. Navre, Z. Werb, A. Lochter, and M. J. Bissell. 2001. 'The interplay of matrix metalloproteinases, morphogens and growth factors is necessary for branching of mammary epithelial cells', *Development*, 128: 3117-31.

Sleeman, K. E., H. Kendrick, A. Ashworth, C. M. Isacke, and M. J. Smalley. 2006. 'CD24 staining of mouse mammary gland cells defines luminal epithelial, myoepithelial/basal and non-epithelial cells', *Breast Cancer Res*, 8: R7.

Soloff, M. S. 1982. 'Oxytocin receptors and mammary myoepithelial cells', *J Dairy Sci*, 65: 326-37.

Soto-Gamez, A., W. J. Quax, and M. Demaria. 2019. 'Regulation of Survival Networks in Senescent Cells: From Mechanisms to Interventions', *J Mol Biol*, 431: 2629-43.

Sousa-Victor, P., S. Gutarra, L. Garcia-Prat, J. Rodriguez-Ubreva, L. Ortet, V. Ruiz-Bonilla, M. Jardi, E. Ballestar, S. Gonzalez, A. L. Serrano, E. Perdiguero, and P. Munoz-Canoves. 2014. 'Geriatric muscle stem cells switch reversible quiescence into senescence', *Nature*, 506: 316-21.

Srivastava, V., T. R. Huycke, K. T. Phong, and Z. J. Gartner. 2020. 'Organoid models for mammary gland dynamics and breast cancer', *Curr Opin Cell Biol*, 66: 51-58.

Stein, T., J. S. Morris, C. R. Davies, S. J. Weber-Hall, M. A. Duffy, V. J. Heath, A. K. Bell, R. K. Ferrier, G. P. Sandilands, and B. A. Gusterson. 2004. 'Involution of the mouse mammary gland is associated with an immune cascade and an acute-phase response, involving LBP, CD14 and STAT3', *Breast Cancer Res*, 6: R75-91.

Stevenson, A. J., G. Vanwalleghem, T. A. Stewart, N. D. Condon, B. Lloyd-Lewis, N. Marino, J. W. Putney, E. K. Scott, A. D. Ewing, and F. M. Davis. 2020. 'Multiscale imaging of basal cell dynamics in the functionally mature mammary gland', *Proc Natl Acad Sci U S A*, 117: 26822-32.

Stewart, T. A., K. Hughes, A. J. Stevenson, N. Marino, A. L. Ju, M. Morehead, and F. M. Davis. 2021. 'Mammary mechanobiology - investigating roles for mechanically activated ion channels in lactation and involution', *J Cell Sci*, 134.

Stingl, J., P. Eirew, I. Ricketson, M. Shackleton, F. Vaillant, D. Choi, H. I. Li, and C. J. Eaves. 2006. 'Purification and unique properties of mammary epithelial stem cells', *Nature*, 439: 993-7.

Stone, S., P. Jiang, P. Dayananth, S. V. Tavtigian, H. Katcher, D. Parry, G. Peters, and A. Kamb. 1995. 'Complex structure and regulation of the P16 (MTS1) locus', *Cancer Res*, 55: 2988-94.

Storer, M., A. Mas, A. Robert-Moreno, M. Pecoraro, M. C. Ortells, V. Di Giacomo, R. Yosef, N. Pilpel, V. Krizhanovsky, J. Sharpe, and W. M. Keyes. 2013. 'Senescence is a developmental mechanism that contributes to embryonic growth and patterning', *Cell*, 155: 1119-30.

Sumbal, J., D. Belisova, and Z. Koledova. 2021. 'Fibroblasts: The grey eminence of mammary gland development', *Semin Cell Dev Biol*, 114: 134-42.

Sumbal, J., A. Chiche, E. Charifou, Z. Koledova, and H. Li. 2020. 'Primary Mammary Organoid Model of Lactation and Involution', *Front Cell Dev Biol*, 8: 68.

Sumbal, J., and Z. Koledova. 2019. 'FGF signaling in mammary gland fibroblasts regulates multiple fibroblast functions and mammary epithelial morphogenesis', *Development*, 146.

Sutherland, K. D., F. Vaillant, W. S. Alexander, T. M. Wintermantel, N. C. Forrest, S. L. Holroyd, E. J. McManus, G. Schutz, C. J. Watson, L. A. Chodosh, G. J. Lindeman, and J. E. Visvader. 2006. 'c-myc as a mediator of accelerated apoptosis and involution in mammary glands lacking Socs3', *EMBO J*, 25: 5805-15.

Suzuki, M., and D. A. Boothman. 2008. 'Stress-induced premature senescence (SIPS)--influence of SIPS on radiotherapy', *J Radiat Res*, 49: 105-12.

Swann, J. B., and M. J. Smyth. 2007. 'Immune surveillance of tumors', *J Clin Invest*, 117: 1137-46.

Taddei, I., M. A. Deugnier, M. M. Faraldo, V. Petit, D. Bouvard, D. Medina, R. Fassler, J. P. Thiery, and M. A. Glukhova. 2008. 'Beta1 integrin deletion from the basal compartment of the mammary epithelium affects stem cells', *Nat Cell Biol*, 10: 716-22.

Talhouk, R. S., M. J. Bissell, and Z. Werb. 1992. 'Coordinated expression of extracellular matrix-degrading proteinases and their inhibitors regulates mammary epithelial function during involution', *Journal of Cell Biology*, 118: 1271-82.

Tanos, T., L. Rojo, P. Echeverria, and C. Brisken. 2012. 'ER and PR signaling nodes during mammary gland development', *Breast Cancer Res*, 14: 210.

Tse, C., A. R. Shoemaker, J. Adickes, M. G. Anderson, J. Chen, S. Jin, E. F. Johnson, K. C. Marsh, M. J. Mitten, P. Nimmer, L. Roberts, S. K. Tahir, Y. Xiao, X. Yang, H. Zhang, S. Fesik, S. H. Rosenberg, and S. W. Elmore. 2008. 'ABT-263: a potent and orally bioavailable Bcl-2 family inhibitor', *Cancer Res*, 68: 3421-8.

Uria, J. A., and Z. Werb. 1998. 'Matrix metalloproteinases and their expression in mammary gland', *Cell Res*, 8: 187-94.

van Deursen, J. M. 2019. 'Senolytic therapies for healthy longevity', *Science*, 364: 636-37.

Van Keymeulen, A., A. S. Rocha, M. Ousset, B. Beck, G. Bouvencourt, J. Rock, N. Sharma, S. Dekoninck, and C. Blanpain. 2011. 'Distinct stem cells contribute to mammary gland development and maintenance', *Nature*, 479: 189-93.

Van Rooijen, N., and A. Sanders. 1994. 'Liposome mediated depletion of macrophages: mechanism of action, preparation of liposomes and applications', *J Immunol Methods*, 174: 83-93.

VanArsdale, T., C. Boshoff, K. T. Arndt, and R. T. Abraham. 2015. 'Molecular Pathways: Targeting the Cyclin D-CDK4/6 Axis for Cancer Treatment', *Clin Cancer Res*, 21: 2905-10.

Veltmaat, J. M., A. A. Mailleux, J. P. Thiery, and S. Bellusci. 2003. 'Mouse embryonic mammogenesis as a model for the molecular regulation of pattern formation', *Differentiation*, 71: 1-17.

Vernon, R. G., and C. M. Pond. 1997. 'Adaptations of maternal adipose tissue to lactation', *J Mammary Gland Biol Neoplasia*, 2: 231-41.

Villiard, E., J. F. Denis, F. S. Hashemi, S. Igelmann, G. Ferbeyre, and S. Roy. 2017. 'Senescence gives insights into the morphogenetic evolution of anamniotes', *Biol Open*, 6: 891-96.

Visvader, J. E., and J. Stingl. 2014. 'Mammary stem cells and the differentiation hierarchy: current status and perspectives', *Genes Dev*, 28: 1143-58.

Wang, C., D. Jurk, M. Maddick, G. Nelson, C. Martin-Ruiz, and T. von Zglinicki. 2009. 'DNA damage response and cellular senescence in tissues of aging mice', *Aging Cell*, 8: 311-23.

Wang, E., and D. Gundersen. 1984. 'Increased organization of cytoskeleton accompanying the aging of human fibroblasts in vitro', *Exp Cell Res*, 154: 191-202.

Wang, Q. A., A. Song, W. Chen, P. C. Schwalie, F. Zhang, L. Vishvanath, L. Jiang, R. Ye, M. Shao, C. Tao, R. K. Gupta, B. Deplancke, and P. E. Scherer. 2018. 'Reversible De-differentiation of Mature White Adipocytes into Preadipocyte-like Precursors during Lactation', *Cell Metab*, 28: 282-88 e3.

Watson, C. J. 2006. 'Involution: apoptosis and tissue remodelling that convert the mammary gland from milk factory to a quiescent organ', *Breast Cancer Res*, 8: 203.

Watson, C. J., and P. A. Kreuzaler. 2011. 'Remodeling mechanisms of the mammary gland during involution', *Int J Dev Biol*, 55: 757-62.

Wiseman, B. S., and Z. Werb. 2002. 'Stromal effects on mammary gland development and breast cancer', *Science*, 296: 1046-9.

Wu, H., L. Pan, C. Gao, H. Xu, Y. Li, L. Zhang, L. Ma, L. Meng, X. Sun, and H. Qin. 2019. 'Quercetin Inhibits the Proliferation of Glycolysis-Addicted HCC Cells by Reducing Hexokinase 2 and Akt-mTOR Pathway', *Molecules*, 24.

Xu, M., T. Pirtskhalava, J. N. Farr, B. M. Weigand, A. K. Palmer, M. M. Weivoda, C. L. Inman, M. B. Ogrodnik, C. M. Hachfeld, D. G. Fraser, J. L. Onken, K. O. Johnson, G. C. Verzosa, L. G. P. Langhi, M. Weigl, N. Giorgadze, N. K. LeBrasseur, J. D. Miller, D. Jurk, R. J. Singh, D. B. Allison, K. Ejima, G. B. Hubbard, Y. Ikeno, H. Cubro, V. D. Garovic, X. Hou, S. J. Weroha, P. D. Robbins, L. J. Niedernhofer, S. Khosla, T. Tchkonia, and J. L. Kirkland. 2018. 'Senolytics improve physical function and increase lifespan in old age', *Nat Med*, 24: 1246-56.

Xu, M., T. Tchkonia, H. Ding, M. Ogrodnik, E. R. Lubbers, T. Pirtskhalava, T. A. White, K. O. Johnson, M. B. Stout, V. Mezera, N. Giorgadze, M. D. Jensen, N. K. LeBrasseur, and J. L. Kirkland. 2015. 'JAK inhibition alleviates the cellular senescence-associated secretory phenotype and frailty in old age', *Proc Natl Acad Sci U S A*, 112: E6301-10.

Xue, W., L. Zender, C. Miething, R. A. Dickins, E. Hernando, V. Krizhanovsky, C. Cordon-Cardo, and S. W. Lowe. 2007. 'Senescence and tumour clearance is triggered by p53 restoration in murine liver carcinomas', *Nature*, 445: 656-60.

Yang, J., M. Liu, D. Hong, M. Zeng, and X. Zhang. 2021. 'The Paradoxical Role of Cellular Senescence in Cancer', *Front Cell Dev Biol*, 9: 722205.

Yosef, R., N. Pilpel, R. Tokarsky-Amiel, A. Biran, Y. Ovadya, S. Cohen, E. Vadai, L. Dassa, E. Shahar, R. Condiotti, I. Ben-Porath, and V. Krizhanovsky. 2016. 'Directed elimination of senescent cells by inhibition of BCL-W and BCL-XL', *Nat Commun*, 7: 11190.

Yuan, J. S., A. Reed, F. Chen, and C. N. Stewart, Jr. 2006. 'Statistical analysis of real-time PCR data', *BMC Bioinformatics*, 7: 85.

Yun, M. H., H. Davaapil, and J. P. Brockes. 2015. 'Recurrent turnover of senescent cells during regeneration of a complex structure', *Elife*, 4.

Zhu, Y., T. Tchkonia, T. Pirtskhalava, A. C. Gower, H. Ding, N. Giorgadze, A. K. Palmer, Y. Ikeno, G. B. Hubbard, M. Lenburg, S. P. O'Hara, N. F. LaRusso, J. D. Miller, C. M. Roos, G. C. Verzosa, N. K. LeBrasseur, J. D. Wren, J. N. Farr, S. Khosla, M. B. Stout, S. J. McGowan, H. Fuhrmann-Stroissnigg, A. U. Gurkar, J. Zhao, D. Colangelo, A. Dorronsoro, Y. Y. Ling, A. S. Barghouthy, D. C. Navarro, T. Sano, P. D. Robbins, L. J. Niedernhofer, and J. L. Kirkland. 2015. 'The Achilles' heel of senescent cells: from transcriptome to senolytic drugs', *Aging Cell*, 14: 644-58.

Zwick, R. K., M. C. Rudolph, B. A. Shook, B. Holtrup, E. Roth, V. Lei, A. Van Keymeulen, V. Seewaldt, S. Kwei, J. Wysolmerski, M. S. Rodeheffer, and V. Horsley. 2018. 'Adipocyte hypertrophy and lipid dynamics underlie mammary gland remodeling after lactation', *Nat Commun*, 9: 3592.

Zygmunt, M., F. Herr, K. Munstedt, U. Lang, and O. D. Liang. 2003. 'Angiogenesis and vasculogenesis in pregnancy', *Eur J Obstet Gynecol Reprod Biol*, 110 Suppl 1: S10-8.

Résumé

La sénescence est une réponse à un stress biologique, caractérisée par un arrêt stable du cycle cellulaire. Néanmoins, les cellules restent métabolliquement actives et acquièrent un phenotype sécrétoire associé à la sénescence, avec la production d'un sécrétome complexe composé de cytokines, chémiokines, facteurs de croissance et modulateurs du remodelage de la matrice extracellulaire. La sénescence est associée à de nombreux processus pathologiques, comme la tumorigénèse et le vieillessement. Cependant, où, quand et comment la sénescence contribue aux processus physiologiques reste méconnu. Pour répondre à cette question, nous avons tiré profit de la glande mammaire (GM), un organe avec une plasticité remarquable pendant le développement post-natal. L'involution de la GM est l'un des évenements majeurs de mort cellulaire et de remodelage tissulaire chez les mammifères, lorsque les cellules épithéliales produisant le lait sont éliminées et que la GM retourne à son état pré-grossesse, attendant la prochaine gestation. Au cours de ma thèse, nous avons montré que la sénescence était induite transitoirement pendant la phase irréversible de l'involution. De plus, le programme de sénescence apparaissait spécifiquement dans les cellules luminales productrices de lait et corrélait à l'expression de l'inhibiteur du cycle cellulaire p16. En parallèle, nous avons établi un nouveau modèle d'organoides pour mimer la gestation, la lactation et l'involution de la GM. Dans ce modèle *ex-vivo*, nous avons aussi relever la présence de cellules sénescentes strictement lors du processus d'involution. Pour évaluer l'impact biologique de la sénescence *in vivo*, nous avons utilisé une méthode de scellement des mamelons pour découpler les phases réversible et irréversible de l'involution. Nous avons dévoilé une association étroite entre le sevrage des hormones lactogéniques qui a lieu lors de la seconde phase d'involution, et l'induction du programme de sénescence. Pour mieux définir les rôles physiologiques de la sénescence pendant l'involution, nous avons traités des souris avec de l'ABT-263, un composé sénolytique induisant l'apoptose des cellules sénescentes. Nous avons observé une altération du remodelage tissulaire suite à l'élimination des cellules sénescentes, avec des alvéoles résiduelles plus larges et un remplissage adipocytaire retardé. De plus, dans des organoides provenant de souris transgéniques p16-3MR, nous avons éliminé les cellules sénescentes avec succès grâce à l'administration de ganciclovir, ce qui a retardé le processus d'involution. Dans leur ensemble, les modèles *in vivo* et *ex-vivo* suggèrent un rôle important de la sénescence pour moduler la phase de remodelage tissulaire dans l'involution de la GM. Enfin, le processus d'involution est intiment lié avec le cancer du sein post-partum, un cancer diagnostiqué dans les 10 ans suivant une grossesse et associé à un mauvais pronostic. Explorer comment la sénescence impacte le microenvironnement lors de l'involution pourrait ainsi fournir de nouvelles connaissances pour mieux comprendre le cancer du sein post-partum.

Abstract

Cellular senescence is a biological stress response characterized by a stable cell cycle arrest. Nonetheless, cells remain metabolically active and acquire a senescence-associated secretory phenotype (SASP), a complex secretome composed of cytokines, chemokines, growth factors, and extracellular matrix remodeling modulators. Senescence is associated with various pathological processes, such as tumorigenesis and aging. However, it is unknown when, where and how senescence contributes to physiological processes. To answer this question, we took advantage of the mammary gland (MG), an organ with remarkable plasticity throughout postnatal development. The MG involution is one of the major mammalian cell death and tissue remodeling events, when milk-producing epithelial cells are removed, and the MG returns to its pre-gestation state, resting for further pregnancy. During my Ph.D., we showed that senescence was transiently induced during the irreversible phase of involution. The senescent program occurred specifically in the alveolar milk-producing luminal cells and correlated with the expression of the cell cycle inhibitor p16. In parallel, we established a novel organoid system to mimic MG gestation, lactation, and involution. In this *ex-vivo* model, we also highlighted the presence of senescent cells strictly during the involution-like process. To assess the biological impact of senescence *in vivo,* we used a teat sealing method to uncouple the reversible and irreversible phases of involution. We unveiled a close association between the withdrawal of lactogenic hormones occurring in the second phase of involution and the induction of the senescence program. To further define the physiological roles of senescence during involution, we treated mice with ABT-263, a senolytic compound inducing apoptosis of senescent cells. Interestingly, we observed an impaired tissue remodeling upon senescence elimination, with larger remaining alveolar structures and delayed adipocyte refilling. Moreover, in organoids from transgenic p16-3MR mice, we successfully removed senescent cells with ganciclovir and delayed the involution-like process. Taken together, both *in vivo* and *ex-vivo* models suggest an essential role of senescence in modulating the tissue remodeling phase of MG involution. Importantly, the involution process is intimately associated with postpartum breast cancer (PPBC), a cancer diagnosed within 10 years following delivery with a poor prognosis. Investigating how senescence impacts the microenvironment during the involution process might provide major insights to understand PPBC.